OPTIMAL SYSTEMS FOR ECHO-LOCATION

BY

RODERICK C. BRYANT

DEPARTMENT OF ELECTRICAL AND ELECTRONIC ENGINEERING

UNIVERSITY OF ADELAIDE

A thesis submitted for the degree of Doctor of Philosophy in:

SEPTEMBER 1985

DEDICATION

This work is dedicated to my dear wife, Anne; fellow mountaineer on our thirteen-year climb to this vantage.

Some imagine that she needs my help to climb mountains. In fact, she prefers rolling hills to rugged mountains but came along for my sake. Often she has had to belay me across patches of scree. Frequently, she has pointed the way up.

For me, the exhiliration of the climb. For Anne, only the view.

ABSTRACT

This thesis is concerned with the factors affecting the performance of pulse echo systems for target localization. Such systems locate a target by estimation of its range and bearing. The thesis is chiefly concerned with situations where Doppler effects are negligible because the relative velocities of receiver, target and scatterers with respect to the transmitter are all small.

In this context, three performance indicators are derived which together can be used to analyze the performance of such a system. By this means, the performance is related to the transmission path characteristics and the energy spectrum of the signal transmitted. Optimal spectra are derived with respect to several performance criteria and their theoretical performances are compared. The theoretical analyses are backed up by computer simulation results.

When the transmission path characteristics are variable or uncertain due to estimation error, a robust system may be required. It is shown that the jointly optimal signal and receiver with respect to a minimax robustness criterion are optimal for a least-favourable transmission path within the class for which the optimization is being performed.

The performance of gated maximum likelihood ranging systems are analyzed to determine the effect of gate width on performance under various conditions. In particular, adaptive systems in which the gate width is coupled to estimated tracking error are analyzed to determine the optimal ratio of gate width to tracking error. A new conditional M.A.P. estimator is then derived which uses the same information but in an optimal way. In particular, the prior information, in the form of a range prediction and a prediction error estimate, is used in a way that minimizes the additional spurious information used. This is done by constructing the conditional prior probability density

function according to a maximum entropy criterion. It is shown that such a system is highly practical, particularly for digital implementation. The performances of various systems are compared by simulation under various conditions and the conditional M.A.P. estimator is shown to consistently yield best performance.

Finally, a case study is undertaken in which robust system optimization and conditional M.A.P. estimation are used. Details of the design of a real time digital system using a linear array of modern signal processing microcomputers are presented. This system was designed for use in robotics experiments for research into automated sheep shearing.

STATEMENT

I hereby certify that this thesis contains no material which has been accepted for the award for any other degree or diploma in any university.

I also declare that, to the best of my knowledge and belief, this thesis contains no material previously published or written by any other person except where due reference is made herein.

I hereby consent to this thesis being made available for photocopying and loan if accepted for the award of the degree of Doctor of Philosophy.

Roderick C. Bryant

ACKNOWLEDGEMENTS

It is a pleasure to acknowledge the debt I owe Prof. R. E. Bogner for the encouragement, the conscientious supervision, the highly rewarding technical discussions and the friendship he has extended to me throughout my candidature. Beyond these things, I owe him the very opportunity to undertake research for a Ph.D. and for this I am profoundly grateful.

To the Australian Wool Corporation also, I express sincere thanks for their imaginative support of the automated mechanical shearing research programme under which I was employed during most of my candidature. In particular I am grateful to Dr. Paul Hudson of the Wool Corporation for the cooperation he has always shown in my dealings with him.

To all the staff and postgraduate students of the Department of Electrical and Electronic Engineering during my candidature I offer thanks for their shared insights and for their active cooperation. Particular thanks are due to the technical staff and to all those involved in the TFB project.

LIST OF SYMBOLS AND ABBREVIATIONS (IN ORDER OF APPEARANCE)

MAP	Maximum A-posteriori Probability.
ML	Maximum Likelihood.
GML	Gated Maximum Likelihood.
$x(t)$	Received Waveform.
$r(t)$	Target echo.
$i(t)$	Interference.
$c(t)$	Clutter.
$n(t)$	Noise.
$p(?)$	Probability density function of ?.
$p(?\|??)$	Probability density function of ? conditional on ??.
$p(?, ??)$	Joint probability density function of ? and ??.
τ	Delay of the target echo.
$\hat{\tau}$	Estimate of target echo delay.
$\bar{\tau}$	Prior expectation of target echo delay.
W	Range gate width.
$LL(??\|?)$	Log-likelihood function of ?? given ?.
$q(t)$	Optimal correlation reference.
$\Phi_{ii}(t_1, t_2)$	Interference Autocovariance Function.
$r_0(\tau)$	Signal component of correlation function.
$\Re$	Detection index.
f_0	Carrier frequency of target echo after interference whitening.
β	Moment bandwidth of target echo after interference whitening.
$Q(f)$	Fourier transform of optimal correlation reference.
$R(f)$	Fourier transform of target echo.
$G_{ii}(f)$	Interference power spectrum.
$y(t)$	Correlation function.

$\acute{y}(t)$	Hilbert transform of correlation function.
$H_T(f)$	Target path transfer function in transmission path model.
$H_c(f)$	Clutter path transfer function in transmission path model.
$G_{nn}(f)$	Noise power spectrum.
$s(t)$	Transmitted signal.
$S(f)$	Fourier transform of transmitted signal.
$G_{ss}(f)$	Power spectral density of constant envelope signal.
T	Duration of signal.
B	Signal bandwidth.
$\Phi_{ss}(t-T)$	Autocorrelation function of the signal.
$R^c(f)$	Fourier transform of compressed target echo.
$G^c_{ii}(f)$	Power spectrum of compressed interference.
$\Re_T$	Inherent detection threshold.
σ^2_τ	Echo delay estimate variance.
$E(?)$	Expectation of ?.
Σ^2_τ	Echo delay estimate variance with informative carrier.
β_0	Second moment of echo energy spectrum after whitening.
G	Antenna gain.
r	Distance from antenna.
S_r	Energy density at distance, r, from the antenna.
E_{0X}	Aperture field polarized in the x direction.
σ_e	Effective aperture area.
β_1	Second moment of transmitted signal spectrum.
P_s	Power of a constant envelope signal.
G_{eff}	Effective antenna gain.
θ	Angle of signal arrival relative to the broadside direction.
$\triangle\tau$	Delay between signal arrival at adjacent sensors.
τ_i	Echo delay at sensor, i.
d	Sensor separation.

c	Velocity of propagation.
L	Length of a sensor array.
$*$	Convolution operator.
N	Number of sensors in an array.
$\Delta\hat{\tau}$	Estimated delay between signal arrival at adjacent sensors.
$\sigma^2_{\Delta\tau}$	Variance of $\Delta\hat{\tau}$.
$(\Delta\theta)^2$	Variance of bearing (or azimuth) estimate.
$\Delta\theta$	Resolution angle.
TRI	Transverse Resolution Index.
TRI	Effective gain per effective unit area of the aperture.
$\vec{\theta}$	Signal parameter vector.
$\chi(\vec{\theta}_1, \vec{\theta}_2)$	Ambiguity function for two signals differing in $\vec{\theta}$.
F	Normalized narrowband signal.
χ_{rq}	Cross-ambiguity function.
α	Incremental fractional velocity.
A	Mean fractional velocity.
$v(t)$	Hilbert transform of target echo.
$w(t)$	Analytic representation of target echo.
$\xi(\tau, f)$	Scattering density in delay-Doppler plane.
$K_c(t, \acute{t})$	Clutter autocovariance function.
$2N_0$	Single-sided Noise power spectral density.
R_T	Frequency band of interest.
R_0	Frequency band of zero signal power.
R_1	Frequency band of non-zero signal power.
DFT	Discrete Fourier Transform.
FFT	Fast implementation of DFT.
MDI	Maximum Detection Index.
MTRI	Maximum Transverse Resolution Index.

MV	Minimum echo delay estimate Variance.
SCR	Signal-to-Clutter Ratio.
SNR	Signal-to Noise Ratio.
$A(\tau)$	Echo-to-reference correlation.
a	Ratio of sidelobe to mainlobe peak values.
erf	Error function.
$\Re_A$	Ambiguity threshold.
$H_M(f)$	Transfer function of matched filter.
SIR	Signal-to-Interference Ratio.
C_s	Signal uncertainty class.
C_i	Interference uncertainty class.
$H(f)$	Receiver filter transfer function.
P_j^D	Element j of designer's strategy vector.
P_k^N	Element k of nature's strategy vector.
$p(?;??)$	Payoff for designer's strategy, ?, and nature's strategy, ??.
p_R	Robust-optimal signal-to-interference ratio.
$H_R(f)$	Robust-optimal matched filter.
(R_R, G_{iR})	Least favourable pair of signal and interference characteristics.
δ	Maximum energy of signal modelling error.
σ_i^2	Interference power.
$L(f)$	Lower bound on interference power spectrum.
$U(f)$	Upper bound on interference power spectrum.
C_T	Target path uncertainty class.
C_c	Clutter path uncertainty class.
δ_T	Maximum power of target path transfer function modelling error.
σ_c^2	Maximum clutter transfer power.

$L_c(f)$	Lower bound on squared magnitude of clutter path transfer function.
$U_c(f)$	Upper bound on squared magnitude of clutter path transfer function.
e_T	Target path transfer function modelling error power.
$H_{TT}(f)$	Normalized target path transfer function.
$H_0(f)$	Nominal normalized target path transfer function.
A	Normalization coefficient for target path transfer function.
A_{min}	Minimum value of normalization coefficient.
P_c	Clutter transfer power.
S_R	Robust-optimal signal Fourier transform.
$H_S(f)$	Receiver filter transfer function with the signal deconvolved.
$H_{TR}(f)$	Least favourable target path transfer function.
$\|H_{cR}(f)\|^2$	Least favourable clutter path transfer function magnitude squared.
$G_R(f)$	Robust-optimal signal power spectrum.
R_U	Frequency band in which the squared magnitude of the least favourable clutter path transfer function is the upper bound.
R_L	Frequency band in which the squared magnitude of the least favourable clutter path transfer function is the lower bound.
R_M	Frequency band in which the squared magnitude of the least favourable clutter path transfer function lies between the bounds.
PDF	Probability Density Function.
RMS	Root-Mean-Square.
σ_e^2	Prediction error variance.
$\vec{\hat{\tau}}$	Vector of previous estimates.

MMSE	Minimum-Mean-Squared-Error.
$H_i(f)$	The ith measured target path transfer function.
A_i	The ith normalization coefficient.
e_i	The ith modelling error power.
E_0	Nominal target path transfer power.
I/O	Input-Output.
DSP	Digital Signal Processing.
FIFO	First-In-First-Out.
FIR	Finite Impulse Response.
A/D	Analog-to-Digital.
CAD	Computer-Aided Design.

TABLE OF CONTENTS

1. INTRODUCTION

§1.0 General Remarks

This thesis is concerned with the optimality of signals, receivers and estimation algorithms for echo-location. For the purposes of this thesis, an echo-location system is any system that aids in the location of a target by transmitting a signal and extracting information from the echo received. The target may be an isolated object within the medium or it may be an arbitrarily defined region within a target surface. The echo-location system may estimate the range and bearing of the target or just the range of any target at a given bearing or the bearing of any target at a specified range. (In the case of focussed systems, the system would typically estimate the range of a target in the focal region).

It is over thirty years since Woodward published his famous analysis [2.1] of these problems. Today, however, there are many relatively new, or emerging, applications of echo-location systems. These include surface imaging systems for robotics [1.1], medical [1.2], industrial [1.3], and geophysical [1.4] applications; and ground-probing radars [1.5]. These are often characteristically different from those that were the subjects of much earlier research. In contrast to more conventional radar and sonar applications, the transmission paths may be complicated by highly coloured absorption properties of the media and by high scattering densities giving rise to low signal-to-clutter ratios. At the same time, Doppler effects are often negligible while the clutter is (at least locally) statistically stationary with range. However, the transmission path characteristics may be subject to a significant degree of variation within the one application.

It was in relation to such an application that the author was motivated to take a fresh look at relevant concepts in estimation theory and to develop a new, comprehensive approach to signal design for a restricted class of conditions relevant to some of these new applications.

Because this thesis covers a rather broad scope of sub-topics, a comprehensive literature review will not be undertaken in detail, here. Instead, each topic will be introduced, with a literature review, in the relevant chapter within the body of the thesis. This chapter, therefore, will be short and restricted to a more general introduction of the sub-topics and the relevant contexts.

Several theorems appear in the text, the proofs of which are rather involved. Those proofs have therefore been provided in appendices which follow all the text. Other appendices contain computer program listings. The appendix numbers are the same as the relevant chapter numbers.

§1.1 Maximum Likelihood Estimation

Chapter 2 is basically a review of signal parameter estimation theory as it applies to echo-location. In particular, the factors affecting the performance of *gated maximum likelihood* (GML) systems are discussed. In some areas, however, established theory has been extended in order to derive fundamental indicators of performance that may be used in later chapters for performance analyses and comparisons and for optimization.

For basic theory and fundamental concepts, the author has drawn heavily on the early radar theory of Woodward [2.1,2.2] and Davies [2.2] and from some of the many excellent texts now available [2.3,2.4,2.5].

The form of transmission path model used exclusively in this thesis is introduced in chapter 2 and is taken from the publications of Kooij [2.7] and Moose [2.6]. The concept of local stationarity of the interference waveform, as interpreted by Moose [2.6], is also adopted here. However, a less restrictive criterion for local stationarity is justified in section 2.3.

The detection index, first introduced by Woodward [2.1] under a different name, is adopted as an indicator of detection performance in sub-section 2.4.1. Threshold effects related to signal detection and ambiguity are also discussed in sub-section 2.4.1, but the signal ambiguity problem is discussed in much more detail in chapter 3.

The expression for range estimate variance first derived by Woodward [2.1] and later shown to correspond to the Cramer-Rao lower bound on estimate variance [2.3,2.4] is adopted as an indicator of range estimate accuracy in sub-section 2.4.2. Other bounds on range estimate variance are also discussed in some detail. In particular, the role of carrier phase in range estimation is discussed, with reference to the early work of Woodward and Davies [2.2] and to the much more recent work of Ziv and Zakai [2.16] and of Weiss and Weinstein [2.17].

A good deal of original work is presented in sub-section 2.4.3 with the result that

a fundamental indicator of transverse resolution is derived. This performance indicator is applicable whether the system is designed to estimate bearing or not. It is shown to be closely related to antenna gain and to bearing estimate variance.

The approach taken by Evans and Kong [2.11], in deriving an expression for the gain of a wideband antenna is combined with the philosophy adopted by Bryant and Bogner [1.1] in order to derive an indicator of transverse resolution performance that takes into account the signal spectrum and the transmission path characteristics. This same indicator is then derived, via a totally independent route, as an indicator of estimate variance for an active bearing estimator.

As a by-product of this analysis,, the form of an active ML estimator of bearing is derived. This estimator is identical to that obtained by Arques [2.15] by a different analysis and, of course, it is very different to the *passive* bearing estimators of more recent authors [2.12,2.13,2.14].

§1.2 Signal Optimization

The topic of signal optimization is the subject of chapter 3. The technique developed is comprehensive in the sense that it provides a unified approach to signal optimization in the context of those types of application that are the chief concern of this thesis.

It incorporates several relevant criteria in a way that allows the designer to provide emphases that reflect the demands of his particular application. The approach is partly inspired by the work of Kooij [2.7] and Moose [2.6] in the late 1960's and early 1970's. However, as well as their criterion of *maximum detection index*, the author employs two others related to range accuracy and transverse resolution. The foundations for this work were laid in chapter 2 where fundamental indicators of performance were derived.

Chapter 3 begins with a review of established signal optimization criteria and approaches in section 3.0. The aim is to show that the more usual approaches taken in the fields of radar and sonar are not efficacious when Doppler effects are negligible and transmission path characteristics are more extreme.

The use of ambiguity functions in signal design is discussed with particular reference to the work of Woodward [2.1], who introduced the ambiguity function. References are also made to the particularly lucid developments of the concept in a text by Helstrom [3.1]. The extension of the concept to cover wideband systems, where Doppler effects are more complicated, is discussed with reference to a paper by Bates [3.2]. The ways in which ambiguity functions can be used in signal design are discussed in sub-sections 3.0.2 and 3.0.3. The mathematical basis for this approach is treated explicitly in sub-section 3.0.3, following the treatment in [3.4]. Reference is made to a number of papers [3.2–3.6] in which a variety of optimization criteria are employed.

In sub-section 3.0.4, the works of Kooij [2.7] and Moose [2.6] concerning signal

optimization according to a detectability criterion are discussed. The attractiveness of their approach is pointed out in sub-section 3.0.5 and the need for its generalization to alternative criteria is argued. A multiple-criteria approach is advocated.

Section 3.1 deals with signal optimization with respect to the simple criteria of *maximum detection index*, *minimum estimate variance* and *maximum transverse resolution index*. The solutions are given in the form of three theorems. In section 3.2, the performances of systems employing signals optimized according to these different criteria are compared theoretically.

Chapter 3 concludes in the development of a technique for combining all three criteria in a mixed criteria optimization approach. This method involves an overall strategy for signal optimization in which priorities can be assigned to three performance constraints such that the higher priority constraints must be met before the remaining performance criteria become effective. The use of this approach is illustrated by examples taken from the authors experience with ultrasonic sensing through wool and these are backed up by simulation results in chapter 5.

Because sections 3.1 to 3.4 deal with optimization of signal power spectra only, an additional section at the end of chapter 3 is devoted to the topic of signal waveform design. That is, the problem of designing a constant envelope waveform with a specified power spectrum is addressed. The pioneering work of Price et al [3.11] is extended to allow arbitrary spectra to be accomodated by means of non-linear chirps.

§1.3 Robust System Optimization

Chapter 4 is devoted to the problem of jointly optimizing the signal and receiver filter according to a robustness criterion when the transmission path characteristics are variable. The criterion used relates to detection performance only. The author's approach is related to the game-theoretic approaches used by other authors [4.4–4.8] for the robust optimization of filters. However, the problem in this case is complicated by having higher dimensionality and more complicated uncertainty class specifications. Nevertheless, a mathematical solution is presented in chapter 4 and solution techniques are described with the aid of a practical example in chapter 6.

§1.4 Conditional MAP Estimation

The main thrust of chapter 5 is towards the development of a conditional maximum a-posteriori probability (MAP) estimation algorithm as an augmented form of the well-known gated maximum likelihood (GML) estimator [2.1–2.4]. Firstly, an optimum form of the GML estimator is presented in which the gate width is related adaptively to the estimated error of the target tracking process. Then, a conditional MAP estimator is derived that uses the same target tracking scheme with the target tracking error estimated in the same way. This conditional MAP estimator is designed according to a minimum information (or maximum entropy) criterion. Several systems are compared in performance over a variety of conditions by means of simulations.

As a by-product of these simulations, many of the theoretical results of chapters 2 and 3 are verified empirically.

§1.5 Acoustic Sensing Through Fleece

Chapter 6 is a case study in which an application of conditional MAP estimation and robust system optimization is described. The system optimization problem is worked through, starting with techniques for constructing transmission path models. The system design is outlined and details are given of the multi-processor based design of the digital signal processing hardware.

The application described in chapter 6 has been the focus of the author's research over the past several years. Details of some of that research are described in [1.1] by the author in collaboration with Prof. R.E. Bogner. This application is very different from historical applications of echo-location. The application is focussed surface imaging at short range through wool. The target surface, the skin of a live sheep, is to be sensed at high speed for control of a shearing robot.

This application involves several elements that are common to many of the emerging applications. The system is for *surface imaging* as a form of *robotic sensing.* It operates through a *highly absorptive* medium and the target is to be detected in the presence of *intense interfering backscatter* from scatterers in the medium. This unwanted clutter is characterized by *local statistical stationarity with respect to range* in the region of the target. However the *transmission path characteristics are highly variable* so that a robust system design is necessary. Finally, the relative velocities between transmitter, target, scatterers and receiver along the beam axis are very small so that *Doppler effects are negligible.*

The characteristics of this problem italicized in the previous paragraph differentiate it from the more conventional applications of echo-location. However, some are shared by many of the emerging applications. It is to be expected, therefore, that the theoretical and practical solutions presented in this thesis will be relevant to the design of many other contemporary applications of echo-location.

2. MAXIMUM LIKELIHOOD ESTIMATION

§2.0 Introductory Remarks

The most fundamental approach to problems in detection and estimation is that which Woodward [2.1,2.2] named the *method of inverse probability.* Generally, we have an effect and we are attempting to discern some aspects of the causal mechanism. We have a parameterised model for that mechanism and we attempt to ascertain the most probable values of the parameters that have resulted in the observed effects.

This technique is known as *Maximum A-posteriori Probability* (MAP) estimation and represents the ideal parameter estimation technique. It turns out that to use this technique we need to know the *a-priori* probability distribution of the parameter to be estimated and this is often a stumbling block.

When such information is not available it seems natural to make an estimate by assuming a uniform prior probability. The corresponding technique is known as *Maximum Likelihood* (ML) estimation [2.1,2.2,2.3,2.4]. A modification of this approach is often used in which the parameter to be estimated is assumed to lie within a certain region or *gate* [2.1,2.2,2.3,2.4]. This method goes by the name, *Gated Maximum Likelihood* (GML) estimation.

This chapter will review what is known about these estimation techniques in order to obtain the structures of GML estimators and to gain insight into the factors affecting their performance. In some areas this knowledge will be extended by original work. This new work will be found in sections 2.3 and 2.4.

Firstly, we shall consider the structures of the estimators and then we shall move on to obtain three performance indicators which indicate the goodness or badness of certain aspects of expected system performance.

Since these indicators depend on the signal design we will be able to use them as signal optimisation criteria in chapter 3.

§2.1 The Maximum Likelihood Estimator of Range

For completeness we briefly review the established principles of ML estimation. Putting the ideas of the previous section into mathematical form, we denote the received waveform by $x(t)$. We assume that this received signal consists of a delayed signal, the target echo, which has been corrupted by additive interference:

$$x(t) = r(t - \tau_0) + i(t) \tag{2.1}$$

The interference, $i(t)$, consists of two statistically independent and jointly normal random components, $c(t)$ and $n(t)$ known as clutter and noise, respectively. These components are generated by different mechanisms and these important differences will be examined later.

Now, $r(t)$ is a known deterministic signal and it is only the presence of interference which prevents us from determining τ precisely from x(t). Because of the interference the value of τ is uncertain but we can describe it by its posterior probability density, $p(\tau|x(t))$.

Now from Baye's rule we have:

$$\begin{aligned} p(\tau, x(t)) &= p(x(t))p(\tau|x(t)) \\ &= p(\tau)p(x(t)|\tau)\,. \end{aligned} \tag{2.2}$$

Hence:

$$p(\tau|x(t)) = \frac{p(\tau)}{p(x(t))} p(x(t)|\tau)\,. \tag{2.3}$$

The left hand side of 2.3 is the posterior probability of τ and we would like to choose our estimate, $\hat{\tau}$, to be that value of τ which maximises 2.3.

The denominator of the first factor on the right tells us nothing about τ. It is an uninformative constant and may be ignored. The numerator of that factor is the prior probability density which is often unavailable.

The second factor in 2.3 is known as the *likelihood function* of τ given $x(t)$. When considered as a function of τ it is not a probability density. It is given the special name, "likelihood", because, in the absence of prior information it indicates the likelihood that received waveform includes a target echo delayed by τ.

We see from 2.3 that when a uniform prior probability is assumed, the approximate posterior density so obtained is simply a scaled version of the likelihood function. The approximate MAP estimate given by the peak of this function is, therefore, the ML estimate of delay.

The usual assumption made in respect of the prior probability is given by:

$$p(\tau) = \begin{cases} const, & \forall \tau : \bar{\tau} - W/2 < \tau < \bar{\tau} + W/2 \\ 0, & otherwise, \end{cases} \tag{2.4}$$

where $\bar{\tau}$ is the prior expectation of τ and W is the width of the *range gate* within which τ is assumed to lie.

The way to obtain a GML estimate is to generate an analogue of the log of the likelihood function, $LL(\tau|x(t))$, within the range gate and locate the peak. We generate the log likelihood function (LLF) because it is relatively easy to do so and this function is monotonic with the likelihood function itself and therefore the peak of the LLF occurs at the same value of τ.

It is well known [2.3,2.4] that the LLF of delay in the presence of normal interference is given (apart from uninformative constants) by:

$$LL(\tau|x(t)) = \int_{-\infty}^{+\infty} x(t)q(t,\tau)dt, \tag{2.5}$$

where $q(t)$ is a correlation reference function defined by the Fredholm integral:

$$r(t_1 - \tau) = \int_{-\infty}^{+\infty} \phi_{ii}(t_1, t_2)\, q(t_2, \tau)\, dt_2, \tag{2.6}$$

where $\phi_{ii}(t_1, t_2)$ is the known interference autocovariance, $E\{i(t_1)i(t_2)\}$. A correlation processor is also obtained in [2.1,2.2] for the more restrictive case of white interference.

Figure 2.1 *Post-Correlation Signal*

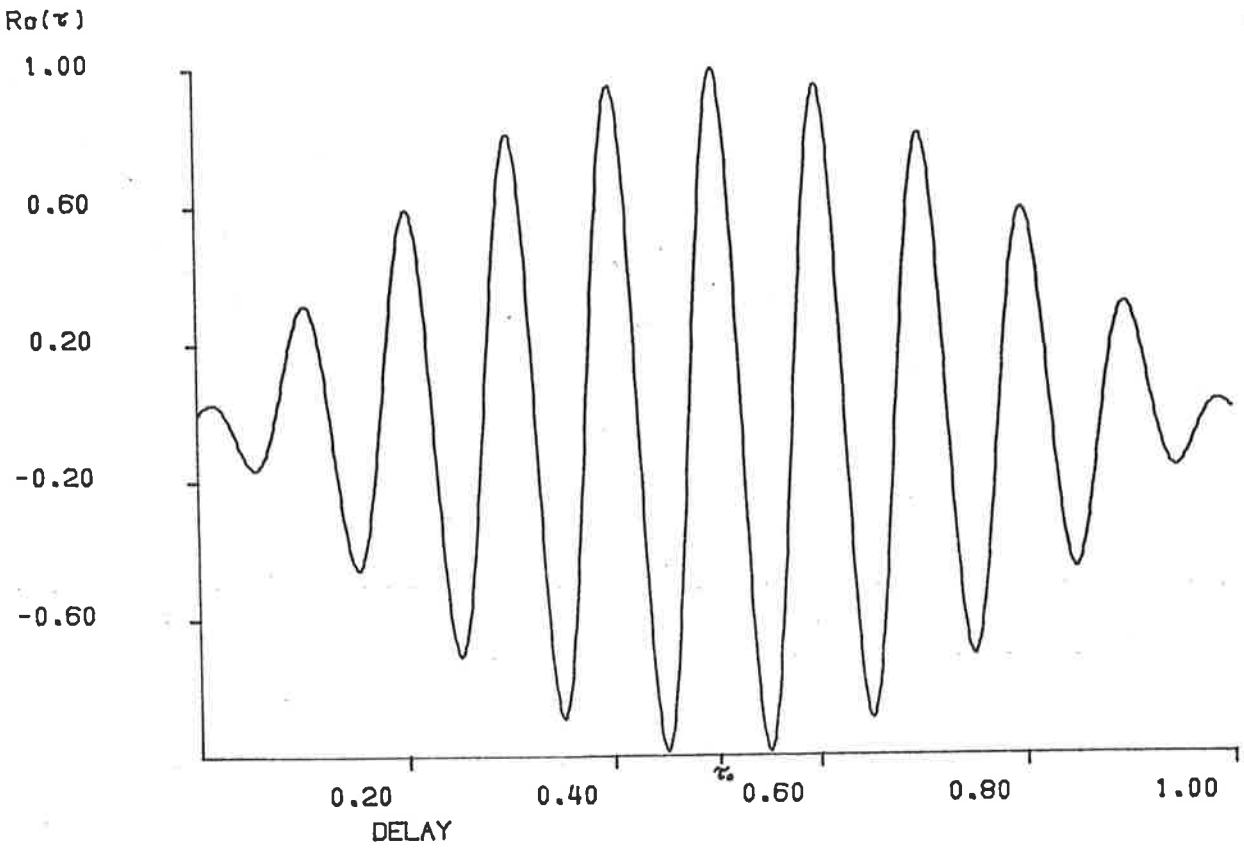

Fig. 2.1 illustrates the nature of the signal component in 2.5 given by:

$$r_0(\tau) = \int_{-\infty}^{+\infty} r(t-\tau_0)\, q(t,\tau)dt \tag{2.7}$$

where τ_0 is the true delay and τ is hypothesized delay. We see that this function consists of an oscillation, or *carrier* component under a more slowly-varying envelope. In most applications, the signal, $r(t)$, is a relatively narrowband signal and the carrier varies much more rapidly than the envelope. When we pick the peak of this signal we use two sources of information, the envelope shape and the carrier phase.

Now, in order for the carrier phase information to be reliable it can be shown that the ratio of the peak signal component in 2.5 to the RMS interference component must exceed a certain value. Otherwise interference may cause peaks of 2.5 near to the envelope peak to exceed the true peak at the envelope peak. Clearly the peak-signal to rms-interference ratio below which this can occur depends on the relationship between the rate of change of the envelope near the peak and the carrier frequency. We denote the square of the peak-signal to rms-interference ratio by $\Re$. The requirement for $\Re$ is obtained in reference [2.5] as:

$$(\Re)^{1/2} >> \frac{f_0}{\beta}, \tag{2.8}$$

where f_0 is the carrier frequency and β is the signal bandwidth. Precise mathematical definitions of these quantities will be presented later.

In practice, in the majority of cases, 2.8 is not met. Furthermore, the carrier phase information is often not preserved at the receiver because of phase errors resulting from reflection from an uneven or inclined target surface. In these circumstances the carrier phase should be treated as an uninformative parameter and averaged out [2.1,2.2,2.3,2.4]. The resulting expression replacing 2.5 is [2.3]:

$$LL(\tau\,||\bar{x}(t)||) = \left|\int_{-\infty}^{+\infty} \bar{x}(t)\bar{q}^*(t,\tau)dt\right|, \tag{2.9}$$

where $\bar{x}(t)$ and $\bar{q}(t)$ are the complex analytic representations of $x(t)$ and $q(t)$ respectively.

Now, if the interference is stationary, then 2.6 becomes:

$$r(t_1 - \tau) = \int_{-\infty}^{+\infty} \Phi_{ii}(t_1 - t_2)\, q(t_2 - \tau)\, dt_2, \tag{2.10}$$

where the autocovariance, $\phi_{ii}(t_1, t_2)$, has been replaced by the equivalent autocorrelation function, $\Phi_{ii}(t_1 - t_2)$ and $q(t_2, \tau)$ now depends only on the difference, $(t_2 - \tau)$. Equation 2.10 is a convolution and it follows that:

$$Q(f) = \frac{R(f)}{G_{ii}(f)}, \tag{2.11}$$

where $Q(f)$, $R(f)$ and $G_{ii}(f)$ are the Fourier transforms of $q(t)$, $r(t)$ and $\Phi_{ii}(t)$ respectively and, hence, $G_{ii}(f)$ is the interference power spectrum.

It follows that, in this case, 2.5 is equivalent to the two- stage filtering operation depicted in Fig. 2.2 in which the received waveform is firstly passed through an interference whitening filter and then through a compression filter. The transfer function of the compression filter is the conjugate match of the transform of the signal output from the whitening filter.

Equation 2.9 is equivalent to the same filtering operation followed by an *enveloping* operation:

$$\begin{aligned} LL(\tau \,||\bar{x}(t)||) &= |y(t) + j\acute{y}(t)|, \\ \textit{where} \qquad y(t) &= \int_{-\infty}^{+\infty} x(t) q(t, \tau) dt \end{aligned} \tag{2.12}$$

and $\acute{y}(t)$ is the Hilbert transform of $y(t)$.

Figure 2.2 *ML Correlation as a Filtering Operation*

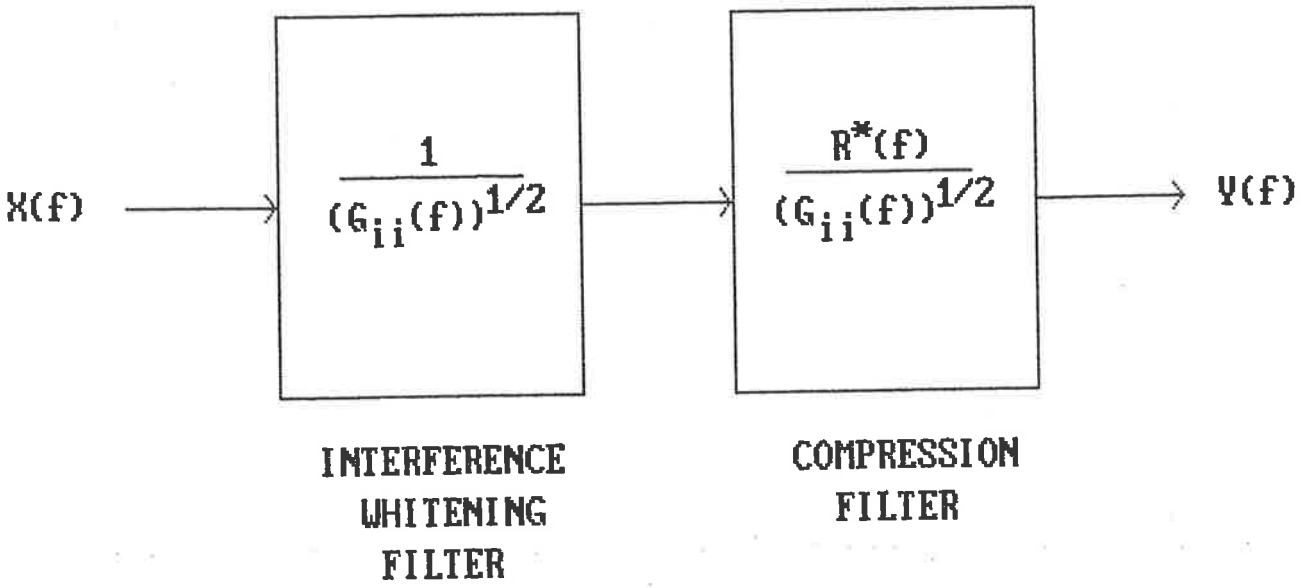

§2.2 A Transmission Path Model

Fig. 2.3 represents a transmission path model which is appropriate for our analysis. This model has appeared previously in the literature [2.6,2.7] in connection with underwater acoustic ranging and is sufficiently general for our purposes.

Now, the restrictions of this model need to be recognised. Firstly, we are assuming that the existence of a random field of scatterers does not cause the target path to be uncertain. This assumption is known in the literature as a *weak scattering* assumption [2.6,2.8]. The approach in chapter 4 allows this assumption to be relaxed by providing for uncertainty in the model.

Secondly, we are assuming that the transmission path impulse responses are time-invariant. This assumption is implicit in the fact that we are using transfer functions of a single frequency variable. It means that no relative motions between transmitter, target, scatterers or receiver are allowed. In practice it means that most of the results derived from this model apply only if Doppler shifts are negligible.

According to this model any transmission path can be fully specified by means of three functions. $H_T(f)$ is the transfer function of a filter representing the path of the target echo. $|H_c(f)|^2$ is the squared magnitude of the stochastic transfer function of a filter representing the combined parallel paths of unwanted echoes from scatterers other then the target. The output from this filter is known as clutter (or, in relation to underwater Sonar, reverberation) and differs from the noise in its dependence on the transmitted signal. The noise power spectral density is given by $G_{nn}(f)$.

As pointed out in chapter 1, this restriction rules out many conventional applications of active ranging systems in the radar and sonar areas. However, this approach is relevant in many emerging applications such as ground-probing radar and surface imaging systems for robotics, medicine industrial applications and oceanography.

Figure 2.3 **Transmission Path Model**

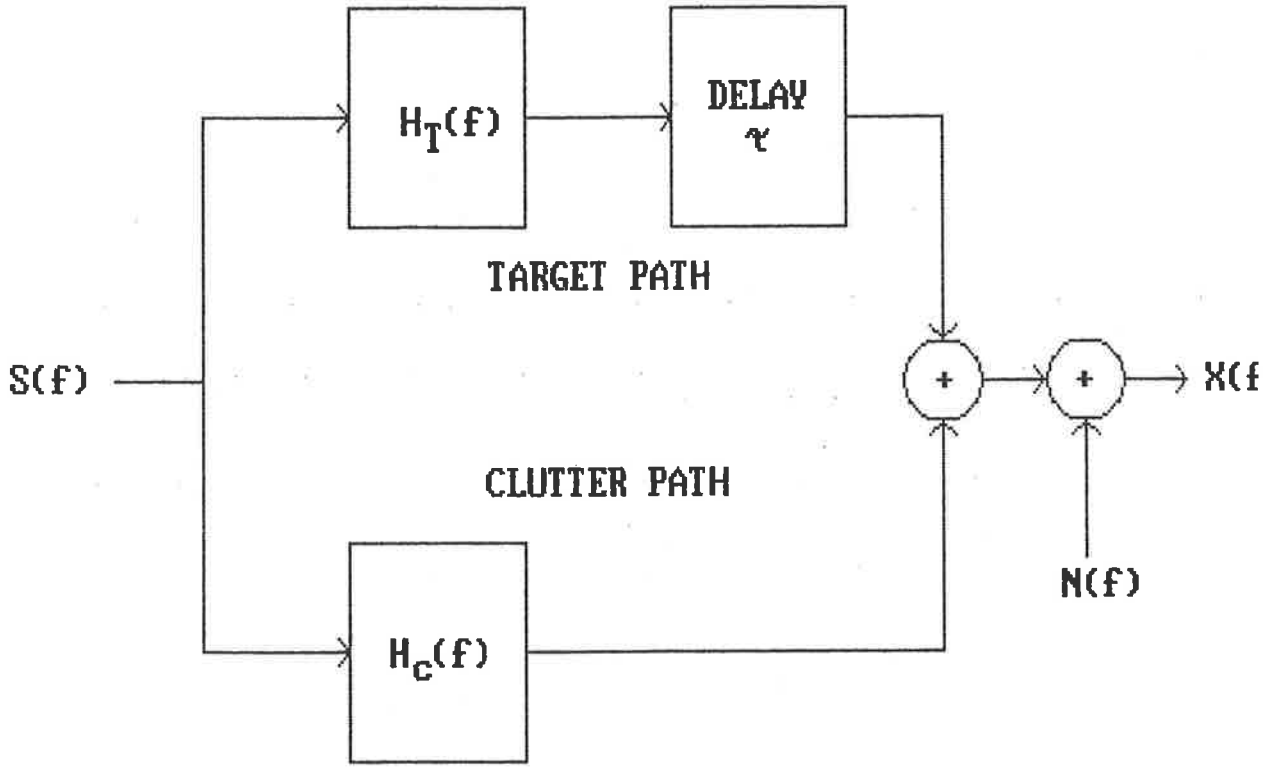

Now, in terms of the model in Fig. 2.3, we have:

$$R(f) = S(f)H_T(f), \tag{2.13}$$

$$G_{ii}(f) = G_{nn}(f) + G_{ss}(f)\,|H_c(f)|^2\,, \tag{2.14}$$

and hence

$$Q(f) = \frac{S(f)H_T(f)}{G_{nn}(f) + G_{ss}(f)\,|H_c(f)|^2}, \tag{2.15}$$

where $S(f)$ is the Fourier transform of the transmitted signal and will be referred to as the *signal*, and $G_{ss}(f)$ is the power spectral density of the signal.

§2.3 Stationarity Conditions

Now, in 2.15, $Q(f)$ depends on $|H_c(f)|^2$ and under certain conditions it is possible to relax the stationarity condition which was applied in deriving 2.10 so that 2.6 becomes:

$$r(t_1 - \tau) = \int_{-\infty}^{+\infty} \Phi_{ii}(t_1 - t_2, \tau)\, q(t_2 - \tau, \tau)\, dt_2. \tag{2.16}$$

Equation 2.16 represents an approximation which is valid when $\phi_{ii}(t_1, t_2)$ is a slowly varying function of t_1 with much greater dependence on the difference, $(t_1 - t_2)$. Equation 2.16 is not valid when ensemble non-stationarity is encountered. Under these conditions, the techniques of chapter 4 may be employed.

Recognising that, apart from a range dependence, 2.16 is again a convolution, we see that:

$$Q(f, \tau) = \frac{R(f)e^{-j2\pi\tau f}}{G_{ii}(f, \tau)}. \tag{2.17}$$

The optimal reference, $q(t, \tau)$, is now a slowly varying function of range, i.e.

$$q(t, \tau) = q(t - \tau, \tau). \tag{2.18}$$

Now, it can be shown [2.6] that the local stationarity condition , allowing the approximations 2.16 to 2.18, is met provided that the covariance function, $\phi_{cc}(t_1, t_2)$, of the clutter path impulse response, $h_c(t)$, is stationary over at least twice the duration of the transmitted signal, to a close approximation.

However, this condition is somewhat restrictive in situations where highly dispersed wideband signals such as chirps or pseudo-random binary sequences are employed. We will see that this condition can be considerably relaxed as a result of recognising that it is not the signal duration that is important but the signal bandwidth.

It is well known [2.9] that a signal of bandwidth B and duration T may be temporally compressed by the factor BT by means of a linear filtering operation. Hence,

if the transmitted signal, $s(t)$, is passed through an appropriate filter then its effective duration can be reduced to $1/B$. We have:

$$\Phi_{ss}(t-T) = s(t) * s(T-t), \tag{2.19}$$

where $\Phi_{ss}(t-T)$ is the compressed signal and the autocorrelation function (of $(t-T)$) of the original signal. The operator, $*$, is the convolution operator.

Now,if $\Phi_{ss}(t-T)$ is transmitted, then, clearly, for local stationarity, the clutter path impulse response must be approximately stationary over a time period of length $2/B$. However, because the clutter path is linear and time-invariant, we can perform the pulse compression at the receiver and so obtain precisely the same clutter function, $c(t)$, as if we had transmitted $\Phi_{ss}(t-T)$ instead of $s(t)$. The conditions at the output of the compression filter will now be:

$$R^c(f) = TG_{ss}(f)H_T(f) \tag{2.20}$$

and

$$G^c_{ii}(f) = TG_{nn}(f)G_{ss}(f) + T\left(G_{ss}(f)\right)^2 |H_c(f)|^2 . \tag{2.21}$$

where the superscript, c, denotes post-compression conditions.

The correlation reference is $q^c(t)$ whose transform is

$$Q^c(f) = \frac{H_T(f)}{G_{nn}(f) + G_{ss}(f)\,|H_c(f)|^2}.$$

The combined effect of signal compression and correlation with $q^c(t)$ is equivalent to correlation with the reference, $q(t)$, whose transform is given by:

$$Q(f) = \frac{S(f)H_T(f)}{G_{nn}(f) + G_{ss}(f)\,|H_c(f)|^2},$$

which is just the ML reference given by 2.15. It follows, therefore, that the appropriate local stationarity condition is given by:

$$\phi_{cc}(t_1,t_2) \approx \Phi_{cc}(t_1-t_2)\,\forall t_1,t_2 : t_1 - t_2 \leq 2/B. \tag{2.22}$$

§2.4 Performance Indicators

It is possible to predict the performance of a ranging system employing ML estimation. To do so we need to analyse its performance in three separate areas. The ranging system performance will depend on its ability to detect the target echo in the presence of the interference, to discriminate against interfering reflecting objects separated from the target in the transverse directions (i.e. at right angles to the beam axis) and to estimate the round-trip delay of the target echo. In analysing system performance in these three areas, we shall identify a number of system parameters which are indicators of system performance. (That is, performance in each of the three areas is directly, solely and monotonically dependent upon the value of the corresponding performance indicator if physical aspects of the system and its environment are fixed.) These indicators will be used as optimization criteria in the next chapter.

2.4.1 Detection Performance

If a ranging system is to perform any useful function at all it must be capable of identifying the target echo in the received waveform. Failure to do so will lead to gross errors as a result of ranging *false targets*. The probability of this happening is related to the value of a system parameter, $\Re$, known as the detection index [2.1].

In most ranging systems, target detection is an explicit function of the system achieved by comparing the gated LLF with a threshold. If the LLF within the gate exceeds the threshold then target detection is indicated. Otherwise it is not. The probability of the target not being detected depends monotonically on the signed difference between $\Re$ and the threshold. The threshold is set by the designer in such a way as to provide the best compromise between the probability of false target detection and the probability of not detecting the target. The value of the threshold therefore depends on the costs associated with those two events.

Now we have met $\Re$ before in equation 2.8 as the square of the peak-signal to rms-

interference ratio and we will find that it has significance in all aspects of performance. $\Re$ may be defined, equivalently, by:

$$\Re = \frac{E\{LL(\tau|x(t)) : r(t-\tau)present\}}{\sqrt{Var\{LL(\tau|x(t)) : r(t-\tau)notpresent\}}}. \tag{2.23}$$

However, $\Re$ has many other physical interpretations [2.1]. It is the value of the peak of the LLF. It is the mean squared value of the post-correlation interference and is also the value of the signal to interference power ratio at the output of the whitening filter (see Fig. 2.2) during the period when the signal is present.

It is shown in [2.1] that the probability of ranging a false target (when explicit target detection is not used) undergoes a rapid transition from very low to very high probability as $\Re$ falls below a value known as the detection threshold, $\Re_T$. Hence, the probability of false target detection and the probability of not detecting the target explicitly are both determined by the relationship between $\Re$ and some threshold value.

The parameter, $\Re$, also has significance in communication theory. To see this we shall take a minor detour. Correlation of the received waveform with $q(t)$, whose transform is specified in 2.11, is equivalent to filtering by convolution with an impulse response given by $q(-t)$. That is, the equivalent filter transfer function is:

$$H(f) = \frac{R^*(f)}{G_{ii}(f)}. \tag{2.24}$$

Filters with transfer functions related to the signal and interference as in 2.24 (apart from an arbitrary scaling) are known as *matched* filters and are widely used in communications. It is not surprising, therefore, that threshold phenomena in relation to $\Re$ are also observed in communications systems.

From any of the interpretations of $\Re$ given above it is possible to obtain:

$$\Re = 2T \int_0^\infty \frac{G_{ss}(f)\,|H_T(f)|^2}{G_{nn}(f) + G_{ss}(f)\,|H_c(f)|^2} df. \tag{2.25}$$

Woodward [2.1] obtains $\Re_T$ implicitly as:

$$\Re_T = 2\ln(W\Re_T\beta) - 2, \tag{2.26}$$

where W is range gate width as before and β^2 is the centroidal second moment of the post-whitening target echo energy spectrum. i.e.

$$\beta^2 = \frac{\int_0^\infty \frac{4\pi^2(f-f_0)^2 G_{ss}(f)|H_T(f)|^2}{G_{nn}(f)+G_{ss}(f)|H_c(f)|^2}df}{\int_0^\infty \frac{G_{ss}(f)|H_T(f)|^2}{G_{nn}(f)+G_{ss}(f)|H_c(f)|^2}df} \tag{2.27}$$

$$and f_0 = \frac{\int_0^\infty \frac{fG_{ss}(f)|H_T(f)|^2}{G_{nn}(f)+G_{ss}(f)|H_c(f)|^2}df}{\int_0^\infty \frac{G_{ss}(f)|H_T(f)|^2}{G_{nn}(f)+G_{ss}(f)|H_c(f)|^2}df}.$$

Here, f_0 is the centroid of the post-whitening target echo energy spectrum or, in other words, the "carrier frequency" of the target echo.

The parameter, β is an important measure of bandwidth which assumes fundamental significance in communications[2.1,2.2,2.10]. We will see shortly that both β and $\Re$ are of great importance in the analysis of range precision.

There remains another phenomenon to investigate in the area of detection performance. We saw in section 2.1 that the fine structure of the post-correlation signal can only contribute range information if the detection index satisfies the inequality given by 2.8. Repeating that here for convenience, we have:

$$(\Re)^{1/2} \gg \frac{f_0}{\beta}.$$

We shall refer to the ratio, $\frac{f_0^2}{\beta^2}$ as the carrier threshold.

In extreme cases, the envelope itself can exhibit a sidelobe structure about the main lobe so that it too may be considered to have a fine structure and an envelope. However, when we looked at the detection threshold, we tacitly assumed that the envelope consisted of a single main lobe and was zero away from the main lobe. This assumption was made by Woodward in deriving equation 2.26.

The existence of envelope sidelobes contributes ambiguity in that a sidelobe may be mistaken for the main lobe if the difference between their peak magnitudes is not sufficiently greater than the rms value of the interference. In situations, also, where the clutter is range-dependant, the existence of sidelobes may increase the rms interference near the peak of the main lobe. However, for reasons which will be discussed in chapter 3 we can avoid explicitly considering that difficulty.

However, no simple inequality such as 2.8 can be derived for application to this problem. Its analysis is considered in detail in chapter 3 and it will be seen that it does have repercussions on the design of signals.

2.4.2 Range Accuracy

The variance of the range estimate under the assumption of perfect target detection was first obtained, approximately, by Woodward [2.1]. His expression was obtained under the assumption, $\Re >> 1$, which is consistent with the assumption of perfect target detection. However, the expression is inaccurate if $\Re < 8$ even if we ignore the possibility of gross range errors due to false target detection. Woodward's expression is:

$$\sigma_\tau^2 = \frac{1}{\Re\beta^2}. \tag{2.28}$$

The expression, 2.28, has been shown to correspond to the Cramer-Rao lower bound on estimation performance [2.3,2.4]. An ***unbiased*** estimator that achieves this bound asymptotically (i.e. as $G_{ii}(f) \to 0$ and hence $\Re \to \infty$) is said to be ***efficient.*** It is also shown in [2.3,2.4] that the ML estimator of delay is unbiased which means that:

$$E\{\hat{\tau}\} = \tau. \tag{2.29}$$

Hence the ML range estimator is optimal in the sense that it can only be improved upon by the use of prior information. Since it is an unbiased estimator we need only concern

ourselves with the estimate variance. There are no sources of systematic error to take into account when analysing the precision of the estimator.

Woodward [2.1] obtained the expression, 2.28, as the approximate variance of the signal component of the posterior distribution under the assumption of uniform prior probability. In [2.2] it is obtained in similar fashion and also as the mean squared error in the peak of the complete posterior density as a result of fluctuations caused by the interference.

We see, then, that the parameter, σ_τ^2, in 2.28 has fundamental significance as an indicator of precision in range estimation. However, one may ask what the range variance would be if the carrier phase is reliable and 2.8 holds so that the LLF is given by 2.5. In this case, the range estimation problem is different because the carrier phase is no longer uninformative. In [2.2] the range variance for this case is derived as:

$$\Sigma_\tau^2 = \frac{1}{\Re\beta_0^2}, \tag{2.30}$$

where β_0 is the second moment of the post-whitening target echo energy spectrum with respect to zero frequency:

$$\beta_0^2 = \frac{\int_0^\infty \frac{4\pi^2 f^2 G_{ss}(f)|H_T(f)|^2}{G_{nn}(f)+G_{ss}(f)|H_c(f)|^2} df}{\int_0^\infty \frac{G_{ss}(f)|H_T(f)|^2}{G_{nn}(f)+G_{ss}(f)|H_c(f)|^2} df}. \tag{2.31}$$

For $\beta << f_0$ we have [2.4]:

$$\Sigma_\tau^2 \approx \frac{1}{\Re f_0^2}. \tag{2.32}$$

However we will not use this expression in this thesis as the condition for its validity is often not satisfied, particularly in acoustic applications.

We see from 2.30 and 2.28 that two different expressions can be obtained for the Cramer-Rao lower bound. Each bound can be approached assymptotically by the relevant estimators for which they are applicable, one of which uses the carrier phase

information and one of which does not. For the estimator that uses carrier phase information, 2.30 gives the performance bound but the estimator only approaches this bound when condition 2.8 holds. For the alternative estimator, 2.28 provides a performance bound that can be approached when $\Re \gg \Re_T$ and $\Re \geq 8$. This is a relaxed requirement as compared with condition 2.8.

We see then that these bounds based on the theory of Cramer and Rao are only useful over certain mutually exclusive regions of $\Re$. Between these regions and below them, exist regions where this theory provides no useful performance bounds.

In [2.16], Ziv and Zakai go some way toward overcoming this difficulty by presenting a new approach to the problem. They are able to obtain a general expression for a lower bound on performance. However a closed analytical form for such a bound on time delay estimation error has not been found[2.17]. As a result, this approach is not useful in the context of the present analysis. Accordingly, we consider independently the problems of detection, estimation without the use of carrier phase and estimation with the use of carrier phase.

Now, substituting 2.27 and 2.25 into 2.28, and 2.31 and 2.25 into 2.30 we obtain:

$$\sigma_\tau^2 = \frac{1}{8\pi^2 T \int_0^\infty \frac{(f-f_0)^2 G_{ss}(f)|H_T(f)|^2}{G_{nn}(f)+G_{ss}(f)|H_c(f)|^2} df} \tag{2.33}$$

and

$$\Sigma_\tau^2 = \frac{1}{8\pi^2 T \int_0^\infty \frac{f^2 G_{ss}(f)|H_T(f)|^2}{G_{nn}(f)+G_{ss}(f)|H_c(f)|^2} df}. \tag{2.34}$$

In most practical situations 2.33 is an appropriate indicator of range precision.

2.4.3 Transverse Resolution

It is very rare indeed for a ranging system to operate in an omnidirectional manner. Generally, the target subtends a relatively small angle at the transponder and it is necessary to direct the signal energy at the target from the transmitter and

to discriminate against interference from other directions at the receiver. In other situations it is necessary to estimate the bearing of a target as well as its range.

Sometimes, as in [1.1] the target is at relatively short range (i.e. not in the far field) and the transmitting and receiving apertures are focussed on the target.

In all these cases, the resolution of the system in directions at right angles to the direction of propagation is an important consideration. We expect this resolution to be fundamentally diffraction limited but there is no well established expression for the transverse resolution of a system of wide relative bandwidth that we can use as a performance indicator.

Now, one way of expressing the transverse resolution of an unfocussed system is by means of its *resolution angle.* The resolution angle, $\triangle\theta$, of such a system is the smallest angle (subtended at the aperture) which can be resolved. Another commonly used parameter for electromagnetic radiating systems is known as *antenna gain.* We shall now derive suitable expressions for these parameters in the context of wideband active ranging systems.

Antenna gain is defined by the formula[2.11]:

$$G = \frac{4\pi r^2 S_r}{E_e}, \tag{2.35}$$

where S_r is received signal energy per unit area at a point in the favoured transmitting direction in the far field at distance, r, from the antenna, and E_e is the signal energy supplied to the aperture. We may interpret antenna gain as the ratio of the energy transmitted by a hypothetical isotropic radiator to that actually transmitted if both radiating systems are to achieve the same energy density, S_r, defined above.

In [2.11], the gain of a wideband antenna is calculated in terms of the transmitted signal energy spectrum under the assumption that the aperture field is a separable

function of space and time and the aperture is planar. i.e.

$$E_{0X}(x,y,t) = E_{0X}(x,y)s(t), \tag{2.36}$$

where E_{0X} is the field in the aperture (Z=0) and is linearly polarized (in the x direction in this example). By using far-field plane-wave angular-spectrum theory the gain of such an antenna is obtained in [2.11] as:

$$G = \frac{4\pi\sigma_e\beta_1^2}{c^2}, \tag{2.37}$$

where σ_e is the effective area of the aperture which is a function of $E_{0X}(x,y)$ and is independent of $s(t)$, c is the velocity of propagation and:

$$\beta_1^2 = \frac{\int_{-\infty}^{+\infty} f^2 |S(f)|^2 df}{\int_{-\infty}^{+\infty} |S(f)|^2 df}. \tag{2.38}$$

We recognize β_1 as the centroidal or "carrier" frequency of the transmitted signal.

Now, in [1.1], it is pointed out that the calculation of effective wideband field patterns in the analysis of the performance of active ranging systems should take account of filtering in the transmission path and the receiver. Wideband acoustic field patterns are obtained numerically in [1.1] by treating individual frequency components separately. The effective contribution of each component is assumed to be in proportion to the post-correlation target echo energy density at that frequency. The total effective field intensity is calculated by summing over the contributions of the individual frequencies. In the continuous case this summation is an integration with respect to frequency.

In order to combine the philosophy in [1.1] with the approach in [2.11] to obtain an expression for effective antenna gain, we will examine the derivation of 2.37 in the hope of generalising it so that it takes into account the effects of the transmission path and the receiver filtering. The interpretation of effective antenna gain, analogous to that given above for antenna gain is as the ratio of the energy transmitted by a hypothetical isotropic radiator to that actually transmitted if both radiating systems are to achieve the same detection index at the receiver.

As a result of these considerations, we see that, to obtain an expression for effective antenna gain we should substitute the post-whitening target echo energy for the transmitted signal energy whenever the field pattern is obtained in the derivation in [2.11].

Now, in the derivation of 2.37 given in [2.11], the denominator of 2.38 is obtained directly as the denominator of 2.35. Hence,

$$G = \frac{8\pi\sigma_e}{c^2 P_s} \int_0^\infty f^2 G_{ss}(f) df, \tag{2.39}$$

where $G_{ss}(f)$ is the signal power spectrum and hence, under our usual assumption of a fixed duration constant envelope signal we can simply replace the denominators of 2.35 and 2.38 with

$$E_s = TP_s, \tag{2.40}$$

where P_s is the constant (during signal transmission) power of the transmitted signal and T is its duration.

To obtain the expression for effective antenna gain defined and interpreted above, it is only necessary to replace the ratio of $G_{ss}(f)$ to P_s in 2.39 (which has the units of time) with the spectral density of the post-correlation signal-to-interference ratio (which also has the units of time). Thus we obtain:

$$G_{eff} = \frac{8\pi T\sigma_e}{c^2} \int_0^\infty \frac{f^2 G_{ss}(f) \left|H_T(f)\right|^2}{G_{nn}(f) + G_{ss}(f) \left|H_c(f)\right|^2} df. \tag{2.41}$$

We will now derive an expression for the resolution angle of an active bearing estimator in which a similar dependence of transverse resolution on the signal spectrum will be found.

Consider the diagram of Fig. 2.4 in which a plane wave signal arrives at a linear array of sensors or antennas from a direction at angle, θ, from the broadside direction of the array. The signal arrives at each sensor with a delay, $\Delta\tau$, between sensors which

Figure 2.4 **Bearing Estimation**

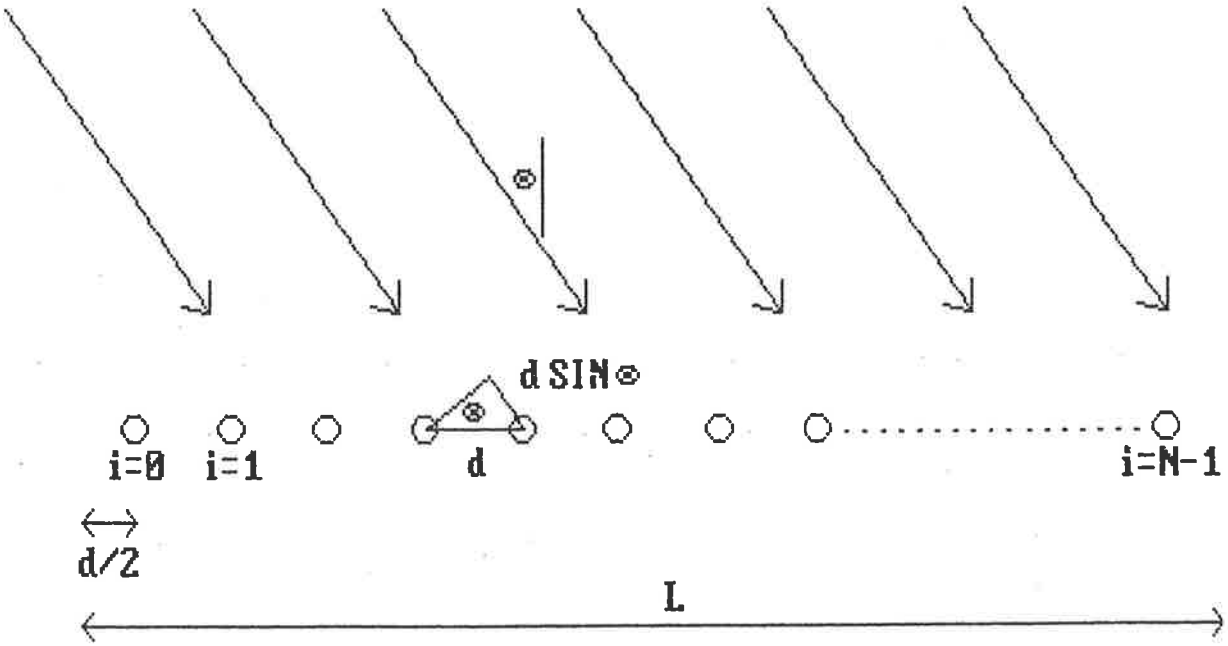

is related to the angle, θ, by the expression:

$$\begin{aligned} \tau_i - \tau_{i-1} &= \Delta\tau \\ &= d/c \sin\theta, \end{aligned} \tag{2.42}$$

where τ_i is the absolute round trip delay to sensor i and d is the sensor separation while c is the velocity of propagation.

If there are N sensors, then

$$d = L/N, \tag{2.43}$$

which defines the array length, L.

Now, there exists a large body of literature dealing with the problem of passive bearing estimation in which the angle, θ is estimated by estimating the delay, $\Delta\tau$, between adjacent sensors in the array when the interference is assumed to be uncorrelated from sensor to sensor [2.12,2.13,2.14]. In the case of passive estimation, no noiseless reference signal is available and the incremental delay between two sensors is obtained by picking the peak of a spectrally weighted cross-correlation of the waveforms from the two sensors. For the ML [2.12] bearing estimator the weighting takes account of the coherence between the two waveforms. In those parts of the spectrum where the coherence is large, there is less uncertainty about the signal. (If the coherence function is 1 then the noise power spectral density at both sensors is zero. If the coherence is zero then the signal power spectral density is zero.) Hence more emphasis is given to spectral regions where the coherence is large and less to those where it is small.

In the case of *active* bearing estimation, however, the concept of coherence between the sensor waveforms is not of direct relevance. This is because the form of the received signal is known in advance. We will also assume that we have a transmission path model for transmission from the transmitter to each sensor. If this model varies from sensor to sensor then it must be characterized for each sensor separately.

The reason for undertaking this analysis here is to underline the fundamental significance of the integral in 2.41 by deriving an expression for resolution angle involving the same integral.

The hypothesised system is one in which a signal is transmitted with a broad beam and an echo is received from a target at each of several sensors, each of which exhibits a broad angular response. The bearing of the target can then be estimated provided the target echo can be reliably detected at each sensor. As when considering range resolution, we assume operation well above the detection threshold.

The approach we will take is to obtain the approximate posterior densities for the absolute round trip delay probabilities at the N sensors by again assuming that the prior probability densities are uniform. This is the usual ML assumption and it incorporates the assumption that the prior probability of the delay difference, $\Delta\tau$, is also uniform. We have:

$$p(\tau_i \,|x_i(t)) \approx kp(x_i(t) \,|\tau_i)\,, \tag{2.44}$$

where the subscript, i, associates the variable with the ith sensor.

Although the carrier phase may be unreliable, the log of the likelihood function in 2.44 is given by 2.5 because any ambiguity in the phase will be removed in the next step. The variance of the probability in 2.44 is therefore given by 2.30. The posterior probability density, $p(\tau_{i-1} \,|x_{i-1}(t))$, is obtained in a similar fashion with the same variance if the two transmission paths are identical (statistically) apart from a delay.

Now we undertake the step in which any ambiguity in the carrier phase will be removed. In order to render the problem mathematically tractable, we have to impose a further restriction. We make the usual assumption[2.12,2.13,2.14] that the interference is independent from sensor to sensor. We also recognise that the delay difference, $\Delta\tau$,

is constrained to lie in the range from $-d/c$ to d/c. i.e.

$$-d/c \leq \Delta\tau \leq d/c$$

and all values within the range are equiprobable.

Hence, provided we restrict our attention to the allowable range of $\Delta\tau$, then $x_i(t)$ contributes no information as to the value of τ_{i-1} and $x_{i-1}(t)$ contributes no information as to the value of τ_i and we may proceed as though τ_i and τ_{i-1} are statistically independent. We have, therefore:

$$\begin{aligned} p\left(\tau_i - \tau_{i-1} | x_i(t), x_{i-1}(t)\right) &= p\left(\tau_i | x_i(t)\right) * p\left(-\tau_{i-1} | x_{i-1}(t)\right) \\ &= k^2 p\left(x_i(t) | \tau_i\right) * p\left(x_{i-1}(t) | - \tau_{i-1}\right) \end{aligned} \tag{2.45}$$

where k is defined in 2.44.

An interpretation of 2.45 is given later in this section where it is shown that the ML estimator of bearing employs established beamforming and beamsteering techniques to locate the target. This is consistent with the analysis given in [2.15].

Now consider Fig. 2.5 which illustrates the relationships between the deterministic components of the probability density functions in 2.45. The important feature to notice is that, because any carrier phase error is observed at both sensors, it is cancelled in 2.45. The deterministic component of the function on the left of 2.45 is a true autocorrelation function (but shifted along the delay axis) The central peak of its fine structure therefore occurs coincidentally with the peak of its envelope.

The carrier phase information is therefore useful provided that ambiguities arising from the presence of interference do not occur. Bearing estimation, however, is unlike range estimation in that these ambiguities can be totally eliminated by ensuring that the sidelobes of the fine structure lie outside the region of interest. The criterion is that the adjacent peaks of the fine structure should be separated by a delay greater than that possible between two sensors. In other words, the sensors must be less than one

Figure 2.5 *Probability Densities for Active Bearing Estimation*

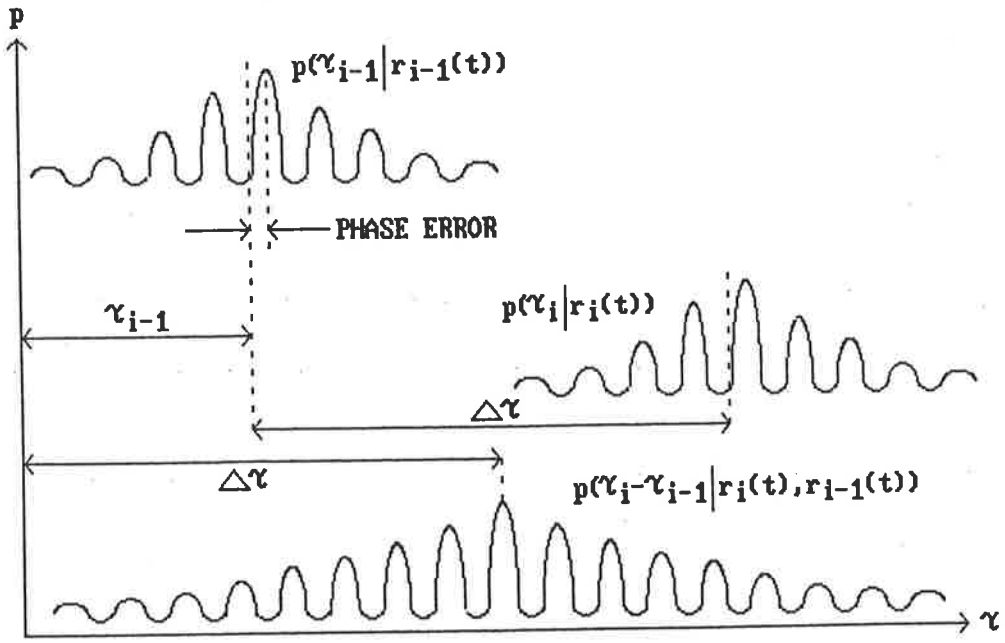

wavelength apart at the carrier frequency which is shown in [2.1] to be f_0 in 2.27. Thus we have:

$$L/N < c/f_0. \tag{2.46}$$

Equation 2.46 is simply the usual criterion for eliminating grating lobes by ensuring that they lie outside the visible region. However, here we see that, for wideband systems, the centroidal frequency, f_0, is the relevant frequency at which the criterion should be met and not, as might be expected, the highest frequency in the band.

Now we wish to know the variance of the approximate posterior density on the left of 2.45. By a well known application of the moment properties of the convolution operator, we have:

$$\sigma^2_{\Delta\tau_i} = \sigma^2_{\tau_i} + \sigma^2_{\tau_{i-1}} = 2\Sigma^2_\tau. \tag{2.47}$$

However, we can obtain $\frac{N(N-1)}{2}$ independent estimates of $\Delta\tau$. Hence:

$$\Delta\hat{\tau} = \frac{2}{N(N-1)} \sum_{i=1}^{N(N-1)/2} (\Delta\hat{\tau})_i, \tag{2.48}$$

and

$$\sigma^2_{\Delta\tau} = \frac{4}{N(N-1)}\Sigma^2_\tau. \tag{2.49}$$

ow, from 2.42 and 2.43 we can obtain:

$$\frac{d\Delta\tau}{d\theta} = \frac{L}{Nc}\cos\theta, \tag{2.50}$$

and if 2.50 is assumed to be approximately constant over small regions of θ, then we can make an approximation as illustrated in Fig. 2.6. We see that:

$$(\Delta\theta)^2 \approx \frac{\sigma^2_{\Delta\tau}}{(d\Delta\tau/d\theta)^2}. \tag{2.51}$$

By substitution from 2.50, 2.49, 2.30, 2.31 and 2.25 we obtain:

$$(\Delta\theta)^2 = \frac{\left(\frac{N}{N-1}\right)c^2}{2\pi^2 T L^2 \cos^2\theta \int_0^\infty \frac{f^2 G_{ss}(f)|H_T(f)|^2}{G_{nn}(f)+G_{ss}(f)|H_c(f)|^2} df}. \tag{2.52}$$

Figure 2.6 *Approximate Derivation of Resolution Angle*

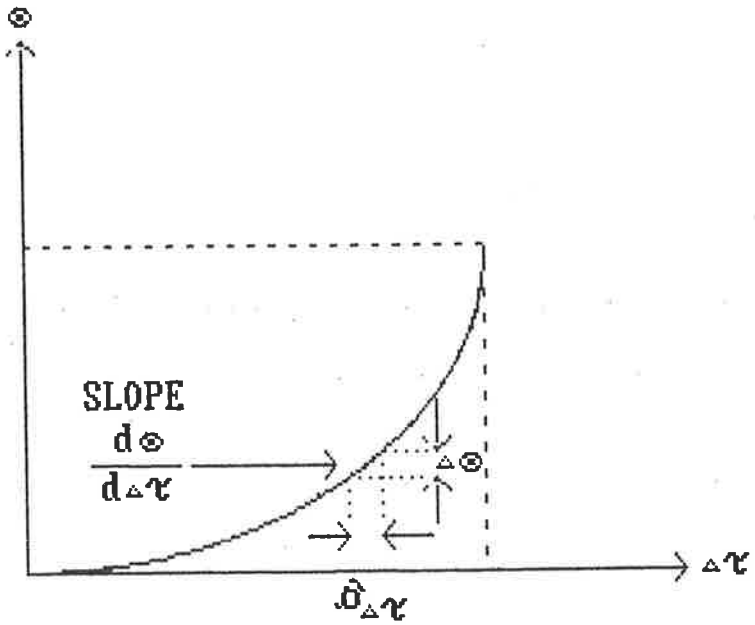

For the continuous case ($N \rightarrow \infty$) in the broadside direction ($\theta = 0$) the reciprocal of 2.51 becomes:

$$\frac{1}{(\triangle\theta)^2} = \frac{2\pi^2 T L^2}{c^2} \int_0^\infty \frac{f^2 G_{ss}(f) \left|H_T(f)\right|^2}{G_{nn}(f) + G_{ss}(f) \left|H_c(f)\right|^2} df. \tag{2.53}$$

Apart from constant factors, we see that 2.41 and 2.53 are identical. The transverse resolution in both cases depends on $G_{ss}(f)$ through the same integral. Now, substituting from 2.53 into 2.41, we obtain:

$$G_{eff} = \frac{4\sigma_e}{\pi L^2} \cdot \frac{1}{(\triangle\theta)^2} \tag{2.54}$$

We recognise $\frac{\pi L^2}{4}$ as the area of a circular aperture of diameter L and thus, if we are considering plane wave arrival from the broadside direction, this is the effective area of the aperture, σ_e. Hence:

$$G_{eff} = \frac{1}{(\triangle\theta)^2}, \tag{2.55}$$

for a circular aperture.

We shall see in the next section that GML estimation of bearing is simply a process of scanning a beam through all angles in the bearing gate or "sector" and choosing that angle corresponding to the greatest observed response. Therefore, the resolution angle is a measure of the effective angular beamwidth of the system. Hence, we can complete our study of transverse resolution by showing that the relationship given in 2.55 can be approximately derived by simple geometrical analysis.

Consider Fig. 2.7 in which a conical beam is illustrated. The centre of the circular transmitting aperture is located at the point of the cone and all the transmitted signal energy, E_T, is transmitted through the cone. (This is a convenient approximation to justify which we need to make the cone subtend a solid angle of say $4\triangle\theta$. This corresponds to ± 2 standard deviations of the bearing estimate.) At distance, r, from

Figure 2.7 *Effective Gain and Resolution Angle*

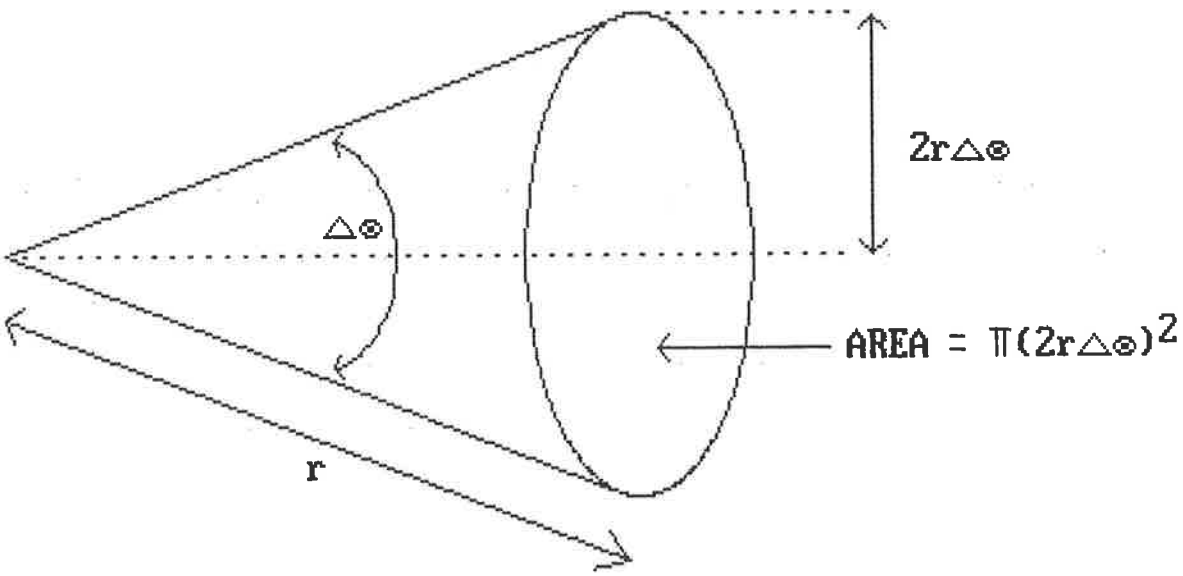

the transmitting aperture, the radius of the cone base is given by $2r\triangle\theta$. Hence, the area of the cone base is $\pi(2r\triangle\theta)^2$. Thus we have:

$$S_r = \frac{E_s}{4\pi r^2(\triangle\theta)^2}$$

and

$$G_{eff} = \frac{1}{(\triangle\theta)^2}.$$

We see then, that equations 2.41 and 2.53 provide consistent measures of transverse resolution although they were derived by totally independent analyses of quite different physical problems. We are entitled to conclude, therefore, that the integral in 2.41 and 2.53 is a fundamental factor in transverse resolution performance.

We define the *transverse resolution index* (TRI) as the gain density of a signal or the effective gain per effective unit area of the aperture. Thus, from 2.41, we have:

$$TRI = \frac{8\pi T}{c^2}\int_0^\infty \frac{f^2 G_{ss}(f)\,|H_T(f)|^2}{\left(G_{nn}(f) + G_R(f)\,|H_{cR}(f)|^2\right)}df. \qquad (2.56)$$

Henceforth, we shall use TRI as a transverse resolution performance indicator in the comparison of signals.

§2.5 The ML Estimator of Bearing

It is interesting to interpret the form of the estimator that chooses $\Delta\tau$ by picking the peak of the probability density on the left of 2.45. Substituting from 2.5, we get:

$$p\left(\Delta\tau \,|x_i(t), x_{i-1}(t)\right) = k' \int_{-\infty}^{+\infty} e^{y_i(\tau)} e^{y_{i-1}(\tau+\Delta\tau)} d\tau, \tag{2.57}$$

where k' is some uninformative constant and

$$y_i(\tau) = \int_{-\infty}^{+\infty} x_i(t) q_i(t,\tau) dt.$$

i.e.

$$p\left(\Delta\tau \,|x_i(t), x_{i-1}(t)\right) = k' \int_{-\infty}^{+\infty} e^{[y_i(\tau)+y_{i-1}(\tau+\Delta\tau)]} d\tau. \tag{2.58}$$

In 2.58 the target echo delay, τ, is treated as an uninformative parameter which is averaged out. This averaging gives rise to the integral in 2.58. The function of range (or echo delay) over which we average is obtained by a three step process. The first step is an optimal filtering of the signal from each sensor as described in section 2.1. The second step is a conventional beamforming process in which signals are delayed and added so as to form a beam in the hypothesized target direction. (The delay between adjacent sensors is $\Delta\tau$.) The third step is a reversible, non-linear distortion of the signal by exponentiation which is necessary for the averaging process to be valid.

The estimate of relative delay, $\Delta\hat{\tau}$, is obtained by choosing the hypothesis, $\Delta\tau$, yielding the largest value in 2.58.

If we wish to estimate bearing and range simultaneously, we do not average out the range information as in 2.58. Instead we pick the peak of the two-dimensional LLF given by:

$$ln p\left(x_i(t), x_{i-1}(t) \,|\tau, \Delta\tau\right) = y_i(\tau) + y_{i-1}(\tau + \Delta\tau). \tag{2.59}$$

We see from 2.59 that conventional beamforming again yields an ML estimate

of bearing when the beam is swept over all angles and the peak in range and bearing is picked. A GML estimate is obtained if a restricted range of angles is swept.

§2.6 Summary and Discussion

In sections 2.1 and 2.2 the problem of ML estimation of round trip delay for range estimation was reviewed. It was discovered that for most cases of practical interest the LLF of delay is given by equations 2.11 and 2.12. However in special cases where the fine structure of the signal is known to carry reliable information and the inequality, 2.8 is satisfied, the appropriate form of the likelihood function is given by 2.5 and 2.11.

A transmission path model, illustrated in Fig. 2.3 is presented in section 2.2. The main restrictions of the model relate to two assumptions. The first of these is a weak scattering assumption in which the target path is assumed to be independent of statistical variations in the clutter path. The second is that there is no relative motion between target, scatterers, transmitter or receiver.

In section 2.3 the stationarity condition necessary for equation 2.11 to be valid is examined. A new criterion for local stationarity is derived in terms of the bandwidth of the transmitted signal rather than its duration. That criterion is given in equation 2.22.

Three system parameters are shown to be of fundamental significance as indicators of performance in section 2.4. The first of these indicates the detectability of the received target echo and is given by equation 2.25. The second indicates the precision with which the target may be localised in range and is given by equation 2.33. The third indicates the transverse resolution of the system and is given by 2.56. Other quantities of interest are given by 2.26 (the detection threshold) and 2.34 (delay estimate variance when carrier phase is used).

The derivation of the third of these parameters in section 2.4 represents a fundamentally new approach to the analysis of transverse resolution. It allows the dependence of the transverse resolution performance of wideband systems on the signal spectrum to be evaluated. The evaluation takes account of interference colouration as well as signal

spectral shaping.

Both the TRI and the detection index are of interest in the analysis and design of communications systems as well as ranging systems. Furthermore, the transmission path model employed in this thesis is well suited to communications applications where the clutter would represent multi-path interference.

Because of the applicability of many of the ideas presented in this chapter to a broader field of application than just active ranging, the results of chapters 3, 4 and 5 should also be regarded as having a broader context.

3. SIGNAL OPTIMIZATION

§3.0 Optimization Criteria

3.0.1 Ambiguity Functions

In chapter 2., a transmission path model was adopted that ignores relative motion between target, transmitter, receiver and scatterers. In practice, this restriction means that all Doppler effects are assumed to be negligible. By *Doppler effect*, I mean the temporal compressions and expansions of echoes that arise as a direct result of such relative motion. If such effects are observed in the frequency domain then they manifest themselves as corresponding frequency expansions and compressions with respect to zero frequency. For narrow band echoes this frequency domain effect can be closely approximated by a frequency shift.

Since most of the existing literature relating to signal optimization for target localization is concerned with Radar or Sonar applications it generally relates to situations where Doppler shifts are not negligible. Initially we shall look at approaches to signal optimization in this broader context before confining our attention to the more restricted class of problems where Doppler effects are negligible.

A large proportion of the literature in this area deals with optimization of the range resolution of a system. The range resolution of a system is its ability to distinguish between multiple targets that are closely spaced in range.

When we considered range accuracy in chapter 2, we did not take into account the possible existence of multiple targets and therefore our range variance indicator is

not also an indicator of range resolution. In the general case, no such indicator has ever been devised and most authors since Woodward [2.1] have studied range resolution in terms of Woodward's *ambiguity function.*

In general, the ambiguity function for two signals differing only in the parameters, $\vec{\theta}$, is [3.1]:

$$\chi\left(\vec{\theta}_1;\vec{\theta}_2\right) = \int_{-\infty}^{+\infty} F\left(t;\vec{\theta}_1\right) F^*\left(t;\vec{\theta}_2\right) dt \tag{3.1}$$

for a narrowband signal, F, with the customary normalization:

$$\chi\left(\vec{\theta};\vec{\theta}\right) = \int_{-\infty}^{+\infty} \left|F\left(t;\vec{\theta}\right)\right|^2 dt = 1. \tag{3.2}$$

For Radar and Sonar, $\vec{\theta} = (\tau, f)^T$, where τ is arrival time and f is Doppler shift. Thus we have:

$$\begin{aligned}\chi\left(-\tau/2,-f/2;\tau/2,f/2\right) &= \int_{-\infty}^{+\infty} r\left(t-\tau/2\right) r\left(t+\tau/2\right) e^{-j2\pi ft}\, dt \\ &= \chi(\tau, f)\end{aligned} \tag{3.3}$$

where r is the target echo.

The central peak of this ambiguity function occurs at the origin and its spread in the delay-Doppler plane is a measure of the "resolvability" of target echoes. It is a fundamental measure of their "resolvability" or "distinguishability" that is independent of the form of the range estimator.

The ambiguity function, 3.3, has a similarly fundamental role to play in relation to clutter performance because clutter must be distinguished from the target signal. In particular, the existence of sidelobes in the ambiguity function may lead to false target detection because target sidelobes may occur coincidentally with clutter main lobes or because the target main lobe may be obscured by clutter sidelobes.

When the interference is coloured we will want to provide spectral emphasis of the ambiguity function, whose role is still fundamental and makes no assumption

about the form of the estimator. However, the problem of what spectral emphasis to use is similar to that encountered in deriving the optimal estimator. Therefore it is not surprising that the ambiguity function generally employed in evaluating the performance of narrowband systems is the *cross-ambiguity* function of the target echo, $r(t)$, with the ML correlation reference, $q(t)$:

$$\chi_{rq}(\tau, f) = \int_{-\infty}^{+\infty} r\,(t - \tau/2)\, q\,(t + \tau/2)\, e^{-j2\pi f t}\, dt. \tag{3.4}$$

Ambiguity functions for wideband signals are difficult to define because echoes from moving scatterers occur with spectral compression or expansion with respect to zero frequency and not just a frequency shift. As a result, the ambiguity function depends on the mean velocity as well as on the differences in arrival times and velocities of the two echoes being compared in the correlation. It is useful, also, to use analytic signals in such definitions.

One such definition is [3.2]:

$$\chi(\tau, \alpha, A) = \left(\frac{1 - A + \alpha}{1 - A}\right)^{1/2} \int_{-\infty}^{+\infty} w(t) w^* \left(\left\{1 - \left[\frac{\alpha}{1 - A}\right]\right\} t + (1 - A + \alpha)\tau\right) dt \tag{3.5}$$

where α is incremental fractional velocity, A is mean fractional velocity, $w(t) = r(t) + jv(t)$ and $v(t)$ is the Hilbert transform of $r(t)$.

For the cross-ambiguity function we could take $y(t) = q(t) + jp(t)$, where $p(t)$ is the Hilbert transform of $q(t)$ and:

$$\chi_{wy}(\tau, \alpha, A) = \left(\frac{1 - A + \alpha}{1 - A}\right)^{1/2} \int_{-\infty}^{+\infty} w(t) y^* \left(\left\{1 - \left[\frac{\alpha}{1 - A}\right]\right\} t + (1 - A + \alpha)\tau\right) dt \tag{3.6}$$

Other definitions have been used for wideband systems but do not illustrate explicitly the dependence on the mean fractional velocity, A.

Generally, it is the magnitude of the ambiguity function that is of interest and often $|\chi|$ is referred to as the ambiguity function.

3.0.2 Clutter Rejection

An important system performance parameter is the signal-to-interference ratio (SIR) at the correlator output and a common criterion for signal optimization is to maximize that parameter[3.3,3.4]. Another common criterion is maximum signal-to-clutter ratio (SCR) at the correlator output[3.6]. Others include maximum detection index[2.7,2.6], maximum correlation processing gain[3.5] and minimum effective ambiguity volume[3.2]. The detection index was defined in subsection **2.4.1.** Correlation processing gain is the gain in signal-to-interference ratio resulting from correlation of the received waveform with the optimal reference, $q(t)$. When the true **ML** filter is being used, the SIR and the detection index are the same. However, if the filter is constrained in some way, this may not be the case [3.3,3.4] and this is why those two criteria have been included separately above.

In this sub-section I will review the standard approach to maximizing SIR or SCR. Usually, in the literature, the received signal is assumed to be of the form, $r(t) = As(t)$, where A is a complex constant while the clutter is characterized by its autocovariance function:

$$\begin{aligned} E\left\{c(t)c^*(t')\right\} &= k_c(t,t') \\ &= \int\int \xi(\tau,f)s(t-\tau)s^*(t'-\tau)e^{j2\pi f(t-t')}d\tau df \end{aligned} \tag{3.7}$$

The function, $\xi(\tau, f)$ represents the scattering density in the range-Doppler plane. The interpretation of this function is most easily understood for a field of discrete scatterers[3.4]:

$$\xi(\tau,f) = \sum_{i,k} \xi_{ik}\delta(\tau-\tau_i)\delta(f-f_k) \tag{3.8}$$

where $\delta(.)$ is the unit impulse function and ξ_{ik} is the Radar cross-section of the $(i,k)_{th}$ scatterer located at (τ_i, f_k) in the range-Doppler plane.

The noise is usually assumed to be white and normal with single-sided power spectral density, $2N_0$.

At the correlator output we thus have:

$$P_s = \left| \int As(t)q^*(t)dt \right|^2 \tag{3.9}$$

$$P_n = 2N_0 \int |q(t)|^2 dt \tag{3.10}$$

$$P_c = 1/2 \int \int q^*(t)k_c(t,t')q(t')dtdt' \tag{3.11}$$

where P_s, P_n and P_c are peak signal power, mean noise power and mean clutter power, respectively.

If $q(t)$ is normalized such that $\int |q(t)|^2 dt = 1$, it can be readily seen from 3.10 that the output noise power is independent of the choice of signal while, from 3.11, the output clutter power depends on $s(t)$ in a complicated way. This dependence can be simplified conceptually by substituting for k_c in 3.11 using 3.7 and 3.4 to obtain:

$$P_c = 1/2 \int \int \xi(\tau, f) \, |\chi_{sq}(\tau, f)|^2 d\tau df \tag{3.12}$$

This is simply the volume integral of the product of the scattering density and the squared magnitude of the cross-ambiguity function. This integral product is often illustrated pictorially as the intersection of the regions contained within the contours of the two-dimensional functions, $\xi(\tau, f)$ and $|\chi_{sq}(\tau, f)|^2$, as in Fig. 3.1.

Since P_s is simply the peak of the ambiguity function squared magnitude, the aim of signal optimization for maximum SCR is to choose $s(t)$ such that the ambiguity given by[2.1]

$$\frac{\int \int |\chi_{sq}(\tau, f)|^2 d\tau df}{P_s} = 1$$

is distributed away from areas of high scattering density in the range-Doppler plane.

When SIR is to be maximized, the value of the peak of the ambiguity function becomes important. Ambiguity is redistributed in such a way that a compromise is reached between maximizing clutter rejection and maximizing the peak signal power at the correlator output.

Figure 3.1 *The Clutter Integral*

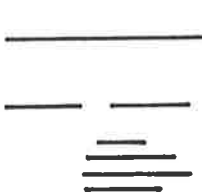

6dB contour of $|\chi_{eq}(\tau, f)|^2$.

6dB contour of $\xi(\tau, f)$.

Contour intersection.

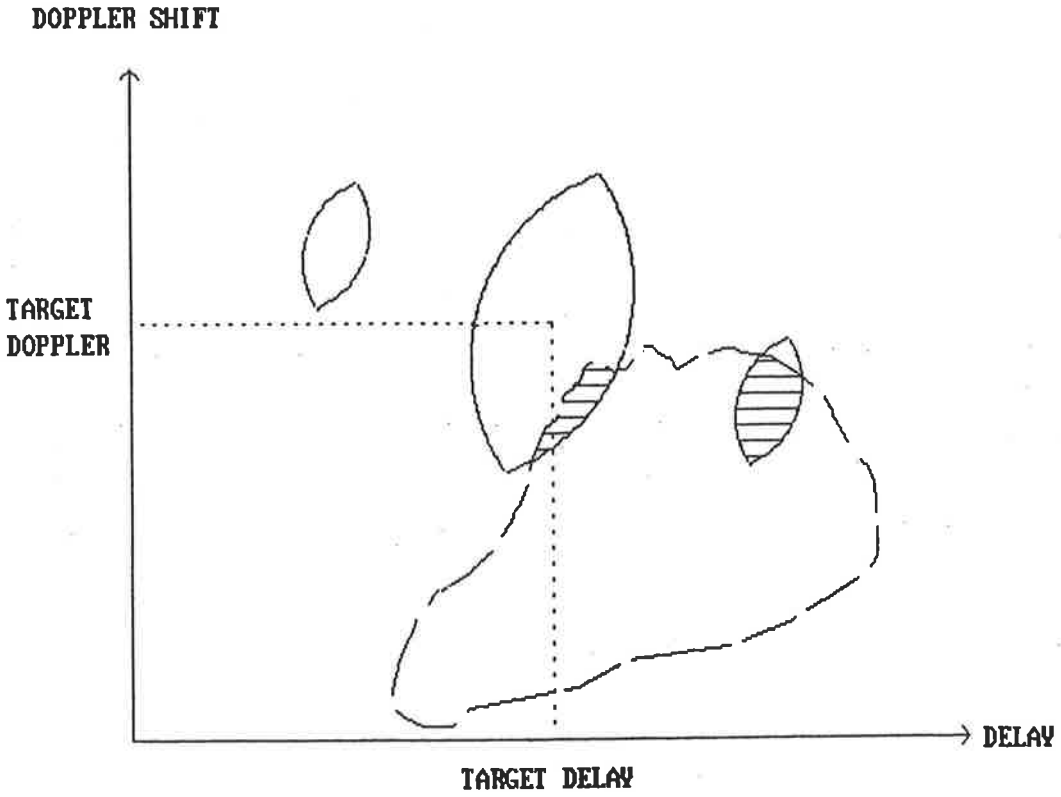

Optimization with respect to either of these criteria is usually undertaken by means of a numerical algorithm or with the aid of diagrams such as Fig. 3.1.

3.0.3 Minimizing Effective Ambiguity Volume

As stated in the previous section, the total ambiguity volume is equal to unity. However,the volume over a finite area of the range-Doppler plane can be minimized by choice of $s(t)$. Bates considers this for wideband signals in [3.2]. Because wideband ambiguity functions are functions of delay and incremental fractional velocity, rather than of delay and Doppler shift, he points out that the integral of the squared modulus of the ambiguity function has the units of time. In order to obtain a unitless value for ambiguity volume, Bates, following Rihaczek, multiplies that integral by the first moment of the energy spectrum of the signal.

This procedure is reasonable since, for wideband signals, the "carrier frequency" may be defined as the centroid of the energy spectrum and, for narrowband signals, Doppler shift is equal to the product of the ratio of the relative velocity to the velocity of propagation and carrier frequency. Hence, the above wideband definition is made conceptually, and indeed numerically consistent with the narrowband definition.

With this definition for ambiguity volume, Bates shows, using 3.5, that the ambiguity volume over a finite range of fractional velocities is monotonically decreasing with signal bandwidth. This volume is therefore minimized by using a signal with a flat spectrum.

3.0.4 Maximizing Detection Index

In chapter 2 we found that the detection index, $\Re$, is an important indicator of detection performance and when the optimal ML filter is employed, $\Re$ corresponds to the SIR. Hence the optimal trade-off between clutter rejection and maximization of received signal energy is found by maximizing $\Re$.

In [2.7], Kooij finds an expression for $G_{ss}(f)$ that maximizes $\Re$ in equation 2.25. The signal power spectrum is given by:

$$G_{ss}(f) = \frac{k_d |H_T(f)| N_0^{1/2} - N_0}{|H_c(f)|^2} \tag{3.13}$$

where k_d is a constant chosen to meet the energy constraint:

$$\int_{-\infty}^{+\infty} G_{ss}(f)df = \frac{E_s}{T_s} = P_s. \tag{3.14}$$

Of course, the same restrictions apply to this result as were imposed in deriving 2.25. In particular, Doppler effects must be negligible and the interference must be locally stationary with range. In addition, the noise was assumed white.

Numerical solutions for particular classes of signals have been found for the case where Doppler effects are allowed[2.6]. However closed form solutions have not been reported.

The author has identified two difficulties in the application of 3.13. The first is that the white noise assumption can be quite unrealistic while the second and more important problem is that 3.13 can yield negative power spectral densities. These two problems are addressed in sub-section 3.1.1.

3.0.5 The Advantages of Multiple Criteria

As discussed in chapter 2, there are many current and emerging applications of target localization techniques for which the restriction to negligible Doppler effects is quite realistic. It is to those applications that this thesis is chiefly addressed. Hence, the approach of Kooij described in the previous sub-section is highly relevant.

However, apart from the difficulties with the application of equation 3.13 which were outlined in the previous sub-section, maximization of detection index as a criterion suffers from other shortcomings. The signal that maximizes the detection index may

only be optimal in a very narrow sense. It is truly optimal only at low signal energies where the detection margin is small and it is essential to maintain as large a margin as possible. Even then, it is not obvious that maximizing the detection index results in maximum detection margin.

The rest of this chapter will be devoted to the development of a theory of optimality in which the performance indicators derived in chapter 2 (detection index, range estimate variance and transverse resolution indicator) are all employed as optimization criteria. Initially we shall look at signal optimization with respect to these simple criteria and later, in sections 3.3 and 3.4, a strategy will be developed for employing all three of the simple criteria simultaneously in computing an optimal signal spectrum.

§3.1 Optimization With Respect to Simple Criteria

3.1.1 Maximizing Detection Index

The expression for the detection index was derived in chapter 2. Repeating 2.25, we have:

$$\Re = 2T \int_0^\infty \frac{G_{ss}(f)\,|H_T(f)|^2}{G_{nn}(f) + G_{ss}(f)\,|H_c(f)|^2} df. \tag{3.14}$$

In this section, we shall derive the signal spectrum that maximizes $\Re$ subject to the energy constraint:

$$\int_0^\infty G_{ss}(f)df = \frac{E_s}{2T} = P_s/2. \tag{3.15}$$

The solution derived by Kooij for the case where the noise is white can be extended to the case of non-white noise by the simple device of inserting a noise-whitening filter in the transmission path model. This was done by the author in [1.1].

However, difficulties were encountered by the author in relation to the form of the solution.These were discussed in the previous section. In addition, we may wish to restrict attention to a limited band of frequencies.Therefore, a generalized solution will be stated here in the form of a theorem which is proven in appendix 3A.

Theorem 1. *Let $G_{ss}(f) = 0 \forall f \notin [f_1, f_2]$. Then the signal power spectral density, $G_{ss}(f)$, that maximizes 3.14 subject to 3.15 is given by:*

$$G_{ss}(f) = \begin{cases} \frac{k_d |H_T(f)| (G_{nn}(f))^{1/2} - G_{nn}(f)}{|H_c(f)|^2} & \forall f \in R_1 \\ 0 & \forall f \in R_0 \end{cases} \tag{3.16}$$

where

$$\begin{aligned} R_1 &= \left\{ f : k_d\,|H_T(f)| > (G_{nn}(f))^{1/2} \right\} \subset R_T, \\ R_0 &= \bar{R}_1, \\ R_T &= [f_1, f_2], \end{aligned} \tag{3.17}$$

and k_d is a non-negative real constant chosen to satisfy the equation:

$$\int_{R_1} \frac{k_d\,|H_T(f)|\,(G_{nn}(f))^{1/2} - G_{nn}(f)}{|H_c(f)|^2} df = P_s/2 \tag{3.18}$$

3.1.3 Maximizing Transverse Resolution Index (TRI)

The problem of maximizing the TRI is rather similar, mathematically, to that of maximizing $\Re$. We shall see that the solution, also, has a very similar form.

Repeating equation 2.56, our problem is to maximize:

$$TRI = \frac{8\pi T}{c^2}\int_0^\infty \frac{f^2 G_{ss}(f)\,|H_T(f)|^2}{G_{nn}(f)+G_{ss}(f)\,|H_c(f)|^2}df, \tag{3.19}$$

subject to the energy constraint given by 3.15. Again the solution will be given in the form of a theorem. The proof of this theorem is identical to that of theorem 1 in appendix 3A except that $|H_T(f)|$ is replaced by $f\,|H_T(f)|$ wherever this appears and $\frac{\Re}{2T}$ is replaced by $\frac{c^2 TRI}{8\pi T}$ wherever this appears.

Theorem 2. *Let $G_{ss}(f) = 0 \forall f \notin [f_1, f_2]$. Then the signal power spectral density, $G_{ss}(f)$, that maximizes 3.19 subject to 3.15 is given by:*

$$G_{ss}(f) = \begin{cases} \frac{k_T f |H_T(f)|(G_{nn}(f))^{1/2} - G_{nn}(f)}{|H_c(f)|^2} & \forall f \in R_1 \\ 0 & \forall f \in R_0 \end{cases} \tag{3.20}$$

where

$$\begin{aligned} R_1 &= \left\{ f : k_T f\,|H_T(f)| > (G_{nn}(f))^{1/2} \right\} \subset R_T, \\ R_0 &= \bar{R}_1, \\ R_T &= [f_1, f_2] \end{aligned} \tag{3.21}$$

and k_T is a non-negative real constant chosen to satisfy the equation:

$$\int_{R_1} \frac{k_T f\,|H_T(f)|\,(G_{nn}(f))^{1/2} - G_{nn}(f)}{|H_c(f)|^2}df = P_s/2. \tag{3.22}$$

3.1.3 Minimizing Range Estimate Variance

From 2.33 we see that the local variance of the range estimate is minimized by maximizing:

$$\frac{1}{\sigma_r^2} = 8\pi^2 T \int_0^\infty \frac{(f-f_0)^2\, G_{ss}(f)\,|H_T(f)|^2}{G_{nn}(f)+G_{ss}(f)\,|H_c(f)|^2}df \tag{3.23}$$

subject to the energy constraint given by 3.15 with f_0 defined by (from 2.27):

$$f_0 = \frac{\int_0^\infty \frac{f G_{ss}(f)|H_T(f)|^2}{G_{nn}(f)+G_{ss}(f)|H_c(f)|^2} df}{\int_0^\infty \frac{G_{ss}(f)|H_T(f)|^2}{G_{nn}(f)+G_{ss}(f)|H_c(f)|^2} df}. \tag{3.24}$$

The solution to this problem is given in the following theorem. The proof of this theorem is identical to that of theorem 1 in appendix 3A except that $|H_T(f)|$ is replaced by $(f - f_0)|H_T(f)|$ wherever this appears and $\frac{\mathcal{R}}{2T}$ is replaced by $\frac{1}{8\pi^2 T \sigma_\tau^2}$ wherever this appears.

Theorem 3. *Let $G_{ss}(f) = 0 \forall f \notin [f_1, f_2]$. Then the signal power spectral density that maximizes 3.23 subject to 3.15 is given by:*

$$G_{ss}(f) = \begin{cases} \frac{k_v|f-f_0||H_T(f)|(G_{nn}(f))^{1/2}-G_{nn}(f)}{|H_c(f)|^2} & \forall f \in R_1 \\ 0 & \forall f \in R_0 \end{cases} \tag{3.25}$$

where

$$\begin{aligned} R_1 &= \left\{ f : k_v |f - f_0| |H_T(f)| > (G_{nn}(f))^{1/2} \right\} \subset R_T \\ R_0 &= \bar{R}_1 \\ R_T &= [f_1, f_2] \end{aligned} \tag{3.26}$$

and f_0 satisfies 3.24 while k_v is a non-negative real constant chosen to satisfy:

$$\int_{R_1} \frac{k_v |f - f_0| |H_T(f)| (G_{nn}(f))^{1/2} - G_{nn}(f)}{|H_c(f)|^2} df = P_s/2. \tag{3.27}$$

§3.2 Performance Comparisons

3.2.1 Computation of Optimal Spectra

The solutions given in theorems 1, 2 and 3 are exact but are not in closed form. It has not been found possible to obtain expressions for the constants, k_d, k_T and k_v. This is because these constants must satisfy the integral equations, 3.18, 3.22 and 3.27 with limits of integration that depend, in turn, on the constants, themselves, through equations, 3.17, 3.21 and 3.26. A further complication arises from the dependance of the solution in Theorem 3 on the centroidal frequency, f_0, given by equation, 3.24. For similar reasons to those cited above in relation to the other constants, f_0 cannot be simply defined in terms of the transmission path model and the signal energy.

Because of the implicit forms of the solutions given in theorems 1, 2 and 3, the computation of optimal spectra necessarily involves iteration to find the constants, k_d, k_T, k_v and f_0. Computer programs have been developed by the author for performing these computations. In each case they involve a fairly straightforward iteration procedure based on Newton's method for obtaining k_d, k_T or k_v.

However, f_0 is obtained by a more complicated algorithm that is designed to cope with the somewhat ill-behaved nature of the centroid with respect to the convergence of iteration procedures under certain conditions. Such procedures operate by hypothesizing a centroid frequency and then computing the optimal spectrum and hence the actual centroid frequency. The hypothesized and actual centroids are then compared and, if they are not sufficiently similar, then a new hypothesis is formed via a formula involving the old hypothesis and the actual centroid resulting from it.

In many cases convergence is obtained by forming the new hypothesis as a weighted mean of the old hypothesis and the resulting actual centroid. A reasonably reliable formula is:

$$f'_{i+1} = \frac{(2f'_i + f_i)}{3} \tag{3.28}$$

where the primed quantities are hypothetical and the subscript is the iteration number.

However, as we shall see, at low signal powers, the minimum variance spectrum tends to contract to the band edges. The result is that it becomes highly sensitive to the hypothesized value of the centroid. The observed effect on the iteration process is that an error in the original centroid hypothesis causes the initial approximation to the spectrum to be concentrated at one of the band edges. The true post-whitening centroid obtained with that signal spectrum , therefore, lies near that band edge. In subsequent iterations, using 3.28 for example, the hypotheses move towards the band edge where the signal energy is concentrated. However, once the hypothetical centroid passes through the centroid of the true optimal spectrum, the signal energy shifts from one band edge to the other.

Under these circumstances, an iteration based on a formula such as 3.28 will be extremely slow to converge if the weighting is too large or will not converge at all if the weighting is too small. A robust and reasonably fast procedure can be obtained by detecting the transition of the actual centroid from one side of the hypothesis to the other. In subsequent iterations the hypothesis is updated using the values of the hypotheses used in previous iterations in such a way that the new hypothesis always moves towards the actual centroid but the step-size relates to the closeness of convergence rather than the difference between the hypothetical and actual centroid values.

Each time the actual centroid swaps from one side of the test value to the other, the updated test value is given by:

$$f'_{i+1} = 1/2\left(f'_i + f'_{i-1}\right). \tag{3.29}$$

On subsequent iterations, when the actual value remains on the same side of the test value, the update formula is:

$$f'_{i+1} = 2f'_i - f'_{i-1}. \tag{3.30}$$

The complete algorithm involves the use of 3.28 initially until the hypotheti-

cal value of f_0 is close to the true value. Subsequently, 3.29 and 3.30 are applied in the manner described. During this latter phase, the algorithm has several important properties. The step-size never increases and always decreases within two iterations. Furthermore, the test value is always updated in the direction of the true centroid (of the optimal spectrum). This combination of properties guarantees the convergence of the algorithm provided numerical problems are not encountered. In practice the author has never encountered such problems with this algorithm.

A listing of the Fortran computer program used in obtaining the minimum variance spectra presented in the following sections is given in appendix 3B. The programs for computing optimal spectra according to the other two simple criteria are not included as they are more straightforward.

3.2.2 A Practical Example

In this section the optimization algorithms already described will be applied to a practical example. The application for which this example is relevant is acoustic sensing through fleece and the interested reader is referred to reference [1.1] for more details. The transmission path was characterized for a particular point on a particular fleece and is indicative only of the type of condition encountered in this application. In this section we are not concerned with uncertainty in the characterization and will treat the problem as if the transmission path characteristics were not subject to variation.

Nevertheless it is important for the designer to be aware of deficiencies and limitations in his transmission path modelling techniques. The techniques used will be highly dependant on the details of the application but some techniques used by the author for the acoustic sensing problem will be presented in chapter 6. However, some aspects of the process are more generally relevant and will be discussed here.

The optimal spectra in theorems 1, 2 and 3 are quite sensitive to spurious detail in the model and for this reason it is necessary to apply spectral smoothing techniques

to eliminate unreliable detail while retaining a reliable estimate of the major spectral features. The approach of the author to this problem is to use selective all-pole spectral modelling which is a form of Maximum Entropy spectral analysis. Readers unfamiliar with these techniques are referred to papers by Makhoul[3.7] and Ulrych and Bishop[3.8] for details.

In some cases the author has found it advantageous to modify the all-pole modelling technique by a method which will be referred to as zero placement. If a signal or impulse response is known to have (or is suspected of having) zeroes in its Z-transform then all-pole modelling is obviously inappropriate. However, we can overcome this difficulty if we can estimate the locations of the zeroes. To eliminate the problem, we cancel each known zero by pole placement prior to the application of the selective all-pole modelling algorithm. Then, once the all-pole model has been obtained, the zeroes are re-inserted.

A listing of a utility program developed by the author to perform this modified form of all-pole spectral estimation is included in appendix 3B. The interested reader will find this relatively easy to follow.

One important point that is worthy of mention here, is that it is usually essential to use the general implementation of the discrete Fourier transform (DFT) rather than the more usual fast Fourier transform (FFT) implementation when applying selective all-pole modelling techniques to spectra. The reason for this is that the length of an FFT must be a power of 2. Now, if the number of frequency bins we have to transform to the autocorrelation domain is not a power of 2 then we might be tempted to use a longer FFT and pad out with extra samples. However, the problem arises with the choice of the padding sample values. Padding with zero-valued samples often yields extremely undesirable effects.

The reason for this is that all-pole modelling techniques can be interpreted as methods in which a parametric spectral model is adjusted to minimize a logarithmic

spectral error function[3.7,3.8]. This function is, of course, highly sensitive to the presence of zero-valued samples in spectra with the result that very biased spectral estimates are obtained. The usual result is that all the modes in the spectrum are assigned very narrow bandwidths. The spectral estimate is then quite small even at small frequency separations from the resonant frequencies. Hence the logarithmic error with respect to the zero-valued frequency samples is kept small.

The following details are not important to the discussion in this section but are included for interest and completeness. A more detailed explanation of the techniques used is included in chapter 6.

The transmission path model used in this section was derived from data obtained at 500kHz sampling and raw power spectra were obtained using a 512-sample FFT algorithm and averaging of the power spectra over a small ensemble of about 10 records. Final smoothing was achieved by the modified all-pole techniques already discussed.

The noise samples were extracted from the time series data by averaging the data over an ensemble of 50 records and then subtracting the average from each record to obtain a noise record. The target signal was obtained by excision of a segment of the averaged data record in the region of the known target delay. The clutter record was obtained by excision either side of the target segment.

The transmission path that we will use as an example is characterized by the three functions given in Fig. 3.2 over the frequency range from 0kHz to 124kHz.

Direct application of our three optimization procedures to this model over that band yields the spectra in Fig. 3.3 at four particular values of signal power, P_s.

It is clear from Fig. 3.3 that the forms of the three optimal spectra can be quite different and that they vary markedly with signal power. However, some very undesirable phenomena are evident in Fig. 3.3C and Fig. 3.3D. We see in these cases that a sizeable proportion of the signal energy is being channelled into part of the

Figure 3.2 *Transmission Path Characteristics*

(0 to 124kHz)

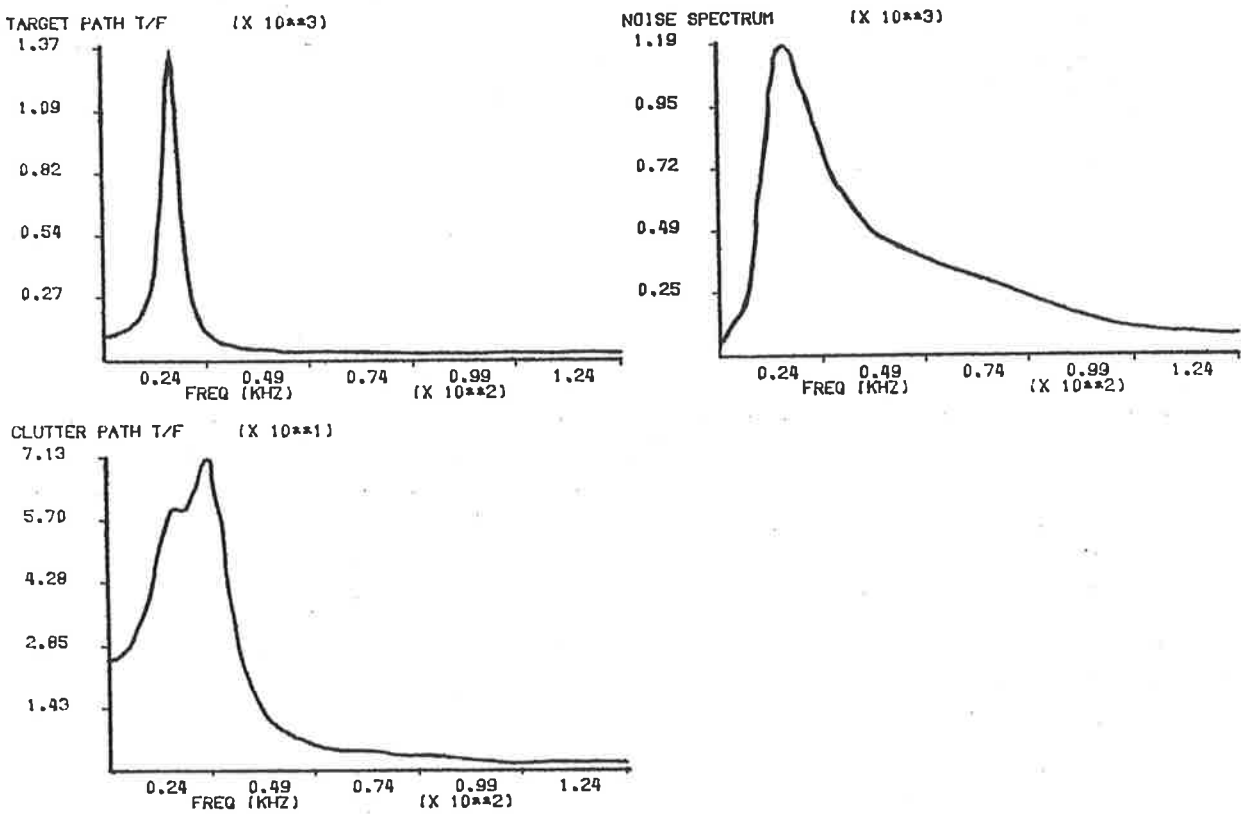

NOTE: For all figures in this thesis, multiply the axis tick labels by the multipliers enclosed in parentheses by the corresponding axis labels.

Figure 3.3 *Optimal Spectra*

(0 to 124kHz)

A) Signal power is 1dB ——— MDI spectra

B) Signal power is 13dB - - - - - - MV spectra

C) Signal power is 27dB — — — — MTRI spectra

D) Signal power is 40dB

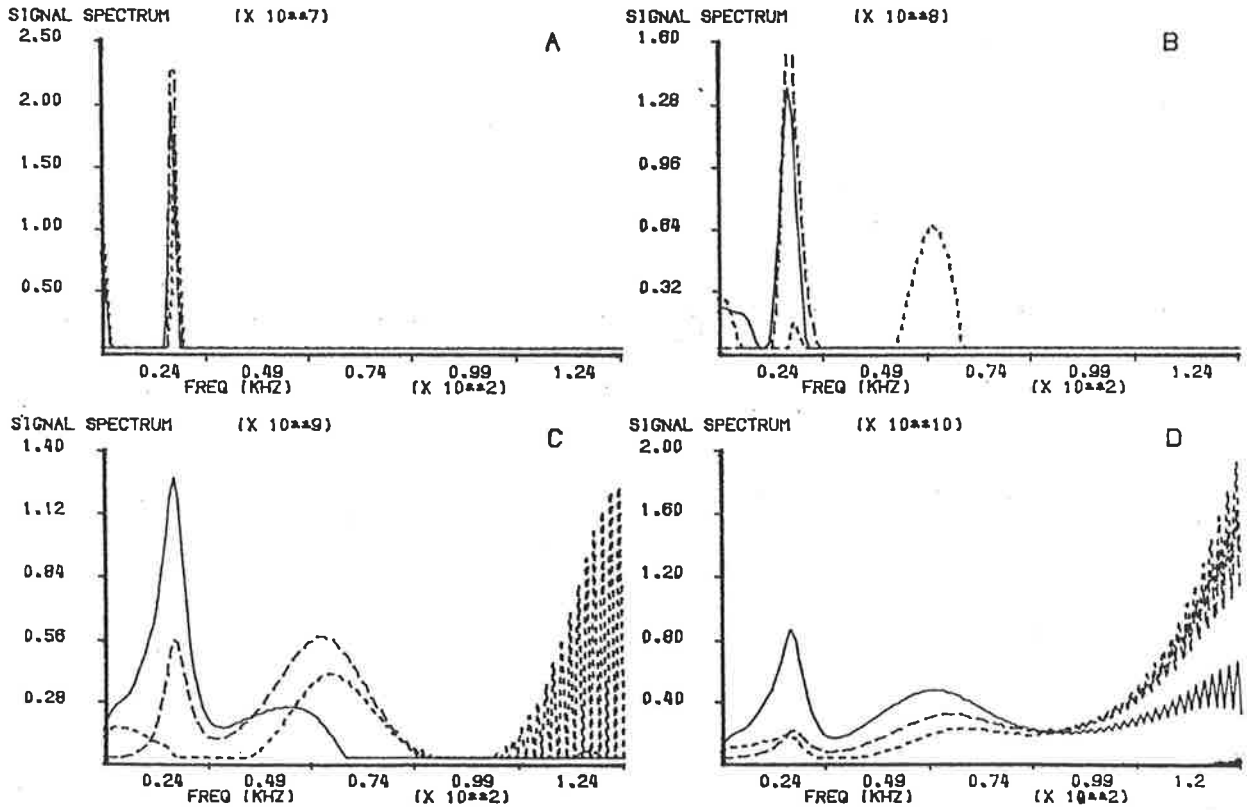

spectrum where, from Fig. 3.2, we see that very little signal power is transmitted either via the target path or the clutter path. The values of the two transfer function magnitudes are so small in this region that the computed optimal spectrum is sensitive to very small perturbations in the spectral estimates. Our spectral estimates are not sufficiently reliable, in this region, for us to have confidence in the resulting signal design.

It is important not to use unreliable data in this way. The way to avoid the problem is to restrict attention to a frequency band in which the transmission path model is believed to be reliable. On inspection of Fig. 3.2, we see that a reasonable frequency band over which to perform our optimization is from 0kHz to 40kHz. However, for other reasons associated with the particular application, such as the existence of acoustic room noise which is difficult to characterize in advance and the undesirability of emitting loud audible sounds, we will perform our optimization above about 10kHz. (The transmission path that we have modeled actually included a 10kHz high pass pre-filter.) Because our three transmission path functions are discrete, having been produced by digital computation, we will actually perform our optimization over the range from 9.8kHz to 39.0kHz.

In this new frequency band the transmission path model may be displayed as in Fig. 3.4. The resulting optimal spectra at various signal powers are illustrated in Fig. 3.5.

Comparing Fig. 3.5 with Fig. 3.4, we see that, at low signal powers, the maximum detection index (MDI) spectrum and the maximum transverse resolution index (MTRI) spectrum have contracted into the centre of the target channel while the minimum variance (MV) spectrum has contracted to the band edges. On the other hand, at high signal powers, all three types of optimal spectra occupy the entire band.

We see that the MV spectrum is always zero at at least one point in the band. This point is the post-whitening target echo spectral centroid frequency, f_0. Energy at this frequency contributes a constant or d.c. value to the post-correlation envelope and

Figure 3.4 Transmission Path Characteristics

(9.8kHz to 39.0kHz)

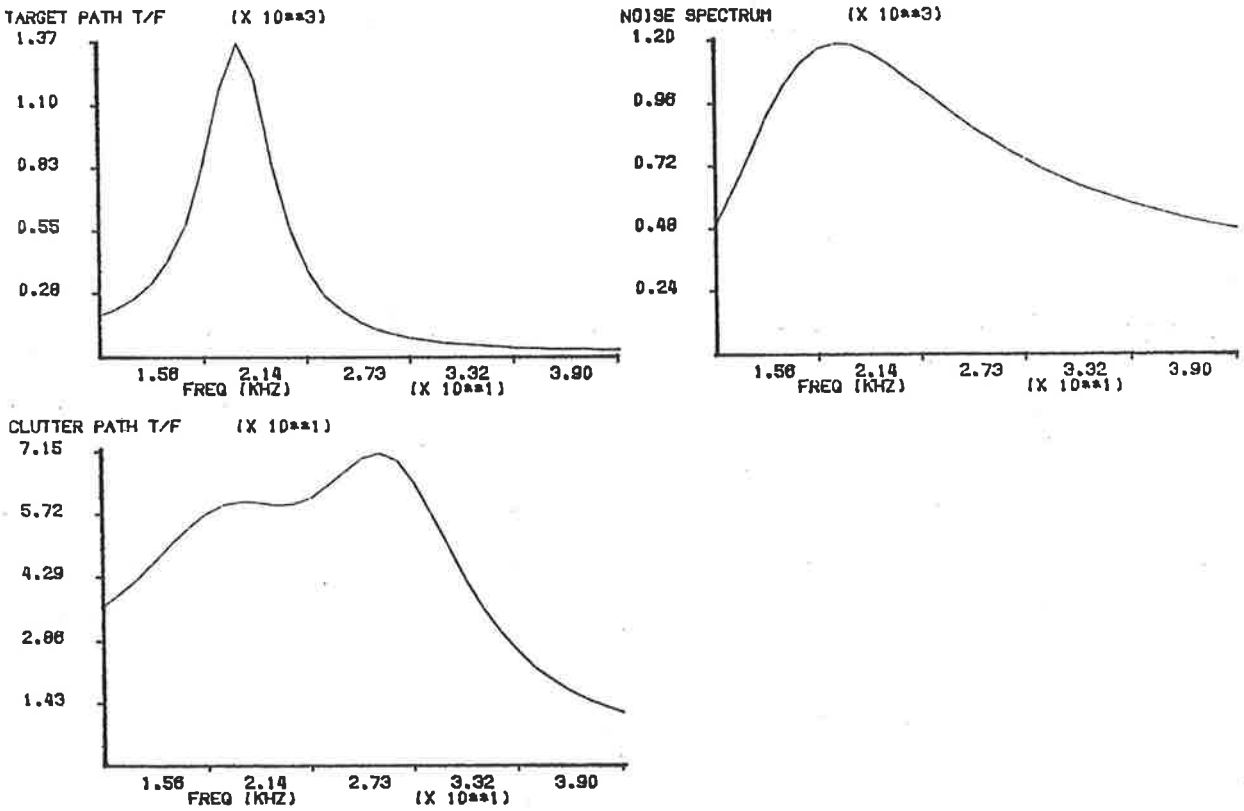

Figure 3.5 *Optimal Spectra*

(9.8kHz to 39.0kHz)

A) Signal power is 1dB ——— MDI spectra

B) Signal power is 13dB - - - - - MV spectra

C) Signal power is 27dB — — — MTRI spectra

D) Signal power is 40dB

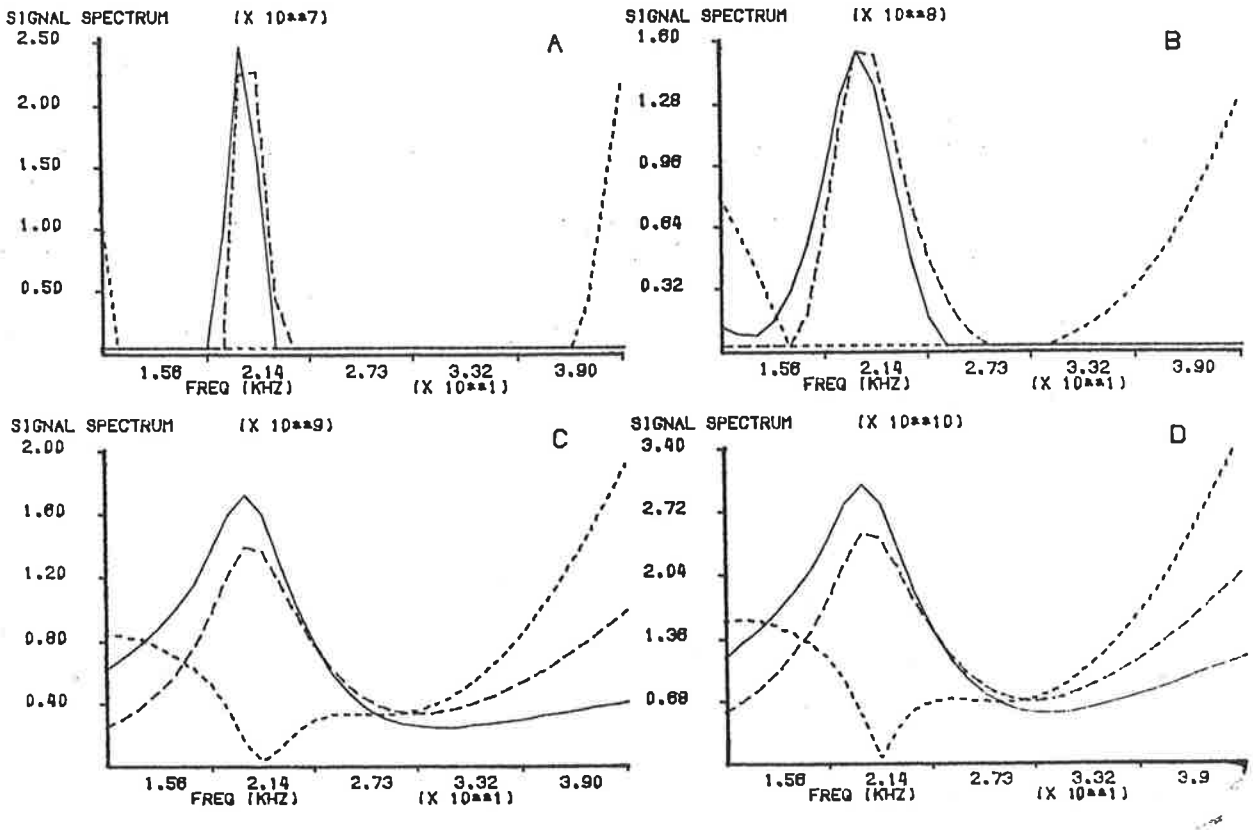

is therefore not useful in aiding in the location of the peak of the envelope.

It is also apparent that the MTRI spectrum is quite similar to the MDI spectrum at all signal powers. In situations where the frequency band of interest is narrow compared to the value of the centre frequency, we can expect this similarity to be even more pronounced than it is here because the simple spectral weighting in equation 3.20 will have negligible effect so that 3.20 and 3.16 will produce almost identical functions.

On the other hand, the MV spectra are very different from the other two at all signal powers and we can usually expect this to be the case, because the MV spectrum will always have a deep null at the spectral centroid of the post-whitening target echo. This null is often located close to the centre of the target channel because it is often located near the peak of the MDI spectrum.

Now it is instructive to compare the performance indicators for these three types of optimal signals over a range of signal powers. In Fig. 3.6, the detection index, the local variance of the range estimate and the TRI are plotted against signal power for each of the three types of optimal spectra. The transmission path model used was that of Fig. 3.4. The spectra were varied with signal power so that they were always optimal.

There are several interesting features of the curves in Fig. 3.6. One is that the curves appear to converge at high signal powers. This is a consequence of the fact that as the signal power is increased the post-correlation signal and interference both become less dependent on the power spectrum of the transmitted signal. To see this we can obtain, using 2.12 to 2.15:

$$R_0(f) = \frac{TG_{ss}(f)\,|H_T(f)|^2}{G_{ss}(f)\,|H_c(f)|^2 + G_{nn}(f)} \tag{3.31}$$

and

$$G_{i0}(f) = \frac{TG_{ss}(f)\,|H_T(f)|^2}{G_{ss}(f)\,|H_c(f)|^2 + G_{nn}(f)} \tag{3.32}$$

where $R_0(f)$ is the post-correlation signal transform and $G_{i0}(f)$ is the post-correlation interference power spectrum. Note that there is an implicit unity-valued constant in

Figure 3.6 *Performance Comparisons*

——— MDI Spectra

- - - - - MV Spectra

— — — MTRI Spectra

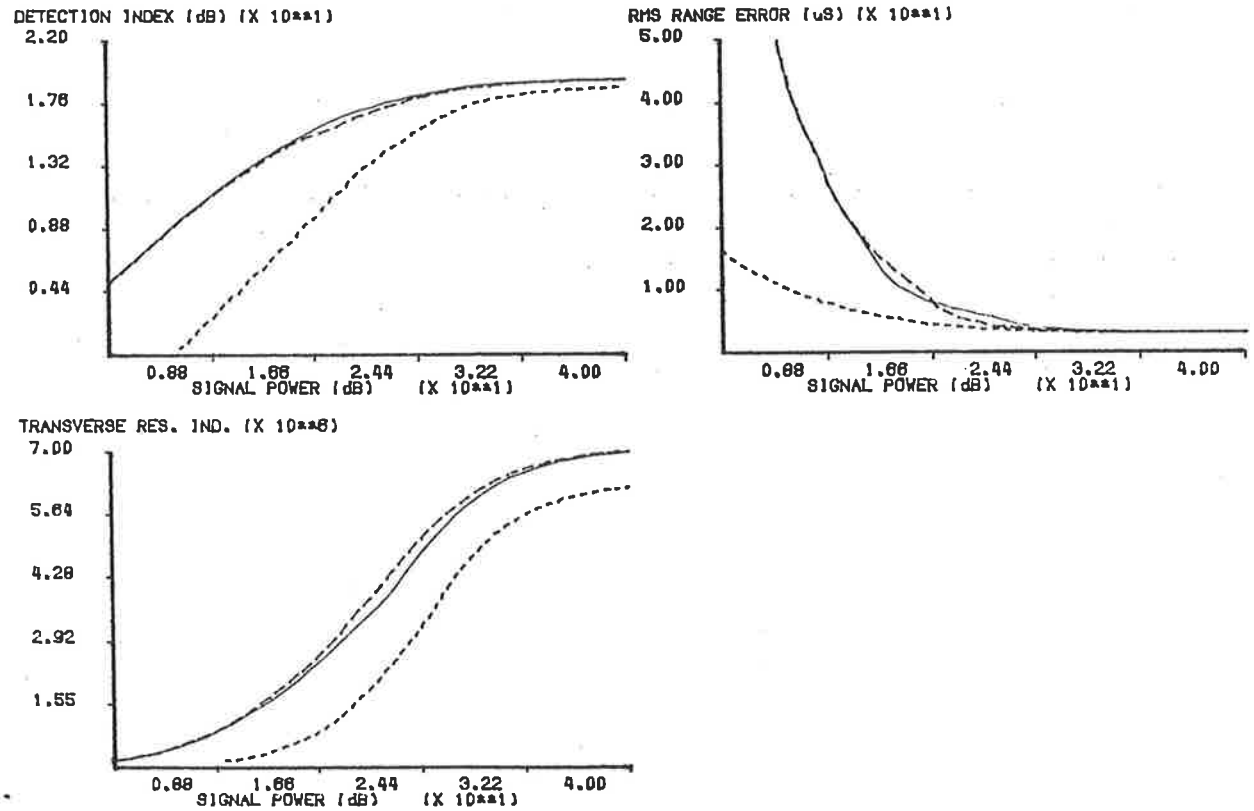

these expressions. This constant arises because we are treating the correlation as a signal waveform even though it is the cross-correlation of two signals. The implied constant restores the units to those of a signal waveform (e.g. volts).

Equations 3.31 and 3.32 are interesting in that the right hand sides are identical. However, this should not be surprising because, if they were not it would be possible to perform another stage of ML filtering which is inconsistent with the optimality of the ML filter. This can be seen by inspection of equation 2.11.

Now, at very high signal powers the noise term in the denominators of 3.31 and 3.32 can be neglected with the result that the signal power spectrum cancels out. This condition can be referred to as the *dominant clutter* condition because the interference power spectrum is dominated by the clutter power spectrum. We see that in the dominant clutter condition the system performance is determined entirely by the target and clutter transfer function magnitudes and the duration of the transmitted signal. We can see this also from 2.25, 2.33 and 2.56.

It is worth noting that the dominant clutter condition can only be achieved if the transmitted signal occupies the full bandwidth. The performance achievable in the dominant clutter condition in different bands may be quite different and will always be poorer in a sub-band than in the full band. However we see from equations 3.17, 3.21 and 3.26 that the three types of optimal spectra will always occupy the full band at sufficiently high signal powers.

From these considerations, we would expect that the curves in Fig. 3.6 would tend asymptotically to a bounding condition as the signal power was increased. Such a phenomenon can be observed in Fig. 3.6.

Another feature of the curves in Fig. 3.6 is that the MTRI and MDI spectra produce similar performance in relation to all three indicators. This is a simple consequence of the fact that, as previously discussed, these spectra tend to be quite similar.

On the other hand, at lower signal powers, the MV spectra produce very different performance figures from those of the other two. This also is not surprising given the very different forms of the spectra. The MV spectra provide a much smaller local variance but also a much lower detection index and a lower TRI than do the other two types of spectra.

Of course, once the detection margin (or $\Re - \Re_T$) drops below about 2 or 3dB (refer to section 2.4.1), the local variance becomes an unreliable indicator of range accuracy and the TRI becomes an unreliable indicator of transverse resolution. We need to obtain curves of detection threshold and thereby construct curves of detection margin before we can complete our performance comparisons. In addition to these, we should consider the effect of the ambiguity phenomenon resulting from the existence of time sidelobes as discussed in sections 2.4 and 3.0.

Using an iterative algorithm based on equation 2.26, it is possible to compute the detection threshold from the range gate width, W, and the moment bandwidth of the post-whitening target echo, β. The results of such computations are displayed, for each of four gate widths, in Fig. 3.7.

The most startling feature of these curves is the way the detection threshold drops abruptly to $-\infty$ at various points. This phenomenon results from the fact that equation 2.26 has no solution if the product, $W\beta$, is too small. Under this condition, the post-correlation target echo main lobe is broader than the range gate. Clearly, in that case, there can be no possibility of false target detection (assuming that the gate is, in fact, located over the target range).

The sharpness of this cutoff in the curves of Fig. 3.7, however, is not an accurate reflection of the way in which prior information can help overcome the detection problem. In fact, the transition is much smoother than indicated by the curves of Fig. 3.7 but equation 2.26 is only valid for $W\beta >> 1$[2.1]. The curves of Fig. 3.7 are conservative. A detailed study of the use of prior information will be undertaken in chapter 5.

Figure 3.7 *Detection Threshold Comparisons*

A) W = 200μ S ——— MDI spectra

B) W = 150μ S - - - - - MV spectra

C) W = 100μ S — — — MTRI spectra

D) W = 50μ S

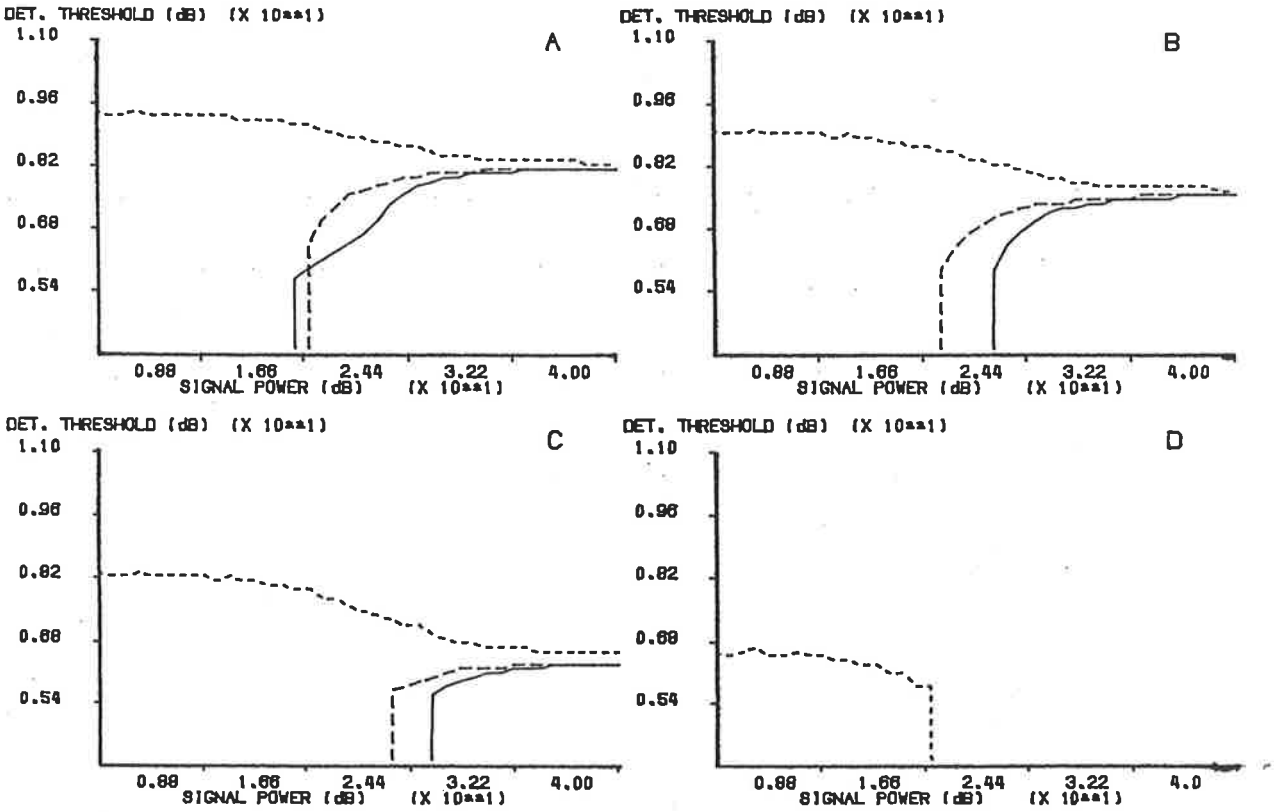

An important feature of these curves is that the MDI spectra consistently provide lower detection thresholds than the other two types of spectra. This is because there is no spectral weighting tending to spread the energy of the MDI signal across the frequency band. In fact, the converse is true in that maximization of the detection index is achieved by concentrating most of the signal energy in the region where the target transfer function is maximum. The result is that β tends to be smaller for MDI spectra and this results in lower detection thresholds.

This is particularly obvious at low signal powers. As the signal power is reduced, the optimal compromise between maximizing SCR and maximizing SNR moves towards maximization of SNR. The result is that the MDI spectrum contracts into the centre of the target channel to maintain the energy in the target echo. As a result, β falls still further so that the detection threshold also drops and, as we shall see shortly, the detection margin is maintained remarkably well.

The MV spectra, on the other hand, respond to this shift in emphasis from clutter to noise by contracting to the band edges. This increases β and hence counteracts to some extent the effect of the reduction in $\Re$ on the local variance, $1/\Re\beta^2$. Hence, as the signal power is reduced, the detection threshold increases.

Fig. 3.8 is a set of curves of detection margin versus signal power derived by subtracting the results depicted in Fig. 3.7 from those of Fig. 3.6A. We see that, if we require a detection margin of 3dB, then the TRI and σ_τ^2 curves of Fig. 3.6 do reliably indicate the performance for the MDI and MTRI spectra. However, for the MV spectra, those curves are only indicative of true performance for signal powers above a certain value that depends on the gate width.

We can find the minimum signal power satisfying the requirement of at least 3dB margin of detection from the curves of Fig. 3.8. For gate widths from 50uS to 200uS it varies from about 16dB to about 19dB. Looking at Fig. 3.6B, we see that this means that the MV spectra give significantly improved range performance only for moderate

Figure 3.8 *Detection Margin*

A) W = 200μ S

B) W = 150μ S

C) W = 100μ S

D) W = 50μ S

——— MDI spectra

– – – – MV spectra

— — — MTRI spectra

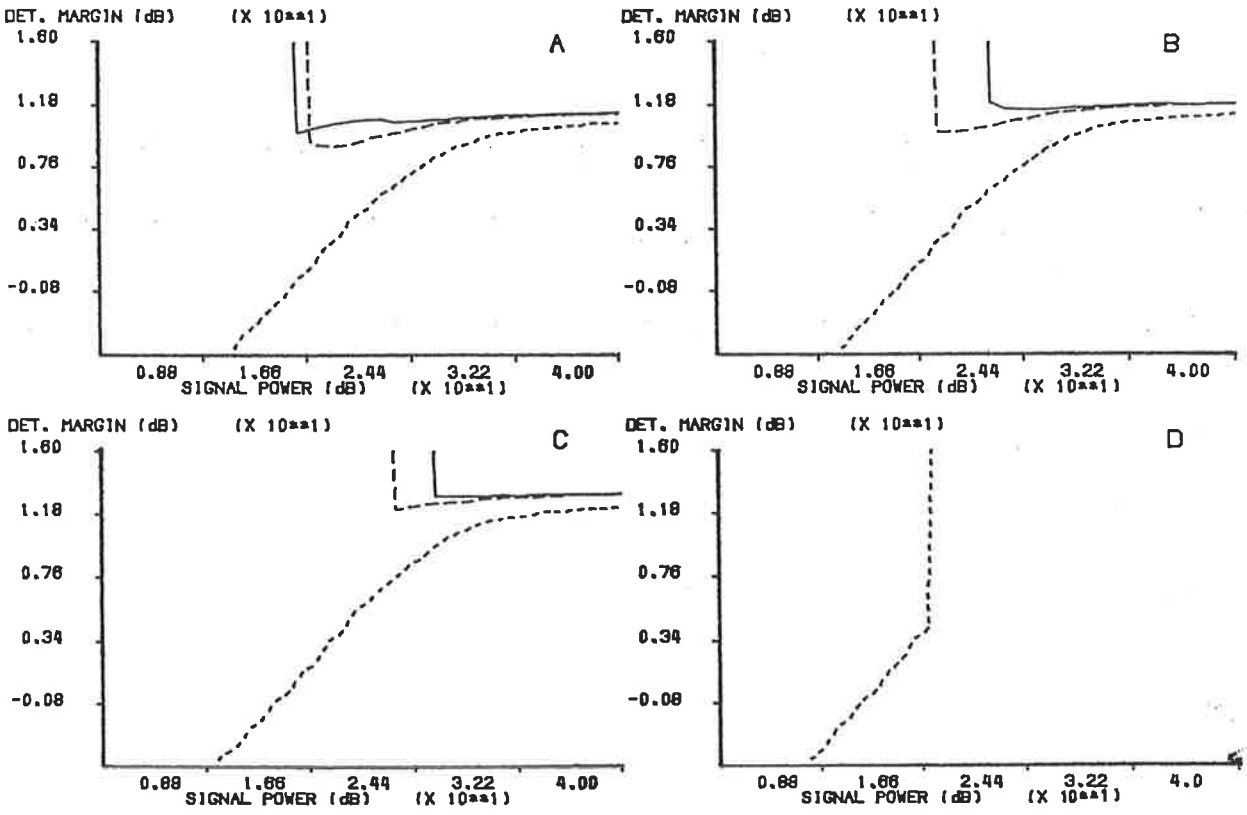

signal power. At lower power, poor detection performance would result in very poor range accuracy. At higher power, the other optimal spectra would yield similar range accuracy to that obtainable with the MV spectra.

Now we turn to the ambiguity problem resulting from the existence of time sidelobes. Our first step in considering this aspect of performance is to inspect the cross-ambiguity functions resulting from the use of some of the spectra we have discussed. Since we have restricted our attention to situations where Doppler effects are negligible, we need only consider the delay dependence of the ambiguity function. Hence we need only inspect the cross-correlation envelope given by:

$$A(\tau) = \left| \int_{-\infty}^{+\infty} \bar{r}(t)\bar{q}^*(t-\tau)dt \right| \tag{3.33}$$

where $\bar{r}(t)$ and $\bar{q}(t)$ are the complex analytic representations of the received target echo, $r(t)$, and the ML reference, $q(t)$, as described in chapter 2.

$A(\tau)$ is the wideband, zero Doppler equivalent of $|\chi_{rq}(\tau, f)|$ which is defined in equation 3.4. $A(\tau)$ is also the signal component of the LLF defined in equation 2.9. It is also the autocorrelation envelope of the post-whitening target echo.

Figs. 3.9 to 3.11 display the ambiguity functions, $A(\tau)$, resulting from the transmission of signals with the spectra displayed in Fig. 3.5. Because of the detail in those figures they have not been superimposed. It is important to realize that these are not the autocorrelation envelopes of the transmitted signals themselves but those of the post-whitening target echoes.

In Fig. 3.9, the ambiguity functions for the MDI signals are displayed. The rapid reduction of local variance with signal power that we saw in Fig. 3.6B is reflected here in the sharpening of the main lobe. There is virtually no sidelobe structure at all.

As expected, a very similar picture can be seen in Fig. 3.11 which corresponds to the MTRI spectra. However, Fig. 3.10 presents a very different picture for the MV spectra. At relatively high signal powers (e.g. $\geq$27dB) a definite sidelobe structure can

Figure 3.9 *Ambiguity Functions for MDI Signals*

A) Signal power is 1dB

B) Signal power is 13dB

C) Signal power is 27dB

D) Signal power is 40dB

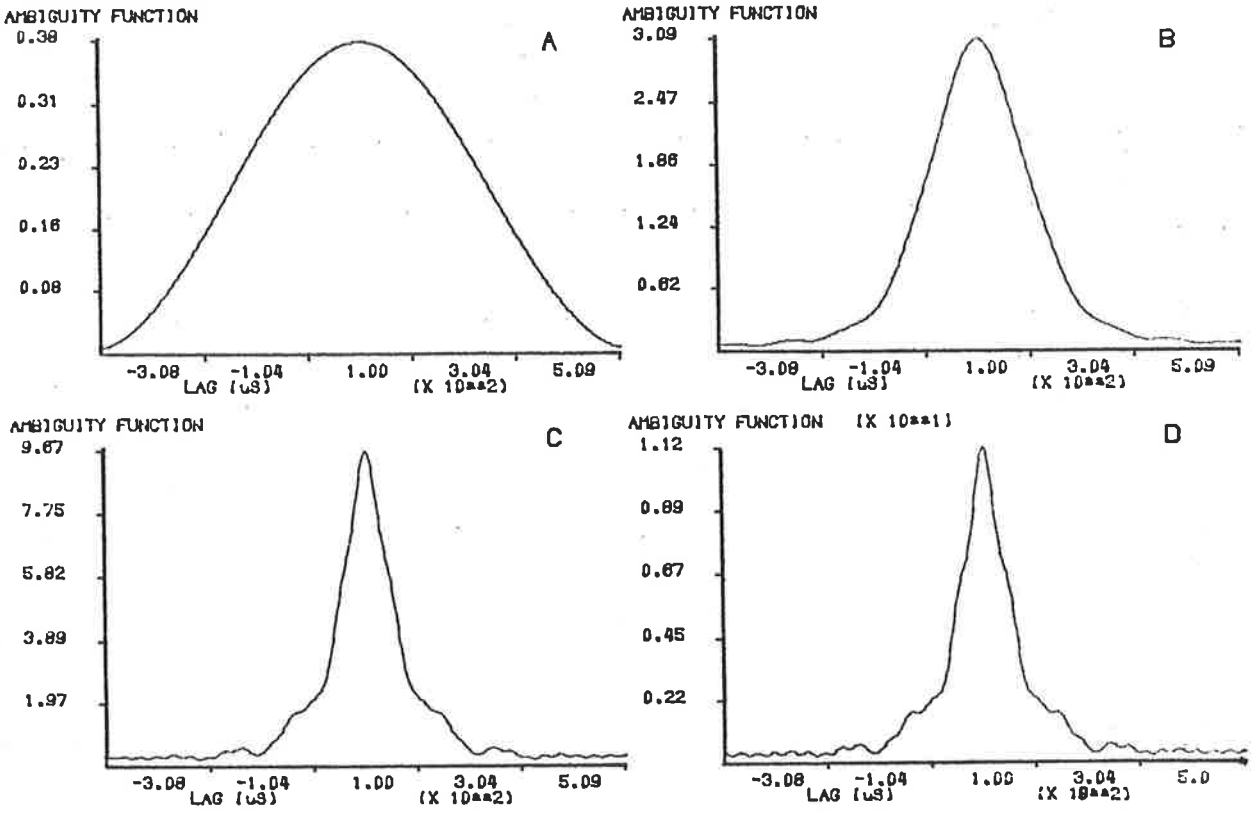

Figure 3.10 *Ambiguity Functions for MV Signals*

A) Signal power is 1dB

B) Signal power is 13dB

C) Signal power is 27dB

D) Signal power is 40dB

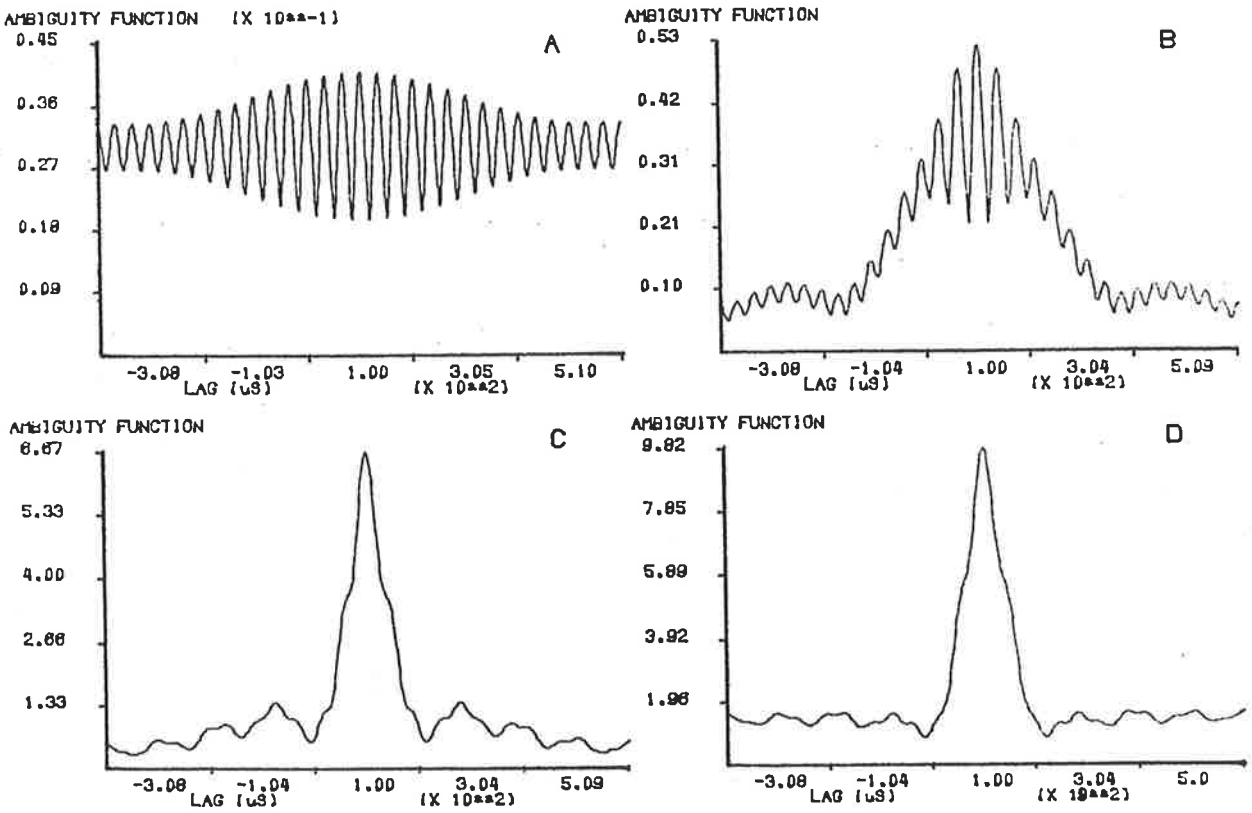

Figure 3.11 *Ambiguity Functions for MTRI Signals*

A) Signal power is 1dB

B) Signal power is 13dB

C) Signal power is 27dB

D) Signal power is 40dB

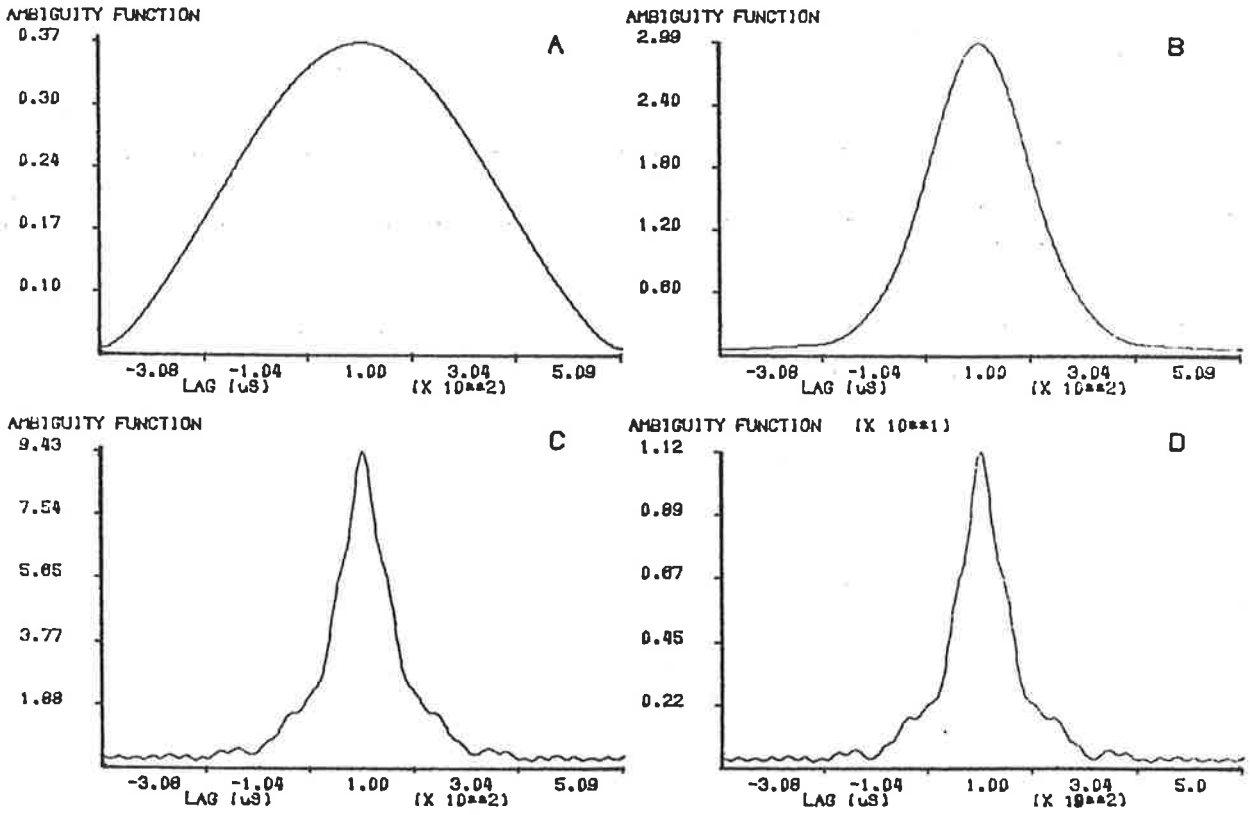

be seen but given the high detection indices achieved, this would present no ambiguity problem. (A more rigorous analysis will be presented soon.) At low signal powers, however, we see that the very sharp main lobe has been maintained but is surrounded by a very complex fine sidelobe structure.

This would represent an ambiguity problem. However, our discussion of detection performance revealed that transmission of MV signals at such low powers (¡16dB) would result in the system operating below threshold. Hence we are not interested in ambiguity at these very low signal powers.

Of more interest are the ambiguity functions associated with MV signals in the 17dB to 25dB region of signal powers where we would expect MV spectra to be most valuable. Fig. 3.12 displays four of these ambiguity functions. We see that the sidelobe structure in these functions is much less pronounced than at the very low signal powers. In fact, the detection indices of over 9dB associated with these conditions (see Fig. 3.6A) is much greater than that necessary to ensure unambiguous detection.

In order to see this it is necessary to perform a mathematical analysis of the ambiguity problem. The two largest sidelobes present the highest probability of producing ambiguous peaks due to additive interference. Now the width of these sidelobes depends on β. Because of the matched filtering, the widths of any interference peaks are similarly dependent on β. As a result, at most one interference peak can occur coincidentally with a sidelobe.

Now the probability that the interference above one sidelobe will exceed the main lobe depends, to a close approximation, only on the ratio of the difference between the peaks of the sidelobe and main lobe and the RMS interference. We will call this ratio the ambiguity ratio, A. The value of the peak of the main lobe is $\Re$ and the RMS interference is $\Re^{1/2}$. Thus if the ratio of sidelobe peak value to main lobe peak value is a, then:

$$\mathrm{A} = \frac{(1-a)\Re}{\Re^{1/2}} = (1-a)\Re^{1/2} \tag{3.34}$$

Figure 3.12 *Ambiguity Functions for MV Signals*

A) Signal power is 18dB

B) Signal power is 20dB

C) Signal power is 22dB

D) Signal power is 24dB

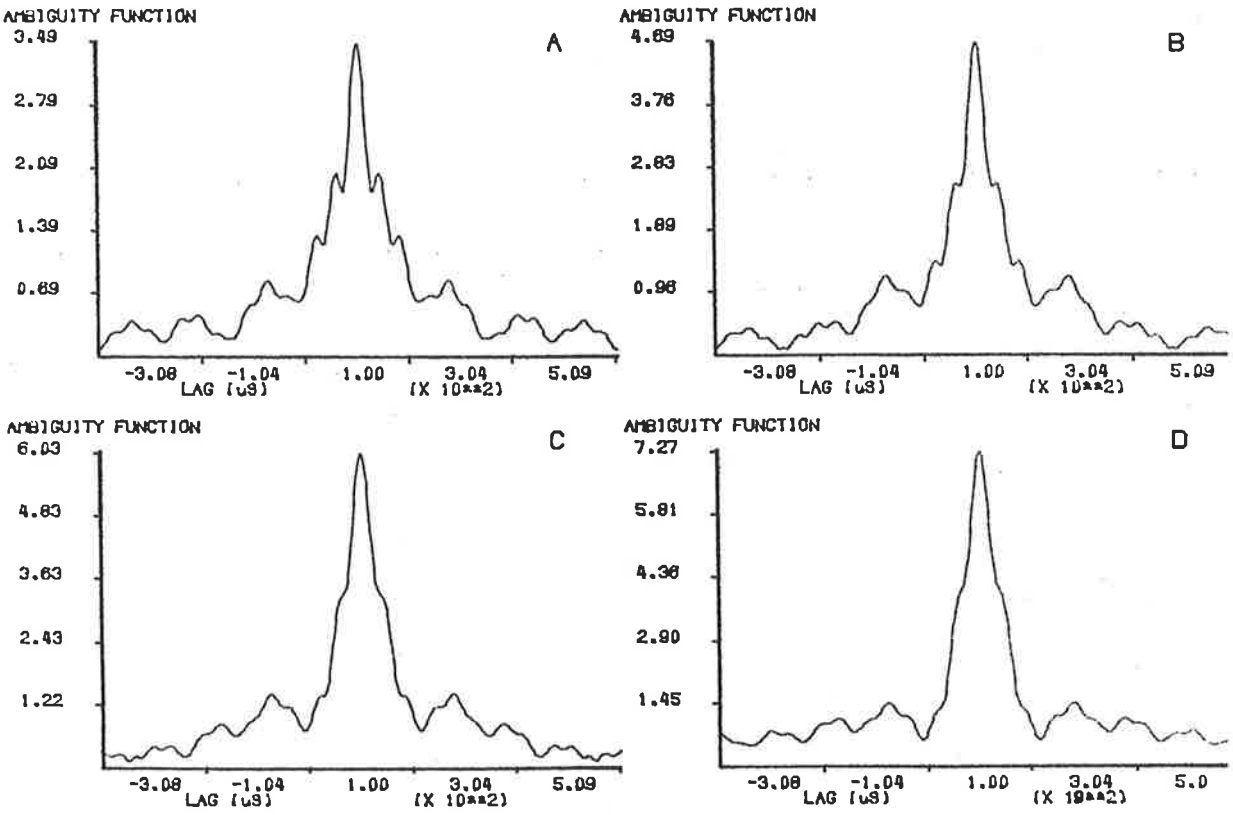

Hence we wish to determine the probability, P_e, that $\Re + n_1 < a\Re + n_2$ where n_1 and n_2 are the noise values at the main lobe and sidelobe peaks respectively and are independent zero mean random variables with variance, $\Re$. Thus, P_e is the probability that $(1-a)\Re < n_2 - n_1$. Now $n_2 - n_1$ is a zero mean normal random variable of variance, $2\Re$. Hence, P_e is the probability that a random variable of unity variance will exceed the value, $\Lambda/\sqrt{2}$. i.e.

$$P_e = 1/2 - erf(\Lambda/\sqrt{2}).$$

However, there are two sidelobes of equal amplitude and the others are too small in relation to the first two to contribute significantly to the ambiguity problem. Hence, the total probability of an ambiguous peak appearing is obtained from the binomial distribution as:

$$\begin{aligned} P_A &= 1 - (1 - P_e)^2 \\ &= 1 - (1/2 + erf(\Lambda/\sqrt{2}))^2. \end{aligned} \tag{3.35}$$

This function has a marked threshold characteristic and we can locate the threshold by solving the equation:

$$P_A = 1/2.$$

$$erf(\Lambda/\sqrt{2}) = 1/\sqrt{2} - 1/2$$

$$\Lambda \approx .7.$$

Thus, for negligible ambiguity, from 3.34 we have the requirement:

$$\Re >> \Re_A = \left(\frac{.7}{1-a}\right)^2. \tag{3.36}$$

It must be remembered however, that this inequality only guarantees unambiguous detection when the nearest sidelobes to the main lobe are much larger than all others.

Now, from Fig. 3.12A, we find that $a \approx .55$. Hence $\Re_A = 3.8dB$. From 3.6A, with a signal power of 18dB, we find that $\Re \approx 11dB$. This is well above the ambiguity threshold, $\Re_A$, justifying the earlier assertion.

In this subsection we have looked at the application of our simple optimization theory as given in theorems 1 to 3 to a practical example. That example is quite extreme in a number of respects. The frequency band of interest is very wide relative to the centre frequency, the transmission path transfer functions are highly coloured and the noise is coloured.

We saw that, for this example, MV spectra can provide a significant improvement in range accuracy over MDI spectra at moderate signal power. At lower power, MV spectra give rise to poor and ambiguous detection. At high power, the performance asymptotically approaches a limiting condition and is not significantly dependent on the signal design, provided the full band is occupied. MTRI spectra tend to be similar to MDI spectra and lead to almost identical performance.

3.2.3 White Environments

In this sub-section we shall apply signal optimization techniques to a somewhat more usual environment. The frequency band of interest is approximately 30kHz wide again, but centred at about 100kHz. The transmission path transfer functions are flat and the noise is white.

Fig. 3.13 displays the optimal spectra obtained at four different signal powers. This time we see that the MTRI spectra are very dissimilar to the MDI spectra at very low signal power but become more similar as the power is increased. The MV spectra are dissimilar to the others at all signal levels.

We see that the MDI spectrum is always flat while the MTRI spectrum has a preference for the high frequency end of the band. The MV spectrum is always zero at the centre frequency and maximum at the band edges. At low signal powers it contracts toward the band edges as it did in the previous example.

In Fig. 3.14 we see the curves produced as the performance indicators vary with signal power. The detection performances of the three types of signals appear

Figure 3.13 *Optimal Spectra - White Environment*

A) Signal power is 1dB ——— MDI spectra

B) Signal power is 13dB - - - - - MV spectra

C) Signal power is 27dB — — — MTRI spectra

D) Signal power is 40dB

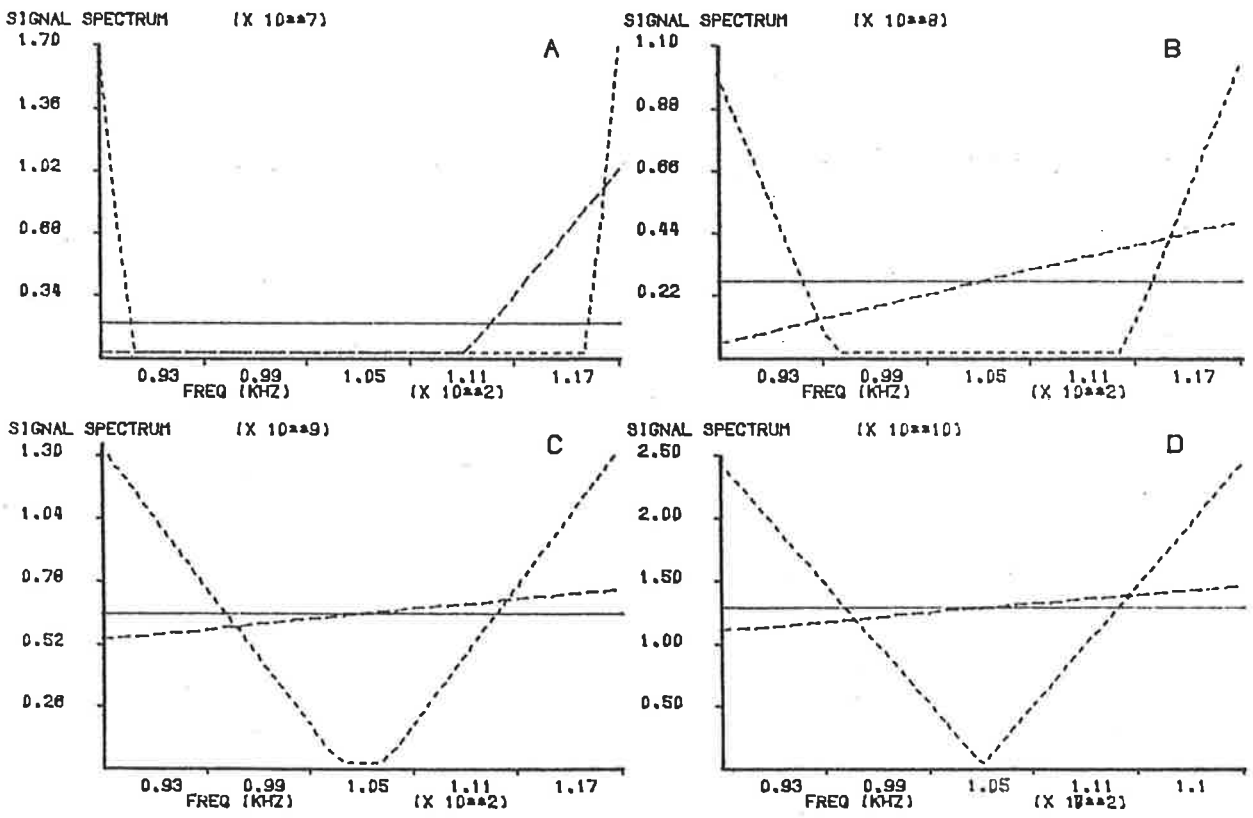

Figure 3.14 *Performance Comparisons - White Environment*

——— MDI Spectra

- - - - - - - MV Spectra

— — — — MTRI Spectra

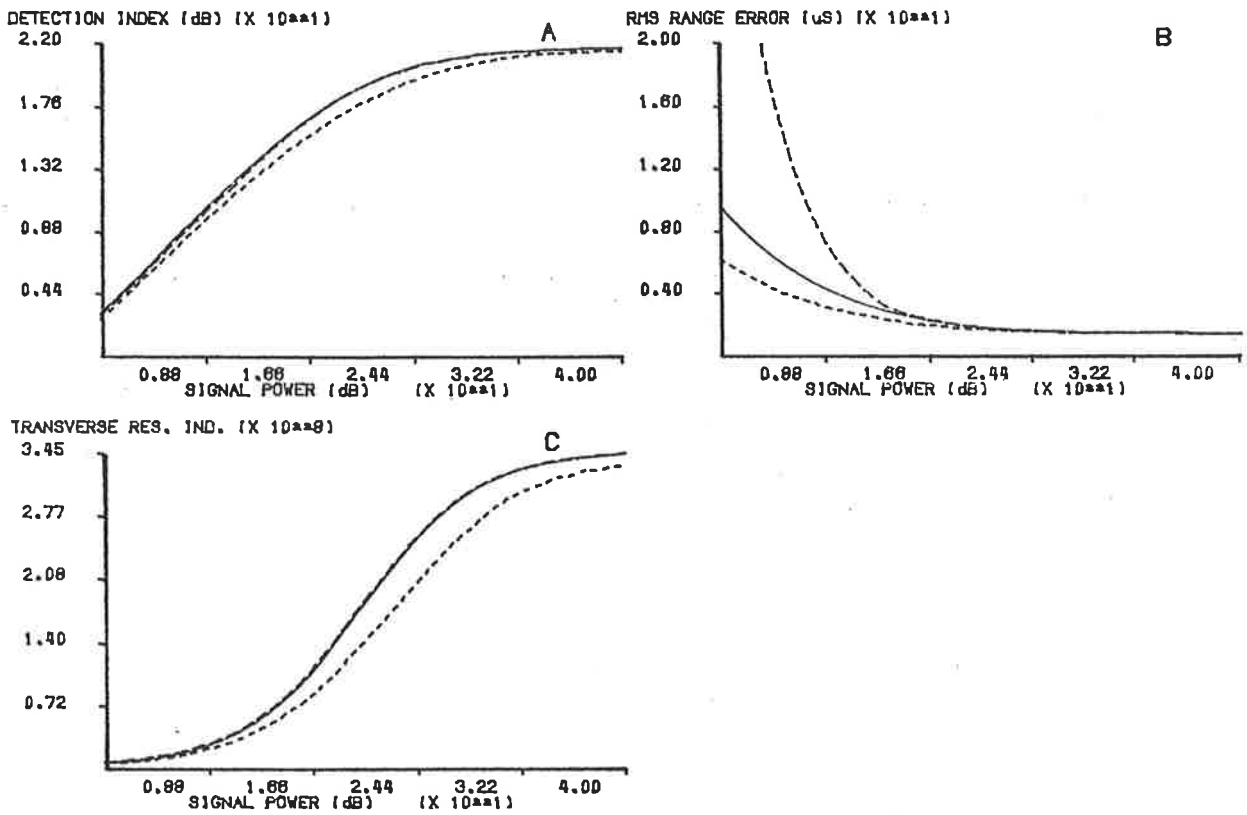

Figure 3.15 *Detection Thresholds - White Environment*

A) W = 200μ S ——— MDI spectra

B) W = 150μ S - - - - - - MV spectra

C) W = 100μ S — — — MTRI spectra

D) W = 50μ S

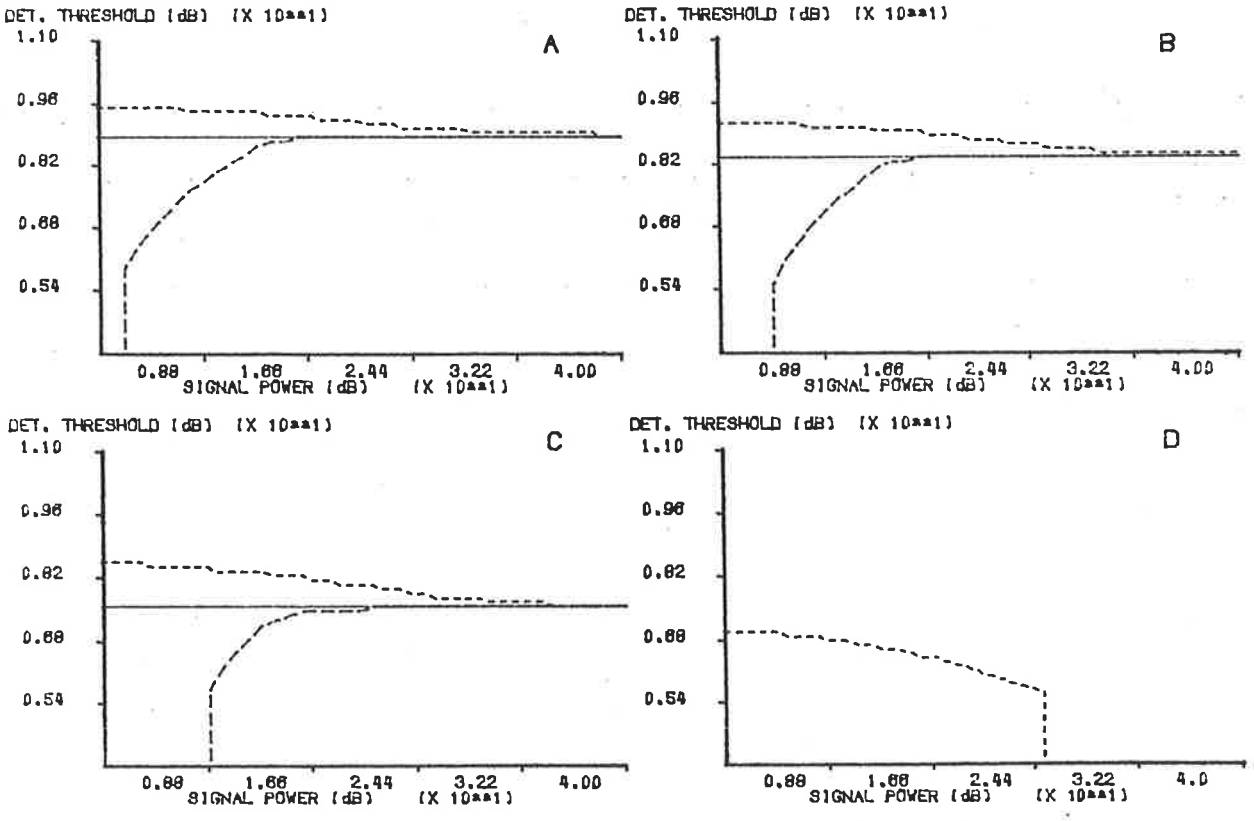

Figure 3.16 *Detection Margins - White Environment*

A) W = 200μ S ——— MDI spectra

B) W = 150μ S - - - - - MV spectra

C) W = 100μ S — — — MTRI spectra

D) W = 50μ S

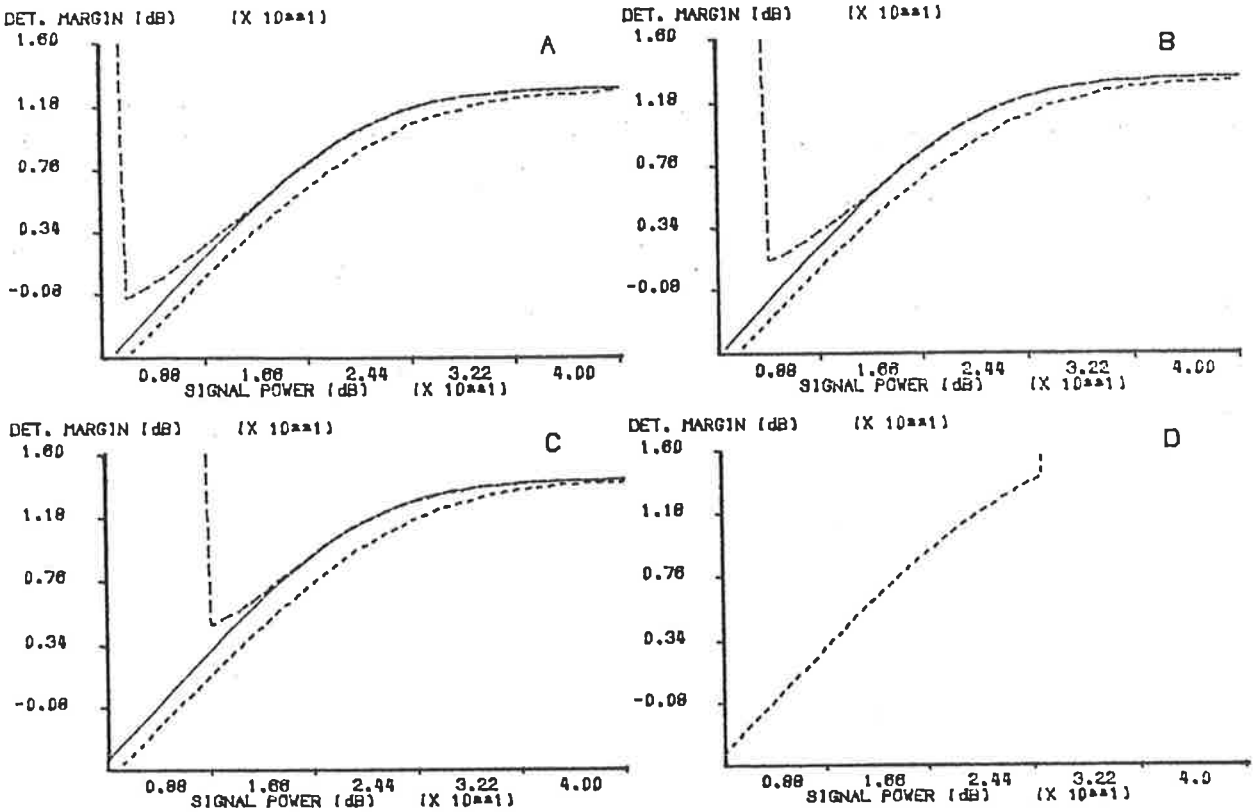

Figure 3.17 *MV Ambiguity Functions - White Environment*

A) Signal power is 1dB

B) Signal power is 13dB

C) Signal power is 27dB

D) Signal power is 40dB

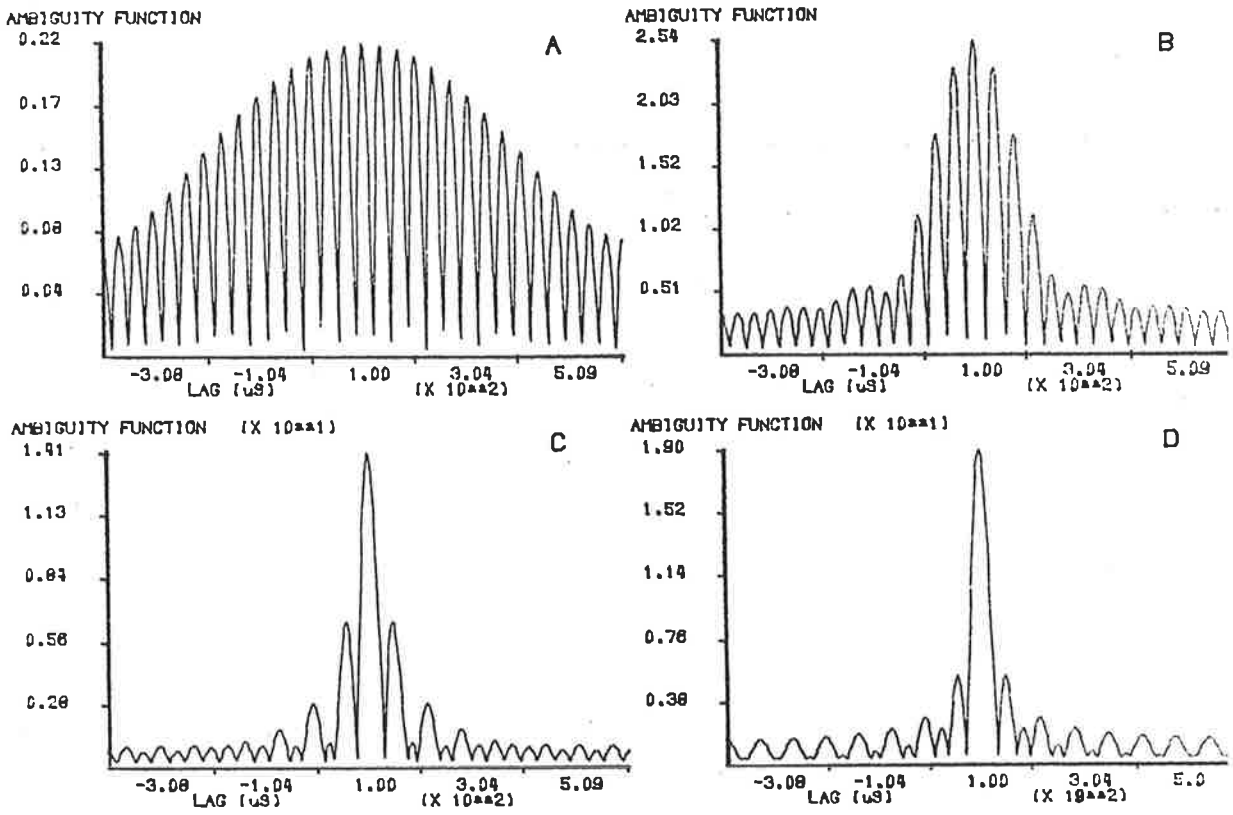

very similar from the detection index curves. However, it is necessary to compute the detection margins to verify this. Fig. 3.15 shows the detection thresholds for various gate widths and Fig. 3.16 shows the detection margins. Again the MDI spectra consistently outperform the others in this respect but never by more than a fraction of 1dB.

The reason for this similarity in spite of the very different spectral distributions is simply that there is no favourable portion of the band for the MDI spectrum to retreat to at low signal power.

From Fig. 3.16 we see that, with a 200uS gate width, the MV spectrum will give improved range accuracy for signal powers in excess of about 13dB because above that power, detection margins of greater than 3dB are achieved. However, from Fig. 3.14B, we find that this improvement is negligible for signal power above 25dB.

At this point we should consider the question of ambiguity. Fig. 3.17 shows the ambiguity functions resulting from the use of MV signals at four signal powers. As before, an extremely highly developed sidelobe structure is evident at low signal power. However, we see a much more obvious sidelobe structure at the higher signal powers than we did previously. This is because the sharp spectral transitions at the band edges are no longer smoothed by the colouration of the transmission path as they were in the previous example.

Of particular interest is the sidelobe performance with signal power in the region of 13dB to 25dB where we expect improved range accuracy from the use of MV signals. Fig. 3.17B is the ambiguity function at a signal power of 13dB. From this figure we find $a \approx .9$ and from equation 3.36 we find $\Re_A = 17dB$. From 3.14A we find that $\Re = 12dB$ which is insufficient to eliminate ambiguity.

At a signal power of 27dB, however, we find from Fig. 3.17c that $a \approx .4$ and from equation, 3.36 we obtain $\Re_A \approx 0dB$. Clearly there is no ambiguity problem here. In fact the ambiguity problem is overcome at a signal power of about 16dB. Hence the

MV spectra give significantly improved range accuracy for signal powers between 15dB and 25dB.

It is also worth noting, in relation to range accuracy, that the MTRI spectra give very poor performance below about 15dB.

The transverse resolution performances of the MTRI spectra and the MDI spectra are virtually identical for this example as we see from Fig. 3.14C. However the MV spectra give somewhat poorer transverse resolution.

We have now compared the performances obtainable using the three types of optimal spectra over a wide range of signal power for two very different transmission paths. We have seen that the usefulness of MV signals is limited by poor detection performance and signal ambiguity. At moderate power, however, they provide improved range accuracy while at high signal power system performance tends to a limiting condition which is independent of the signal provided the full band is occupied. We have also seen that the MV signals produce somewhat poorer transverse resolution than the other types except at very high signal powers. The MTRI signals, on the other hand, do not produce significantly improved transverse resolution over MDI signals and often, in fact, have very similar spectra to the MDI signals.

For any particular application the true optimal spectrum will provide a compromise between the performances of these simple optima. The question of how to effect such a compromise is the subject of the next section.

§3.3 Optimization With Respect to Mixed Criteria

We saw in the previous section that very poor detection performance can result from the use of MV signals at low signal powers. Minimum local variance is not an adequate criterion under these conditions as local variance is not a reliable indicator of range accuracy. In some situations, also, MV signals may not provide the transverse resolution required. Clearly, it would be useful to know how to compromise between the simple criteria in order to obtain a signal design that was best suited to a particular application.

Usually, we want to optimize with respect to one criterion, subject to constraints on the other two performance indicators. Typically, we want to minimize the local variance subject to the requirements of reliable and unambiguous detection and adequate transverse resolution. The detection requirements can be achieved by requiring that the detection index be greater than some minimal value and the transverse resolution requirement can be achieved by ensuring that the TRI exceeds a certain value. However, initially we shall look at the problem of minimizing the local variance subject to strict equality constraints on $\Re$ and TRI.

We have seen in the previous section that $\Re$ is a good indicator of detection margin in that MDI signals generally yield the largest detection margins. Therefore a detection margin constraint is equivalent to a constraint on $\Re$. Similarly, MDI signals have the best sidelobe performance, while, for any given signal spectrum, unambiguous detection will be effected provided the detection index provides some margin (say 3dB) above the ambiguity threshold. Hence, the unambiguous detection requirement also corresponds to a constraint on $\Re$. Of course, the constraint value to choose depends intimately on the details of the particular transmission path and the choice of frequency band. Designer intervention in the optimization process is necessary, in that several attempts with different constraint values may be necessary before an appropriate choice is made. The advantage of simplifying the detection constraints to a simple constraint

on $\Re$ in this way, however, is that the mathematical analysis is simplified considerably.

We now have two simple, strict equality constraints which may be expressed mathematically as:

$$2T\int_0^\infty \frac{G_{ss}(f)\,|H_T(f)|^2}{G_{nn}(f)+G_{ss}(f)\,|H_c(f)|^2}df = \Re_{min} \tag{3.37}$$

and

$$\frac{8\pi T}{c^2}\int_0^\infty \frac{f^2 G_{ss}(f)\,|H_T(f)|^2}{G_{nn}(f)+G_{ss}(f)\,|H_c(f)|^2}df = TRI_{min} \tag{3.38}$$

where $\Re_{min}$ and TRI_{min} are constraint values determined by the designer.

As well as meeting these constraints we wish to minimize the range estimate variance, given by 3.23 subject to the additional power constraint given by 3.15. The solution to this problem is given in the following theorem which is proven in appendix 3C.

Theorem 4. *Let $G_{ss}(f) = 0 \forall f \notin [f_1, f_2]$. Then the signal power spectral density, $G_{ss}(f)$, that maximizes 3.23 subject to 3.15,3.37 and 3.38, if it exists, is given by:*

$$G_{ss}(f) = \begin{cases} \dfrac{\left(k_v^2(f-f_0)^2+k_T^2 f^2+k_d^2\right)^{1/2}|H_T(f)|(G_{nn}(f))^{1/2}-G_{nn}(f)}{|H_c(f)|^2} & \forall f \in R_1 \\ 0 & \forall f \in R_0 \end{cases} \tag{3.39}$$

where

$$\begin{aligned} R_1 &= \left\{ f : \left(k_v^2(f-f_0)^2 + k_T^2 f^2 + k_d^2\right)^{1/2} |H_T(f)| > (G_{nn}(f))^{1/2} \right\} \subset R_T \\ R_0 &= \bar{R}_1 \\ R_T &= [f_1, f_2] \end{aligned} \tag{3.40}$$

and k_v, k_T and k_d are non-negative constants chosen to satisfy simultaneously 3.15, 3.37 and 3.38.

The solution given in theorem 4 is not simply a combination (linear or otherwise) of the solutions given in theorems 1 to 3 for at least two reasons. Firstly, the definitions of the frequency regions, R_1 and R_0, are not the same in any two of the theorems. Secondly, the value obtained for the centroidal frequency, f_0, is not, in general, the

same in the solution of theorems 3 and 4. Nevertheless, there is a correspondence between the values of $\Re_{min}$ and k_d and between those of TRI_{min} and k_T in that an increase in one of the constraint values in 3.37 or 3.38 always results in an increase in the value of the corresponding coefficient in 3.39. This can be seen from an inspection of the proof of theorem 4 in appendix 3C.

Now, the solution of Theorem 4 is not guaranteed to exist. It may not exist for one or more of several reasons. Firstly, the left hand side of 3.37 may always be greater than the right when the other constraints are met. Secondly, the left hand side of 3.38 may always be greater than the right when the other constraints are met. Thirdly, the left hand side of 3.37 may always be less than the right when the other constraints are met or, fourthly, the left hand side of 3.38 may always be less than the right when the other constraints are met. We require a strategy for dealing with these various conditions.

The first and second of the above conditions are advantageous in that our constraint(s), 3.37 or(/and) 3.38 is(/are) more than met. In this case the optimal solution is obtained by simply eliminating the offending constraint. Inspection of the proof in appendix 3C reveals that the solution to the new problem is obtained by setting the corresponding coefficient in 3.39 to zero.

The third and fourth conditions are rather more difficult to deal with. The author has adopted the following strategy. Detection performance takes top priority, followed by transverse resolution. Therefore, if 3.38 cannot be met subject to the other constraints then the solution adopted is to use the signal spectrum that maximizes TRI subject to 3.15 and 3.37. It is easily deduced from the proof of theorem 4 that the solution to this problem is obtained by dropping the constraint, 3.38 and setting k_v to zero. If neither 3.38 nor 3.37 can be met then we simply revert to the simple criterion of maximum detection index subject to 3.15.

In practice, the designer looks at various solutions obtained by using different

constraint values. The detection and ambiguity thresholds are also taken into account before the choice is made of the spectrum best suited to the application. In order to facilitate such investigations, the author has developed a computer program that implements the solution strategy outlined in the preceding paragraph. A listing is included in appendix 3B. The program involves four nested iteration loops to obtain the constants, k_v, k_T, k_d and f_0.

The form of the solution in R_1 has been modified slightly from that given in 3.39 to an equivalent form given by:

$$G_{ss}(f) = \frac{k_v \left((f - f_0)^2 + k_T'^2 f^2 + k_d'^2 \right)^{1/2} |H_T(f)| \left(G_{nn}(f) \right)^{1/2} - G_{nn}(f)}{|H_c(f)|^2} \qquad (3.41)$$

in which $k_T = k_v k_T'$ and $k_d = k_v k_d'$.

This modification ensures that the power constraint given in 3.15 can always be met by adjustment of only the one coefficient, k_v. This simplifies the procedures for updating k_T and k_d from one iteration to the next.

The overall solution is achieved by a relatively simple process in which several simple decisions are made at each iteration step. The procedure starts with k_d and k_T set to zero. The inner two iteration loops correspond to the simple MV optimization process under this condition. This MV solution is then tested for adherence to the detection index constraint (equation 3.37). If the constraint is met or more than met, then k_d is left at zero and the TRI constraint (equation 3.38) is tested. If not then iteration around the inner three loops obtains a solution satisfying the detection index constraint.

This third level of iteration continues until either the constraint is met or the first term in the numerator of 3.41 (involving the factor $|f - fo|$) is making negligible contribution to the signal power. This condition indicates that the constraint is not achievable, in which case the hypothesized solution being tested is chosen as the overall

solution. This solution is a very close approximation to the MDI solution because k_T is zero and k_v is close to zero.

The outer iteration loop attempts to achieve the TRI constraint (equation 3.38) by means of an algorithm analogous to that discussed in relation to the third loop. Again, this procedure is terminated if the constraint is met or if the $|f - fo|$ term in the numerator of 3.41 is making negligible contribution to the signal power.

§3.4 Examples of Mixed Criteria Optimization

As a means of illustrating the use of the mixed criteria optimization technique described in the previous section, two examples of its application to the transmission path of Fig. 3.4 will be discussed.

In the first of these examples, the TRI was unconstrained. This was achieved by running the computer program for mixed criteria optimization with TRI_{min} set to zero. The detection index constraint, $\Re_{min}$, was set to 14dB.

The resulting signal spectra at various signal powers are displayed in Fig. 3.18. Comparing these results with those of Fig. 3.5, we see that, at signal powers of 1dB and 13dB, the spectra are MDI spectra, while at 27dB and 40dB they are MV spectra. (Note that signal power is adjusted to within .1dB of the required value - this accounts for some small differences in absolute power density.)

Fig. 3.19 displays the curves of the three performance indicators for comparison with Fig. 3.6. Comparing the detection index curves, we see that, below about 12dB in signal power, the mixed criteria optimal spectra give identical performance to the MDI spectra. From 12dB to about 21dB in signal power, the detection index is constant at 14dB. Above 21dB in signal power, the detection index achieved is that achieved with the MV spectra.

Looking at the curves of range error, we see that the range error curve for the mixed criteria optimal spectra drops sharply away from the MDI curve above about 13dB and is close to the MV curve above about 17dB. These comparisons clearly illustrate the way in which detection performance can be traded for range accuracy.

The TRI curve has been presented for completeness. Again we see a transition region below which the performance is as for the MDI spectra and above which it is as for the MV spectra.

In the next example, $\Re_{min}$ was set to 10dB and TRI_{min} was set to 2.6×10^6. The

Figure 3.18 *Optimal Spectra - Mixed Criteria*

(Unconstrained TRI)

A) Signal power is 1dB

B) Signal power is 13dB

C) Signal power is 27dB

D) Signal power is 40dB

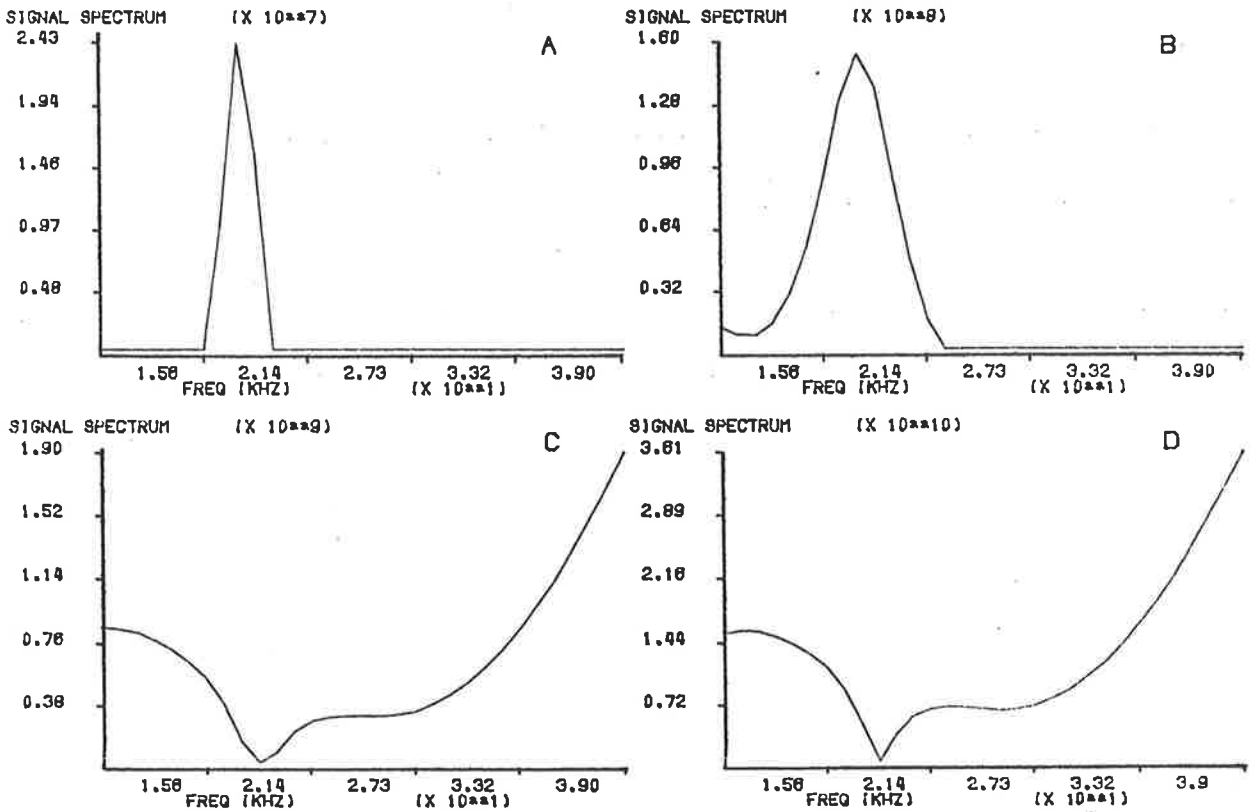

Figure 3.19 Performance Indicators for Mixed Criteria Optimal Spectra

(Unconstrained TRI)

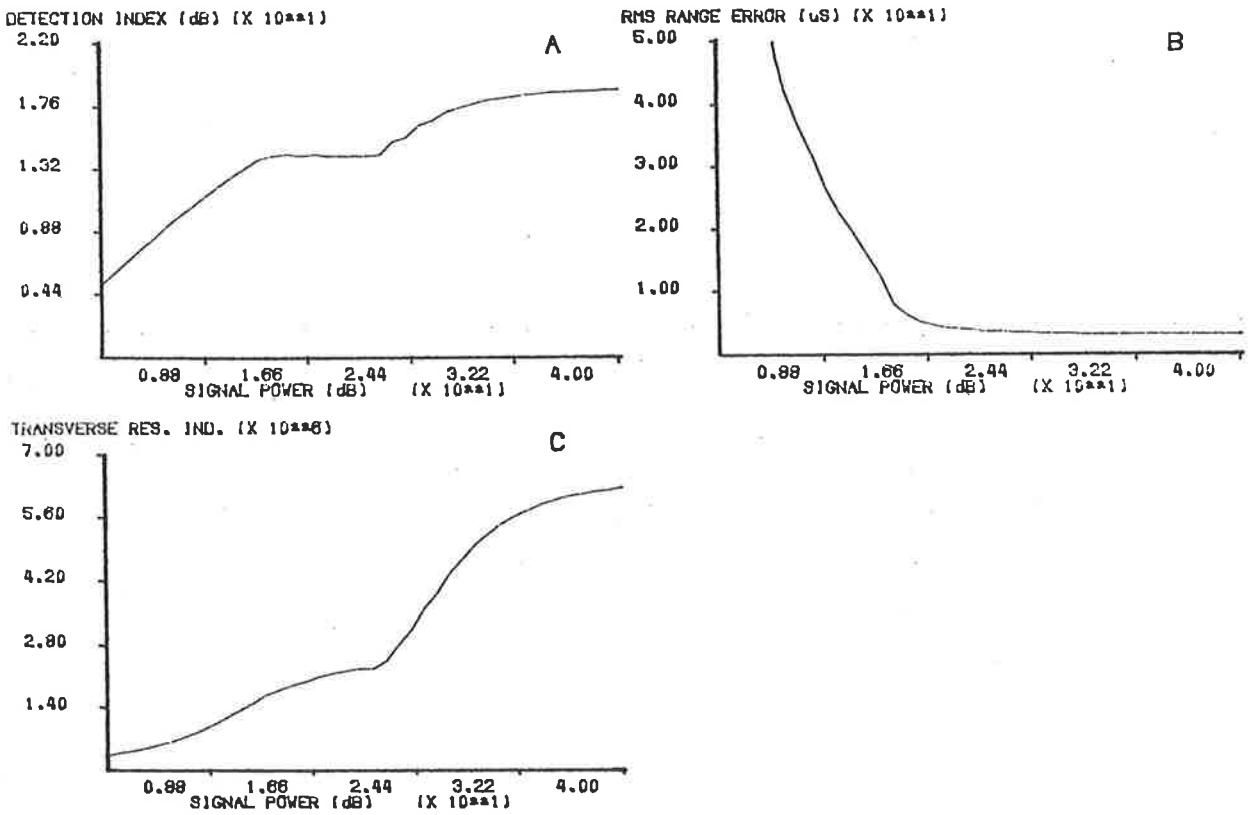

Figure 3.20 *Optimal Spectra - Mixed Criteria*

A) Signal power is 1dB

B) Signal power is 13dB

C) Signal power is 27dB

D) Signal power is 40dB

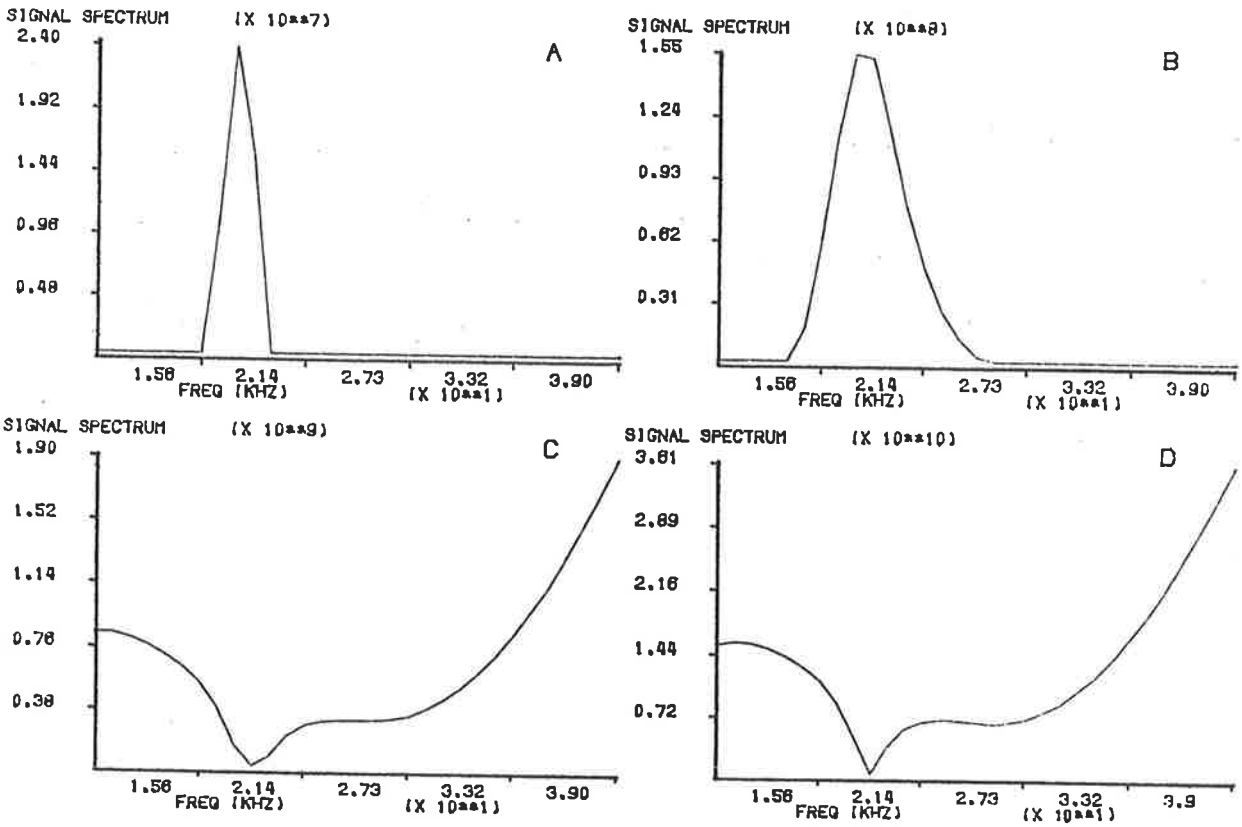

spectra obtained are illustrated in Fig. 3.20. Comparison with Fig. 3.5 reveals that the spectrum is that of an MDI spectrum at a signal power of 1dB. By 13dB, the transition to MTRI spectra has been completed and by 27dB the spectrum is an MV spectrum.

The performance curves are presented in Fig. 3.21. Only one of the two transition regions is evident in these curves because of the close similarity in performance of the MTRI and MDI spectra. The obvious transition is that from MTRI spectra to MV spectra which occurs for signal powers between about 16dB and 24dB. In this region the TRI is held at 2.6×10^6, the detection index actually drops slightly and the range error drops sharply below the MTRI curve to meet the MV curve.

Figure 3.21 *Performance Indicators for Mixed Criteria Optimal Spectra*

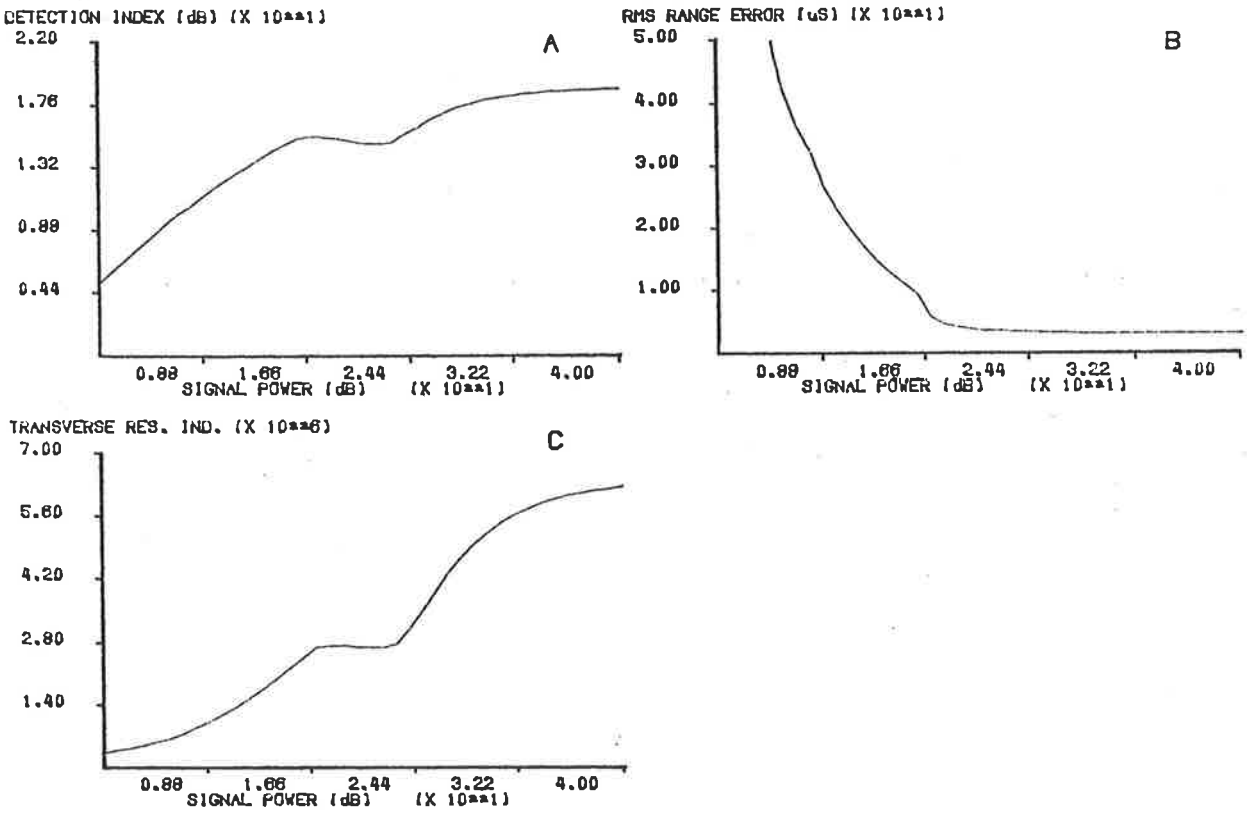

§3.5 Signal Waveform Design

When the transmitted signal is subject to a peak power limitation and is to be transmitted with a limited duration, then the signal energy will be maximized by the transmission of a constant envelope signal. In fact, in a number of places in the preceding chapters, the explicit assumption was made that the signal to be transmitted was a constant envelope signal. In this section we shall see how arbitrary signal spectra can be obtained approximately by the design of a constant envelope waveform.

We shall consider two types of constant envelope waveform. These are phase-modulated sinusoids and binary signals[3.9,3.10]. The selection and design of such signals is usually discussed with reference to their ambiguity functions in the range-Doppler plane. However, from the discussions and results in this chapter, we see that such considerations are unnecessary here. This is partly because considerations of clutter rejection and signal ambiguity have already been taken into account in the spectrum design. It is also due, in part, to the fact that we are addressing a somewhat atypical problem. The transmission path characteristics may be very complicated, Doppler effects are negligible and the clutter is evenly distributed in range in the vicinity of target range.

Now, binary signals are often used (usually to modulate sinusoidal carriers) because of the close approximations to impulsive autocorrelations that can be achieved with certain classes of them. The extremely low level range sidelobes that can be achieved are advantageous in many situations. However, such autocorrelations transform to nearly white power spectra over the frequency band of interest. Hence such signals are of limited use in our application and methods of tailoring the spectrum of long binary sequences to within the accuracy required have not been found.

An important class of phase-modulated sinusoidal signals is the class pioneered by Price et al[3.11]. *Chirps* or swept frequency signals are used extensively in pulse compression Radar and Sonar. They are usually linear chirps in which the instantaneous

frequency is swept at a constant rate across the band, producing a linear frequency-time trajectory. The spectrum of a linear chirp approximates the rectangular shape that might be expected from simple-minded instantaneous frequency considerations and the closeness of this approximation depends on how quickly the instantaneous frequency traverses the band[3.11].

Similarly, the spectrum of a chirp with a non-linear frequency-time trajectory can be made to approximate any required power spectrum closely, provided it does not traverse any part of the frequency band too quickly. The way in which the design can be achieved is indicated in Fig. 3.22. The technique involves constructing a chirp so that the derivative of its time-frequency trajectory is proportional to the required power spectral density at each point in the frequency band of interest.

The method amounts to:

1) Numerical computation of $\int_{f_1}^{f} G_{ss}(f)df$ for all frequencies in the band, $[f_1, f_2]$, to give a function proportional to the time-frequency trajectory. (i.e $dt/df = G_{ss}(f)$.)

2) Scaling of this function so that the maximum time equals the required signal duration. This produces the time-frequency trajectory, $t(f_i)$ where t is time and f_i is instantaneous frequency. This function is stored in an array in the waveform design computer program. The indices of that array represent frequency bin numbers.

3) Synthesis of a chirp by computing $\sin(2\pi \int_0^t f_i(t)dt)$ at incremental values of t corresponding to sampling instants. Because of the way the time-frequency trajectory must be represented in the computer (see para. 2)), the integral in the above function is computed by treating the trajectory as a function quantized in frequency as well as time.

The listing of a computer program to perform these computations is included in appendix 3B. An example of the accuracy with which required spectra may be approximated is given in Fig. 3.23.

Figure 3.22 *Chirp Design Concept*

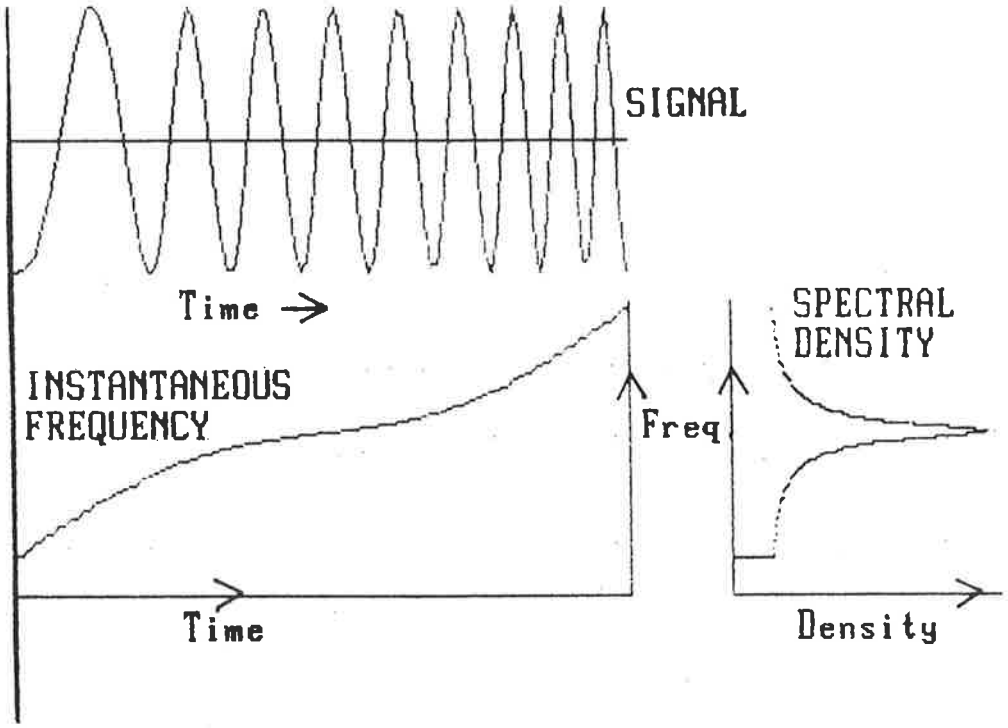

Figure 3.23 Chirp Power Spectrum

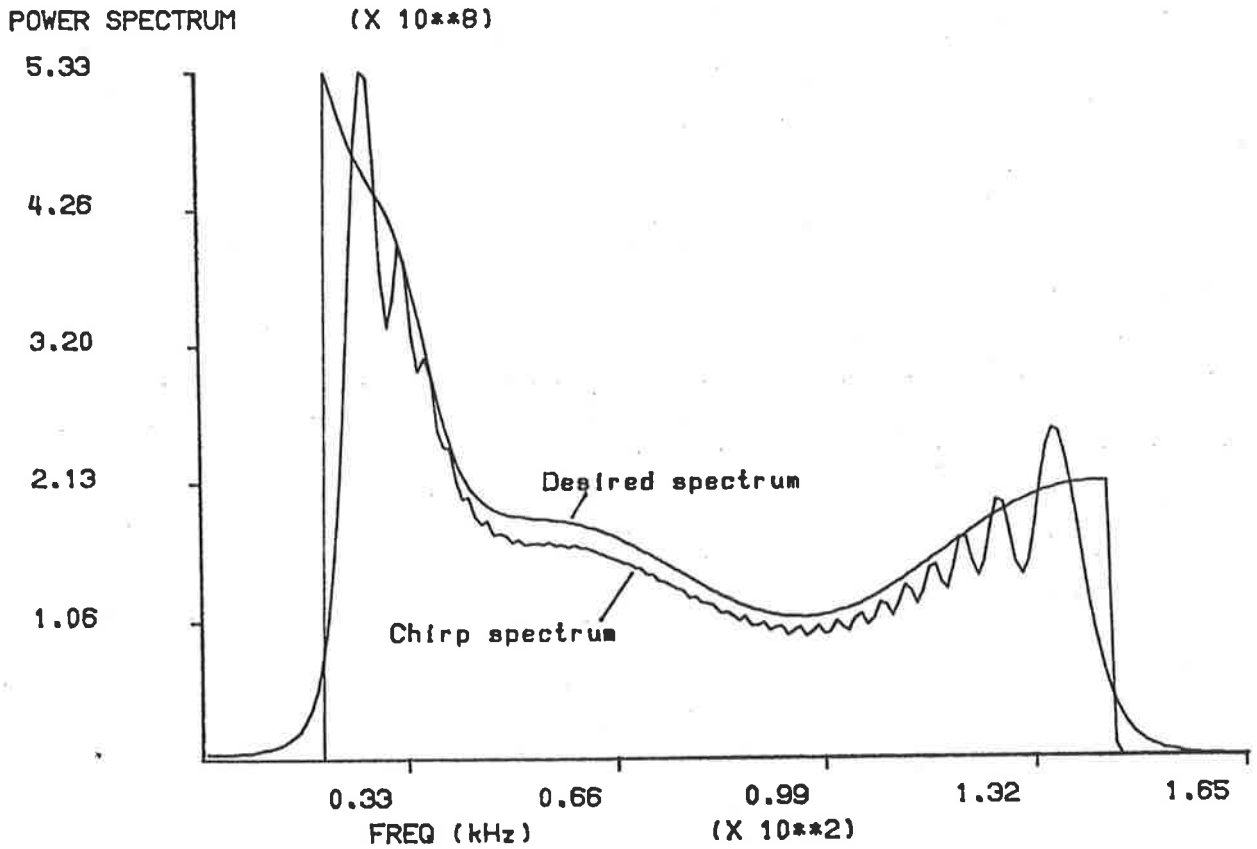

This section completes the study of signal optimization in this thesis except for the important class of problems in which the transmission path characteristics are uncertain. The problem of jointly optimizing the signal and receiver filter under such uncertainties is studied in the next chapter.

4. OPTIMIZATION FOR UNCERTAIN MODELS

§4.0 Introductory Remarks

Often the designer is confronted with a situation where a precise specification for the transmission path is difficult or impossible to obtain. There are two classes of such situations. In one class, exact measurements of the target and clutter transmission path transfer functions are not available and the designer does not have complete confidence in the estimates that are. In the other class of problem, the transmission path characteristics are known to vary and hence there must be an uncertainty included in the specification of those characteristics.

Clearly, in such situations, the techniques of the previous chapters are inadequate as they may only be applied when the transmission path characteristics are precisely specified. A more sophisticated approach is needed which takes account of the uncertainties present in the problem.

There are two established approaches to this sort of problem. One may design an adaptive system which tunes itself to the characteristics of the path within certain bounds. Alternatively, one may design a non-adaptive system which is optimized according to a robustness criterion. This criterion is chosen to ensure that the resulting system performs well, but not necessarily optimally, for any transmission path within a particular uncertainty class.

The first of these approaches can often result in very complex system designs with attendant problems of high cost and unreliability. For some classes of problem

such an approach is justifiable. However, the design of a real-time system for transmission path identification, as would be required here, would be complex in the extreme. Furthermore, in some cases of practical interest, such as ultrasonic sensing of sheepskin through the fleece [1.1] variations in transmission path characteristics occur much more rapidly than an adaptive system could be expected to track accurately.

In this chapter we shall explore the second approach in which the signal to be transmitted and the receiver filter are jointly optimized according to a max-min robustness criterion. In section 4.1 we will examine the formulation and solution of the robust filter design problem as reported elsewhere in the literature. Section 4.2 is devoted to the formulation and solution of the somewhat more complicated problem described above.

§4.1 Robust Matched Filters

The term *matched filter* is the generic name applied to the class of filters that are designed to maximize the *signal-to-interference ratio at the signal peak (SIR)* at the filter output. A matched filter must be designed for a particular signal input in the presence of stationary noise having a certain known power spectrum. The output SIR of a general filter is given by:

$$SIR = \frac{\left|\int_{-\infty}^{+\infty} R(f)H(f)df\right|^2}{\int_{-\infty}^{+\infty} G_{ii}(f)|H(f)|^2 df} \tag{4.1}$$

where

$R(f)$ is the Fourier transform of the signal

$H(f)$ is the filter transfer function

$G_{ii}(f)$ is the interference power spectrum

It is, perhaps, remarkable that maximization of SIR by the choice of $H(f)$ yields an expression proportional to $H(f)$ as given in 2.24. The filter specified in the latter equation was chosen to yield the log-likelihood function of delay at its output. The matched filter is given by the expression:

$$H_M(f) = \frac{kR^*(f)}{G_{ii}(f)} \tag{4.2}$$

This expression differs from 2.24 only in that an arbitrary scale factor, k, may be applied.

The maximum SIR given by 4.1 with $H(f) = H_M(f)$ reduces to:

$$SIR_{MAX} = \int_{-\infty}^{+\infty} \frac{|R(f)|^2}{G_{ii}(f)} df \tag{4.3}$$

This is exactly equal in value to the expressions for detection index given by 2.23 and 2.25.

This correspondence between matched filtering and correlation techniques for delay estimation will justify the approach taken in section 4.2. However, we will now

explore the problem of robust optimization of $H(f)$ in 4.1 when $R(f)$ and $G_{ii}(f)$ are uncertain.

The approach reported several times in recent years [4.1,4.2,4.3,4.4,4.5] is one in which the minimum SIR encountered for any pair of signal and interference within specified classes for $R(f)$ and $G_{ii}(f)$ is maximized by choice of $H(f)$. In other words, the designer chooses $H(f)$ to optimize the worst case performance. A similar approach has been reported for Wiener filters [4.1,4.2,4.6,4.7,4.8].

The problem lends itself to a *game theoretic* formulation in which the players are the designer and nature. The designer has a set of strategies, $\{H(f)\}$, and nature has a set of strategies, $C_s \times C_i$, which is the cartesian product of the uncertainty classes, C_s and C_i corresponding to $R(f)$ and $G_{ii}(f)$ respectively. The *payoff* for the designer is the SIR which we will denote by $p(H; R, G_{ii})$. We can arbitrarily assign a payoff of $(-p(H; R, G_{ii}))$ for nature. The problem can then be described formally as a *two-person zero-sum* game [4.9,4.10].

If the strategies, $H(f)$ and $(R(f), G_{ii}(f))$ can be considered *mixed* strategies then the game is guaranteed a solution by the *fundamental theorem* of game theory [4.10]. A mixed strategy is one which can be expressed as a linear combination over a finite set of *pure* strategies. The vector of coefficients is a probability vector known as the *strategy function* and the payoff for a pair of strategy functions is given by the expected payoff over the matrix of pairs of pure strategies. We have

$$H(f) = \sum_j P_j^D H_j(f),$$

$$(R(f), G_{ii}(f)) = \sum_k P_k^N (R(f), G_{ii}(f))_k,$$

$$p(H; R, G_{ii}) = \sum_j \sum_k p(H_j; (R, G_{ii})_k) P_k^N P_j^D,$$

in which the probability, P_j^D is the j_{th} element of the designer's strategy function (or vector) and P_k^N is the k_{th} element of nature's strategy function (or vector).

In general, however, the strategies cannot be considered mixed and it will be necessary to prove that a solution exists. Nevertheless, we can gain insight into the problem by considering the form of the solution given by the fundamental theorem.

Formulating the problem, we wish to find the function, $H(f)$, such that:

$$SIR = p_R = \underset{\{H(f)\}}{MAX} \; \underset{C_o \times C_i}{MIN} \; p(H; R, G_{ii}), \tag{4.4}$$

in which p_R is defined.

By the fundamental theorem [4.10] we have:

$$\begin{aligned} p_R &= \underset{C_o \times C_i}{MIN} \; \underset{\{H(f)\}}{MAX} \; p(H; R, G_{ii}) \\ &= \underset{C_o \times C_i}{MIN} \; p(H_M; R, G_{ii}), \end{aligned} \tag{4.5}$$

where $H_M(f)$ is the matched filter for $R(f)$ and $G_{ii}(f)$. That is

$$p_R = p(H_R; R_R, G_{iR}), \tag{4.6}$$

where $H_R(f)$ is the matched filter for the *least favourable* pair of signal and noise characteristics, $R_R(f)$ and $G_{iR}(f)$.

This solution, denoted by $(H_R; R_R, G_{iR}; p_R)$ represents a *saddlepoint* of the game. That is to say, for natures strategy, (R_R, G_{iR}), the designer can only reduce his payoff, $p(H; R_R, G_{iR})$, by varying H from H_R. Similarly, for the designers strategy, H_R, nature can only reduce her payoff, $(-p(H_R; R, G_{ii}))$ (and thereby increase the designers payoff) by varying (R, G_{ii}) from (R_R, G_{iR}). Hence, the *value* of the game, p_R, represents the worst payoff the designer can expect for his strategy, H_R, and the best payoff he can expect for nature's strategy,(R_R, G_{iR}).

The various references [4.1–4.5] dealing with robust matched filtering deal with particular problems in which the signal and interference uncertainties are specified in

various ways. The solutions are rarely, if ever, in closed form and generally involve unknown constants which must be solved for recursively. Since the formulations are not in the forms of mixed strategy games, it is necessary to show that the solutions do exist. The formulation and solution given in [4.1] are presented in slightly modified form below. This formulation closely resembles that presented in the next section for our joint (signal and filter) optimization problem. The original form was two-dimensional.

The criterion for optimization is again given by 4.4 with $p(H; R, G_{ii})$ given by 4.1 and the uncertainty classes specified as:

$$C_R = \left\{ R(f) : \int |R(f) - R_0(f)|^2 df \leq \delta \right\}, \tag{4.7}$$

$$C_i = \left\{ G_{ii}(f) : L(f) \leq G_{ii}(f) \leq U(f); \int G_{ii}(f) df = \sigma_i^2 \right\}, \tag{4.8}$$

where $R_0(f)$ is the nominal signal and δ is the maximum modeling error energy. $G_{ii}(f)$ is specified as lying between upper and lower bounds given by $L(f)$ and $U(f)$ respectively and the total interference power is specified to be σ_i^2 .

The solution presented in [4.1] is given in implicit form as:

$$R_R(f) = \frac{R_0(f) G_{iR}(f)}{G_{iR}(f) + c}, \tag{4.9}$$

$$G_{iR}(f) = \begin{cases} U(f) & \forall f \in R_U \\ L(f) & \forall f \in R_L \\ \frac{|R_R(f)|}{k} & \forall f \in R_M \end{cases} \tag{4.10}$$

$$\begin{aligned} \textit{where } R_U &= \{ f : kU(f) < |R_R(f)| \}, \\ R_L &= \{ f : |R_R(f)| \leq kL(f) \}, \\ R_M &= \{ f : kL(f) < |R_R(f)| \leq kU(f) \}, \end{aligned} \tag{4.11}$$

and the non-negative constants, k and c are chosen to satisfy:

$$c^2 \int \frac{|R_0(f)|^2}{[G_{iR}(f) + c]^2} df = \delta \tag{4.12}$$

$$\textit{and } \int_{R_L} L(f) df + \int_{R_U} U(f) df + \frac{1}{k} \int_{R_M} |R_R(f)| df = \sigma_i^2. \tag{4.13}$$

4.12 and 4.13 are derived from 4.7 and 4.8 by substitution from 4.9 and 4.10.

Necessary and sufficient conditions for the existence of non-negative constants, k and c satisfying 4.12 and 4.13 are derived in [4.1]. A sufficient condition is that $L(f)$, $U(f)$ and $|R_0(f)|$ are all finite and non-negative (consistent with their definitions) and that $L(f)$ and $U(f)$ are non-zero when $|R_0(f)|$ is non-zero. Also, if either δ or σ_i are zero, then the solution exists.

The solution may be interpreted in interesting ways. For example, the forms of H_R and p_R are consistent with an interpretation in which the constant, c, represents a white noise component added to the interference to account for the uncertainty in $R(f)$. Another observation is that R_R and G_{iR} are the most similar in shape of all the pairs of signals and interference spectra in the class $C_R \times C_i$ when the signal modeling error is assumed to be maximal. (This is equivalent to saying that R_R and G_{iR} are chosen to make H_R as flat as possible.)

The method of formulation, the form of the solution and the technique of proof given for this problem in [4.1] all contribute to the approach taken in the next section. However, there is no direct correspondence between the two problems.

§4.2 Robust Combinations of Signals and Filters

In the previous section we saw that the ML filter presented in chapter 2 is closely related to that class of filters known as matched filters, which are designed to maximize the SIR at the filter output. In fact the SIR for a matched filter is equal to the detection index introduced in chapter 3. Furthermore, we saw in chapter 3 that signals optimized with respect to a minimum local variance criterion could perform very poorly in relation to detection performance compared to those chosen to maximize the detection index.

We are led by these considerations to the approach taken in this chapter for dealing with uncertainties in the transmission path model. Firstly, our robust system must have good detection performance and it follows that we must optimize with respect to a detectability criterion. Secondly, we expect detection performance to depend on SIR.

Our approach, therefore, will be to maximize the minimum SIR over the uncertainty class of transmission paths by choice of the signal, $S(f)$, and the receiver filter, $H(f)$. We will see that, if we assume a fixed duration constant envelope signal as in chapter 3 then we need only optimize $G_{ss}(f)$, the signal power spectrum and $H_R(f)$, the optimum filter, must be specified in terms of the particular signal implementation, $S(f)$. The problem solution is fully defined, in analogy to the result discussed in the previous section, by specification of the least favourable transmission path.

Our first step, in developing this approach must be to determine how we shall specify the transmission path uncertainties. The starting point will be the precise transmission path model described in chapter 2 and summarized diagramatically in Fig. 2.3. That model was completely specified by means of three functions. $H_T(f)$ modeled the target path transfer function. $|H_C(f)|^2$ modeled the squared magnitude of the stochastic transfer function of the clutter path. $G_{nn}(f)$ represented the noise power spectrum. Our uncertain model will involve specified uncertainties in some of these functions.

Now, according to the discussion in section 4.0, these uncertainties arise as a result of imprecise estimation or because of variations in the transmission path characteristics. The noise power spectrum, $G_{nn}(f)$, however, is readily obtained, in most cases, by means of a passive measurement. Furthermore, because the noise is often generated in the front-end of the receiver or in the close proximity of the receiver, $G_{nn}(f)$ is usually quite stable. For these reasons we will assume that $G_{nn}(f)$ can be precisely specified.

The transmission path transfer functions, on the other hand, do require uncertain specifications and we will start by considering a direct analogy to the uncertain signal and noise models of the previous section. $H_T(f)$ will be taken as analogous to R(f) and $|H_c(f)|^2$ will be treated as an analogue of $G_{ii}(f)$. Thus we have:

$$C_T = \left\{ H_T(f) : \int |H_T(f) - H_0(f)|^2 \, df \leq \delta_T \right\} \tag{4.14}$$

$$C_c = \left\{ |H_c(f)|^2 : \; L_c(f) \leq |H_c(f)|^2 \leq U_c(f); \; \int |H_c(f)|^2 \, df = \sigma_c^2 \right\} \tag{4.15}$$

The forms of these specifications are appealing because the values of δ_T, $L_c(f)$ and $U_c(f)$ could be readily estimated by processing a representative set of measurements. However, they do suffer from some drawbacks which were much less relevant in the analogous example discussed in [4.1]. These difficulties only arise when the uncertainties being specified arise from variability in the actual transmission path.

Consider,firstly, how one would go about constructing a specification for C_T. One would presumably have available a set of functions, $H_T(f)$ belonging to the class to be modeled. (Methods for obtaining these functions will be discussed in chapter 6) Let us assume,for the purpose of this discussion, that this set is known to include bounding functions of the class for which the inequality in 4.14 is an equality. We could choose $H_0(f)$ to be the mean of the functions of the set and find δ_T for 4.14 by evaluating the integral in 4.14 for each function in our representative set. However, this approach might yield an unnecessarily large value for δ_T. In other words the class C_T might be broader

than necessary to accommodate all the functions in our set of measurements. A better way to choose $H_0(f)$ would be to select the function which minimized the maximum value of the integral in 4.14 over the set of measurements. This approach would yield a class, C_T, as defined in 4.14, which was just sufficiently broad to accommodate all the functions in our representative set.

The question arises, however, as to whether the form of the specification, 4.14, prevents us from reducing the size of C_T even further. To what extent this is true depends on the nature of the uncertainty being modeled.

In some cases of practical interest such as ultrasonic sensing through fleece [1.1] an important contribution to the variability of $H_T(f)$ arises from variations in the medium attenuation and this has important implications in the context of the present discussion. The medium attenuation is usually coloured. However we can illustrate rather simply the inadequacy of the specification in 4.14 by considering a flat attenuation.

Imagine that the only source of variation in $H_T(f)$ was a flat attenuation which varied by an order in magnitude. Then we should be able to specify $H_T(f)$ exactly apart from a scale factor. However, if we construct a specification as in 4.14, the class prescribed will include a wide variety of different colourations and phase responses, few of which can exist in the true class being modeled. In fact the specification would be so broad as to be virtually useless as a description of the transmission path.

A considerable improvement can be obtained by specifying C_T in the following way:

$$C_T = \left\{ \begin{array}{c} H_T(f): \qquad H_T(f) = AH_{TT}(f), \\ e_T = \int_{f_A}^{f_B} |H_{TT}(f) - H_0(f)|^2 \, df \leq \delta_T, \\ A \geq A_{min} \end{array} \right\} \tag{4.16}$$

where f_A and f_B represent the frequency bounds within which we wish to perform our optimization.

When constructing a specification of the form given in 4.16 from a set of mea-

surements, one would minimize the size of the class, C_T by choosing A for any function, $H_T(f)$, in the set of measurements, such that the corresponding error energy, e_T as defined in 4.16, is minimized. $H_0(f)$ is chosen to minimize the maximum value of e_T over the set of measurement functions when A is chosen in this fashion for each function.

The construction of such a specification from a set of measurements is a somewhat complex procedure. However the form of this specification more closely represents the types of uncertainties which would have to be represented in practice. Later in this chapter and in chapter 6 we will consider obtaining an approximate robust optimum solution by applying techniques which avoid these difficulties and those associated with computing an exact mathematical solution.

The specification, 4.15, also needs modifying. This is because, in practice, the integral in 4.15 can be expected to vary significantly over the true class of conditions to be represented in many situations. A better specification is:

$$C_c = \left\{ \begin{array}{c} |H_c(f)|^2 : \; L_c(f) \leq |H_c(f)|^2 \leq U_c(f); \\ P_c = \int_{f_A}^{f_B} |H_c(f)|^2 \, df \leq \sigma_c^2 \end{array} \right\} \tag{4.17}$$

The remaining shortcoming of the form of the model represented by 4.16 and 4.17 is that it does not take account of dependencies which may exist between the variations in $H_T(f)$ and those in $|H_c(f)|^2$, and between A and $H_{TT}(f)$.The penalty paid for not taking these dependencies into account may be a reduction in detection index over the true class of conditions encountered because the system will be optimized for robust performance over a broader class than necessary. However, 4.16 and 4.17 remain relatively simple and further complication is probably unjustified.

We have now developed suitable forms for the specifications of the target and clutter path transfer function classes. We now need to derive an expression for SIR in terms of the signal power spectrum, the noise power spectrum and the target and clutter path transfer functions. Once we have such an expression (for the payoff in our game)

we can attempt to maximize its minimum value over the classes of transfer functions (nature's strategies) by choice of the signal power spectrum and the receiver filter (the designer's strategy).

Restating our problem explicitly, we wish to find $H_R(f)$ and $S_R(f)$ (where "R" denotes a robust-optimal function) such that the minimum value of $p\left(H_T, |H_c|^2 ; H, S\right)$ over the classes, C_T and C_c given in 4.16 and 4.17 is maximized, where:

$$p\left(H_T, |H_c|^2 ; H, S\right) = \frac{\left|\int_{f_A}^{f_B} S(f) H_T(f) H(f) df\right|^2}{\int_{f_A}^{f_B} \left[G_{ss}(f) |H_c(f)|^2 + G_{nn}(f)\right] |H(f)|^2 df} \tag{4.18}$$

where $G_{ss}(f)$ is the power spectrum of the signal, $S(f)$. Note that $p\left(H_T, |H_c|^2 ; H, S\right)$ is simply the SIR obtained by substitution into equation 4.1. It may also be regarded as the designer's payoff with the pair of arguments to the left of the semi-colon representing nature's strategy and those to the right of the semi-colon representing the designer's strategy.

Now, equation 4.18 still involves the Fourier transform, $S(f)$, of the transmitted signal. We shall therefore manipulate it so that it only involves the power spectrum of the transmitted signal. This simplifies the solution process. Without loss of generality, we can write:

$$H(f) = K S^*(f) H_s(f)$$

which defines $H_s(f)$ and where K is an arbitrary constant.Further, if S(f) is a constant envelope signal of duration T then 4.18 can be written:

$$p\left(H_T, |H_c|^2 ; H, G_{ss}\right) = \frac{T\left|\int_{f_A}^{f_B} G_{ss}(f) H_T(f) H_s(f) df\right|^2}{\int_{f_A}^{f_B} \left[G_{ss}(f) |H_c(f)|^2 + G_{nn}(f)\right] |H(f)|^2 df} \tag{4.19}$$

The saddlepoint solution to this problem is fully specified by the least favourable pair of target and clutter transfer functions, $H_{TR}(f)$ and $|H_{cR}(f)|^2$ from within the classes, C_T and C_c. H_R and G_R are optimal for this least favourable choice, with G_R

being the robust-optimal signal power spectrum. The saddlepoint is defined by:

$$p\left(H_T,|H_c|^2;H_R,G_R\right)\geq p\left(H_{TR},|H_{cR}|^2;H_R,G_R\right)\geq p\left(H_{TR},|H_{cR}|^2;H,G_{ss}\right) \quad (4.20)$$

This solution is given in the theorem below which is proved in Appendix 4.

Theorem 5. *For the classes, C_T and C_c, and the noise power spectrum, $G_{nn}(f)$, the robust filter and signal pair (H_R,G_R) satisfying 4.20 is that pair which is optimal for the pair of least-favourable transfer functions defined by:*

$$H_{TR}(f) = \frac{A_{min}H_0(f)\left(G_{nn}(f)+G_R(f)\,|H_{cR}(f)|^2\right)}{G_{nn}(f)+G_R(f)\left(|H_{cR}(f)|^2+c\right)} \quad (4.21)$$

$$|H_{cR}(f)|^2 = \begin{cases} U_c(f) & \forall f\in R_U \\ L_c(f) & \forall f\in R_L \\ \frac{G_R|H_{TR}(f)|-k_1G_{nn}(f)}{k_1G_R(f)} & \forall f\in R_M \end{cases} \quad (4.22)$$

$$\textit{where:}\qquad G_R(f) = \begin{cases} \frac{k_2|H_{TR}(f)|(G_{nn}(f))^{1/2}-G_{nn}(f)}{|H_{cR}(f)|^2} & \forall f\in R_T\cap\bar{R}_0 \\ 0 & \forall f\in R_0 \end{cases} \quad (4.23)$$

$$\left.\begin{aligned} R_U &= \{f: k_1\left[G_R(f)U_c(f)+G_{nn}(f)\right] < G_R(f)\,|H_{TR}(f)|\}\subset R_T \\ R_L &= \{f: k_1\left[G_R(f)U_c(f)+G_{nn}(f)\right] \geq G_R(f)\,|H_{TR}(f)|\}\subset R_T \\ R_M &= \bar{R}_L\cup\bar{R}_U\subset R_T \\ R_0 &= \left\{f: A_{min}k_2\,|H_{TR}(f)|\leq (G_{nn}(f))^{1/2}\right\}\subset R_T \\ R_T &= \{f: f_A<f\leq f_B\} \end{aligned}\right\} \quad (4.24)$$

The non-negative constants, k_1, k_2 and c must be chosen to satisfy the three equations below and a sufficient condition for their existence is that $G_{nn}(f)$, $|H_0(f)|$, $L_c(f)$ and $U_c(f)$ are all finite, non-negative real functions on R_T and that γ_T and σ_c^2 are finite non-negative real numbers while P_s is a finite positive real number. We have:

$$\int_{R_T}|H_{cR}(f)|^2\,df = \sigma_c^2 \quad (4.25)$$

$$c^2\int_{R_T}\frac{|H_0(f)|^2}{\left[|H_{cR}(f)|^2+c\right]^2}df = \gamma_T \quad (4.26)$$

$$\int_{R_0 \subset R_T} G_R(f)df \;=\; P_s \tag{4.27}$$

Equations 4.25 and 4.26 arise from the constraints within the class descriptions for the clutter path transfer function and the target path transfer function, respectively. Equation 4.27 arises from the signal energy constraint. In general it will be necessary to solve 4.25-4.27 iteratively for k_1, k_2 and c.

An explicit form of the above solution is derived in Appendix 4 in which the right hand sides of the equations, 4.21-4.24, and both sides of the equations,4.25-4.27 are cleared of H_{TR}, H_{cR} and G_R. An interpretation of this result is presented in section 4.3. The solution is:

$$|H_{TR}(f)| \;=\; \begin{cases} \frac{A_{min}|H_0(f)|U_c(f)+c/k_2(G_{nn}(f))^{1/2}}{U_c(f)+c} & \forall f \in R_U \\ \frac{A_{min}|H_0(f)|L_c(f)+c/k_2(G_{nn}(f))^{1/2}}{L_c(f)+c} & \forall f \in R_L \\ A_{min}\,|H_0(f)| - k_1 c & \forall f \in R_M \end{cases} \tag{4.28}$$

$$\arg\left(H_{TR}(f)\right) \;=\; \arg\left(H_0(f)\right) \forall f \in R_T \tag{4.29}$$

$$|H_{cR}(f)|^2 \;=\; \begin{cases} U_c(f) & \forall f \in R_U \\ L - c(f) & \forall f \in R_L \\ \frac{A_{min}k_2|H_0(f)|-(G_{nn}(f))^{1/2}}{k_1 k_2} - c & \forall f \in R_M \end{cases} \tag{4.30}$$

$$\left.\begin{aligned} R_U &= \left\{ f : k_1 k_2 \left(U_c(f) + c\right) < A_{min} k_2 \,|H_0(f)| - \left(G_{nn}(f)\right)^{1/2} \right\} \subset R_T \\ R_M &= \left\{ f : k_1 k_2 \left(L_c(f) + c\right) < A_{min} k_2 \,|H_0(f)| - \left(G_{nn}(f)\right)^{1/2} \right\} \subset R_T \\ & \qquad A_{min} k_2 \,|H_0(f)| - \left(G_{nn}(f)\right)^{1/2} \le k_1 k_2 \left(U - c(f) + c\right) \\ R_L &= \left\{ f : A_{min} k_2 \,|H_0(f)| - \left(G_{nn}(f)\right)^{1/2} \le k_1 k_2 \left(L_c(f) + c\right) \right\} \subset R_T \\ R_0 &= \left\{ f : A_{min} k_2 \,|H_0(f)| - \left(G_{nn}(f)\right)^{1/2} \le 0 \right\} \subset R_T \end{aligned}\right\} \tag{4.31}$$

k_1, k_2 and c are then chosen to satisfy:

$$\begin{aligned} &\int_{R_U} U_c(f)df + \int_{R_L} L_c(f)df \\ &\qquad + \int_{R_M} \left(\frac{A_{min} k_2 \,|H_0(f)| - \left(G_{nn}(f)\right)^{1/2}}{k_1 k_2} - c \right) df \;=\; \sigma_c^2 \end{aligned} \tag{4.32}$$

$$c^2 \int_{R_U} \frac{|H_0(f)|^2}{(U_c(f)+c)^2} df + c^2 \int_{R_L} \frac{|H_0(f)|^2}{(L_c(f)+c)^2} df + c^2 k_1 k_2 \int_{R_M} \frac{|H_0(f)|^2}{\left[A_{min} k_2 |H_0(f)| - (G_{nn}(f))^{1/2}\right]^2} df = \delta_T \tag{4.33}$$

$$k_1 k_2 \int_{R_M} (G_{nn}(f))^{1/2} df + \int_{R_U} (G_{nn}(f))^{1/2} \frac{A_{min} k_2 |H_0(f)| - (G_{nn}(f))^{1/2}}{U_c(f)+c} df + \int_{R_L \subset \bar{R}_0} (G_{nn}(f))^{1/2} \frac{A_{min} k_2 |H_0(f)| - (G_{nn}(f))^{1/2}}{L_c(f)+c} df = P_s \tag{4.34}$$

The resulting form of G_R is:

$$G_R(f) = \begin{cases} \frac{A_{min} k_2 |H_0(f)| - (G_{nn}(f))^{1/2}}{U_c(f)+c} (G_{nn}(f))^{1/2} & \forall f \in R_U \\ \frac{A_{min} k_2 |H_0(f)| - (G_{nn}(f))^{1/2}}{L_c(f)+c} (G_{nn}(f))^{1/2} & \forall f \in R_L \subset \bar{R}_0 \\ k_1 k_2 (G_{nn}(f))^{1/2} & \forall f \in R_M \\ 0 & \forall f \in R_0 \end{cases} \tag{4.35}$$

The existence of non-negative constants, k_1, k_2 and c satisfying 4.32-4.35 is also proved in Appendix 4 under certain minor restrictions. As a by-product of that analysis we see that 4.32 can be solved for k_1 given any allowable values for k_2 and c. Similarly, 4.33 can always be solved for c provided $\delta_T \leq E_0$ and 4.34 can always be solved for k_2.

An appropriate procedure for solving these simultaneous equations recursively, is presented in chapter 6 along with the listing of a computer program that implements the procedure. The convergence properties of this procedure are also investigated in chapter 6.

§4.3 Discussion

The solution given by 4.21 to 4.35 can be interpreted in several interesting ways. It appears that c represents a white component added to the squared magnitude of the clutter path transfer function. To see this from equations 4.23 and 4.2 by substitution from equation 4.21, we can obtain:

$$G_R(f) = \frac{(G_{nn}(f))^{1/2}\left[A_{min}k_2|H_0(f)| - (G_{nn}(f))^{1/2}\right]}{|H_c(f)|^2 + c} \tag{4.36}$$

$$\text{and } H_R(f) = \frac{A_{min}H_0(f)}{G_{nn}(f) + G_R(f)\left(|H_{cR}(f)|^2 + c\right)} \tag{4.37}$$

It is immediately apparent, from comparison of 4.36 and 4.37 with equations 3.16 and 2.15, respectively (taking into account that $H_R(f)S_R(f)$ is proportional to the optimal correlation reference), that this robust optimum solution is also optimum for a pair of transmission path characteristics given by:

$$H_T(f) = A_{min}H_0(f)$$

$$|H_c(f)|^2 = |H_{cR}(f)|^2 + c$$

Another observation is that $H_{TR}(f)$ and $|H_{cR}(f)|^2$ are chosen such that the function $|H_R(f)|^2 G_R(f)$ is as flat as possible. In R_M, for example, we have:

$$|H_R(f)|^2 G_R(f) = \frac{|H_{TR}(f)|^2 (G_R(f))^2}{\left[G_{nn}(f) + G_R(f)|H_{cR}(f)|^2\right]^2} = k_1^2$$

An interpretation of this is that the least-favourable transmission path is that which allows the designer to use the least *overall* colouration to obtain optimum performance. A similar interpretation applies to the robust optimum matched filter result discussed in the previous section.

A result which was fully expected is that the value of A_{min} does not affect the robust optimum solution. This can be seen by inspecting 4.36 and 4.37. In 4.36 k_2 is

adjusted to provide the required signal power. Hence any change in the value of A_{min} will always be offset by a change in the value of k_2. In 4.37 A_{min} simply scales the optimum filter transfer function and therefore has no effect on the SIR. The nett result is the same as if we simply dropped the third inequality from the specification, 4.16, provided we adhere to the same procedure in constructing that specification.

We can summarize the characteristics of the least favourable transmission path (with A retained for completeness) as follows:

1)	$A = A_{min}$.	The mean magnitude of the target path transfer function is minimal.
2)	$e_T = \delta_T$.	The modeling error of the target path transfer function is maximal. That is to say, the transfer function is as different from the nominal transfer function as possible.
3)	$P_c = \sigma_c^2$.	The clutter path transfer function has maximum "power".
4)	$\arg(H_{TR}(f)) = \arg(H_0(f))$.	The phase response of the target path is that of the nominal target path.
5)	$\lvert H_R(f)\rvert^2 G_R(f)$ is as flat as possible.	The optimum overall colouration provided by the signal and filter pair is minimal.

These characteristics can aid in identifying, approximately, the least favourable path as discussed later.

The importance of Theorem 5 lies in the fact that its proof demonstrates that, for a realistic formulation of the problem, a solution exists. In order to design the robust optimum system one must firstly identify the least favourable path. It is possible to do

this approximately without solving the equations, 4.32 to 4.35.

For example, we may have a set of pairs of functions, $\left(H_T(f), |H_c(f)|^2\right)$. Then, we can simply compare their optimal detection indices and choose the pair yielding the smallest value.

One advantage of this approach is that it does take account of the dependencies between A, $H_T(f)$ and $|H_c(f)|^2$ discussed in the previous section. It can therefore be expected to produce a less conservative result.

In Chapter 6 this approach is compared to the alternative of specifying the uncertainty classes as in 4.16 and 4.17 and then solving for the solution given in Theorem 5. A practical example is used to illustrate the comparison.

5. CONDITIONAL M.A.P. ESTIMATION

§5.0 Using Prior Information

Woodward[2.1] once wrote, in relation to signal parameter estimation, "guesswork destroys information". What he meant was that using guesswork in performing an irreversible process on a signal prevents any later process from extracting information from the signal by using more reliable prior information. The way to extract from a signal the maximum quantity of information about a parameter is to use all available relevant prior information in the process.

In chapter 2, we saw that ML estimation is a process in which no prior information is used while MAP estimation uses *all* the prior information that exists. This is because MAP estimation explicitly uses the prior probability density function (PDF) of the parameter being estimated. Furthermore, it uses that function in an optimal way. Now the prior PDF contains *all* the prior information about the parameter. It is not surprising, therefore, that, as we shall shortly see, in several senses, MAP estimation is optimal.

However, the statement that the MAP estimator uses the prior PDF in an optimal way requires justification and an explanation. The MAP estimator uses the prior PDF together with the LLF to construct the posterior PDF as we saw in chapter 2. The MAP estimate is then chosen to maximize that posterior PDF. Thus it is the most probable value of the parameter, taking in to account all the relevant information that exists.

Furthermore, if the posterior PDF is symmetrical, the MAP estimate is the min-

imum mean squared error (MMSE) estimate of the parameter [2.3,2.4]. This symmetry requirement is often satisfied approximately in practice. The reason is, simply, that there are usually a large number of independent contributions to our uncertainty about the value of the parameter to be estimated. Hence, we can invoke the central limit theorem[5.1] to show that the posterior PDF is approximately normal and therefore closely symmetrical. Usually, we want to minimize the mean squared error and we can do this by choosing the MAP estimate if we can obtain such an estimate.

However there is a difficulty with the implementation of MAP estimation techniques in practical signal parameter estimation applications (particularly in real time). The problem is that, nearly always, much of the prior information about the parameter to be estimated is unavailable to the estimator. It exists, and could be assembled into a prior PDF if time permitted and the necessary mechanism for doing so existed. However, such a scheme is usually quite impractical.

In section 5.2, a simpler problem will be tackled in which only the most readily available prior information is used in an optimal, yet practical way. However, the conventional approach is to use GML estimation as defined in chapter 2. Now a parameter gate represents an explicit and usually inaccurate assumption about the nature of the prior PDF. Hence, GML estimation involves guesswork in an irreversible operation and, therefore, the destruction of useful information.

Nevertheless, GML estimation is, and will continue to be, a highly practical and efficacious estimation technique. In many applications, the penalty paid for using guesswork in this way is small while the cost of incorporating a more optimal use of prior information might well be prohibitive.

In this chapter we will investigate the performance and design of both GML and conditional MAP range estimators. The investigation will be carried out with the aid of simulation software developed by the author for the purpose and will, incidentally, provide empirical verification of many of the theoretical results of chapters 2 and 3.

§5.1 Range Gating

5.1.1 Locked Range Gates

The relationship between range gate width and performance has been investigated in chapters 2 and 3. We have seen theoretical evidence that the detection threshold falls as the range gate width is reduced. Indeed, as we have seen, sufficiently narrow gates can eliminate the detection problem entirely.

Based on this evidence alone, we might be led to the conclusion that the smaller the gate the better the performance. However, there are, of course, other factors to consider and these will be examined in the next subsection. These factors only become evident when we look at a practical implementation of range gating in which the gate must track the target.

In this subsection, however, we shall examine the performance of a system employing a hypothetical range gate that is always locked on to the target in order to verify the theoretical results of chapters 2 and 3 prior to extending them in the remainder of this chapter. Our investigation will involve gathering simulation results for comparison with the corresponding theoretical results that were obtained in chapter 3.

The operation of a system employing the optimal spectra of chapter 3 through the transmission path of Fig. 3.4 has been simulated. In the simulations, one hundred post-correlation waveform envelopes were generated for each signal tested. These were all produced by independent random processes that will be explained shortly. Each of four different post-correlation processing techniques was applied to each of the hundred post-correlation waveform envelopes and the root-mean-square (RMS) estimation error was computed for each technique for each signal.

The form of the post-correlation waveform envelope was computed by the construction of the transform of the complex analytic waveform, transforming it to the

time domain and computing its magnitude. The frequency domain computation simply involved computing $R_0(f)$ as given by equation 3.31 from the signal power spectrum, $G_{ss}(f)$, and the transmission path characteristics and an additive complex interference transform whose squared magnitude was given by $2G_{i0}(f)$ as given in equation 3.32. The factor of two accounts for the contribution of the Hilbert transform of the interference to the complex analytic interference power[2.1].

The interference sequence was constructed by first generating a sequence of independent random complex variables whose magnitude had a variance of 2. This sequence actually represents the transform of the complex analytic post-whitening interference. This sequence is then multiplied by the square root of a discrete form of $G_{i0}(f)$.

The way in which the white interference transform was generated is of some interest. The individual real and imaginary samples are all independent of each other and of unity variance. Furthermore, the samples were generated in such a way that their distribution was closely normal. It is an assumption of the derivation of the ML estimator that the time domain white interference be normally distributed and, from the central limit theorem, we find that that assumption corresponds to an assumption of normally distributed interference samples in the frequency domain also. Each frequency domain sample represents a summation over many time domain samples. It was appropriate, therefore, in the simulations, to use samples that were approximately normally distributed.

Such normally distributed random samples were obtained by adding together twelve samples whose distribution was uniform in the range from 0. to 1. and subtracting the value, 6., from the result to remove the mean. It is well known[5.1] that a random variable, uniformly distributed over a unity range has a variance of $\frac{1}{12}$ and that the variances of independent random variables add when the corresponding variables are summed. It follows that the samples generated by the above method had unity variance. It is also well known[5.1] that summing just three uniformly distributed random

numbers produces a number with a nearly normal distribution (at least within two standard deviations of the mean). It follows, then, that the required close approximation to a normal distribution was easily achieved by the above procedure.

Finally,the transform of the post-correlation waveform was set to zero for negative frequencies,while, for positive frequencies, the transform was obtained by adding $R_0(f)$ to $2G_{i0}(f)$. Hence, the inverse transformation (via a 512 point FFT) produced a complex analytic sequence in the time domain, as required.

An additional feature was added in that the target delay was made to vary randomly by simply shifting the complete post-correlation waveform envelope by a discrete amount obtained by quantization of a white, normally distributed, zero mean, random number. The RMS value of this number was specified by the user of the simulation program. The reason for this feature will not become clear until the next subsection because the results in this subsection were obtained by centring the range gate on the shifted time origin which always corresponded to the peak of the target echo.

Plotted in Fig. 5.1 is the RMS delay estimate error obtained by simulation using MDI signals with a 200uS range gate for the transmission path of Fig. 3.4 over a range of signal power. The theoretical local variance of chapter 3 is also plotted. We see that there is very close agreement and as predicted in chapter 3, we see no threshold phenomenon associated with poor detection performance. The discrepancy at low signal power is consistent with the local variance estimate being a lower bound to which the true variance tends assymptotically.

Fig. 5.2 displays a similar comparison for MV signals. For any signal power above about 18dB we again see that the agreement is very good. At lower powers we see the effects of signal ambiguity and poor detection. For example, between 14dB and 16dB in signal power the curve is at its steepest because this is the location of the detection threshold. Above 16dB in signal power, the curve flattens out but steepens again above 17dB as the ambiguity threshold is reached. All this is in excellent agreement with the

Figure 5.1 *Range Accuracy with MDI Signals*

(Range gate is 200μS locked)

——— Simulation results

– – – – – Theoretical Estimate

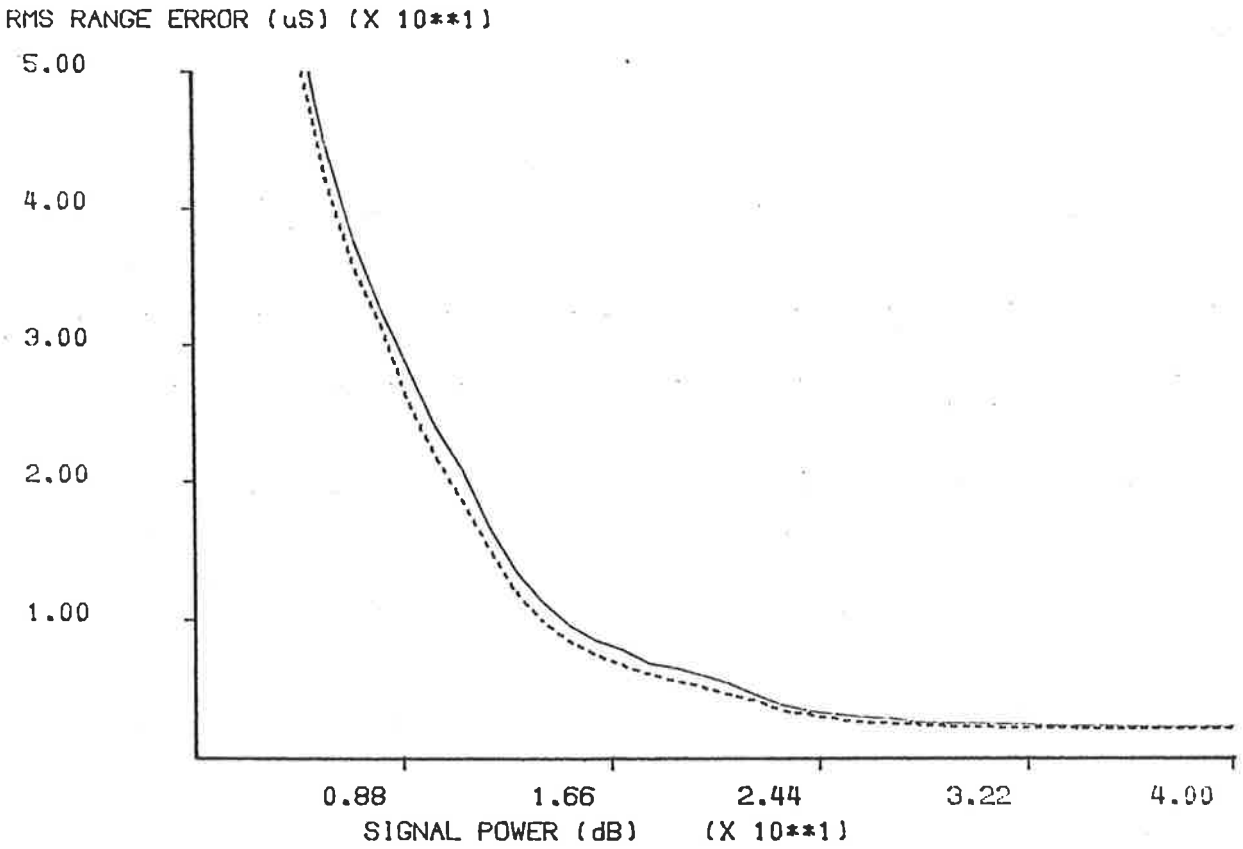

Figure 5.2 *Range Accuracy with MV Signals*

(Range gate is 200μS locked)

——— Simulation results

– – – – – Theoretical Estimate

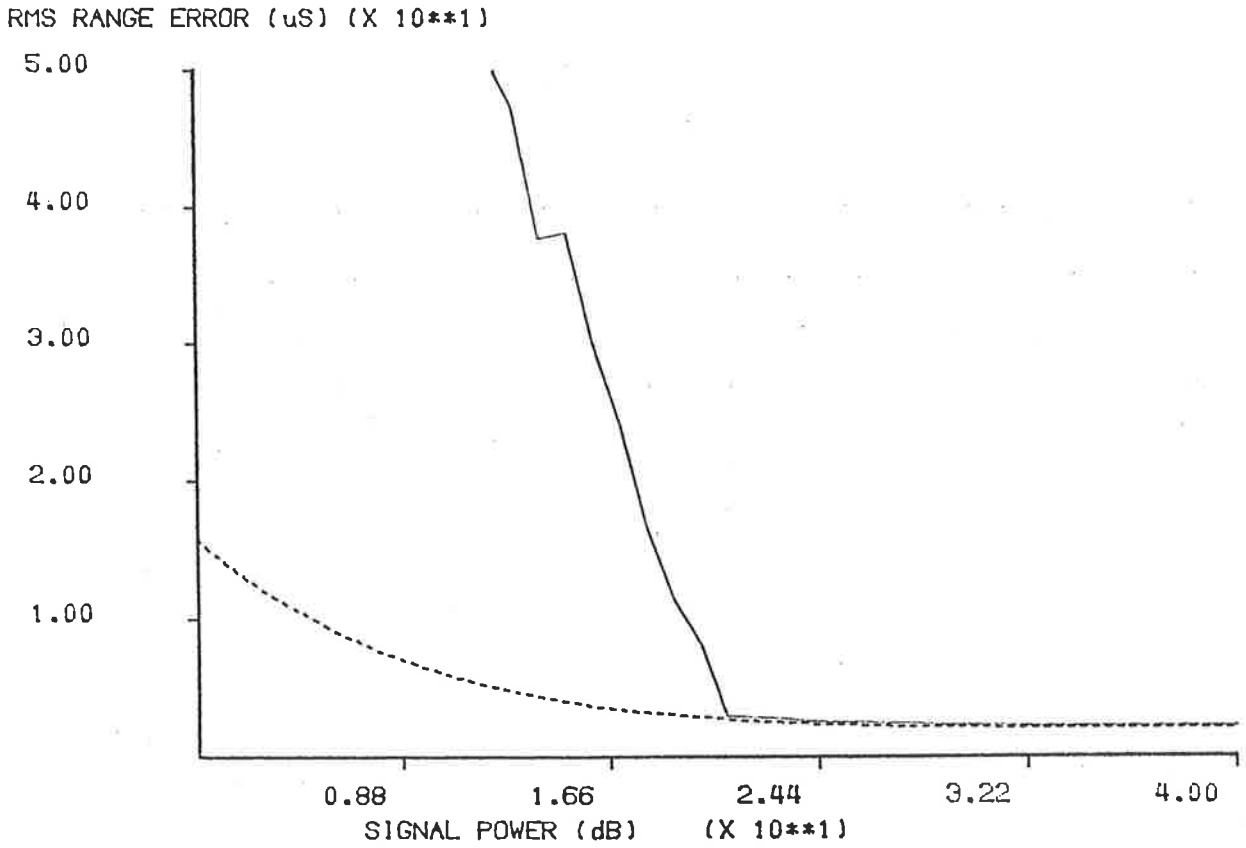

analyses and theoretical results of chapter 3.

Fig. 5.3 compares the simulation results with the theoretical results for mixed criteria signals. The latter signals were obtained using a detection index constraint of 14dB. Again we observe an excellent agreement except in the region of 16dB in signal power where some deterioration in performance is evident due to signal ambiguity. Even with this problem, however, the mixed optimum signals still yield performance better than or equal to that obtained with either of the other two types of signal at all signal powers. The greatest gains over the performance with MDI spectra are made in the region of signal power from about 14dB to 25dB as expected. Direct comparison reveals that an improvement of more than a factor of two in range accuracy are achievable in this region by the use of mixed criteria optimum spectra rather than MDI spectra. Furthermore a vast improvement over MV signals is evident for any signal power below about 22dB because of the ambiguity and detection problems encountered with the latter types of signal at low signal power. Here again we have excellent agreement with the analyses of chapter 3.

5.1.2 Tracking Range Gates

Practical systems, of course, cannot use range gates that are locked onto the target. The gate must always be centred on a prediction of the target delay and that prediction is often based on previous estimates of the target delay. We shall call this type of gate a tracking range gate.

The question that arises is how narrow to make the gate. As we reduce the gate width, the detection problem is reduced because, as we have seen in chapters 2 and 3, the detection threshold falls as the gate width is reduced and may even disappear completely. However, at the same time, the probability of missing the peak of the target echo completely (because it lies outside the gate) increases. We shall call the occurrence of this phenomenon (of missing the target) a gating error.

Figure 5.3 *Range Accuracy with Mixed Criteria Optimum Signals*

(Range gate is 200μS locked, detection index constraint is 14dB)

——— Simulation results

– – – – Theoretical Estimate

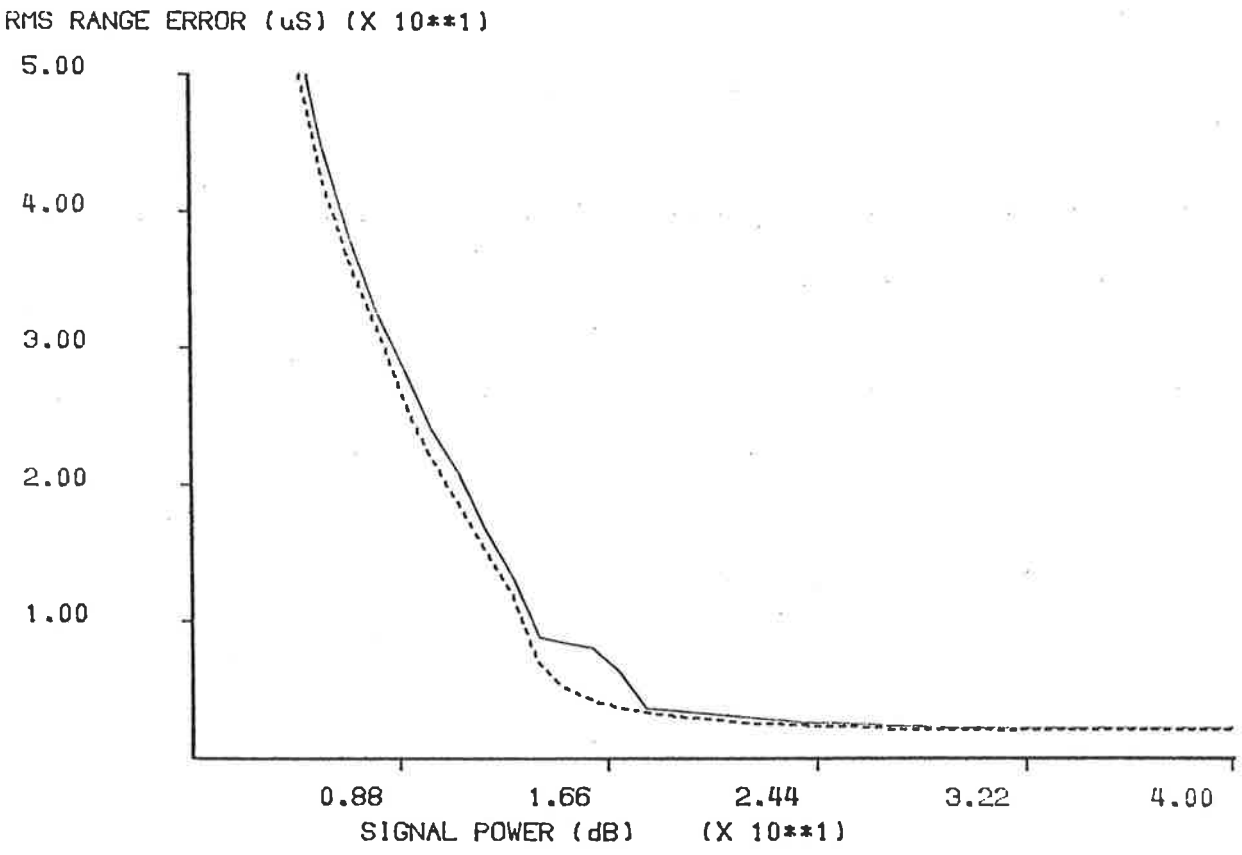

There are two obvious ways of approaching the problem theoretically, based on different assumptions about the way in which the prediction error is distributed. The use of a range gate is most consistent with the assumption that the prediction error is rectangularly distributed. If this is so and the gate width is made equal to the width of that rectangle, then the GML estimator will be using all the useful information in the received waveform but ignoring the spurious information outside the region of range within which the target is known to lie. However, the estimator only has available to it the estimated variance of the prediction, rather than the width of the error distribution. Since this is in direct proportion to that width, however, it is possible to set the gate width equal to the width of the assumed rectangular error distribution. The gate width is chosen such that a rectangular error distribution having the same width as the gate would have a variance equal to the estimated variance of the prediction. The variance of a rectangular distribution is simply related to the width of the rectangle and thus we have:

$$\sigma_e^2 = \frac{W^2}{12} \tag{5.1}$$

where σ_e^2 is the prediction error variance and W is the range gate width in units of delay.

In other words, we should choose:

$$W = 3.5\sigma_e. \tag{5.2}$$

If the prediction PDF *is* rectangular, then this choice will ensure that the probability of a gating error is very small while keeping the detection threshold low thereby minimizing the estimate variance.

In practice, however, a more reasonable assumption is that the prediction is distributed normally. Such an assumption can in fact be justified without reference to the prediction process. This avenue will be explored in the next section.

Under a Gaussian assumption, we can adjust our gate width to provide any

required probability of gating error. That probability is given by:

$$P_g = 1 - 2erf\left(\frac{W}{2\sigma_e}\right) \tag{5.3}$$

From 5.3, for example, we see that, for a range gate width of $4\sigma_e$, the probability of a gating error is about .05 while for a gate width of $2\sigma_e$ it is about .32.

In practice, the estimate variance is a complicated function of the gate width depending on the local variance, the probability of false detection within the gate and the distribution of prediction errors outside the gate. Gating errors can be disastrous in that the system may completely lose track of the target as a result of such errors. The probability of this happening is dependent on the predictability of the target range and on the details of the prediction process.

The simulation methods employed in this sub-section are designed to illustrate the concepts described above, rather than to simulate realistically any particular implementation. Two adaptive tracking gates have been simulated whose widths were related to an estimate of the RMS prediction error. This estimate adapts during the "run" of one hundred pulse-echo cycles.

The initial prediction was the unshifted time origin, which was the mean target delay. The initial error estimate was $\frac{1}{\sqrt{12}}$ times the width of the data window which was 1024uS. Thereafter, the prediction was the mean of ten previous range estimates, with all estimates prior to the commencement of the run being set to mean target range. The error estimate was the root-mean-square of all the actual estimate errors to that point in the run.

The independent random variations in the target delay mentioned in subsection 5.1.1 represent unpredictable variations in the range of an actual target. The predictability of the target range can thus be adjusted by specifying the RMS value of this random variation. The fact that the mean target delay is constant simplifies the prediction process but does not detract from the generality of the results.

Figure 5.4 *Adaptive GML Estimation with MV Signals*

(RMS unpredictable target range variation is $5\mu S$)

——— $W = 2\sigma_e$

– – – – $W = 4\sigma_e$

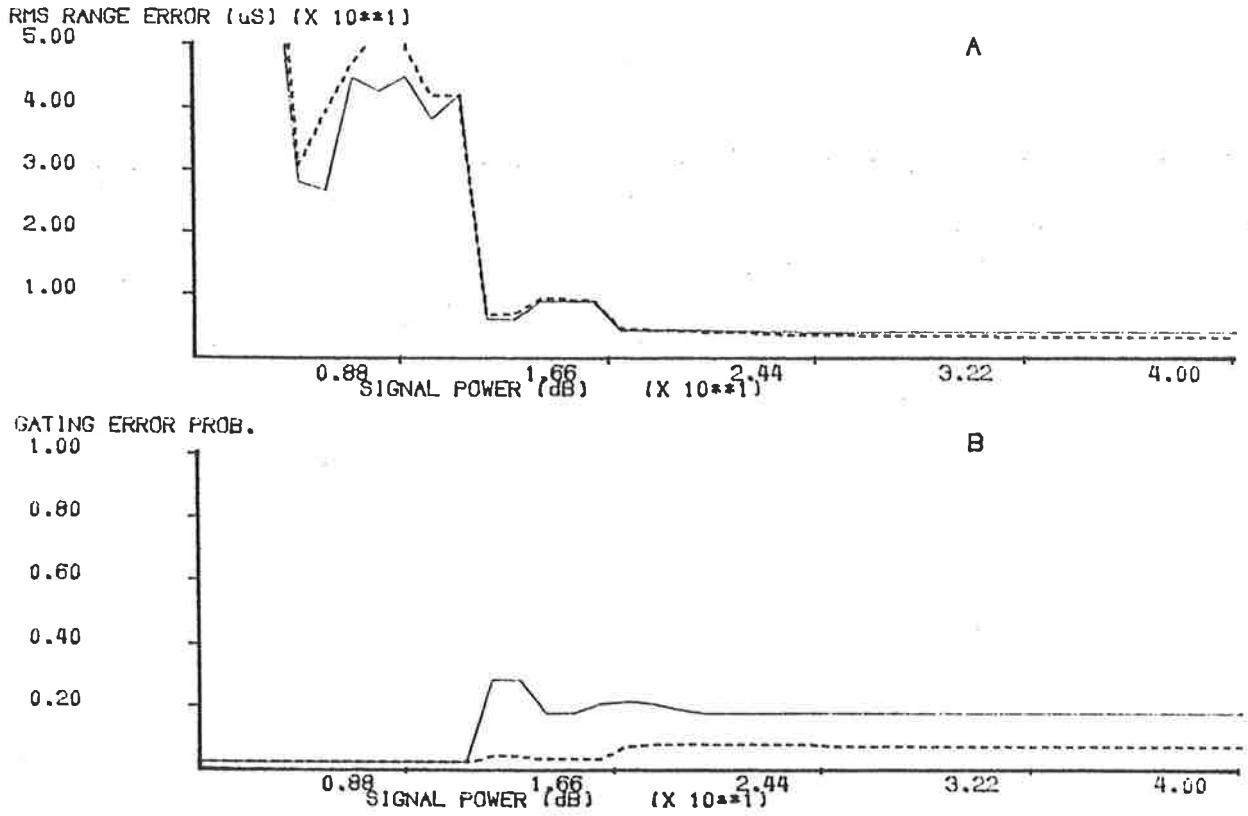

Figure 5.5 *Adaptive GML Estimation with MV Signals*

(RMS unpredictable target range variation is $50\mu S$)

——————— $W = 2\sigma_e$

– – – – – $W = 4\sigma_e$

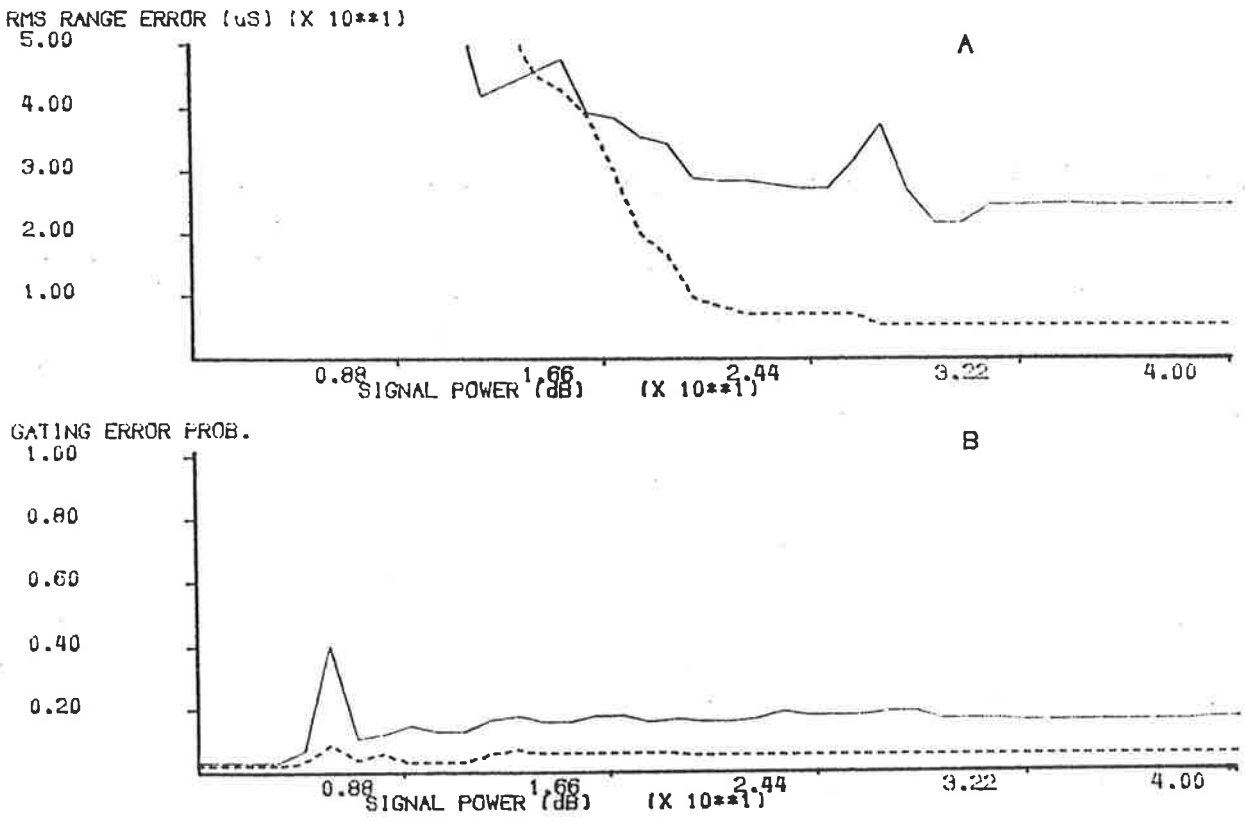

The results displayed in Figs. 5.4 and 5.5 were obtained for two different ratios of gate width to estimated RMS prediction error; namely 2 and 4. Fig. 5.4A represents the error that would be observed for a highly predictable target with RMS unpredictable variation of delay being only 5uS. Fig. 5.5A displays the results obtained for a very unpredictable target whose unpredictable delay variations had an RMS value of 50uS. In both cases MV signals were employed for a range of signal power. Figs. 5.4A and 5.5A should be analyzed in conjunction with Figs. 5.4B and 5.5B which display the corresponding gating error probabilities.

Now, in Fig. 5.4A, we see that the detection threshold has a much more pronounced effect in that the curves are extremely steep over a narrow range of signal power. The reason for this is the positive feedback effect provided by the coupling between the prediction error and the gate width. The gate is always wide at the start of a run. If the signal power is such that the system is operating well below threshold for this wide gate, then the gate will remain wide. This is because the estimate will be distributed uniformly in the gate with a large variance so that the prediction error will also be large. If, however, the system is in the threshold region for the initial wide gate, then the estimate will not be distributed uniformly in the gate and the estimate variance will be small enough so that the prediction error will be reduced from its original assumed value. As a result, the gate width will be reduced, the detection threshold will drop, the detection margin will rise and the estimate error will fall still further.

As a result of this effect, an adaptive gate width can extend the usefulness of a system to much lower signal power because the initially wide gate allows the target to be acquired by the process just described until the gate width is narrow enough to eliminate detection problems within the gate. This can be seen by comparing Fig. 5.4A with Fig. 5.1.

Below this initial threshold, we see that there exists a region of signal power in which the curves are somewhat erratic but the steepness of the threshold region is

abruptly discontinued. The gating error probability has been reduced virtually to zero in this region because the prediction error is dominated by estimation error due to false target detection within the gate. This error is confined within the gate so that a very small proportion of the prediction error is distributed outside the gate. Because the target is so predictable, the system needs only to detect the target occasionally in order to keep track of it. However, at low enough signal power, the system cannot keep track of the target without opening the gate still further and this explains the second threshold that is just evident in the curves of Fig. 5.4A at the lowest signal powers for which they are visible.

Above the main threshold the curves exhibit a plateau that is brought about by ambiguity in the signal but we see that this is overcome at a slightly lower signal power than was the case with the fixed 200uS range gate and has a much less serious effect on the estimation error. This is simply because, if the main lobe is detected often enough, the gate width can be reduced to exclude the sidelobes most of the time and thus reduce the ambiguity.

At high signal power we see from Fig.5.4B that the gating error probabilities are fairly independent of signal power but are very dependent on the ratio of gate width to RMS prediction error as expected. This dependence is reflected in the estimation error curves of Fig. 5.4A where we see that the wider gate performs better.

The gating error probability is not simply predictable from equation 5.3 for narrow gates because, for a number of reasons, the prediction error is not normally distributed when using narrow gates. The main reason for this is as follows. Using a narrow gate causes the system to lose track of the target frequently with the result that the prediction error increases and the gate opens to reacquire the target. As has already been discussed, under these conditions, the prediction error is distributed almost entirely within the gate. Thus a system with a small ratio of gate width to RMS prediction error is continually hunting for the target, with its gate opening and closing

as it does so. The result is that the gating error probability is lower than otherwise might be expected. The gating error probability for the wider gate represented in Fig. 5.4 is almost precisely the value predicted, indicating that a system using such a gate is much less prone to ***hunt***.

Comparing the performances of the two systems, we see that the wider gate gives smaller error above threshold and the two gates exhibit similar threshold phenomena.

In the case of a highly unpredictable target, the dependance of performance on gate width above threshold is much more marked because gating errors result in much larger estimation error magnitudes so that the "narrower" gate hunts over a bigger region of delay. This can be seen in Fig. 5.5A where the RMS estimation error at high signal power varies by a factor of 4 or more between the two gate width ratios.

Looking at the curve for a gate width of $4\sigma_e$ we see that it is similar to that for a 200uS fixed gate as in Fig. 5.1. This is not surprising because over most of the range for which the curve is visible in Fig. 5.5A, the estimation error is much smaller than the unpredictable target delay variations so that the prediction error is dominated by the unpredictable delay variations. Hence the RMS prediction error is approximately 50uS, resulting in a gate width of 200uS. We see then, that when the target delay varies in a very unpredictable fashion, there is little to be gained from using an adaptive gate width except during target acquisition.

Figs. 5.6A and 5.6B were obtained in the same way as Figs. 5.4A and 5.5A respectively except that MDI signals were used. In Fig. 5.6A, we see that there is no evidence of detection problems for either of the systems except at very low signal power where both systems exhibit the sharp thresholds that we saw in the previous example. An important feature of these curves, however, is that, at low signal power, the range accuracy is much better than predicted from the theory of chapter 3. The reason is that prior information is being used to locate the target approximately while more precise information is extracted from the signal. Since the target delay is highly predictable,

Figure 5.6 *Adaptive GML Estimation with MDI Signals*

(RMS unpredictable target range variation is: A) 5μS and B) 50μS)

——— $W = 2\sigma_e$

– – – – – $W = 4\sigma_e$

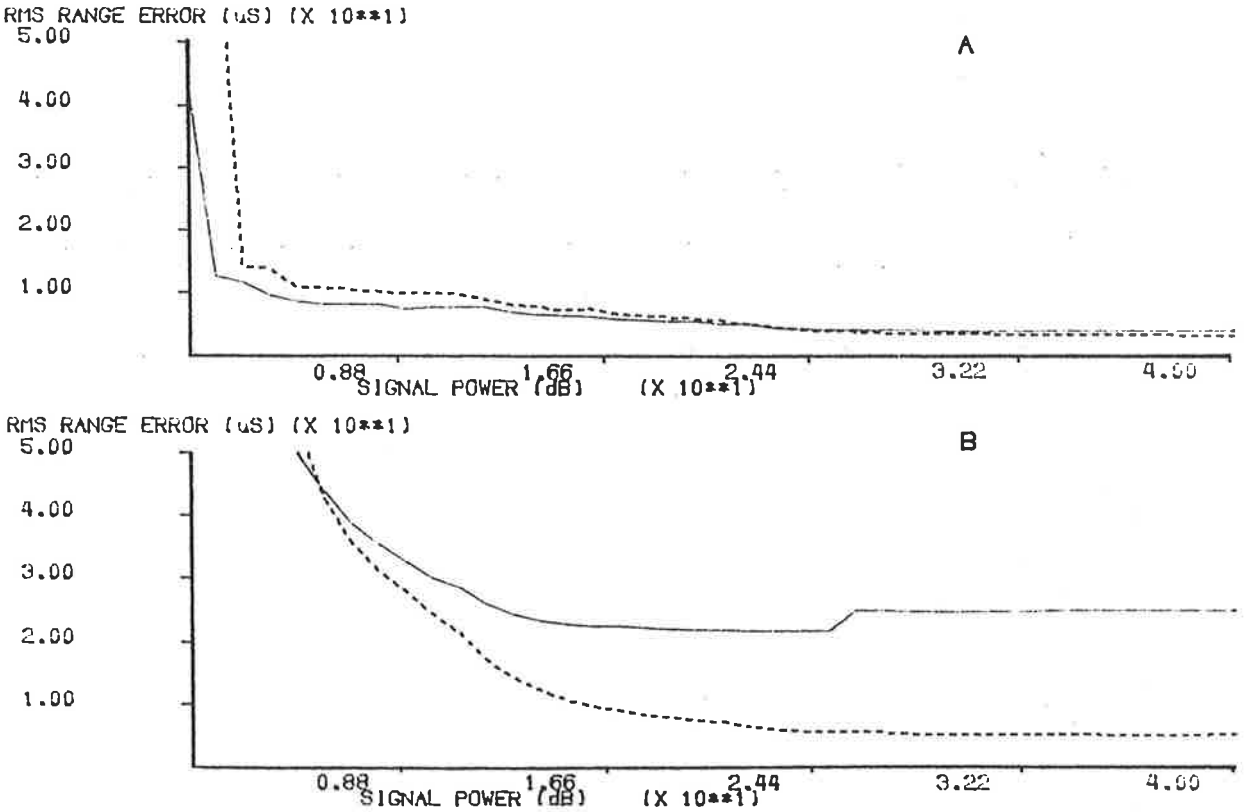

little information need be extracted from the signal to keep the prediction error small. As a result the narrower gate performs better at low signal power but worse at high signal power where most of the information is extracted from the signal.

As indicated in Fig. 5.6B, however, when the target delay is highly unpredictable, narrow gates perform better only at extremely low signal power and they perform very poorly indeed at high signal power. Again, the performance of the "wider" gate is similar to that predicted from theory for a fixed gate, indicating that adaptive gate widths provide little advantage when ranging unpredictable targets.

Summarizing the conclusions of this subsection, we have found that adaptive range gates give much enhanced detection performance if the target is highly predictable at some small expense in range accuracy. In addition, the effects of signal ambiguity can be greatly reduced by the use of adaptive gates when the target is predictable. However, the detection threshold appears to be largely independent of the ratio of gate width to RMS prediction error. For unpredictable targets, on the other hand, little is to be gained from using an adaptive gate over a gate of fixed width. Narrower gates give very poor performance in this case because gating errors result in excessive hunting.

§5.2 The Conditional MAP Estimator

5.2.1 Deriving The Estimator

We saw in the previous section that improved performance can result from the use of tracking range gates. In particular, the effects of signal ambiguity can be greatly reduced and the effective detection threshold can be lowered by several dB. However, to ensure good performance, the gate width must be adjusted according to the situation. In order for the system to acquire the target, gates need to be either broad or adaptive in the sense that the gate width is related to the estimated prediction error. Furthermore, if the target delay is highly predictable and the detection index is low, then a narrow range gate will perform best but in any other situation the gate width should be at least 3.5 to 4 times as large as the RMS prediction error.

An important insight into these various relationships can be gained by considering the underlying probabilistic principles. The system that performs best in any particular situation will be the one that best approximates the MAP estimator.

The prior information incorporated in an adaptive tracking range gate is derived only from previous estimates. Hence the approximate prior probability distribution represented by such a gate is in fact an approximate prior probability density conditional on the values of previous estimates. Hence, an estimator employing such a gate could be called an approximate conditional MAP estimator because it locates the peak of an approximate conditional posterior probability density.

However, we have seen that the performance of such an estimator can be very suboptimal and this is because of the nature of the approximations made. In the simulations, two parameters of the conditional prior probability were derived from the previous estimates using a simple model of the target dynamics (i.e. the target does not move). They were the predicted target delay and the estimated prediction error. Usually, this is all one can expect to extract from a small number of previous estimates.

Having only the mean and variance of the conditional prior distribution, we then constructed, in effect, a PDF with a precise rectangular shape. In other words, we used guesswork in constructing the conditional prior PDF and injected highly unreliable information into it. Sometimes the guesswork "paid off" because the true PDF was not very dissimilar from that we constructed. In general, however, we need much more information, particularly about the source of the predicion error, before we can construct a rectangular PDF that approximates closely the true prior PDF.

An alternative approach is to form the log of a non-rectangular PDF and add it to the LLF before picking the peak. This frees the designer from the constraint to a rectangular PDF. In particular, it allows the designer to construct the PDF that incorporates the least information additional to the mean and variance.

This concept of incorporating the minimum information, or equivalently the maximum entropy, into a distribution has long been recognized as a criterion for prior probability distributions in MAP estimation[5.2]. In this subsection that principle is applied to signal parameter estimation in what is believed to be an original manner.

It is well known[5.2] that the maximum entropy PDF having a known mean and variance is Gaussian. Hence the most appropriate conditional prior PDF to construct is given by:

$$p\left(\tau|\vec{\hat{\tau}}\right) = \frac{1}{\sigma_e\sqrt{2\pi}} exp\left[-\frac{(\tau-\bar{\tau})^2}{2\sigma_e^2}\right] \tag{5.4}$$

where $\vec{\hat{\tau}}$ is the vector of previous estimates, $\bar{\tau}$ is the predicted target delay derived from those previous estimates and σ_e is the estimated RMS prediction error.

Now the first factor in 5.4 is uninformative in that it does not depend on hypothesized target delay, τ. Hence it may be ignored. The log of the second factor is simply an inverted parabola centred at the predicted delay and with the coefficient, $\frac{1}{2\sigma_e^2}$. The conditional MAP estimate is obtained by adding this inverted parabola to the LLF and locating the peak.

This conditional MAP estimation process should not be confused with sequential estimation or recursive estimation schemes (even though it does involve recursion). A sequential estimator of range would use a number of echoes sequentially to make one range estimate. Each echo waveform would be used to improve the range estimate until the required accuracy was achieved. Such a scheme could only be applied if the target range was not time varying. More typically, sequential estimation is used for signal estimation. In this context it has limited applicability to target localization problems in that such sequential filtering schemes are potentially faster than the ML correlation technique discussed in previous chapters. However, such techniques involve considerable complexity in their implementation and are certainly not optimal with respect to system performance.

A recursive estimator can be used to give a MMSE estimate by filtering raw estimates using a model of the target dynamics incorporated into a predictor-corrector form of state-variable filter. This is a form of generalized Wiener filtering known as Kalman filtering[5.3]. If we applied this technique directly to the output of a ML estimator we would not do as well as with a conditional MAP estimator because we would be using guesswork in an irreversible fashion to obtain the raw estimates. We could not expect, for example, to lower the detection threshold by this method.

However, we could incorporate a recursive estimation scheme after a conditional MAP estimator. In fact, we can use such a scheme to perform the predictions required for conditional MAP estimation and to provide the prediction error estimates. This concept is not new. Kalman filters have been used for target tracking in Radars for many years[5.4].

5.2.2 Performance Comparisons

The conditional MAP estimator uses all the readily available information in an optimal way. However, it does not construct an accurate posterior PDF because it does

not use all the prior information that exists. Therefore we would not expect it to give the best possible performance. Nevertheless, we would expect it to perform better than any of the GML estimators that we have considered in most situations.

In Fig. 5.7 the performances of the adaptive GML estimators are compared to that of the conditional MAP estimator for predictable and unpredictable targets using MV and MDI signals. The situations are exactly as described in the previous section and exactly the same post-correlation waveforms were used for all three estimators. We see that the conditional MAP estimator consistently outperforms both of the adaptive GML estimators.

We can conclude from these comparisons and the theoretical discussion of the previous subsection, that the conditional MAP estimator will consistently outperform any other estimator using similar sources of information when used in a variety of conditions. Under certain conditions that are especially favourable to another estimator, that estimator may perform better than the conditional MAP estimator described. However it is impossible to predict this better performance without using *additional information* to that used by the estimator itself. Hence we could not design a system to take advantage of the fact that a particular estimator was especially favoured by the conditions without using more prior information than we have assumed to be available in this study.

5.2.3 Practical Implementation

In order to perform conditional MAP estimation it is necessary to make predictions, to estimate prediction error and to construct a parabola to subtract from the LLF. All these things are most easily done digitally if the required processing speed can be realized. Methods of digital implementation of real time MAP estimators are discussed in the next chapter.

A question that arises is how best to make the predictions. The optimal predictor

Figure 5.7 *Performance Comparisons*

A) MV signals Delay variation is 5μS

B) MV signals Delay variation is 50μS

C) MDI signals Delay variation is 5μS

D) MDI signals Delay variation is 50μS

——— MAP

– – – – – Adaptive GML ($W = 2\sigma_e$)

— — — Adaptive GML ($W = 4\sigma_e$)

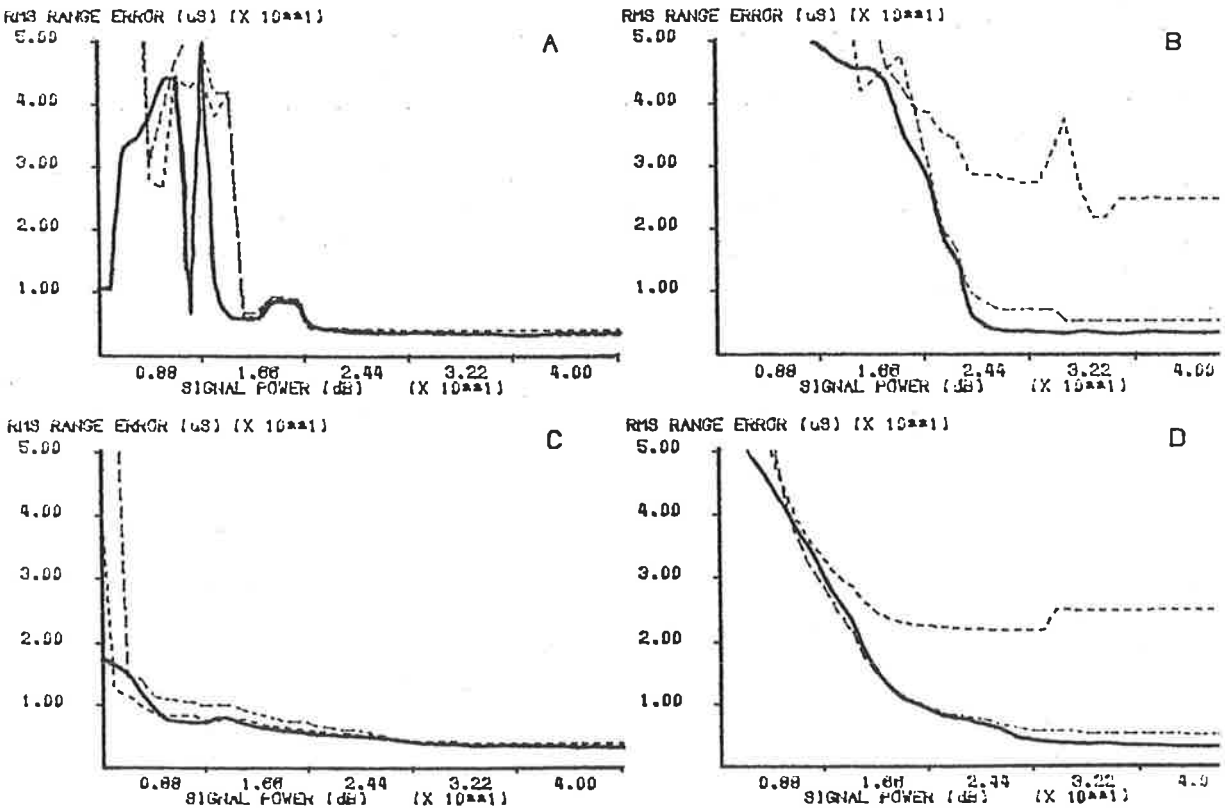

for such an application will use as much information about the target dynamics as can be incorporated. However this might demand greater complexity than can be justified.

Practical prediction schemes will be as varied as are the applications of target localization. For example, in one application with which the author is familiar[1.1], the skin of a sheep was to be ranged through the wool using a focussed acoustic ranging system. In this case, movement of the target surface in the direction of propagation was negligible. Nevertheless, the target had "dynamics" because the focussed sensor scanned the surface and the surface range varied from point to point. Range estimates for nearby points on the skin constituted the vector of previous estimates and one prediction process that was used involved the use of a complex statistical model of the sheepskin shape. The model was derived from an extensive statistical evaluation of sheepskin shapes [5.5]. It was originally intended for use in controlling a shearing system with the help of less sophisticated sensors than the acoustic system.

In more typical examples, simple models of the target dynamics may be incorporated in adaptive Kalman filters as mentioned in subsection 5.2.1. In still simpler cases, linear predictive techniques may suffice.

In situations where a conditional MAP estimator is not feasible because of implementation problems, an adaptive tracking range gate may yield much better performance than a tracking range gate of fixed width. Unless it is known that the target is highly predictable and the detection index is small, the gate width should be adjusted to 3.5 to 4 times the estimated prediction error for best performance.

6. A CASE STUDY - Acoustic Sensing Through Fleece

§6.0 Acoustic Sensing Through Fleece

Most of the work reported in this thesis was motivated by the author's involvement in a research project aimed at assessing the feasibility of sensing sheepskin through full fleece and, if possible, developing the techniques necessary. Such a sensing system, able to deliver range information to a robot controller in real time, would be extremely useful in the development of an automatic shearing mechanism utilizing sensory feedback. For more detailed background information on this project, the interested reader is referred to [1.1] and [6.1].

Two different approaches are under consideration. In one approach, the focussed sensing system ranges points just ahead of the cutter during the actual shearing operation. All the experimental work to date has been related to this approach. An alternative approach that may be viable is less restricted in its transverse resolution because the available aperture area is not nearly so limited by mechanical constraints. In this latter approach, each *patch* to be shorn would be imaged very rapidly prior to shearing. The robot would then keep track of variations in the skin shape (due to breathing etc.) by using other, less sophisticated sensors operating behind the point of cut.

It is perhaps worth mentioning here that experience so far with automated shearing apparatus strongly supports the hypothesis that such techniques will be a good deal more humane than traditional methods [6.1]. The hundreds of sheep shorn by robot mechanisms have sustained far fewer injuries than they would have as a result of human

shearing. All of these injuries were trivial in nature, requiring virtually no treatment at all. Furthermore, the animals appear to be less stressed when handled by machine than when handled by humans.

Currently, there are some important developments underway in the acoustic sensing project. The most important relates to the design and manufacture of the focussed array of transducers. Current developments are expected to yield an improvement in received signal energy of better than 15dB. Once this work is complete, the transmission path will be characterized again, taking into account the new array and also the noise generated by the cutter. This noise has not been considered explicitly before although an assessment of its likely effects was made during an earlier phase of the project.

The case study in this chapter, therefore, does not follow the case through to a final system design. However, the approach, the techniques and the details of the implementation are all indicative of the ways in which the theory developed in this thesis can be applied in practice.

Basically, this acoustic sensing system is a focussed ranging system. The focussing is achieved by placing small transducers on part of a spherical surface centred at the point of focus. The aperture is constrained to be relatively small by mechanical considerations. As a result, a fixed focus may be used because the depth of focus is consistent with the range variations expected. More complicated focussing patterns can be achieved by varying the shape of the surface on which the transducers lie [1.1].

In principle, focussing can be achieved electronically also. The approach is similar to the "phased array" approach used in electronic beamsteering and beamforming for antennas. In receiving antenna arrays of this type, phase shifts are introduced into each channel (one channel corresponds to one array element) such that the phase of a signal from the direction of the main beam would be the same at the output of each channel. The channels are then summed to obtain a single receiving channel with some required antenna beam pattern. Transmitting arrays can be treated in a similar fashion. In the

case of a wideband transducer array, focussing can be achieved by introducing delays into each channel such that the total delay of a signal emitted from the focus is the same at the output of each channel. Similarly the overall delay from a signal source to a focus via each element of a transmitting array can be adjusted to be identical. The ways in which electronic focussing may be utilized in a sheepskin sensing or imaging system are yet to be investigated in detail. However, some important limitations are immediately apparent.

Firstly, the use of signals of long duration (as are described later) precludes the use of "dynamic focussing" for the receiving array unless a correlator is provided for each array element. "Dynamic focussing" is a technique in which the receiving array focus is always maintained at a range consistent with the elapsed time (since pulse transmission). By this means, the target is always kept in focus. When signals of long duration are employed, however, elapsed time from commencement of pulse transmission has a different relationship to range for each point in the signal waveform. Hence, at any point in time there is ambiguity as to what range to focus on. If, however, there is a correlator provided in each channel, then the electronic focussing can be undertaken at the correlator outputs since the system is linear. At that point, each point on the waveform corresponds to a particular range rather than an elapsed time. The cost of such an approach, however, would be prohibitive.

Secondly, electronic beamforming would be expensive in such an application because signals of wide time-bandwidth product are employed and low noise amplifiers and delay elements of similarly wide time-bandwidth product would be required for each channel.

Colouration of the target path transfer function arises from several mechanisms. By far the most important, however, is the highly frequency-dependant absorption characteristic displayed by wool. Dispersion of the target echo also occurs because the echo results from specular reflection of a non-plane wave from an extended surface.

Clutter arises from scattering from particles that contaminate the wool and from the wool itself. The clutter path impulse response is, of course, stochastic. Its statistics are non-stationary with range because of the range-dependant absorption losses. However, it can be shown to be locally stationary at target range according to the stationarity condition of equation 2.22.

Because the wool thickness, density and curliness varies and the degree of contamination varies, the transmission path transfer functions are also highly variable. As a result, the transmission path model must include uncertainty as discussed in chapter 4. As we shall see, the main problem with which we are faced is that of ensuring that the target echo can be detected. The delay associated with detected echoes can nearly always be estimated with sufficient accuracy for our purposes. The robust optimization techniques of chapter 4 are therefore highly relevant to this problem.

The other main difficulty with which we must contend is that of implementing a system that will provide rapid response. The shearing head could be moving at up to 1m/sec. (Nevertheless, because the transducer array is always moving closely parallel to the skin with its beam axis orientated approximately at right angles to the skin, Doppler effects are negligible.) Because such high speeds are involved and because the cutter is always in close proximity to the skin, an update interval of only 4msec is required. We shall see that this requirement translates into very demanding specifications for the signal processor design.

In this chapter we shall consider the application of the techniques of chapter 4 to the problem of designing such a sheepskin sensing system starting from the construction of a transmission path model. We shall look at the system design of the complete sensor and in more detail at the design of the signal processing section that implements the conditional MAP estimation algorithm of chapter 5. We will also look briefly at a potentially important new approach to the architectural design of digital signal processors that was given initial impetus by the requirements of this sheepskin sensor.

We shall not consider many important related matters that lie outside the scope of this thesis. These include, the nature of the transducer design, details of how the range predictions for MAP estimation are obtained and details of the robot design and the robot control philosophy. The interested reader is referred to [1.1,6.1,6.2] for such published material as exists on related topics not discussed here.

§6.1 Constructing Transmission Path Models

The first step in developing a system design for such a sensing system is to design the transduction and focussing system. Once this has been done, the transmission path can be characterized. In our case, the transmission path characteristics are variable. Hence, we require a set of transmission path models representing a class of characteristics.

Each member of the set will consist of the three functions: the target path transfer function, the squared magnitude of the clutter path transfer function and the noise power spectrum. In our case, because the noise is generated in the receiver front end, all the noise power spectra are identical. In other words, the noise power spectrum is not uncertain because it does not depend on the variable fleece conditions.

The ways in which these functions are obtained depend on the details of the application. In our case, there is no way in which separate target and clutter path characteristics can be directly measured. It is therefore necessary for us to deduce them from the total response.

The approach taken is to obtain an ensemble of total impulse responses at one point on a fleece; average over the ensemble to eliminate noise and then excise the target path and clutter path impulse responses from the total response. An ensemble of noise records is obtained by subtracting the "noiseless" response from each of the original total responses. The noise power spectrum is then obtained as the mean squared magnitude of the Fourier transforms of these noise records.

This technique is repeated for as many different fleece conditions as are considered necessary to define the uncertainty in the transmission path characteristics. For illustrative purposes, we shall only use three points in the following analysis although one would normally use more than this. Fleece conditions vary markedly from point to point on any one fleece and we would probably need four or five points to characterize

one fleece. They also vary from fleece to fleece and thus we might require twenty or more members for our set of transmission path models to fully characterize the uncertainty in the transmission path characteristics.

In our case there exists a further complication. Our transducer array suffers from a transmitter-to-receiver coupling problem that gives rise to *self-clutter* or *self-response*. This is an acoustical response of the receiver to the transmission of a signal from the transmitter. It is a problem because the transmitting and receiving elements are interspersed and the aperture dimensions are of the same order as the distance from the sensing array to the skin. Since a signal of long duration is transmitted, this means that this acoustically coupled signalhas not died out before the target echo is received. Because the transducers are excited by a very large signal voltage, this self-clutter is nonlinearly related to the signal transmitted. It turns out that the transmission of an impulsive signal excites a large self-response. At the same time, most of the acoustic energy of the transmitted impulse is absorbed by the wool so that the wanted impulse response is very weak.

Under normal conditions, at target delay, the self-clutter has decayed to the extent that it does not swamp the returning echoes. However, when an impulse is transmitted, the self-clutter is in fact the dominant component of the total response. As a result, it is necessary to estimate the self-response of the array in the absence of other echoes and to subtract this from the total response.(In the experimental sensing system it is also stored and cancelled by simple subtraction.)

The self-response estimate is obtained by averaging over a number of responses to eliminate noise. Each member of the ensemble is obtained as the impulse response of the array when pointed at an absorbing panel. This panel is simply a peice of soft polyurethane foam with a textured surface such as is commonly used in packaging. It is placed obliquely to the beam axis at relatively long range where the array is very unfocussed and any residual echoes from it do not lie within the range gate used.

Figure 6.1 *Noise Power Spectrum*

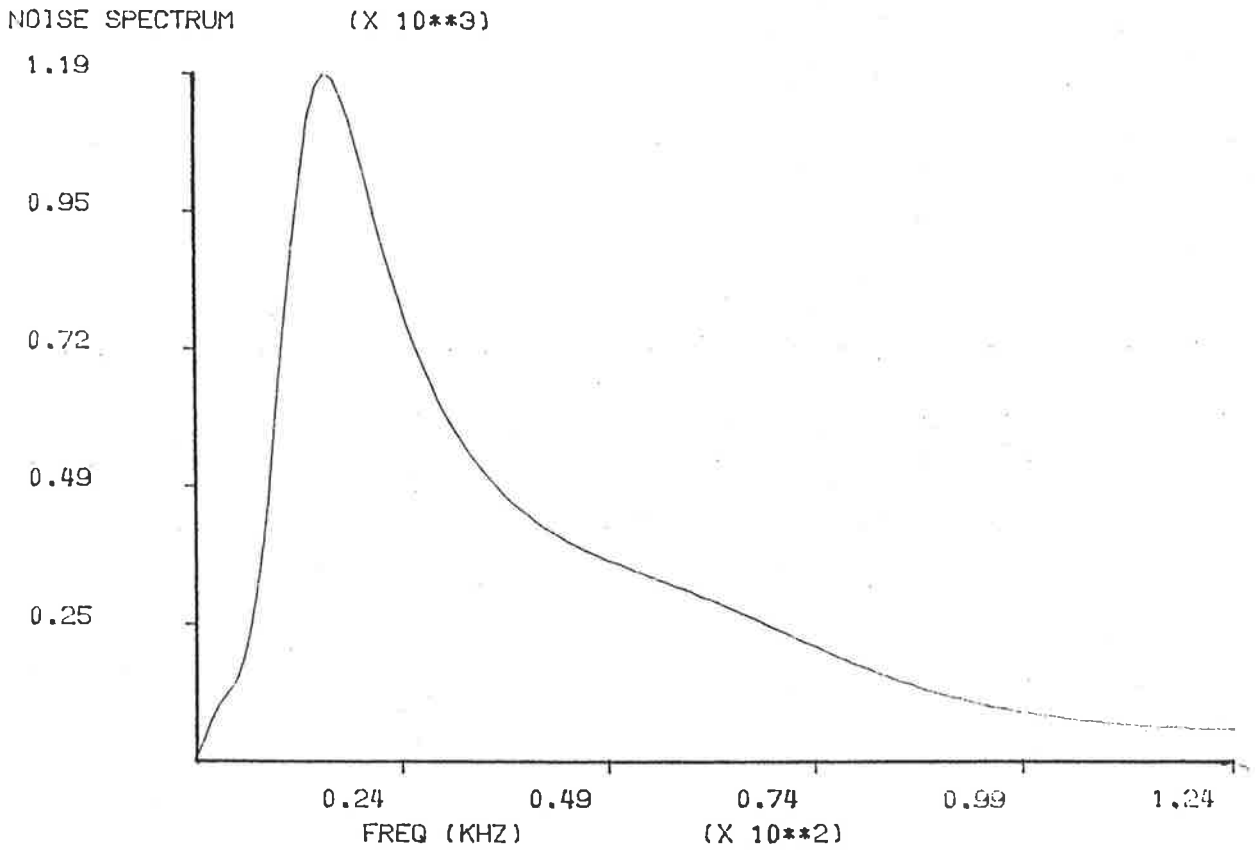

Figure 6.2 *Estimation of the Target Path Impulse Response*

A) Total impulse response after averaging.

B) Impulse self-response after averaging.

C) Total impulse response after subtracting self-response.

D) Excised target path impulse response.

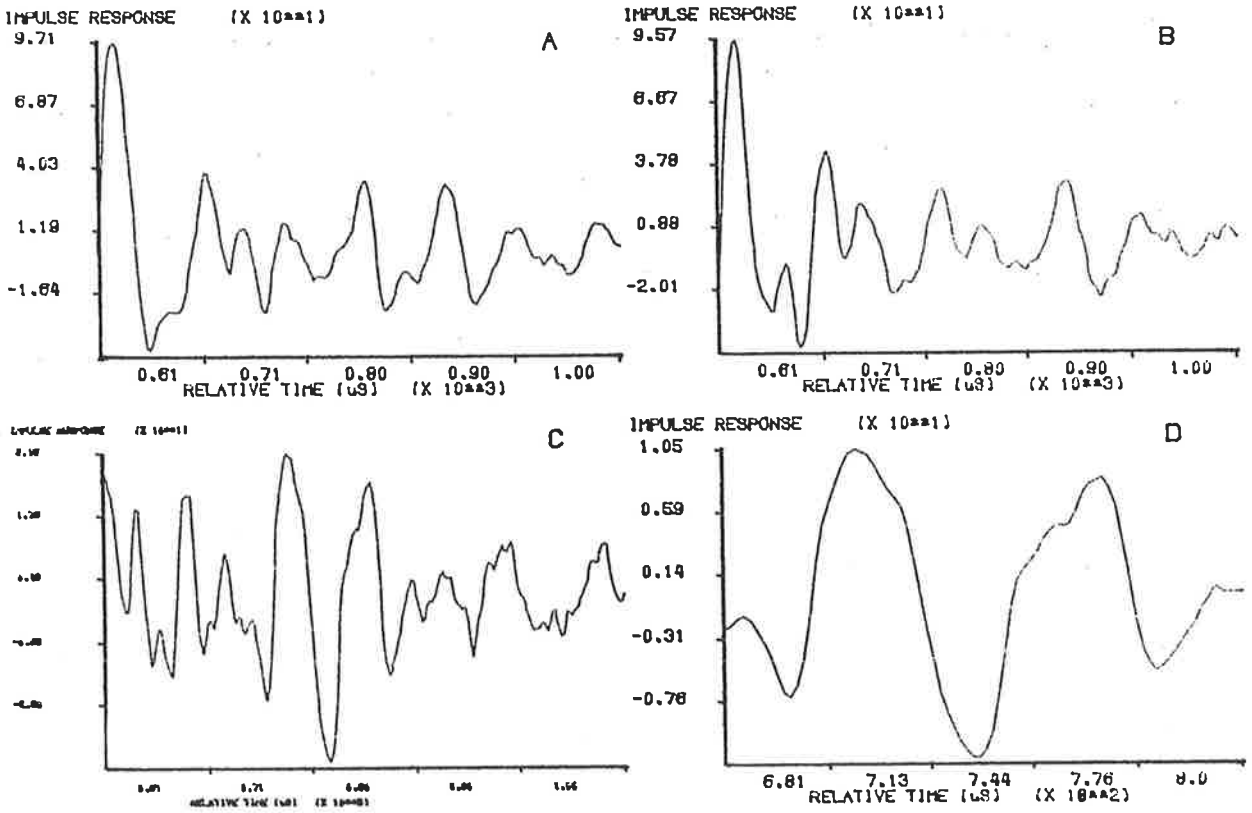

Fig. 6.1 displays the noise power spectrum common to all the transmission paths in the set we shall consider. Fig. 6.2 illustrates how the self-clutter is eliminated from a total response after the noise has been averaged out. Fig. 6.2A is the total response after averaging. Fig. 6.2B is the self-response of the array. Fig. 6.2C is the result of subtracting the self-response from the total response. The target echo is clearly distinguishable from the clutter. Prior knowledge of the target range allows the target echo to be excised giving the target path impulse response of Fig. 6.2D.

Admittedly, the target path impulse responses obtained in this manner are corrupted by clutter. Nevertheless, they represent the best estimates obtainable. Since the clutter varies from point to point, the variations in our target path impulse response estimates for those points will reflect the uncertainty arising from this contamination. Eventually we will construct a class description for our target path transfer function and the uncertainty in it will be due, in part, to these estimation errors. Mostly, however, it will be due to actual variations in the target path transfer function under different fleece conditions.

Finally, with Fig. 6.1, Fig. 6.3 represents one member of our set of transmission path characteristics which was obtained in the manner described in this subsection. Fig. 6.3A is the target path impulse response which, being real rather than complex, is more convenient to display than the transfer function. Fig. 6.3B is, in fact, the squared magnitude of the target path transfer function corresponding to the impulse response of Fig 6.3A. Fig. 6.3C is the squared magnitude of the clutter path transfer function.

Figure 6.3 *First Transmission Path Model*

A) Target path impulse response.

B) Squared magnitude of target path transfer function.

C) Squared magnitude of clutter path transfer function.

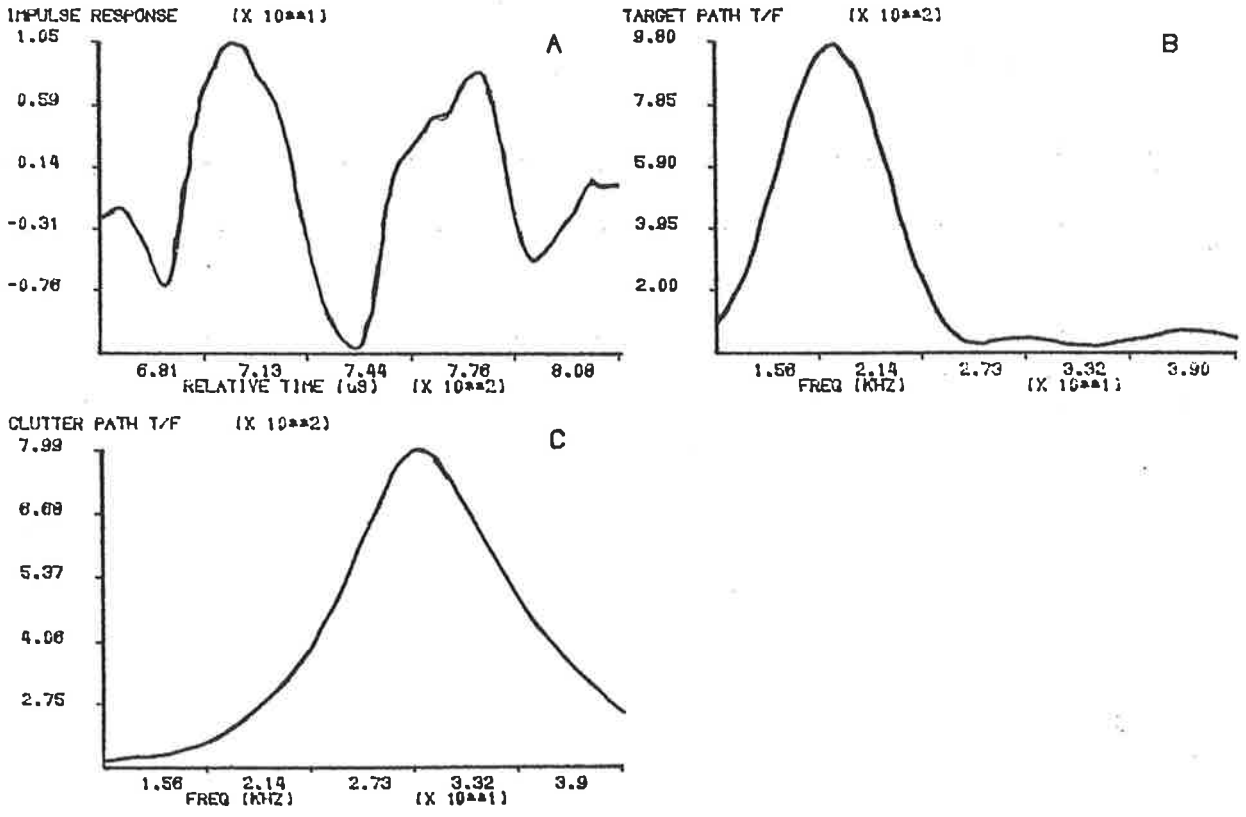

§6.2 Robust Signal Optimization

6.2.0 Preamble

The robust optimization technique of chapter 4 consisted of four main steps. The first of these was considered in the previous section. That is, the task of constructing a set of transmission path models defining the class of conditions to be optimized for. The set we shall consider in our case study is displayed in Figs. 6.1, 6.3, 6.4 and 6.5. The format was explained in the previous section.

The second step is considered in the next sub-section. This is the problem of constructing a class description appropriate for the solution technique of chapter 4.

Subsection 6.2.2 reports on implementation of the third and fourth steps. In the third step, the least favourable transmission path within the class is identified and in the final step the MDI signal spectrum for this least favourable path is designed. This signal spectrum is robust-optimal for the class of transmission paths when used in conjunction with the jointly robust-optimal receiver filter. The filter is the optimal filter for the transmitted signal and the least favourable transmission path.

To complete the study, the detection indices obtainable with various combinations of signals and transmission paths are computed and comparisons are made to show, amongst other things, that the computed robust-optimal solution does, in fact represent a saddle-point solution to our minimax optimization problem as is proven theoretically in appendix 4.

6.2.1 Constructing a Class Description

The aim of this sub-section is to show how a class description can be constructed in the form described by equations 4.16 and 4.17. The class to be described should be no broader than necessary to accomodate the transmission paths represented in the set of transmission path models obtained by measurement.

Figure 6.4 *Second Transmission Path Model*

A) Target path impulse response.

B) Squared magnitude of target path transfer function.

C) Squared magnitude of clutter path transfer function.

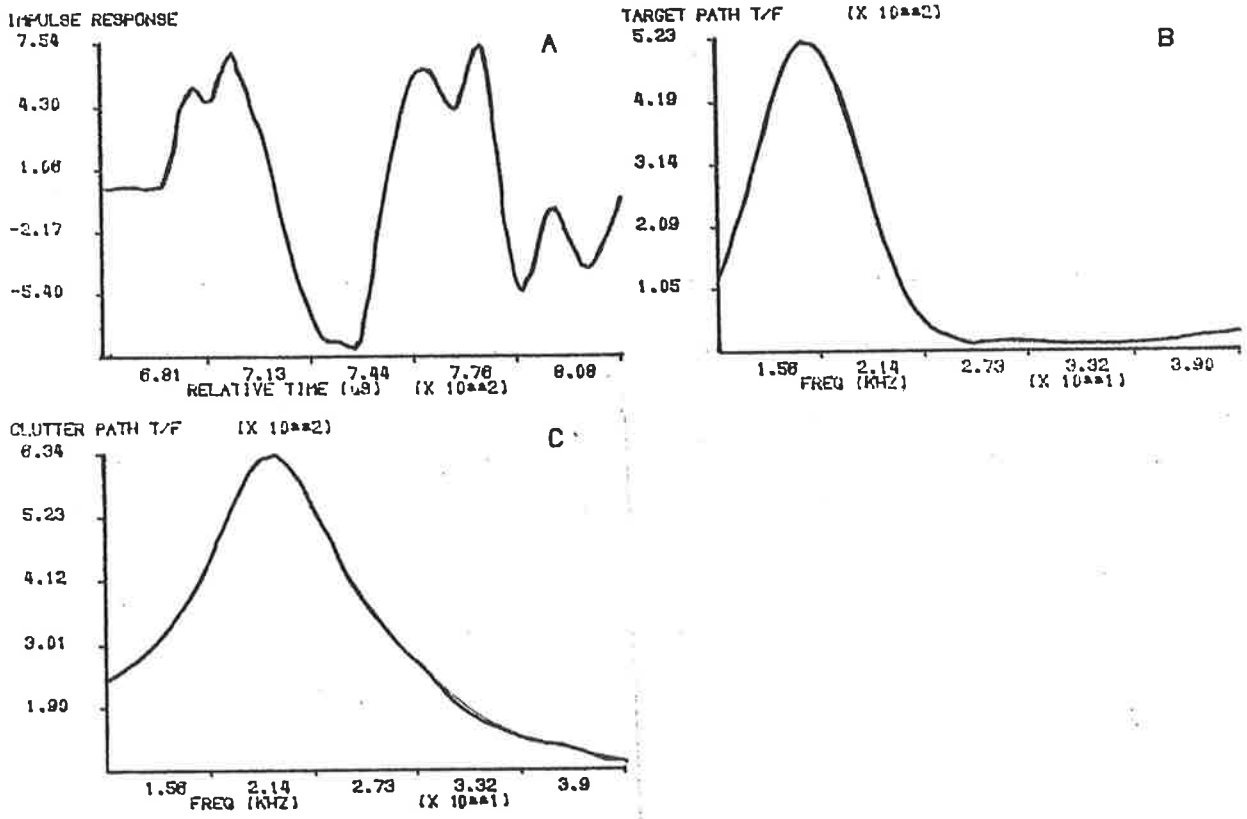

Figure 6.5 *Third Transmission Path Model*

A) Target path impulse response.

B) Squared magnitude of target path transfer function.

C) Squared magnitude of clutter path transfer function.

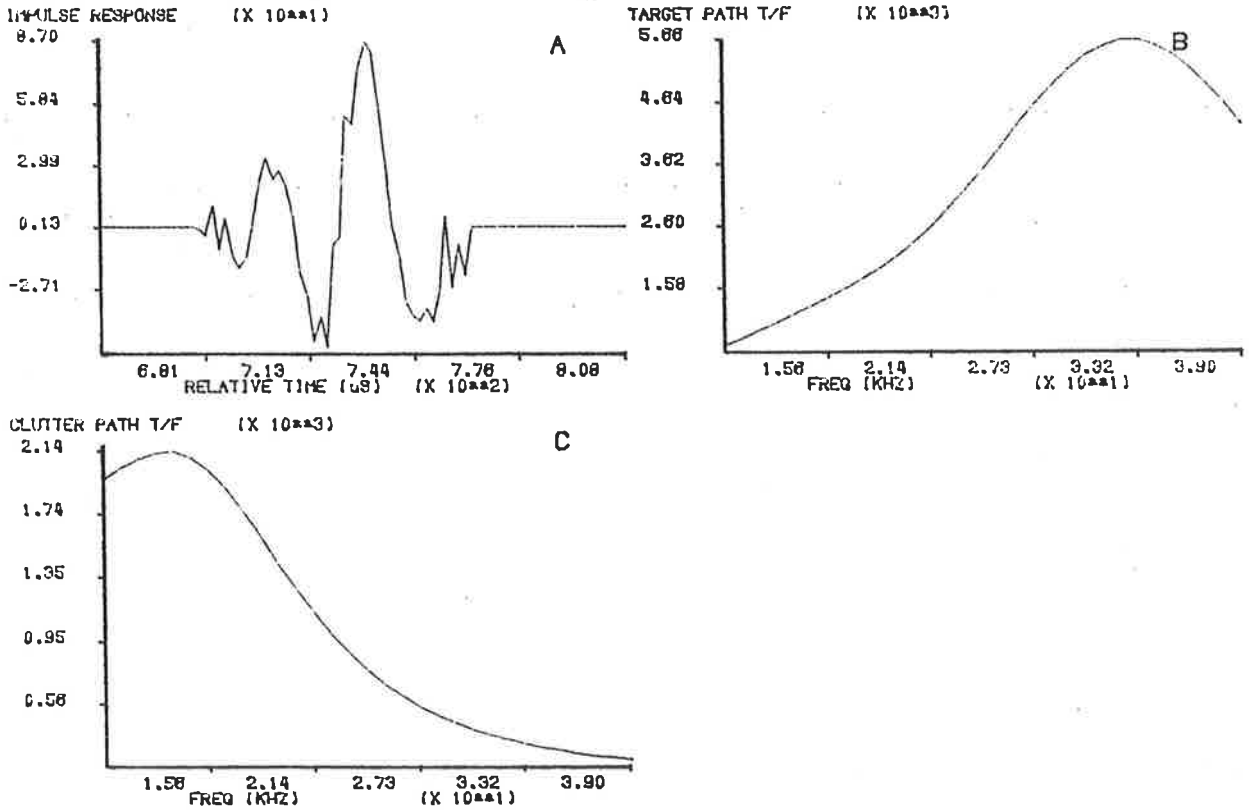

Equation 4.16 describes a class of target path transfer functions, $C_T = \{H_T(f)\}$. As discussed in chapter 4, we need to find a nominal transfer function, $H_0(f)$, an error power, δ_T and a minimum scale factor, A_{min}. The scale factor for each member of the set of measured target path transfer functions should be chosen to give the best (i.e. MMSE) fit to the nominal target path transfer function. Under that condition, the maximum value, δ_T, of the modelling error power (i.e. the power in the difference between a target path transfer function and the nominal target path transfer function) over the set of measured functions should be minimized by the choice of the nominal function.

Now let the *ith* measured function be represented by $H_i(f)$ and the corresponding scale factor be A_i while the corresponding modelling error power is e_i. Then we have:

$$e_i = \int_{f_1}^{f_2} \left| \frac{H_i(f)}{A_i} - H_0(f) \right|^2 df \tag{6.1}$$

$$= \int_{f_1}^{f_2} \left(\frac{H_i(f)}{A_i} - H_0(f) \right) \left(\frac{H_i(f)}{A_i} - H_0(f) \right)^* df \tag{6.2}$$

where $*$ represents the conjugation operation. Thus:

$$e_i = \frac{1}{A_i^2} \int_{f_1}^{f_2} |H_i(f)|^2 \, df + \int_{f_1}^{f_2} |H_0(f)|^2 \, df - \frac{2}{A_i} \int_{f_1}^{f_2} (H_0(f) H_i^*(f)) df. \tag{6.3}$$

e_i is minimized by setting $\frac{de_i}{dA_i} = 0$ in 6.4,

$$\frac{de_i}{dA_i} = \frac{-2}{A_i^3} \int_{f_1}^{f_2} |H_i(f)|^2 df + \frac{2}{A_i^2} \int_{f_1}^{f_2} (H_0(f) H_i^*(f)) df, \tag{6.4}$$

giving:

$$A_i = \frac{\int_{f_1}^{f_2} H_i^2(f) df}{\int_{f_1}^{f_2} \left(H_0(f) H_i^*(f) \right) df}. \tag{6.5}$$

This yields:

$$e_i = \int_{f_1}^{f_2} |H_0(f)|^2 df - \frac{\left[\int_{f_1}^{f_2} \left(H_0(f) H_i^*(f) \right) df \right]^2}{\int_{f_1}^{f_2} |H_i(f)|^2 df}. \tag{6.6}$$

Now, the maximum value over the index, i, of e_i in equation 6.6 is to be minimized by the choice of $H_0(f)$. However, we clearly need to apply a constraint to the scaling of $H_0(f)$. Otherwise 6.6 could be minimized by setting $H_0(f) = 0 \forall f$. Therefore, we constrain the nominal transfer power to equal a constant:

$$\int_{f_1}^{f_2} |H_0(f)|^2 df = E_0. \tag{6.7}$$

The choice of E_0 is not important. In the final description, E_0 and δ_T are both inversely related to the square of A_{min} in the sense that if we quadruple the value of E_0 used in our algorithm for constructing the class description, then δ_T will be quadrupled and A_{min} will be halved.

In fact, the computer program whose listing appears in appendix 6, implements the algorithm in such a way that A_{min} is always set to unity. This means that $H_0(f)$ is scaled so that it is directly comparable with the transfer functions in the original measurement set and has the least favourable (i.e. the smallest) magnitude allowable in the class.

Now, it is clear that the value of e_i can always be reduced by making $H_0(f)$ more like $H_i(f)$ subject to the constraint, 6.7. The simplest way to do this is to compute:

$$H_0(f) = aH_0(f)_{old} + bH_i(f), \tag{6.8}$$

where the constants, a and b are chosen such that 6.7 is met and some required reduction in e_i is achieved.

There are two obvious consequences of this simple observation. Firstly, the function, $H_0(f)$, that minimizes the maximum value of e_i over the index i, must be a linear combination of the transfer functions, $H_i(f)$. If it is not, then we can equate it to a linear combination of those transfer functions and some foreign function. Hence, we must be able to reduce the maximum value of e_i by reducing the contribution of that foreign transfer function via equation 6.8 and such reduction is not compatible with

$H_0(f)$ minimizing the maximum of e_i. Secondly, the minimum value of the maximum e_i over the index, i, is achieved when:

$$e_i = e_j \; \forall i, j \leq N \tag{6.9}$$

where N is the number of transfer functions in the measurement set. If (6.9) was not met then the maximum value of e_i could be reduced by increasing the contribution of the ith transfer function to the linear combination yielding $H_0(f)$ via (6.8).

Equations (6.5) to (6.9) are used within the computer program whose listing is given in appendix 6. This program constructs the most appropriate class description of equation (4.16) for the target path transfer function from the set of measured target path transfer functions by computing $H_0(f)$ and δ_T iteratively and setting $A_{min} = 1$. It also outputs the value of E_0 defined in equation (6.7) for a reason that will become clear shortly.

This same program also constructs the class description of equation 4.17 for the clutter path transfer function. It does so by straightforwardly finding the upper and lower bounds on the square of the clutter path transfer function and the upper bound on the clutter path transfer power, σ_c^2, over the set of measured clutter path transfer functions.

There are virtually no limitations on the use of this program. The only complicated section is the iteration used in finding $H_0(f)$. In that iteration, one coefficient in the linear combination of measured transfer functions used to compute $H_0(f)$ is updated at each iteration. The one associated with the transfer function giving the biggest error power, e_i, with respect to the nominal transfer function is updated. The update equation is:

$$a_{i_{new}} = a_{i_{old}} \sqrt{\frac{e_i}{e_1}}, \quad with \; H_0(f) = c \sum_i a_i H_i(f),$$

where c is chosen to satisfy equation (6.7). The coefficient, a_1, is never updated and the procedure is terminated when all e_i are close in value to e_1.

In the author's experience, this procedure always converges as one would expect from the discussion leading to the statements of equations (6.8) and (6.9).

Now, we have three transmission path models in our measurement set. They are represented in Figs. 6.2 to 6.5 and Fig. 6.1. We can see that the models of Figs. 6.3 and 6.4 are much more similar than either is to that of Fig. 6.5. In fact, Figs. 6.3 and 6.4 correspond to very unfavourable fleece conditions. From the discussion of section 4.3, it is clear that Fig. 6.5 represents a much more favourable transmission path. This is because the transfer function magnitudes are much greater, the target and clutter paths are spectrally very dissimilar and the target path exhibits a relatively wide bandwidth.

We would expect the least favourable transmission path on the fleece to have characteristics somewhat similar to those of Figs. 6.3 and 6.4. For this reason, two class descriptions were generated in order that the results could be compared. One was generated using all three of the measurement-based models and the other was based on the models of Figs. 6.3 and 6.4 only.

The first class description, based on all three models, is represented in Fig. 6.6 and the second, based on the least favourable two models is represented in Fig. 6.7. The various parameter descriptions are also given on those figures. The important difference between these two is that Fig. 6.6 represents a much broader class description than does Fig. 6.7. This is evident from the fact that the maximum modelling error power, δ_T, is some twenty times larger in Fig. 6.6 than in Fig. 6.7 while the nominal transfer power is only about three times as large.

In the next sub-section the least favourable transmission paths within these two classes are identified. We shall see that the least favourable transmission path corresponding to the class description of Fig. 6.6 is far more unfavourable than that corresponding to the class description of Fig. 6.7.

Figure 6.6 *Transmission Path Class Description (Full Set)*

$$\gamma_T = 863 \times 10^3 ; \quad E_0 = 1.25 \times 10^6 ; \quad \sigma_c^2 = 31.2 \times 10^3$$

A) Nominal target path impulse response.

B) Nominal squared magnitude of target path transfer function.

C) Bounds on squared magnitude of clutter path transfer function.

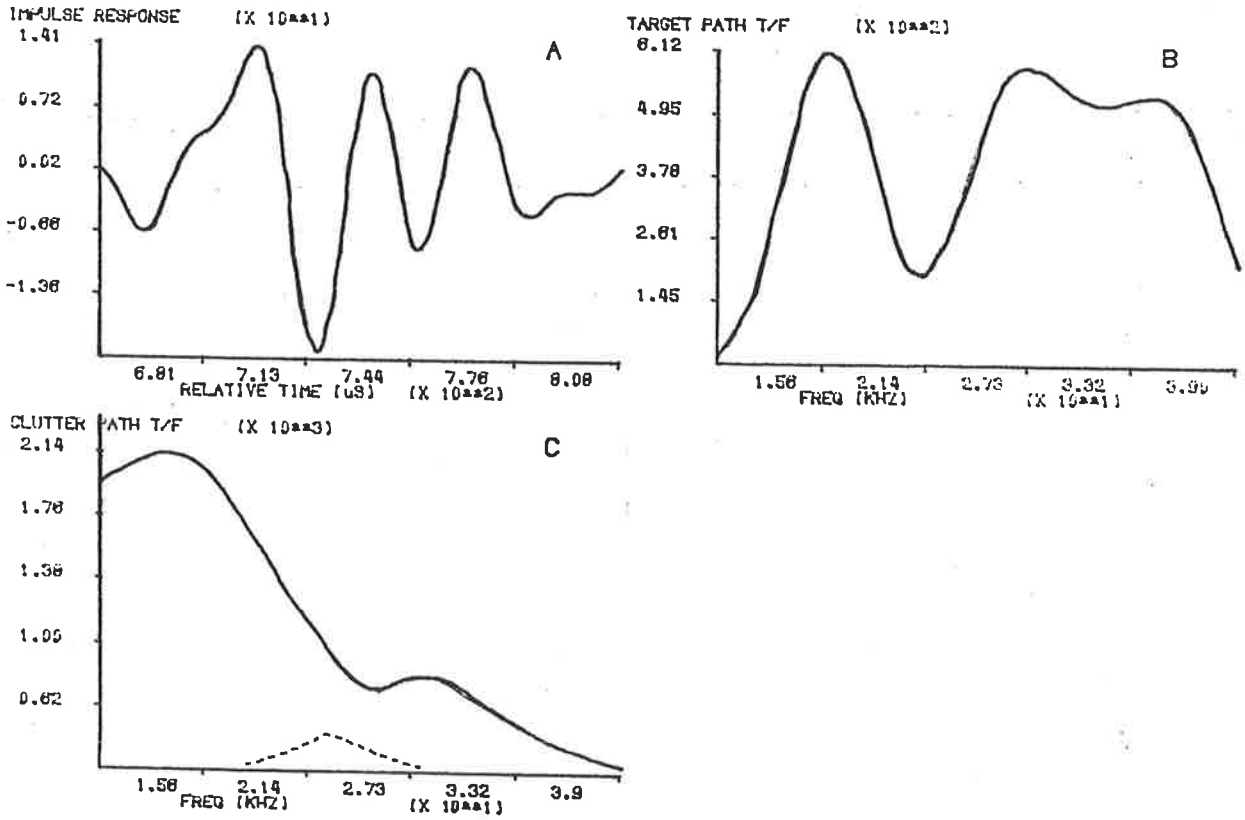

Figure 6.7 *Transmission Path Class Description (Restricted Set)*

$$\gamma_T = 42.5 \times 10^3 ; \qquad E_0 = 439 \times 10^3 ; \qquad \sigma_c^2 = 12.6 \times 10^3$$

A) Nominal target path impulse response.

B) Nominal squared magnitude of target path transfer function.

C) Bounds on squared magnitude of clutter path transfer function.

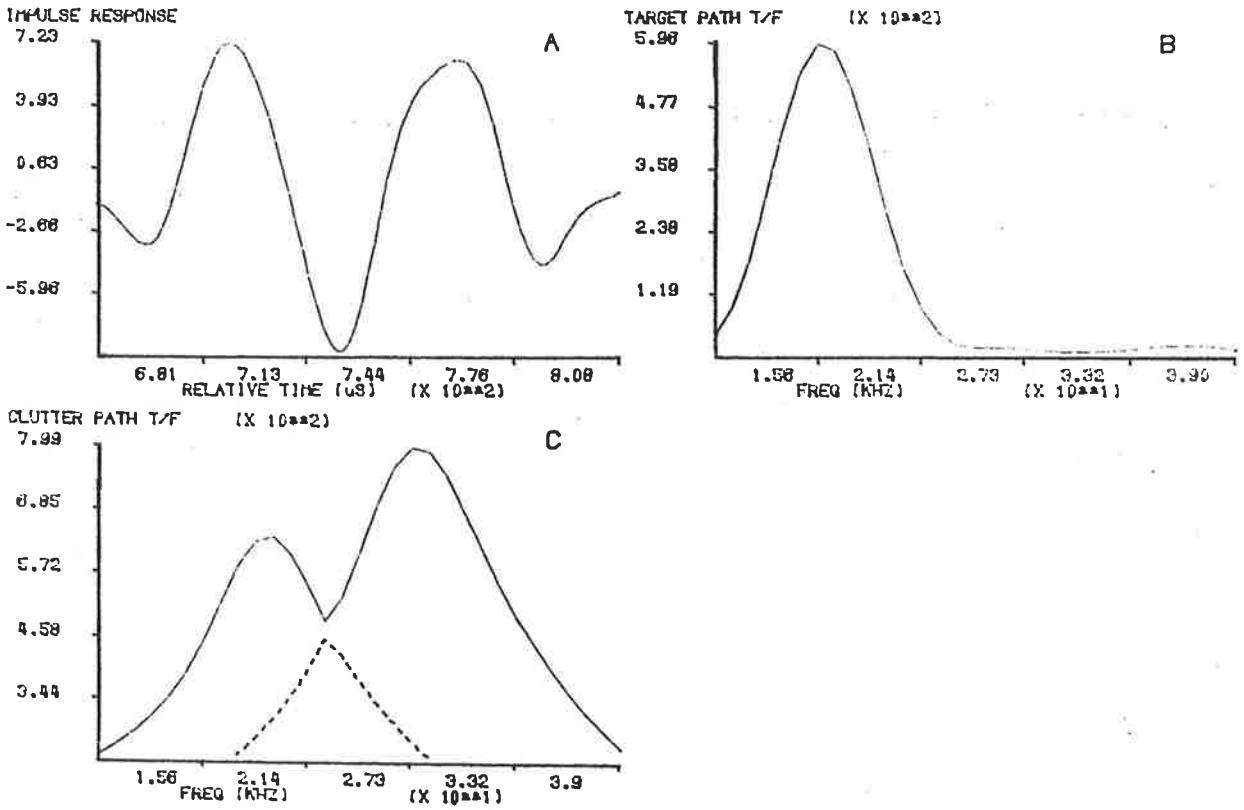

6.2.2 Identifying The Least Favourable Transmission Path

In order to identify the least favourable transmission path within a class described by equations of the forms of equations 4.16 and 4.17, it is necessary to simultaneously solve the three integral equations 4.32 to 4.34.

This problem is simplified by recognizing that each of the three equations are always soluble for one of the three unknown constants given any values for the other two provided certain minor restrictions are met. This was shown in appendix 4. Equation 4.33, however, may not be soluble for c if the condition, $\delta_T \leq E_0$, is not satisfied.

In theory, a solution can always be found provided the target path modeling error power, δ_T, in the transmission path class description, does not exceed the nominal target path transfer power, E_0, as discussed in appendix 4. However, this solution is approached iteratively in practice and care must be taken in devising the iterative procedure to ensure that the procedure is as robust as possible.

In practice, difficulties can arise if δ_T approaches E_0 as equation 4.32 may produce arithmetic overflows in solution due to the choice of an unfavourable trial value for c during the iteration process. In order to minimize the probability of this happening, the procedure should be organized as three nested iteration loops with the outermost loop solving equation 4.32 for k_1. The other two loops solve equations 4.33 and 4.34 for c and k_2 respectively in either order.

A computer program for performing this procedure is listed in appendix 6 after the listing of the class description program. The author has found this program to be very robust. For example, from Fig. 6.6, we find that, for the first of our two class descriptions, $\delta_T \approx .7E_0$ and yet the program is still able to compute a solution.

The least favourable transmission paths within the classes represented in Figs. 6.6 and 6.7 are presented in Figs. 6.8 and 6.9 respectively.

The most important feature of Fig. 6.8 is that the class description of Fig. 6.6 is

Figure 6.8 *Least Favourable Transmission Path Model*

(Broad Class Description)

A) Target path impulse response.

B) Squared magnitude of target path transfer function.

C) Squared magnitude of clutter path transfer function.

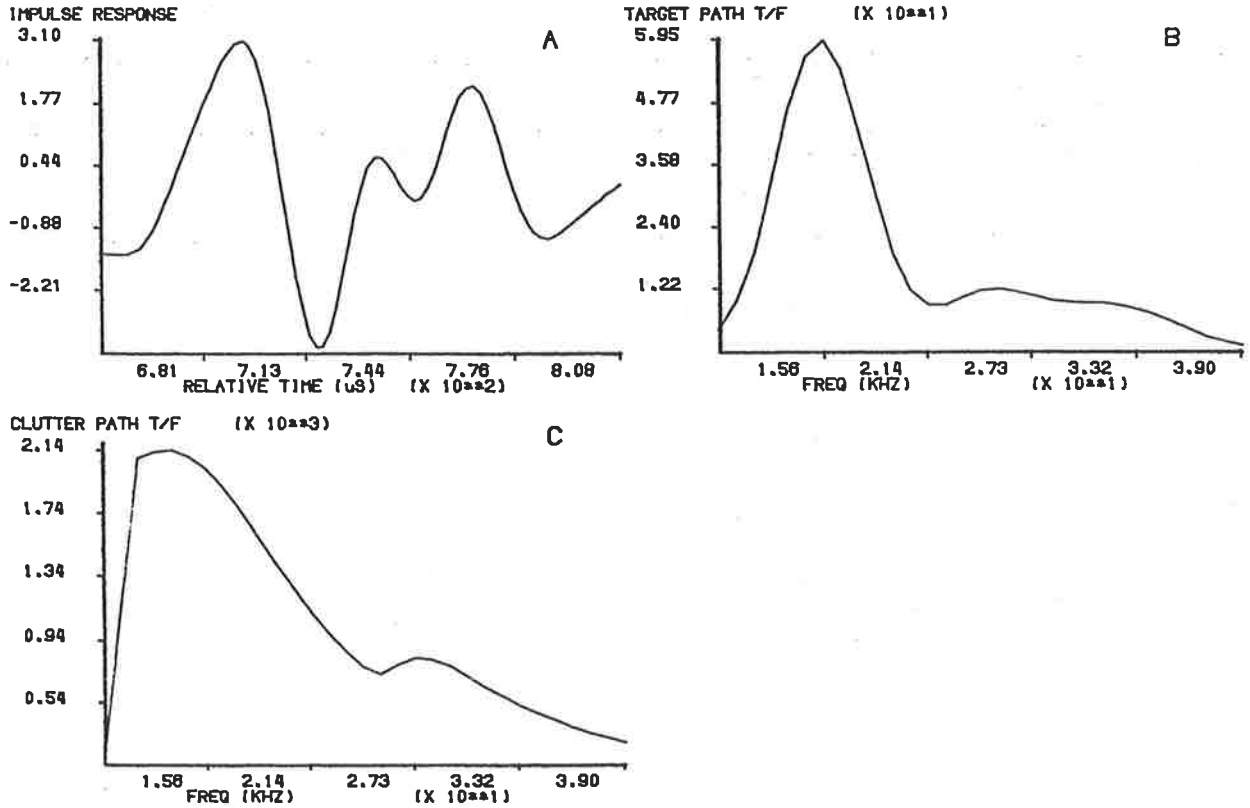

Figure 6.9 *Least Favourable Transmission Path Model*

(Restricted Class Description)

A) Target path impulse response.

B) Squared magnitude of target path transfer function.

C) Squared magnitude of clutter path transfer function.

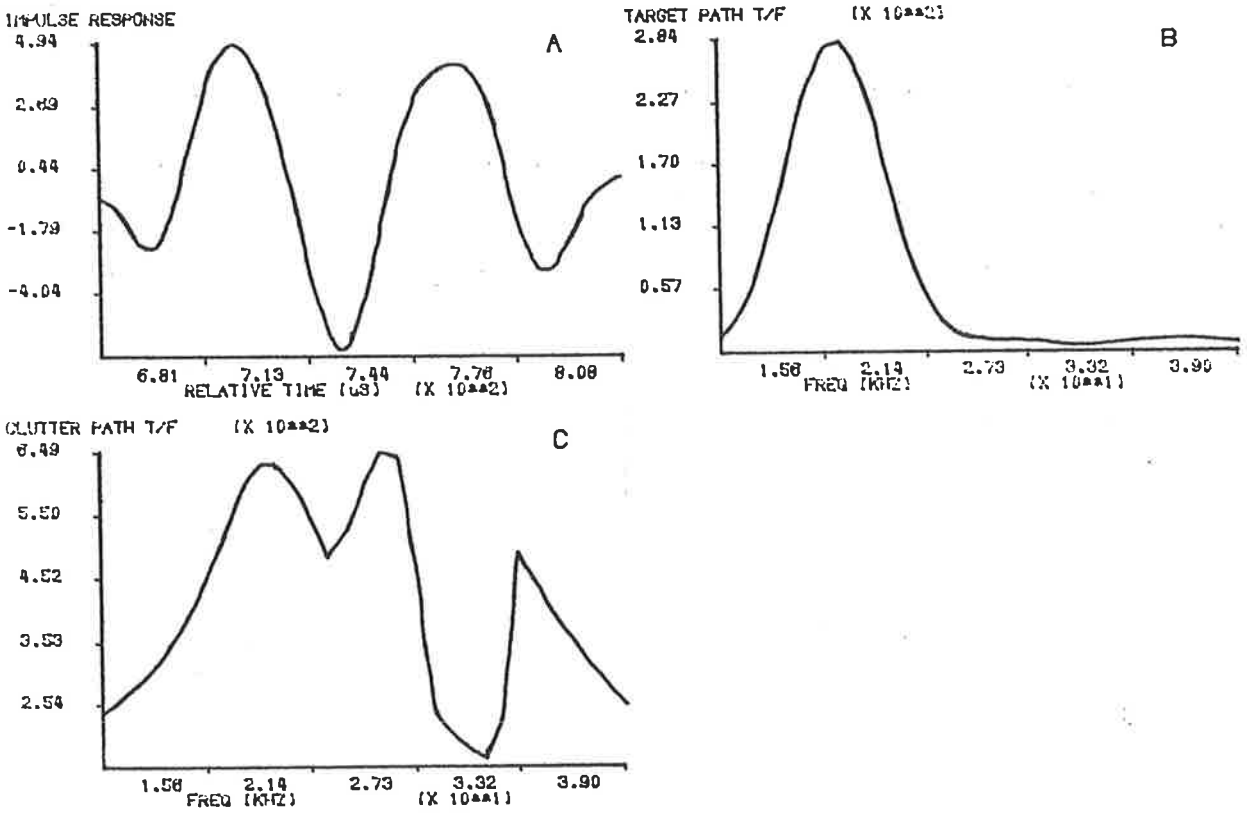

is so broad that a quite unrealistic combination of target and clutter path colourations has been selected. The author's experience, as reflected in the set of measured characteristics in Figs. 6.3 to Fig. 6.5, indicates that the least favourable characteristics obtained on actual fleece exhibit peak clutter path responses at frequencies well above the corresponding peak target path responses. In Fig. 6.8, however, we see that the robust optimization procedure has selected a clutter path transfer function with the frequency of its peak just slightly below that of the target path transfer function. Furthermore, the magnitude of that peak is unrealistically large. Such large clutter path responses are exhibited in practice only in conjunction with large target path responses under highly favourable fleece conditions.

The solution to this problem is to simply exclude highly favourable transmission path characteristics from consideration when constructing the class description. A representative set of transmission path models should be assembled from among the less favourable models found in practice. In identifying the less favourable models, the designer can refer to the unfavourable characteristics listed in section 4.3, most of which are clearly unfavourable from elementary considerations.

In our case, we shall simply proceed to use the second of our transmission path class descriptions based on the less favourable two models in our set of three measurement based models. That description is presented in Fig. 6.7 and the resulting least-favourable transmission path is characterized in Fig. 6.9.

We are now in a position to examine the robustness of the two solutions generated. This will be done by computing and comparing the maximal detection indices obtainable with optimum signals for each transmission path. In table 6.1 each of the three measurement-based models and the two least-favourable models is represented. Optimal signal spectra have been computed for each of the five models and each optimal spectrum has been coupled with each path to obtain a complete table of detection indices.

TABLE 6.1 DETECTION INDEX COMPARISONS

	SPEC 1	SPEC 2	ROBUST SPEC 1	SPEC 3	ROBUST SPEC 2
PATH 1	12.0	11.9	12.0	8.2	11.3
PATH 2	6.7	6.8	6.7	4.2	6.4
ROBUST PATH 1	3.1	3.0	3.1	.7	2.8
PATH 3	18.4	18.7	19.3	21.2	20.9
ROBUST PATH 2	-7.9	-8.1	-7.4	-7.4	-6.9

The name, "ROBUST PATH 1" in table 6.1, refers to the least-favourable path associated with the restricted class of transmission paths described in Fig. 6.7. "ROBUST PATH 2" refers to the least-favourable path associated with the broad class of transmission paths described in Fig. 6.6. "PATH 1", "PATH 2" and "PATH 3" refer to the transmission paths modeled in Figs. 6.3 to 6.5 respectively. Similarly, "ROBUST SPEC 1" refers to the robust optimum signal spectrum for the restricted class of transmission paths while "ROBUST SPEC 2" refers to that for the broad class. "SPEC 1", "SPEC 2" and "SPEC 3" refer to the MDI signal spectra for the three transmission paths numbered 1 to 3 above.

The table has been set up in such a way that the restricted class of transmission paths can be readily considered independently. Only the three columns and the three rows at top left of table 6.1 are relevant when considering the restricted class in isolation.

We see from this portion of the table that no signal spectrum considered yields a higher detection index for any particular transmission path than the MDI spectrum for that path. We also see that, for any signal spectrum, the lowest detection index is obtained as a result of transmission through that path that was selected as the least-favourable path.

This latter result is not surprising but would not be invariably true. The least-favourable path is not defined as being least-favourable in that sense. It is least-favourable in the sense that *optimal* performance through that path is worse than that achievable through any other path in the class.

Turning again to the top left portion of table 6.1, we see that the combination of least-favourable path and MDI signal for that path (the robust optimum signal for the class) does indeed constitute a saddlepoint among those paths and signals represented in the table. The corresponding table entry is at least as large as any other in the corresponding row (row 3) and is smaller than any other in the corresponding column.

Similar comments to all those above in relation to the restricted class of transmission paths also apply when considering the broad class represented in the complete table. However, additional comments can be made about the complete set of results. Firstly, we see that the third of the measured transmission paths (row 4 of table 6.1) is much more favourable than any other represented in the table. This supports the earlier assertion. Secondly, the least-favourable transmission path within the broad class is far less favourable than any other represented in the table. Finally, we see that the robust optimum spectrum for the broad class of transmission paths (column 5 of table 6.1) yields poorer performance than the robust optimum spectrum for the restricted class (column 3 of table 6.1) for the transmission paths from that restricted class (rows 1 to 3 of table 6.1).

The results discussed in the preceding paragraph indicate that, in broadening the class description, we have traded performance in the restricted class for performance outside that restricted class. This, of course, is the principle of robust optimization. However, the class description was broadened to accomodate an additional highly favourable path. We would prefer to trade performance through this highly favourable path for performance elsewhere, if possible. Instead, the effect of broadening the class description has been to cater for extremely unfavourable paths which, according to

empirical evidence, simply do not occur in practice.

This aspect of the problem was discussed earlier in this subsection. The approach taken as a result of that discussion was to restrict the class description by excluding highly favourable measured characteristics when formulating the class description. This meant that the resulting class description did not embrace unrealistic transmission path characteristics such as those of Fig. 6.8.

An alternative and less mathematical approach to robust optimization results from the realization that tables such as 6.1 can be interpreted as game matrices. The game theoretic formulation of the problem in chapter 4 uses a class description that effectively allows interpolation between the transmission paths represented in the measurement set. Another approach, however, is to construct a large measurement set which effectively does not require interpolation. The class of transmission paths for which we would optimize would then be defined directly by the measurement set itself.

Guided by the theoretical results of chapter 4, we could then hope to find a saddlepoint solution to our game problem by constructing a game matrix like table 6.1. To do this we would use all the transmission path characteristics represented in our measurement set. Each element, D_{ij}, in the matrix would represent the SIR obtainable through transmission path i using a signal and receiver filter jointly optimized for transmission path j. A saddlepoint would correspond to an entry that was the maximum in the corresponding row and the minimum in the corresponding column. However, such a saddlepoint may not exist and in that case the more mathematical approach used earlier in this subsection should be employed.

In Fig. 6.10, the robust optimum signal spectra obtained using the two transmission path class descriptions of Figs. 6.6 and 6.7 are compared. We see that they are quite different. Consistent with the analysis of chapter 4, we find that the least-favourable path of the broader class is associated with a flatter optimum signal spectrum. However, that transmission path is not a realistic one for the reasons given earlier. For this

Figure 6.10 *Robust Optimum Signal Spectra*

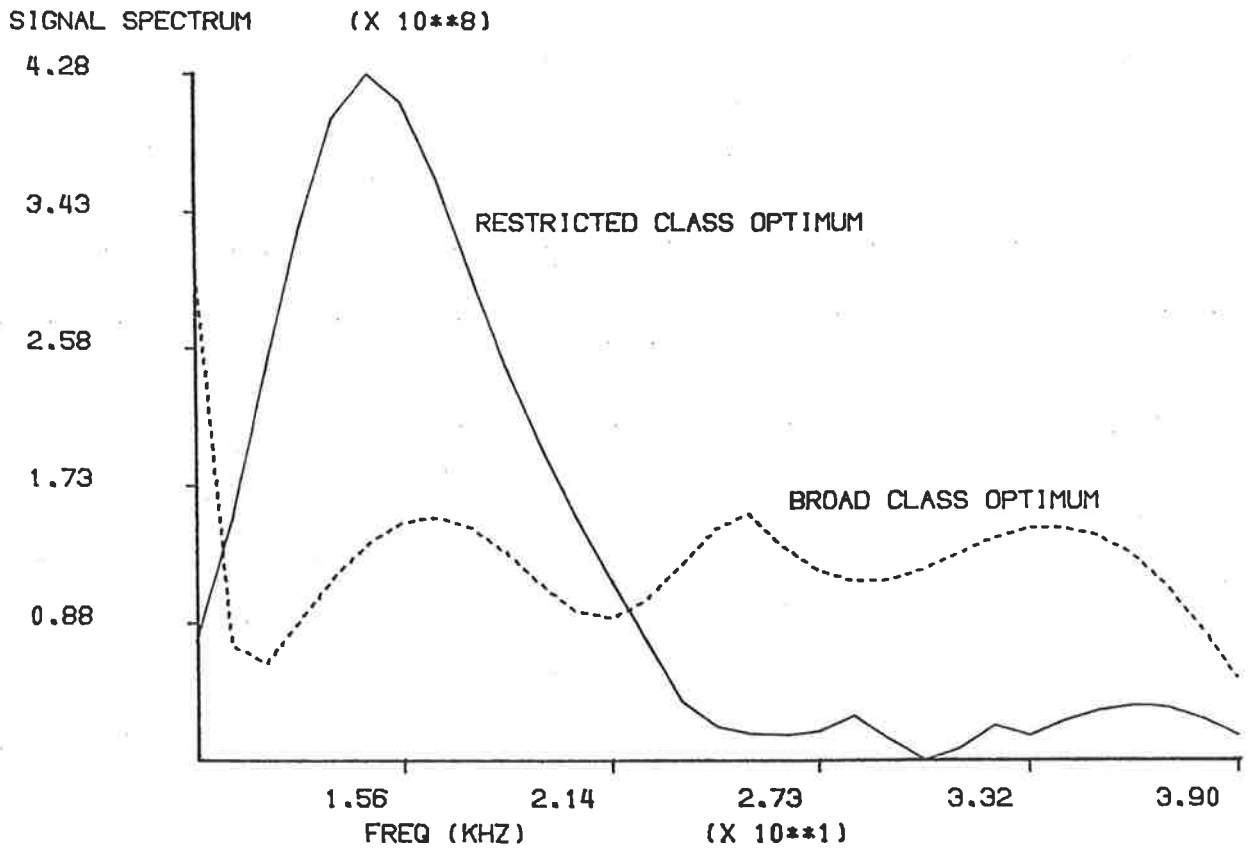

reason, the designer should choose to use the robust optimum signal spectrum for the restricted class of transmission paths.

§6.3 Sensing System Design

6.3.1 Current System Design

In this subsection we shall look at the way in which a digital sensing system for use in the automated shearing experiments was implemented. Fig. 6.11 provides an overall timing diagram.

We see from the figure that the host computer must provide, every 4mS (approx.), an 8-bit range prediction and an 8-bit confidence indication. The latter is inversely related to the estimated RMS prediction error. The host is also responsible for generating a timing pulse at, nominally, 4mS intervals and a reset pulse whenever convenient and desirable. The main function of the reset pulse is to initiate an internal test sequence within the sensor as indicated in Fig. 6.11. Such checking facilities were considered necessary because of the potentially disastrous consequences of undetected sensor failure.

This ultrasonic ranging system is designed to estimate the distance from the sensing head to the sheepskin through the wool at approximately 4mS intervals under the control of the host computer. The sensing head is a focussed array of small ultrasonic transducers. Transmitting and receiving transducers are interspersed throughout the array and all the transmitting transducers are connected in parallel as are all the receiving transducers. The sensing head is focussed at a nominal range of 120mm by spherical curvature of the array. It has a depth of focus in the order of 40mm.

The electronics of the ranging system consists of four main sections. There is a main processor, a transmitting section, a receiving section and a correlator. In addition, there are units that interface these sections, perform logic and timing functions and provide self-test and diagnostic facilities. The overall arrangement is as indicated in the block diagram of Fig. 6.12.

Figure 6.11 *Automated Shearing Sensor Timing*

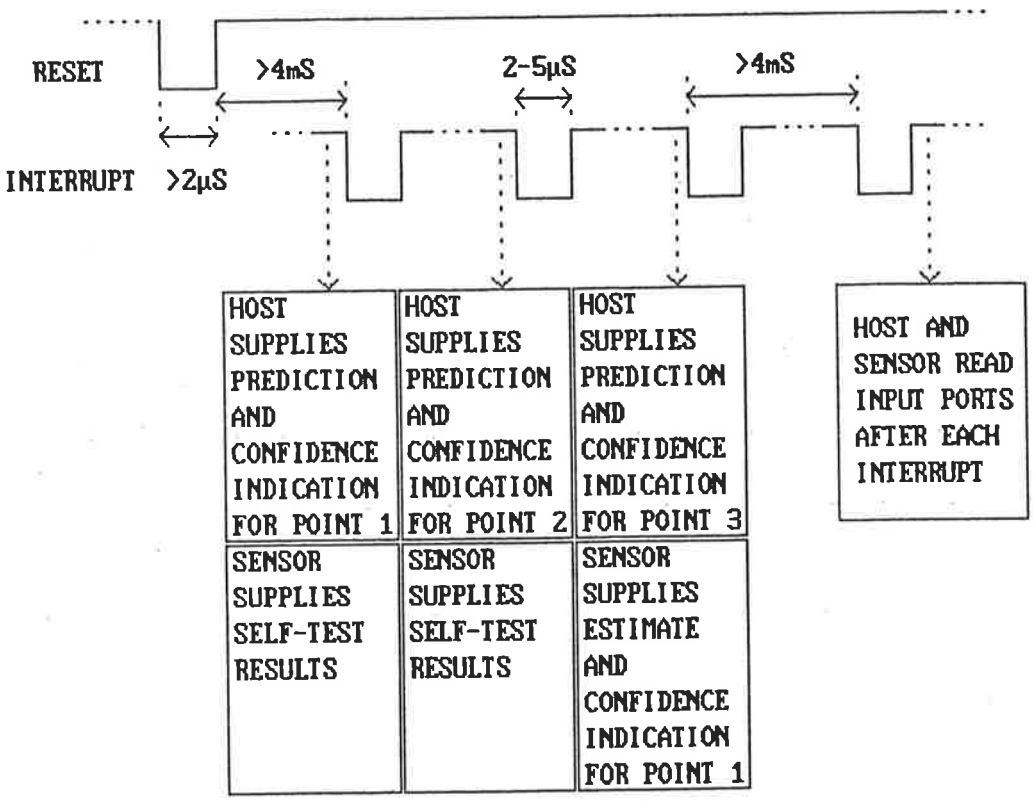

Figure 6.11 *Acoustic Sensor Block Diagram*

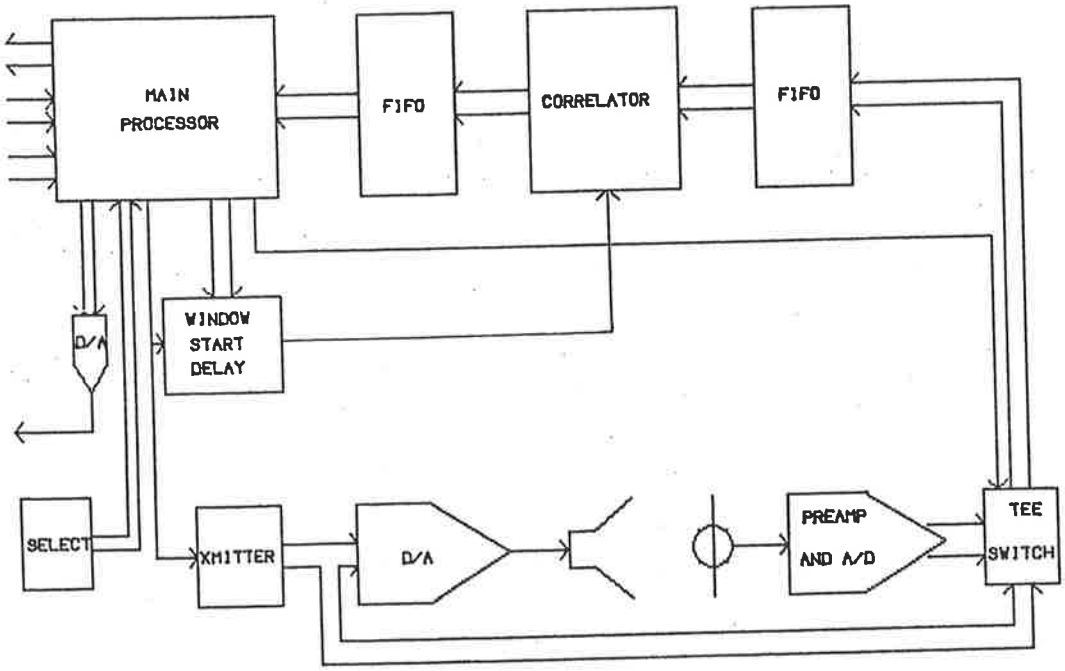

A conditional MAP estimation scheme, as described in chapter 5, is implemented in the blocks marked "CORRELATOR" and "Main Processor". The correlator is required to correlate the received waveform with 160 reference samples over 128 lags in under 3mS. This demanding specification is achieved by employing four TMS32010 signal processors in a linear array. Each of the processors runs an identical program and a single 20MHz clock supplies all four processors. Synchronization between the stages is achieved by resetting all four processors simultaneously at the commencement of the data acquisition sequence within each 4mS interval and then allowing the interstage communication flags to synchronize the stages. Figs. 6.13 and 6.14 detail the correlator hardware design.

The TMS32010 code for the correlator is quite simple. In-line code is used for computing the sum-of-products, resulting in an improvement of almost a factor of two in computation speed over a looped structure. All outputs are output to latches immediately they become available with no handshaking. Availability of input data is indicated to a processor by the setting of its "BIO" flag. This simplified I/O process is made possible by ensuring that all processors run identical programs. Such an approach results in a highly efficient implementation with very low overheads for I/O and interstage synchronization without the need for expensive multi-port random access memory (RAM) blocks between stages. (The only overhead associated with output results from the execution of "OUT" instructions. Extra overheads accumulate during input owing to the testing of the "BIO" flag. However, synchronization is achieved with the transfer of the first datum and thereafter input overheads are absolutely minimal and no overheads are associated with synchronization.)

It is worth noting that this same approach can be applied to the implementation of any non-recursive algorithm because such algorithms can always be distributed between stages in such a way that all stages run identical programs and all I/O is in one direction only. (For recursive algorithms, the approach would have to be modified. For an informative discussion on the design of multi-processor DSP systems, the interested

Figure 6.13 *Correlator Block Diagram*

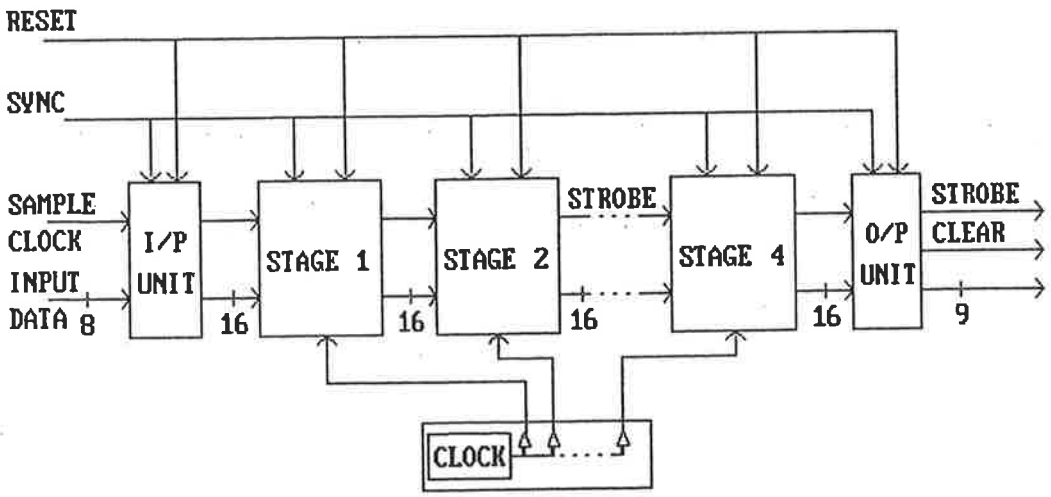

Figure 6.14 Correlator Stage Design

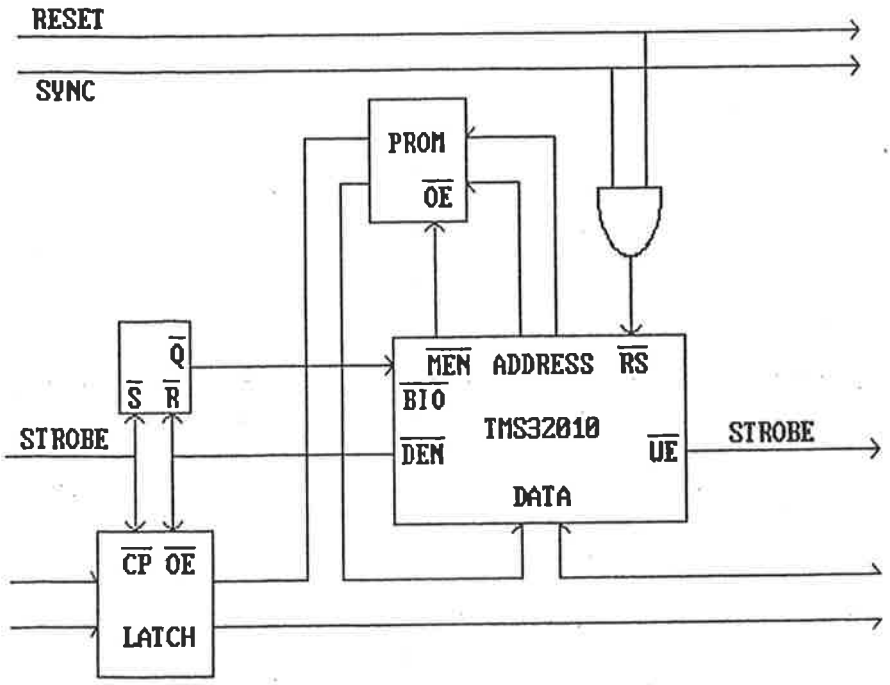

reader is referred to [6.6]) The concept is amenable to extension to allow the design of two-dimensional modular structures for high speed implementation of FFT processors. Such processors could be used to implement correlators to much more demanding specifications [6.5] than those associated with the application being described here. A listing of the correlator code is given in appendix 6.

The correlator is decoupled from the A/D convertor at its input and from the post-correlation processor at its output by the use of high density First-In-First-Out (FIFO) memories. These devices can be asynchronously accessed at input and output and provide FULL and EMPTY flags. The use of such FIFO buffers frees the correlator and post-correlator to input data at their own rate and allows pipelining of the correlation and post-correlation processing tasks.

A single TMS32010 processor performs the post-correlation processing as well as all the communication and control tasks of the sensing system. The post-correlation processing is performed sample by sample and consists of the tasks of enveloping, biasing and peak-picking. The term, "biasing" as used here, refers to the process of adding a parabolic weighting to the envelope as described in chapter 5.

The enveloping operation is performed approximately allowing it to be performed at high speed. The true envelope of a wideband signal is obtained as the RMS sum of the signal and its Hilbert transform. (i.e. as the magnitude of the complex analytic signal.) In our case the Hilbert transform is approximated by means of a 15-element FIR filter. Such techniques are well known[6.3]. The need to evaluate square roots in computing the envelope is avoided by the use of another approximation which obtains the envelope as a simple non-linear function of the signal and Hilbert transform. Errors resulting from these approximations have been estimated at less than six percent.

6.3.2 Trends For The Future

This multi-processor approach to the implementation of high speed DSP systems

is capable of realizing throughput rates suitable for a very wide range of sensing and imaging tasks[6.4,6.5,6.6]. In principle it is possible to combine this approach with efficient computation methods based on the FFT [6.4,6.5].

However, in order to obtain maximum benefit from the multi-processor concept, the architecture of the constituent processor should reflect the I/O intensive nature of such applications and the complexity of the data flow in typical DSP algorithms. The TMS32010 represents a highly successful compromise between the architectural requirements of a microprocessor controller and those of a DSP processor. Nevertheless, its architecture is not optimal for multi-processor applications.

In order to investigate practical alternatives in the architectural design of processors for multi-processor applications, a group of researchers at the University of Adelaide, including the author, set about designing a new architecture optimized for complex sum-of-product computations in a multi-processor environment[6.4]. The author's involvement was directly motivated by the need for a high speed DSP system in the sheepskin sensing project. The result is illustrated in Fig. 6.15.

The main features of the architecture are the separate on-chip I/O processors, the four-quadrant structure and the ring bus. Less obvious features include self-incrementing data pointers, data pointer control registers, loop counters and various flags for conditional jumps, and a load-immediate facility for initializing pointers and registers as well as data locations.

The single most important insight behind this design is the realization that maximum multiplier speed does not necessarily ensure maximum throughput. Our aim was to find ways to trade multiplier speed for speed of data handling so that a balance could be struck between the two capabilities. The use of several shift-and-add type multipliers helps to achieve this balance. The total chip area devoted to multiplication is much less than with one fast combinatorial multiplier, leaving more area for data handling. Equally importantly, the multiply input and output data is now dispersed

Figure 6.15 TFB Architecture

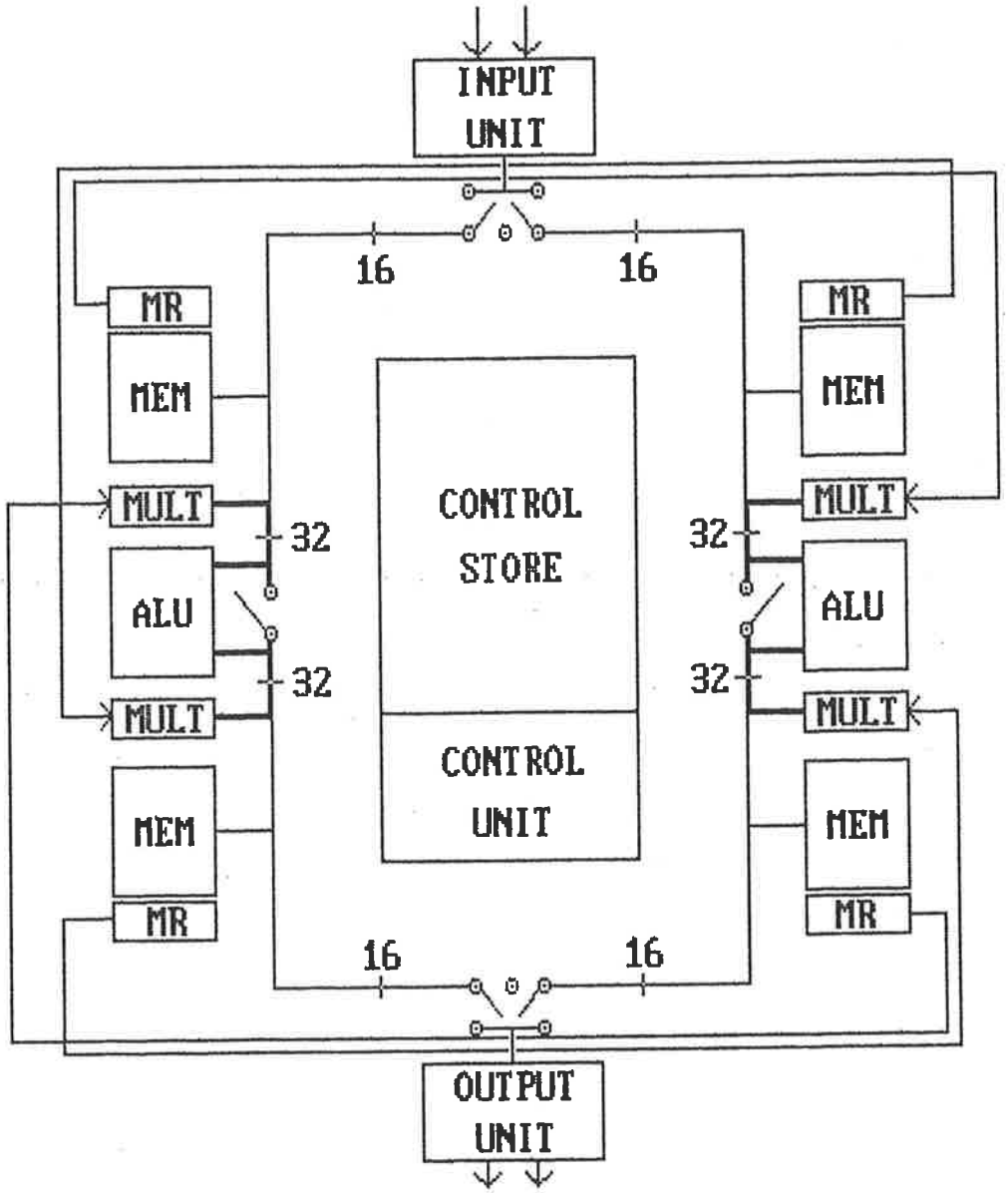

among several physical locations on the chip reducing the potential for bottlenecks.

The segmented ring bus structure provides flexible wideband channels of communication within the chip and a similar motive was behind the decision to use multiple memories. The choice of a four-quadrant structure resulted from an early decision to directly cater for complex arithmetic. Each complex multiply involves four real multiplications and the input data naturally falls into four different categories.

Finally, a 16-pin input port and a 16-pin output port were provided. It was envisaged that these ports would be configurable as 8-bit half-ports and that both synchronous and asynchronous modes of communication would be selectable. In order to reduce I/O overheads to a minimum, on-chip I/O processors were provided to handle the tasks of data formatting and timing in accordance with the selected communication mode. (The modes catered for include double-byte transmission through each half-port.)

The resulting structure allows all data handling, subtractions, additions, shifts and I/O to be pipelined with multiplication in typical algorithms. The design is particularly well suited for complex FFT computation in a parallel-pipelined system involving a two-dimensional array of processors. Such systems are described in [6.5]. By a conservative esimate, an array of 320 such processors could achieve a throughput rate of 50Msamples/sec for the continuous stream computation of 1024-sample FFT.

This architecture forms the basis of a major design exercise being undertaken by a team of VLSI design researchers at the University of Adelaide. Their aims are to develop software tools and design methodologies for CAD design of large VLSI systems as well as to investigate high performance silicon structures suitable for integration at this level. They are working in close collaboration with The Microelectronics Centre of North Carolina and have collaborative links with Bell Laboratories in New Jersey. At the time of writing, all the processing elements of the architecture described above have been designed and simulated. The memories, I/O processors and bus structures have also been designed and simulated in part. Some of these elements have been or are in

the process of being fabricated preparatory to hardware testing. The remaining element is, of course, the control structure which is still being designed. At this stage, there appears to be no significant impediment to the implementation of our architecture. In fact, despite initial concern about the problems imposed by the internal communications, the designers have found that the structure is quite practical for VLSI implementation.

§6.4 Some Results

The system described in sub-section 6.3.1 has not yet been used in robotics experiments. However, an earlier design, described in [1.1], was used in robotics experiments with live sheep. This earlier system was developed before the arrival of the TMS32010 in the market-place. It utilized a NEC μPD7720 signal processor for post-correlation processing and a multi-module structure employing five TRW multiply-accumulators for correlation. (The correlator was developed by the author during 1982/83 to a much more demanding specification than that detailed in section 6.3.1. At that time, the precise requirements were not yet known and the system was developed as a laboratory tool for exploratory experiments both on the bench and with the robot.)

Fig. 6.16 is a frame taken from a videotape of robotics experiments conducted in the automated shearing laboratory at the University of Western Australia. This frame shows the use of acoustic sensing to sense the skin of a live sheep for control of the robot arm while traversing the heavily matted belly wool. The sensing system used was that described in [1.1] and mentioned above. The transducer array can be seen mounted at the end of the robot arm in place of the usual cutter assembly. (Actual shearing was not being attempted in this experiment.)

Fig. 6.17 is another frame from the same videotape showing a plot generated during another experiment. The top trace shows the range estimates from the sensor plotted as a function of time. Random peak-to-peak variations in the skin-to-sensor range estimates of about 2mm are indicated in the top trace. The second trace is a testing signal. The third trace shows the vertical position of the array which was being controlled by the robot to achieve the required range of 120mm. The bottom trace shows the range estimate confidence parameter produced by the sensing system. This is, in fact, proportional to the log of the conditional posterior probability of the range estimate. A small initial confidence is seen to rise rapidly as the target is acquired and to remain high subsequently as the robot tracks the skin.

Figure 6.16 *Robotics Experiments - Setup*

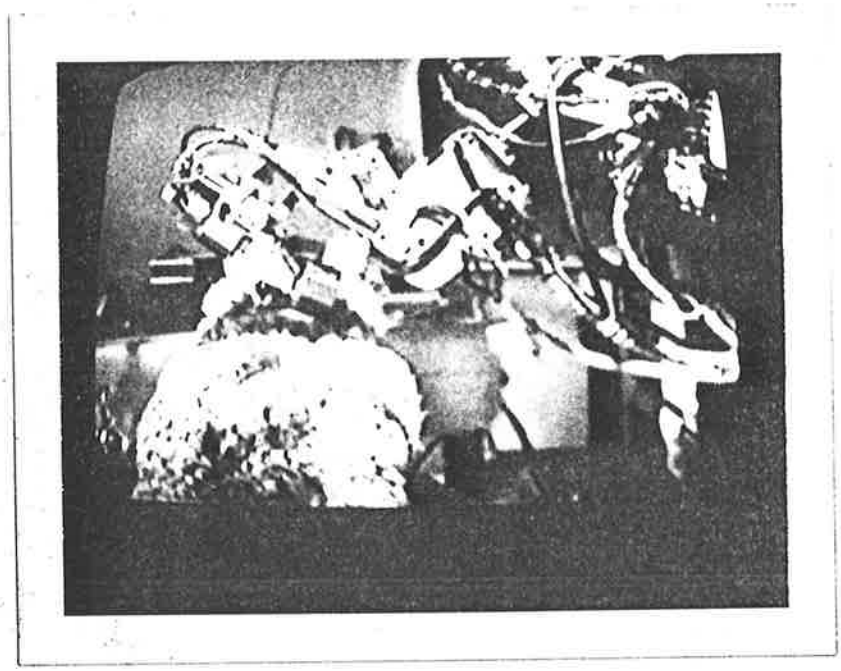

Figure 6.17 ***Robotics Experiments - Some Results***

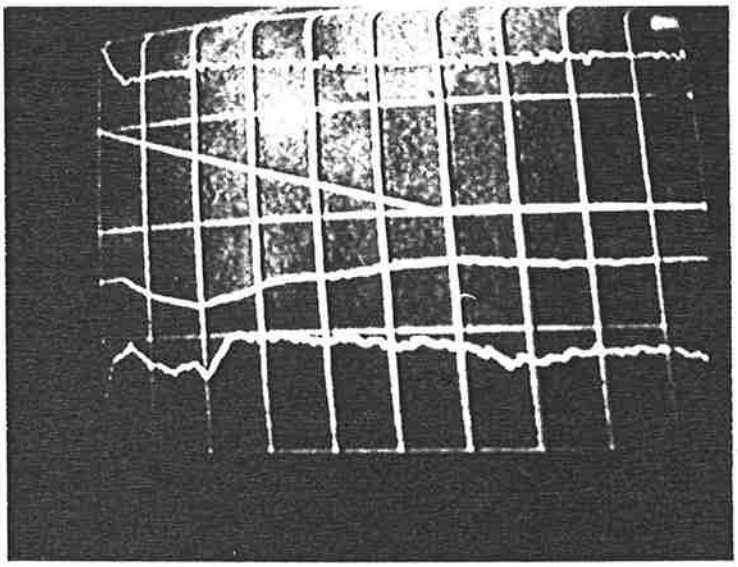

As a result of experiments such as those described briefly above, particularly unfavourable wool conditions have been identified and characterized. Studies such as that of section 6.2 have indicated a need to redesign the transducers to lower the resonant frequency, to increase the peak sensitivity and to reduce performance variations between array elements. This work is now at an advanced stage and, meanwhile, new signal processing electronics have been developed as described in section 6.3.1.

The prognosis for the outcome of the project is that acoustic sensing through the fleece will be proven feasible as a robotic sensing technique in experiments during early 1986. Economically, the sensor design outlined in sub-section 6.3.1 is definitely viable for such an application and is expected to be varied little for future use. However, additional facilities, such as a one-dimensional beamsteering capability, are under investigation.

The possibility of using a higher resolution patch-sensing approach, as discussed in section 6.0, still remains to be assessed in detail. It may be that the surface could be scanned sequentially in raster fashion. In this case, the basic signal processing hardware would require little modification but the system would require augmenting if electronic beam-steering techniques are to be employed. (Mechanical beam-steering may well prove uneconomic.) On the other hand, a faster multi-dimensional processing technique based either on tomography or on parametric model fitting may be necessary or desirable. In this case, a new signal processing system will have to be developed and the VLSI architecture described in subsection 6.3.2 may well be very important in this context. In either case, however, the author expects that the signal design principles and methodology introduced in this thesis will remain important to the continued success of the project.

7. CONCLUSIONS

§7.0 General Remarks

The focus of this thesis is a special class of echo-location applications. Grouped within this class are a wide variety of sensing and surface-imaging applications, most of which have emerged only recently. For this class, Doppler effects are negligible, unwanted backscatter may be intense and the medium may be characterized by highly-coloured absorption properties. In addition, the transmission path characteristics may be highly variable.

For such systems, conventional approaches to system design may be inadequate. We have seen, in chapters 3 and 5, for example, that system performance may be very sensitive to the shape of the signal power spectrum. Furthermore, there are several different aspects of system performance which react independently, in general, to changes in the signal power spectrum. We therefore need to take these dependences into account by using a design procedure that operates on a more complicated transmission path model than is conventionally employed. On the other hand, conventional techniques for signal optimization have little to offer if Doppler effects are not present and the clutter is stationary with range.

This thesis aims to provide a complete system design methodology for such applications. The designer who applies this methodology can feel sure that his design is optimal in a sense that is meaningful in terms of his particular set of competing performance demands.

I have looked for ways in which the signal, the receiver filter, the post-correlation

processor and even the digital processing architecture can be optimized according to relevant criteria. To this end, a number of separate but interrelated investigations have been undertaken in the body of this thesis. Conclusions were presented in the relevant chapters, but the complete set has been compiled in the next section. The restrictions under which the various theoretical results were obtained are also given.

These theoretical restrictions are examined in more detail in section 7.2. Difficulties associated with generalization of the theory are discussed there.

§7.1 Detailed Conclusions

7.1.1 Estimation Theory

The form of the Maximum Likelihood estimator of range by echo-location has long been known. The process involves correlation of the echo with a range-dependent reference signal over all ranges. The estimate is obtained as the range associated with the highest correlation. This form of estimator only becomes practical when prior knowledge is used to restrict attention to a finite region of the range axis. The resulting estimator is known as a Gated Maximum Likelihood estimator.

An important simplification can be made if the interference is statistically stationary or locally stationary with range. In that case the reference signal is independent of range apart from a simple time shift, or is only slowly varying with range. The correlation process can then be viewed as a straightforward linear filtering process involving interference-whitening and matched filtering of the interference-whitened target echo.

My only original contribution in this area is the derivation of the new criterion for local stationarity given by equation 2.22. This condition is less restrictive than that applied by Moose [2.6] but is more consistent. It is particularly relevant where signals of high time-bandwidth product are used. If the noise is stationary, then the interference is locally stationary provided the covariance of the clutter path impulse response, $\phi_{cc}(t_1, t_2)$, depends only on the difference between t_1 and t_2, to a close approximation, over a time period of $2/B$ where B is the signal bandwidth. The requirement imposed by Moose [2.6] was applied over a time period of $2T$ rather than $2/B$ where T was the signal duration.

The Gated Maximum Likelihood estimator of bearing (and, similarly, that of azimuth) by echo-location using an array of sensors, has been derived by Arques [2.15]. It involves scanning a beam across the bearing gate (or sector) and choosing the bearing associated with the peak post-correlation response. The correlation reference is the

same as that used in GML range estimation. In chapter 2, I obtained the same result independently of Arques by a different derivation.

The bearing estimate can be obtained for a target at a particular range, in which case the log-likelihood function generated by the scanning process is a function of bearing only. Alternatively, the estimate can be obtained within a range gate and a sector. In this case, both bearing and range are being estimated and the log-likelihood function is produced by the combined effects of scanning and correlation over a lag region. The LLF is then a two-dimensional function of range and bearing. The concept is easily extended to three dimensions if azimuth is to be estimated also.

The accuracy of these ML estimation procedures depends on the signal power spectrum, the signal duration, the transmission path characteristics and, in the cases of bearing and azimuth, the shape and size of the transmitting aperture. The way in which range estimate variance depends on these factors has been known since Woodward [2.1] analyzed the problem. However, the equivalent expression for bearing estimate variance is derived by me in chapter 2. I also derive an expression for the effective gain of a wideband antenna used for echo-location. It turns out that there is a direct reciprocal correspondence between these two expressions of transverse resolution. I have therefore defined a quantity which I have called the transverse resolution index and which is common to both expressions.

The range estimate variance, the TRI and a third quantity, often appearing in the literature, the detection index, have been used extensively within this thesis as indicators of performance. They all depend, in different ways, on the signal power spectrum, the signal duration and the transmission path characteristics. They are sufficient to indicate all aspects of system performance for comparison between systems and for optimization purposes.

In chapter 5, an original derivation yields a new estimator of range known as a conditional MAP estimator. The concept may readily be extended to estimation

of bearing and azimuth. This estimator is obtained as an augmented form of GML estimator but has superior performance. Its performance is, in fact, superior to that of an optimal form of GML estimator that uses an adaptive tracking range gate. The width of this gate is controlled such that it is always related to the estimated RMS tracking error.

The conditional MAP estimator uses the same information as this optimal form of GML estimator but it minimizes the amount of additional spurious information used. It does this by constructing the log of the conditional prior probability density function according to a minimum information (or maximum entropy) criterion. This function turns out to be an inverted parabola that must be added to the LLF prior to peak-picking.

In the case of digital implementation, such a scheme is highly practical, adding only slightly to the computational load in typical applications. An example is given in chapter 6.

In cases where an adaptive tracking range gate is more practical, mathematical analysis and empirical evidence (obtained by simulation in chapter 5) indicates that the gate width should be adjusted to about 3.5 to 4 times the estimated RMS tracking error in most cases. If the target is highly predictable and the detection index is very small then a system employing a narrower adaptive tracking gate may perform better. However, such a system will be continually hunting for the target with its gate opening and closing as it repeatedly loses and reacquires the target.

7.1.2 Signal Optimization

Four theorems have been presented in chapter 3 that provide analytic solutions to signal optimization problems. In each case, only the signal power spectrum is specified. Later in the same chapter a method for designing a non-linear chirp with the required power spectrum is given and the listing of a computer program for this task is provided

in appendix 3B. In the case of each theorem, also, the solution is not in closed form. The solution of one or more integral equations is required in order to obtain the values of constants in the solution. Again, program listings are provided in appendix 3B.

Three of the four theorems deal with optimization with respect to the three performance indicators that were introduced in chapter 2 and discussed in the previous subsection of this chapter, section 7.1.1. The fourth allows two of these criteria to be introduced as constraints in the problem of optimizing with respect to the third criterion.

Finally, a complete signal optimization strategy has been presented in which the three criteria are effective only according to their priority. Detection performance is always assigned highest priority. This means that the detection index must be greater than or equal to a specified constraint value before either of the other criteria become effective. Either of the other criteria may have next highest priority. If transverse resolution has next highest priority, then both the detection index and the TRI must be greater than or equal to specified constraint values before range accuracy becomes effective as an optimization criterion.

This strategy is implemented in a computer program, the listing of which has been provided in appendix 3B. It gives the designer the flexibility to assign priorities and objectives that reflect the requirements of his application. Nevertheless, it may be that the simpler approach of optimization with respect to one simple criterion also has a place. For one example, a multi-mode echo-location system might well be optimized according to different criteria in different modes. For another, a robust system to operate in a very adverse environment would probably be optimized according to a detection criterion as in chapters 4 and 6.

Many theoretical results have been presented in chapter 3 to illustrate the methods. Most of these results have been supported by simulation results in chapter 5 which are in excellent agreement with the theoretical results.

Methods for constructing transmission path models have been discussed in chapters 3 and 6. They involve ensemble averaging of impulse responses to extract noise and estimate its power spectrum, simple excision of the target echo from the composite echo and power spectral estimation using all-pole modelling to remove spurious detail. I have developed a variant of all-pole modelling that I call all-pole modelling with zero-placement and which has been presented in chapter 3. This can help overcome the shortcomings of all-pole modelling when the system being modelled is known to have zeros in its transfer function. None of these methods will be ideal for all applications, however, and they should be taken as indicative only of the way in which such transmission path models can be obtained.

7.1.3 Robust System Optimization

Despite the flexibility of the signal optimization techniques presented in chapter 3, there exist applications that fall well within the ambit of this thesis and yet are not catered for by the theory of chapters 2 and 3. The application described in chapter 6 is one of these.

The difficulty here is that the transmission path characteristics are uncertain. In the case of the example in chapter 6, the uncertainty arises from two sources. Firstly, there is measurement error which results from the process via which the target impulse response must be extracted from the clutter in order to characterize the transmission path. Secondly, and more importantly, the transmission path characteristics can vary significantly in a quite unpredictable fashion.

The first step in dealing with this problem is to construct a transmission path class description. A transmission path is then described as belonging to this class if its characteristics fall between the limits prescribed in the class description. The class should be as narrow as possible and yet broad enough to accommodate all transmission path characteristics associated with the problem. The form of the class description also

needs to be amenable to the mathematical treatment that is to follow.

A mathematical form for such a transmission path class description has been presented and justified in chapter 4. Techniques for constructing a class description of that form have been given in chapter 6 and the listing of a computer program for producing one from a set of measured transmission path characteristics has been provided in appendix 6.

Chapter 4 also included a theorem that gave the robust jointly optimal pair of signal power spectrum and correlation reference for a specified transmission path class description. Again, the solution is not in closed form but requires the simultaneous solution of a set of integral equations for the values of three constants in the mathematical solution.

The optimization criterion applied is that the pair of signal and receiver filter should maximize the minimum detection index over the class of transmission paths. The problem was presented in chapter 4 like a problem in game theory. Consistent with this approach, the solution, when it exists, is in the form of a saddlepoint. That is, the robust optimal system is designed to maximize the detection index for a least-favourable transmission path within the class. The optimal system performs worst for this least-favourable path. The solution is guaranteed to exist unless the transmission path class description is exceptionally broad. A more precise requirement is stated in appendix 4.

An interesting interpretation of the mathematical form of the solution to this problem is that the least-favourable path is coloured in such a way that the optimal system design for that path (and the robust-optimal system design for the transmission path class) displays the least overall colouration. That is, the product of the optimum signal spectrum with the optimum receiver filter power transfer function is as flat as possible. In addition, the other parameters of the signal path are as unfavourable as possible. Hence, the attenuation of the target path is as large as possible and the clutter

is as intense as possible.

An example of this mathematical approach to robust optimization has been presented in chapter 6 and the listing of a computer program for computing the least-favourable transmission path model has been provided in appendix 6. In addition, a more straightforward approach has been described that will often produce a solution more simply. In this approach, the designer computes the optimum (for maximum detection index) pair of signal and receiver filter for each member of his set of measured transmission path characteristics. He then constructs a game matrix in which each combination of system design and transmission path model has a corresponding entry. The entries are the values of detection index obtained with those combinations.

Hopefully, the designer will be able to identify a saddlepoint in the matrix. However, a saddlepoint is not guaranteed to exist. Furthermore, unless a large number of transmission path measurements are used, a saddlepoint solution obtained by this method may not be the true global saddlepoint of the problem. Nevertheless, this approach also has a theoretical advantage in that the coupling that usually exists between the clutter path characteristics and the target path characteristics (they do not vary completely independently) is reflected in the way in which the problem is formulated.

In the problem formulation of chapter 4 the mathematical form of the transmission path class description does not reflect such interdependence. This can lead to difficulties as we saw in the example of chapter 6 where transmission path characteristics associated with highly favourable paths were combined with others associated with highly unfavourable paths to produce a very unrealistic least-favourable transmission path model. The overall result of such a process is a highly conservative design that performs poorly over the true class of transmission paths for which it has supposedly been optimized. This type of difficulty can largely be overcome, however, by simply excluding highly favourable transmission paths from the analysis when constructing the transmission path class description.

7.1.4 Digital Implementation

The problem of implementing an optimal echo-location system for a high speed application has been considered with the aid of an example in chapter 6. Multi-processor digital system design was advocated and ways of minimizing I/O and synchronization overheads were discussed.

Non-recursive algorithms such as fast Fourier transforms, block correlations and continuous transversal filters are typical of echo-location systems. They can be implemented in multiprocessor structures in which all constituent processors run identical programs and are synchronized via their I/O links. All data flow is in one direction only. All output data is output as it becomes available with no handshaking. The availability of input data is indicated to the receiving processor by means of a hardware flag. Each stage is synchronized to the preceding stage by simply waiting for data to become available.

This approach simplifies the design problem and minimizes overheads. In some cases, however, two or more unalike sections of an algorithm must run on separate processors. In this case, the need for precise synchronization can be eliminated by inserting a First-In-First-Out memory between the stages, effectively decoupling the two processes.

An examination of processor architectures best suited for use as constituent processors in such multi-processor applications was also undertaken in chapter 6. The desirability of flexible, wideband I/O facilities was highlighted. In addition, a way of facilitating compromise between multiplier speed and data-handling capacity was advanced in the form of a multiplicity of shift-and-add type multipliers and a segmented bus structure.An example of such an architectural design in which I was heavily involved was given in chapter 6. The detailed design of a CMOS VLSI implementation of it is not yet finished. However, conservative performance estimates indicate that it will be about 7 times faster than the Texas Instruments TMS32010 signal processor in

multiprocessor FFT applications. In such applications, also, it will require no additional circuitry, except perhaps, depending on the application, for data reordering at input or output.

§7.2 Extensions of the Theory

The conditional MAP estimator presented in chapter 5 uses previous estimates of target range in an optimal way to aid in estimation of the current target range. I have previously described this algorithm as a "look-behind" algorithm [1.1]. This terminology arises naturally in the context of surface imaging when echoes from points over a large area of a surface are being processed in a sequential manner to produce a surface map. In that context, I have also investigated the possibility of developing a conditional MAP estimator that uses unprocessed (or partly processed) echoes from nearby points on the surface to aid in the estimation of surface range at the current point. This type of estimator is called a "look-ahead" estimator [1.1]. Encouraging results have been obtained with an approximate look-ahead algorithm [1.1]. Such an extension to the theory of chapter 5, if it could be demonstrated to be of significant utility, might well be valuable. In other respects, however, there are few theoretical restrictions relevant to the derivation in chapter 5. Prior information can be used in this way to augment any GML estimator.

The theory of chapters 2, 3 and 4, on the other hand, is restricted to situations where Doppler effects are negligible and the clutter is at least locally stationary in a statistical sense. The first of these restrictions might well be important. There may be applications, which do not meet this restriction, to which the theory of chapters 3 and 4 could otherwise be usefully applied. If the clutter is uniformly distributed in range and velocity in a region around the target, then the conventional approaches to signal optimization (as described in section 3.0) have little to offer. If, at the same time, the transmission path is complicated by highly-coloured absorption, coloured noise and differences between the target and clutter paths, then my approach may be useful if it can be extended to take account of significant Doppler effects.

However, attempts to remove the restriction on relative motion by extending the transmission path model to include convolution of the clutter power spectrum with an

assumed Doppler distribution have not been successful. The two main reasons for this are that the resulting optimization problems are very complicated and yet the model still does not cater for wideband Doppler effects.

It seems then, that a completely new approach to the problem will be necessary if a satisfactory solution is to be found. That is to say, it appears that we cannot simply extend the theory of chapters 3 and 4 to cater for non-zero Doppler distribution of the clutter and target echoes.

§7.3 Concluding Remarks

In this thesis, I have reviewed and extended the theory pertaining to the design of echo-location systems. Chapter 2 pertains to the design and performance analysis of ML estimators of range, bearing and azimuth. Chapter 3 deals with the design of signals to optimize performance with respect to range estimation accuracy, target detectability and transverse resolution. Chapter 4 concerns the robust optimization of target detection performance by joint design of the signal and correlation reference. Chapter 5 introduces conditional MAP estimation as an optimal approach to echo location when the target is being tracked and range predictions and estimates of the prediction error are available.

The theory is backed up by simulation results presented in Chapter 5. In addition, Chapters 3, 4, 5 and 6 are replete with details of practical techniques for transmission path modelling and for implementing the design theory. Computer program listings are supplied in the relevant appendices.

To round out the thesis, Chapter 6 presents a case study in which many of the principles and techniques are put to the test of practical application. This case study goes as far as a practical system design involving the implementation of the real-time DSP algorithms in an array of modern signal processing microprocessors. As well as demonstrating the practicality of the design theory, these latter sections on system implementation explore the factors affecting the efficiency of DSP multiprocessor systems. Finally, a new processor architecture is presented that takes advantage of the lessons learnt in that exploration. While I cannot claim sole responsibility for that architecture, it was my implementation problem that prompted its design and I believe I made a significant contribution to that design.

My aim in writing this thesis was to present a comprehensive design methodology for a certain class of echo location system. I believe I have achieved that aim. The methodology presented was certainly influenced at many points in its evolution by the contributions of my supervisor, Prof. R. E. Bogner. In fact, we have had a number

of joint publications on related topics. Nevertheless, I regard the work presented in this thesis as essentially and substantially my own except as indicated in the previous paragraph and in the Acknowledgements.

APPENDIX 3A: PROOF OF THEOREM 1

The proof of theorem 1 will be undertaken in two steps. In the first step the form of the solution in R_1 will be derived. In the second step it will be shown that the transmission of any signal power in R_0 will result in a reduction of the detection index.

Extremization in R_1

For the first step in our proof we need to derive the signal power spectrum, $G_{ss}(f)$, that maximizes the integral:

$$\frac{\Re}{2T} = \int_{R_1} \frac{G_{ss}(f)\,|H_T(f)|^2}{G_{nn}(f) + G_{ss}(f)\,|H_c(f)|^2} df \qquad (3A.1)$$

subject to the power constraint (from 3.15):

$$\int_{R_1} G_{ss}(f) df = P_s/2. \qquad (3A.2)$$

i.e. (provided $G_{ss}(f) > 0$ everywhere in R_1) maximize:

$$\frac{\Re}{2T} = \int_{R_1} \left[\frac{|H_T(f)|^2}{|H_c(f)|^2} - \frac{G_{nn}(f)\,|H_T(f)|^2}{|H_c(f)|^2\, G_{nn}(f) + |H_c(f)|^4\, G_{ss}(f)} \right] df \qquad (3A.3)$$

subject to 3A.2.

The constrained extremization thus reduces to minimizing:

$$\Upsilon = \int_{R_1} \left[\frac{|H_T(f)|^2\, G_{nn}(f)}{|H_c(f)|^2\, G_{nn}(f) + |H_c(f)|^4\, G_{ss}(f)} + \lambda G_{ss}(f) \right] df \qquad (3A.4)$$

where λ is a Lagrange multiplier.

Now, if we let $\Upsilon = \int_{R_1} F(f)df$, then the solution is given by the Euler-Lagrange equation:

$$\frac{dF(f)}{dG_{ss}(f)} = 0.$$

i.e.

$$\lambda - \frac{|H_T(f)|^2 G_{nn}(f) |H_c(f)|^4}{\left(|H_c(f)|^2 G_{nn}(f) + |H_c(f)|^4 G_{ss}(f)\right)^2} = 0. \qquad (3A.5)$$

Equation 3A.5 reduces to:

$$(G_{ss}(f))^2 + \frac{2G_{nn}(f)}{|H_c(f)|^2} G_{ss}(f) + \frac{(G_{nn}(f))^2}{|H_c(f)|^4} - \frac{|H_T(f)|^2 G_{nn}(f)}{\lambda |H_c(f)|^4} = 0. \qquad (3A.6)$$

Of the two mathematical solutions to 3A.6, only the following can be positive:

$$G_{ss}(f) = \frac{k_d |H_T(f)| (G_{nn}(f))^{1/2} - G_{nn}(f)}{|H_c(f)|^2} \qquad (3A.7)$$

where $k_d^2 = 1/\lambda$.

From the definition of R_1, we see that the numerator of 3A.7 is strictly positive over R_1. Hence 3A.7 is a valid solution in R_1. This completes the first step in the proof.

Band of Zero Power

Now, consider the possibility of transmitting some power, P_1, in R_1 and some, P_2, in a region, R_2, within R_0 so that $P_s = P_1 + P_2$. If R_2 is chosen appropriately, the spectrum, $G_2(f)$, that maximizes $\frac{\Re}{2T}$ in R_2 will be given by:

$$G_2(f) = \frac{k_2 |H_T(f)| (G_{nn}(f))^{1/2} - G_{nn}(f)}{|H_c(f)|^2} \tag{3A.8}$$

where k_2 is chosen such that

$$\int_{R_2} G_2(f) df = P_2/2. \tag{3A.9}$$

R_2 will be chosen such that 3A.8 is positive everywhere in R_2.

Now, for P_2 negligibly small, the spectrum, $G_1(f)$, that maximizes $\frac{\Re}{2T}$ in R_1 will be given by:

$$G_1(f) = \frac{k_1 |H_T(f)| (G_{nn}(f))^{1/2} - G_{nn}(f)}{|H_c(f)|^2} \tag{3A.10}$$

From 3A.8 and 3A.10, we can write:

$$\frac{\Re}{2T} = \int_{R_1 \cup R_2} \left[\frac{|H_T(f)|^2}{|H_c(f)|^2} - \frac{G_{nn}(f) |H_T(f)|^2}{|H_c(f)|^2 G_{nn}(f) + |H_c(f)|^4 G_{ss}(f)} \right] df \tag{3A.11}$$

and, substituting for $G_{ss}(f)$, we obtain:

$$\begin{aligned} \frac{\Re}{2T} = & \int_{R_1 \cup R_2} \frac{|H_T(f)|^2}{|H_c(f)|^2} df \\ & - \frac{1}{k_1} \int_{R_1} \frac{|H_T(f)| (G_{nn}(f))^{1/2}}{|H_c(f)|^2} df \\ & - \frac{1}{k_2} \int_{R_2} \frac{|H_T(f)| (G_{nn}(f))^{1/2}}{|H_c(f)|^2} df. \end{aligned} \tag{3A.12}$$

From 3A.12, we get:

$$\frac{\partial(\frac{\Re}{2T})}{\partial k_1} = \frac{1}{k_1^2} \int_{R_1} \frac{|H_T(f)| (G_{nn}(f))^{1/2}}{|H_c(f)|^2} df \tag{3A.13}$$

and

$$\frac{\partial(\frac{\mathcal{R}}{2T})}{\partial k_2} = \frac{1}{k_2^2}\int_{R_2} \frac{|H_T(f)|\,(G_{nn}(f))^{1/2}}{|H_c(f)|^2}df. \tag{3A.14}$$

But

$$\frac{dP_1}{dk_1} = 2\int_{R_1} \frac{|H_T(f)|\,(G_{nn}(f))^{1/2}}{|H_c(f)|^2}df. \tag{3A.15}$$

Hence

$$\frac{dk_1}{dP_2} = \frac{-1}{2\int_{R_1} \frac{|H_T(f)|(G_{nn}(f))^{1/2}}{|H_c(f)|^2}df}. \tag{3A.16}$$

Similarly,

$$\frac{dk_2}{dP_2} = \frac{1}{2\int_{R_2} \frac{|H_T(f)|(G_{nn}(f))^{1/2}}{|H_c(f)|^2}df}. \tag{3A.17}$$

From 3A.13, 3A.14, 3A.16 and 3A.17, we obtain:

$$\frac{d(\frac{\mathcal{R}}{2T})}{dP_2} = \frac{1}{2}\left(\frac{1}{k_2^2} - \frac{1}{k_1^2}\right) \tag{3A.18}$$

Now, since $P_1 < P_s$, we have $k_1 < k_d$ and from 3.17 we see that $k_2 > k_d$ for $G_2(f)$ to be positive in R_2. Hence, from 3A.18, $\frac{d(\frac{\mathcal{R}}{2T})}{dP_2}$ is strictly negative and it follows that $\frac{\mathcal{R}}{2T}$ is maximized by setting $P_2 = 0$. Hence the complete solution is given by 3.16.

Q. E. D.

APPENDIX 3B: PROGRAM LISTINGS FOR CHAPTER 3

§AP3B.1 MV Optimization Program

```
      PROGRAM VARIAN
C PROGRAM TO COMPUTE THE OPTIMAL SIGNAL SPECTRUM FOR RANGE ESTIMATION
C GIVEN A TRANSMISSION PATH MODEL. THE MODEL CONSISTS OF A SET OF DATA
C FILES WHICH ARE ASSUMED TO REPRESENT COMPONENTS OF THE MODEL AS
C FOLLOWS:
C       "SIGSPEC" CONTAINS THE SQUARED MAGNITUDE OF THE TARGET
C                 PATH TRANSFER FUNCTION.
C       "CLSPEC"  CONTAINS THE SQUARED MAGNITUDE OF THE CLUTTER
C                 PATH TRANSFER FUNCTION.
C       "NSPEC"   CONTAINS THE POWER SPECTRUM OF LOCALLY GENERATED
C                 NOISE.
C THE OPTIMUM SPECTRUM IS OUTPUT TO FILE: "OPTSPEC.BIN".
C ALL SIGNALS ARE ASSUMED SAMPLED AT 500KHZ AND ALL SPECTRA ARE ASSUMED
C TO BE BASED ON 512-POINT FFT.

      REAL LPSPEC(128),LPCLUT(128),S(128),NSPEC(128),K,NEWK
      LOGICAL FLAG

      OPEN(1,ERR=100,FILE='SIGSPEC.BIN',STATUS='OLD',ACCESS='SEQUENTIAL'
     1 ,FORM='UNFORMATTED')
      OPEN(2,ERR=100,FILE='CLSPEC.BIN',STATUS='OLD',ACCESS='SEQUENTIAL'
     1 ,FORM='UNFORMATTED')
      OPEN(6,ERR=100,FILE='NSPEC.BIN',STATUS='OLD',ACCESS='SEQUENTIAL'
     1 ,FORM='UNFORMATTED')
      OPEN(7,ERR=100,FILE='DETIND.VAR',STATUS='NEW',ACCESS='SEQUENTIAL'
     1 ,FORM='UNFORMATTED')
      OPEN(8,ERR=100,FILE='ESTVAR.VAR',STATUS='NEW',ACCESS='SEQUENTIAL'
     1 ,FORM='UNFORMATTED')
      OPEN(4,ERR=100,FILE='TRI.VAR',STATUS='NEW',ACCESS='SEQUENTIAL'
     1 ,FORM='UNFORMATTED')
C READ IN TRANSFER FUNCTION SQUARED MAGNITUDES
C WHICH MUST BE DIVIDED BY THE SQUARE OF THE TRANSMITTED IMPULSE
C MAGNITUDE (10V) EXPRESSED IN UNITS OF THE QUANTIZATION STEP (.1*9/256 V)
      DO 10 I=1,128
      READ(1) SAMP
      LPSPEC(I) = SAMP/(2840.*2840.)
      READ(2) SAMP
      LPCLUT(I) = SAMP/(2840.*2840.)
  10  CONTINUE

C READ IN NOISE PSD
      DO 200 I=1,128
      READ(6) NSPEC(I)
 200  CONTINUE

C GET FIRST AND LAST FREQUENCIES AND SIGNAL POWERS
      TYPE *,'SPECIFY FIRST AND LAST FREQUENCIES (BIN NOS.)'
      ACCEPT *,I1,I2
      TYPE *,'SPECIFY FIRST AND LAST SIGNAL POWERS (dB)'
      ACCEPT *,IDB1,IDB2

C COMPUTE THE INITIAL ESTIMATE OF THE SPECTRAL CENTROID
C OF THE POST-WHITENING TARGET SIGNAL
   5  CN = 0.0
      CD = 0.0
      DO 11 I=I1,I2
      CN = CN+I*LPSPEC(I)/LPCLUT(I)
      CD = CD+LPSPEC(I)/LPCLUT(I)
  11  CONTINUE
      C = CN/CD
```

```
      DO 145 IDB=IDB1,IDB2
      OPEN(3,ERR=100,FILE='OPTSPEC.VAR',STATUS='NEW',ACCESS='SEQUENTIAL'
     1 ,FORM='UNFORMATTED')
      PREQ = 10**(FLOAT(IDB)/10.)
      OLDK = 0.
      K = 1.E4
      OLDP = 0.
      FLAG = .FALSE.

C COMPUTE THE MINIMUM VARIANCE SIGNAL SPECTRUM USING K
C ITERATE ON CENTROID
  90  CN = 0.0
      CD = 0.0
      PS = 0.0
      DO 70 I=I1,I2
      S(I) = (K*977*ABS(FLOAT(I)-C)*
     & SQRT(LPSPEC(I)*NSPEC(I))-NSPEC(I))/LPCLUT(I)
      IF (S(I).LT.0.0) S(I) = 0.0
      PS = PS+S(I)*LPSPEC(I)*977
      SS = S(I)*LPSPEC(I)/(NSPEC(I)+S(I)*LPCLUT(I))
      CN = CN+I*SS
      CD = CD+SS
  70  CONTINUE

C COMPUTE SIGNAL POWER
C POWER = SUM(P.S.D.*UNITS*BIN-WIDTH)
      P = 0.
      DO 250 I=I1,I2
 250  P = P+S(I)
      P = P*26E-12*977

C IF SIGNAL POWER NOT AS REQUIRED THEN RECOMPUTE OPTIMAL SPECTRUM
 255  PC = ABS(P/PREQ-1)*100
      IF (PC.LE.1.) GO TO 75
      IF ((P-OLDP).EQ.0.) THEN
        NEWK = 2*K
      ELSE
        NEWK = K+(K-OLDK)*(PREQ-P)/(P-OLDP)
        IF (NEWK.LE.0) NEWK = (K-OLDK)/2+OLDK
      ENDIF
      OLDK = K
      K = NEWK
      OLDP = P
      GO TO 90

C IF CENTROID NOT CORRECT THEN UPDATE AND TRY AGAIN
  75  CCC = CC
      CC = C
      C = CN/CD
      IF (ABS(CC-C).LT..5) GOTO 260
      IF (((CC.GT.CCC).AND.(C.LT.CC)).OR.
     & ((CC.LT.CCC).AND.(C.GT.CC))) THEN
        FLAG = .TRUE.
        C = (CC+CCC)/2
      ELSE
        IF (FLAG) THEN
          C = 2*CC-CCC
        ELSE
          C = (2*CC+C)/3
        ENDIF
      ENDIF
      GO TO 90
```

```
C WRITE OUT OPTIMUM SPECTRUM
 260  DO 263 I=1,I1-1
 263  S(I) = 0.
      DO 266 I=I2+1,128
 266  S(I) = 0.
      DO 110 I=1,128
 110  WRITE(3) S(I)

C COMPUTE THE VARIANCE OF THE DELAY ESTIMATE USING THE OPTIMUM
C SIGNAL SPECTRUM CORRESPONDING TO K
      SIGMA = 0.0
      DO 20 I=I1,I2
      IF ((S(I).LE.0).AND.(NSPEC(I).LE.0)) THEN
        DEL = 0.
      ELSE
        DEL = ((FLOAT(I)-C)**2)*S(I)*LPSPEC(I)
        DEL = DEL/(NSPEC(I)+S(I)*LPCLUT(I))
      ENDIF
  20  SIGMA = SIGMA+DEL
      SIGMA = 2000/(8*3.1416*3.1416*(977**3)*SIGMA)
      WRITE(5,31)
  31  FORMAT(1H ,//)
      WRITE(5,30) SIGMA
  30  FORMAT(1H ,'DELAY ESTIMATE VARIANCE IS ',E9.3,' SECS**2')
      SIGMA = SQRT(SIGMA)*1.0E6
      WRITE(8) SIGMA
      WRITE(5,50) SIGMA
  50  FORMAT(1H ,'CORRESPONDING TO AN RMS ERROR OF ',F9.3,' US')

C COMPUTE THE VALUE OF THE TRANSVERSE RESOLUTION INDEX
C USING THE OPTIMUM SIGNAL SPECTRUM CORRESPONDING TO K
      TRI = 0.0
      DO 220 I=I1,I2
      IF ((S(I).LE.0).AND.(NSPEC(I).LE.0)) THEN
        DEL = 0.
      ELSE
        DEL = (FLOAT(I)**2)*S(I)*LPSPEC(I)
        DEL = DEL/(NSPEC(I)+S(I)*LPCLUT(I))
      ENDIF
 220  TRI = TRI+DEL
      TRI = (977**3)*TRI
      TRI = 8*3.1416*.0005*TRI
      TRI = TRI/(340*340)
      WRITE(4) TRI
      WRITE(5,230) TRI
 230  FORMAT(1H ,'TRANSVERSE RES. INDEX IS ',E9.3,
     & 'PER SQ. METRE')

C OUTPUT THE VALUE OF THE DETECTION INDEX (SIR)
      D = 10*ALOG10(CD*977/2000)
      WRITE(7) D
      WRITE(5,120) D
 120  FORMAT(1H ,'THE DETECTION INDEX IS ',F6.2,' DB')

      CLOSE(3)
 145  CONTINUE
      STOP

 100  WRITE(5,40)
  40  FORMAT(1H ,'ERROR DURING FILE OPENING')
      STOP
      END
```

§AP3B.2 All-pole Spectral Estimation Program with Zero Placement

```
      PROGRAM DURBIN

C PROGRAM TO SMOOTH A POWER SPECTRUM BY MODIFIED SELECTIVE
C MEM SPECTRAL ESTIMATION USING DURBIN'S ALGORITHM AND
C ZERO PLACEMENT.

      CHARACTER INFILE*31,OTFILE*31,CH
      DIMENSION A(20),R(20),S(256)
      COMPLEX X(512),Y(256),Z(10),ZJ
      REAL JJ

 10   TYPE *,'SPECIFY INPUT FILE: '
      ACCEPT 15,INFILE
 15   FORMAT(A31)
      OPEN(1,ERR=40,FILE=INFILE,STATUS='OLD',ACCESS='SEQUENTIAL'
     1 ,FORM='UNFORMATTED')
      REWIND(1)
      GO TO 50
 40   WRITE(10,60) IER
 60   FORMAT(18H FILE OPEN ERROR- ,I5)
      GO TO 10

 50   TYPE *,'SPECIFY OUTPUT FILE: '
      ACCEPT 15,OTFILE
      OPEN(2,ERR=80,FILE=OTFILE,STATUS='NEW',ACCESS='SEQUENTIAL'
     1 ,FORM='UNFORMATTED')
      GO TO 90
 80   WRITE(10,60) IER
      GO TO 50

 90   TYPE *,'SPECIFY PREDICTION ORDER: '
      ACCEPT *,NP

      TYPE *,'SPECIFY NUMBER OF ZEROES TO BE PLACED'
      ACCEPT *,NZ
      DO 95 I=1,NZ
      TYPE *,'SPECIFY POSITION OF NEXT ZERO (ZREAL,ZIMAG)'
      ACCEPT *,ZREAL,ZIMAG
      Z(I) = CMPLX(ZREAL,ZIMAG)
 95   CONTINUE

      TYPE *,'SPECIFY FIRST AND LAST SAMPLE: '
      ACCEPT *,ISAMP,LSAMP
      IF (ISAMP.LT.1) ISAMP = 1
      NSAMP = LSAMP-ISAMP+1

C READ IN DATA
      X(NSAMP+1) = (0.,0.)
      DO 120 I=1,ISAMP-1
 120  READ(1)
      READ(1) SAMP
      X(1) = CMPLX(SAMP,0.)
      DO 130 I=2,NSAMP
      READ(1) SAMP
      X(I) = CMPLX(SAMP,0.)
 130  X(2*NSAMP+2-I) = X(I)

C INSERT POLES TO CANCEL KNOWN ZEROES
      Z1 = (1.,0.)
      DO 145 I=1,NZ
 145  X(1) = X(1)/CABS(Z1-Z(I))
      DO 135 J=2,NSAMP
```

```
      JJ = 3.1416*(J-1)/NSAMP
      ZJ = CMPLX(COS(JJ),SIN(JJ))
      DO 135 I=1,NZ
      X(J) = X(J)/CABS(ZJ-Z(I))
 135  X(2*NSAMP+2-J) = X(J)

C TRANSFORM TO AUTOCORRELATION DOMAIN
      CALL DFT(X,2*NSAMP,Y,NP+1)
      DO 140 I=1,NP+1
 140  R(I) = REAL(Y(I))/(2*NSAMP)

C APPLY MEM TO AUTOCORRELATION FUNCTION
      CALL DURB(R,A,NP,G)

C OBTAIN MEM SPECTRAL ESTIMATE FROM PREDICTOR COEFFICIENTS
      DO 150 I=1,NP+1
 150  X(I) = CMPLX(A(I),0.)
      DO 160 I=NP+2,2*NSAMP
 160  X(I) = (0.,0.)
      CALL DFT(X,2*NSAMP,Y,NSAMP)
      DO 170 I=1,NSAMP
      S(I) = REAL(Y(I)*CONJG(Y(I)))
      S(I) = G*G/S(I)
 170  CONTINUE

C OUTPUT LEADING ZERO SAMPLES
      SAMP = 0.
      DO 255 I=1,ISAMP-1
 255  WRITE(2) SAMP

C REINSERT ZEROES AND OUTPUT
      Z1 = (1.,0.)
      SAMP = S(1)
      DO 245 I=1,NZ
 245  SAMP = SAMP*CABS(Z1-Z(I))
      WRITE(2) SAMP
      DO 240 J=2,NSAMP
      JJ = 3.1416*(J-1)/NSAMP
      ZJ = CMPLX(COS(JJ),SIN(JJ))
      SAMP = S(J)
      DO 235 I=1,NZ
 235  SAMP = SAMP*CABS(ZJ-Z(I))
 240  WRITE(2) SAMP

C OUTPUT TRAILING ZERO SAMPLES
      SAMP = 0.
 250  READ(1,END=260)
      WRITE(2) SAMP
      GOTO 250

 260  STOP
      END
```

```
      SUBROUTINE DURB(CS,A,NP,G)
      DIMENSION A(20),AP(0:20,0:20),E(0:20),CS(*)
      REAL K(20)

C DURBIN'S ALGORITHM
      E(0) = CS(1)
      DO 15 I=0,NP
      AP(I,0) = 0.0
      AP(0,I) = 0.0
 15   CONTINUE
      DO 20 I=1,NP
      K(I) = CS(I+1)
      DO 30 J=1,(I-1)
      K(I) = K(I) + AP(I-1,J)*CS(I-J+1)
 30   CONTINUE
      K(I) = -K(I)/E(I-1)
      AP(I,I) = K(I)
      DO 40 J=1,(I-1)
      AP(I,J) = AP(I-1,J)  + K(I)*AP(I-1,I-J)
 40   CONTINUE
      E(I) = (1-K(I)*K(I))*E(I-1)
 20   CONTINUE
      A(1) = 1.
      DO 50 J=1,NP
      A(J+1) = AP(NP,J)
 50   CONTINUE

C COMPUTE GAIN PARAMETER
      G = SQRT(E(NP))

      RETURN
      END
```

```
      SUBROUTINE DFT(DAT,N,S,NV)

C COMPUTE NV COMPLEX POINTS FROM AN N-POINT
C COMPLEX SEQUENCE BY DFT. MODIFIED FROM AN
C ORIGINAL ROUTINE BY D. FENSOM

      COMPLEX W(512),Z,DAT(*),S(*)
      CON=-8.*ATAN2(1.,1.)/FLOAT(N)
      DO 100 I=1,N
 100  W(I)=CEXP(CMPLX(0.,CON*FLOAT(I-1)))
      DO 300 I=1,NV
      Z=CMPLX(0.,0.)
      DO 200 J=1,N
      IA=MOD((I-1)*(J-1),N)+1
 200  Z=Z+DAT(J)*W(IA)
 300  S(I)=Z
      RETURN
      END
```

§AP3B.3 Mixed Criteria Optimization Program

```
      PROGRAM MIXUP
C PROGRAM TO COMPUTE THE OPTIMAL SIGNAL SPECTRUM FOR RANGE ESTIMATION
C GIVEN A TRANSMISSION PATH MODEL. THE MODEL CONSISTS OF A SET OF DATA
C FILES WHICH ARE ASSUMED TO REPRESENT COMPONENTS OF THE MODEL AS
C FOLLOWS:
C       "SIGSPEC" CONTAINS THE SQUARED MAGNITUDE OF THE TARGET
C                 PATH TRANSFER FUNCTION.
C       "CLSPEC"  CONTAINS THE SQUARED MAGNITUDE OF THE CLUTTER
C                 PATH TRANSFER FUNCTION.
C       "NSPEC"   CONTAINS THE POWER SPECTRUM OF LOCALLY GENERATED
C                 NOISE.
C THE OPTIMUM SPECTRUM IS OUTPUT TO FILE: "OPTSPEC.BIN".
C THREE PERFORMANCE INDICATOR FILES ARE ALSO PRODUCED. THEY ARE CALLED
C "DETIND.MIX", "ESTVAR.MIX" AND "TRI.MIX".
C ALL SIGNALS ARE ASSUMED SAMPLED AT 500KHZ AND ALL SPECTRA ARE ASSUMED
C TO BE BASED ON 512-POINT FFT.

      REAL LPSPEC(128),LPCLUT(128),S(128),NSPEC(128),
     & KV,NEWKV,KD,NEWKD,KT,NEWKT
      LOGICAL FLAG,DFIRST,TFIRST,DONLY

      OPEN(1,ERR=100,FILE='SIGSPEC.BIN',STATUS='OLD',ACCESS='SEQUENTIAL'
     1 ,FORM='UNFORMATTED')
      OPEN(2,ERR=100,FILE='CLSPEC.BIN',STATUS='OLD',ACCESS='SEQUENTIAL'
     1 ,FORM='UNFORMATTED')
      OPEN(6,ERR=100,FILE='NSPEC.BIN',STATUS='OLD',ACCESS='SEQUENTIAL'
     1 ,FORM='UNFORMATTED')
      OPEN(7,ERR=100,FILE='DETIND.MIX',STATUS='NEW',ACCESS='SEQUENTIAL'
     1 ,FORM='UNFORMATTED')
      OPEN(8,ERR=100,FILE='ESTVAR.MIX',STATUS='NEW',ACCESS='SEQUENTIAL'
     1 ,FORM='UNFORMATTED')
      OPEN(4,ERR=100,FILE='TRI.MIX',STATUS='NEW',ACCESS='SEQUENTIAL'
     1 ,FORM='UNFORMATTED')
C READ IN TRANSFER FUNCTION SQUARED MAGNITUDES
C WHICH MUST BE DIVIDED BY THE SQUARE OF THE TRANSMITTED IMPULSE
C MAGNITUDE (10V) EXPRESSED IN UNITS OF THE QUANTIZATION STEP (.1*9/256 V)
      DO 10 I=1,128
      READ(1) SAMP
      LPSPEC(I) = SAMP/(2840.*2840.)
      READ(2) SAMP
      LPCLUT(I) = SAMP/(2840.*2840.)
   10 CONTINUE

C READ IN NOISE PSD
      DO 200 I=1,128
      READ(6) NSPEC(I)
  200 CONTINUE

C GET FIRST AND LAST FREQUENCIES AND SIGNAL POWERS,
C AND CONSTRAINTS.
      TYPE *,'SPECIFY FIRST AND LAST FREQUENCIES (BIN NOS.)'
      ACCEPT *,I1,I2
      TYPE *,'SPECIFY FIRST AND LAST SIGNAL POWERS (dB)'
      ACCEPT *,IDB1,IDB2
      TYPE *,'SPECIFY DETECTION INDEX REQUIRED (dB)'
      ACCEPT *,DREQ
      TYPE *,'SPECIFY TRI REQUIRED'
      ACCEPT *,TREQ
```

```
C COMPUTE THE INITIAL ESTIMATE OF THE SPECTRAL CENTROID
C OF THE POST-WHITENING TARGET SIGNAL
   5  CN = 0.0
      CD = 0.0
      DO 11 I=I1,I2
      CN = CN+I*LPSPEC(I)/LPCLUT(I)
      CD = CD+LPSPEC(I)/LPCLUT(I)
  11  CONTINUE
      C = CN/CD

C REPEAT FOR ALL REQUIRED SIGNAL POWERS AT
C 1dB INTERVALS
      DO 145 IDB=IDB1,IDB2

      OPEN(3,ERR=100,FILE='OPTSPEC.MIX',STATUS='NEW',ACCESS='SEQUENTIAL'
     1 ,FORM='UNFORMATTED')

C INITIALIZE
      PREQ = 10**(FLOAT(IDB)/10.)
      OLDKV = 0.
      KV = 1.E4
      OLDP = 0.
      KD = 0.
      KT = 0.
      CC = C
      FLAG = .FALSE.
      DFIRST = .TRUE.
      TFIRST = .TRUE.
      DONLY = .FALSE.

C COMPUTE THE MINIMUM VARIANCE SIGNAL SPECTRUM USING KV,
C KD AND KT. ITERATE ON CENTROID.
  90  CN = 0.0
      CD = 0.0
      PV = 0.
      PT = 0.
      PD = 0.
      DO 70 I=I1,I2
      SV = 977*ABS(FLOAT(I)-C)*SQRT(LPSPEC(I)*NSPEC(I))/LPCLUT(I)
      ST = KT*977*FLOAT(I)*SQRT(LPSPEC(I)*NSPEC(I))/LPCLUT(I)
      SD = KD*SQRT(LPSPEC(I)*NSPEC(I))/LPCLUT(I)
      SSV = (977*ABS(FLOAT(I)-C))**2
      SST = (KT*977*FLOAT(I))**2
      SSD = KD**2
      S(I) = (KV*SQRT((SSV+SST+SSD)*(LPSPEC(I)*NSPEC(I)))
     & -NSPEC(I))/LPCLUT(I)
      IF (S(I).LT.0.0) THEN
        S(I) = 0.0
        SV = 0.
        ST = 0.
        SD = 0.
      ENDIF
C COMPUTE "PARTIAL POWERS"
      PV = PV+SV
      PT = PT+ST
      PD = PD+SD
      SS = S(I)*LPSPEC(I)/(NSPEC(I)+S(I)*LPCLUT(I))
C COMPUTE NUMERATOR AND DENOMINATOR OF CENTROID FREQ.
      CN = CN+I*SS
      CD = CD+SS
  70  CONTINUE
```

```
C COMPUTE SIGNAL POWER
C POWER = SUM(P.S.D.*UNITS*BIN-WIDTH)
      P = 0.
      DO 250 I=I1,I2
 250  P = P+S(I)
      P = P*26E-12*977

C IF SIGNAL POWER NOT AS REQUIRED THEN RECOMPUTE OPTIMAL SPECTRUM
 255  PC = ABS(P/PREQ-1)*100
      IF (PC.LE.1.) GO TO 75
      IF ((P-OLDP).EQ.0.) THEN
        NEWKV = 2*KV
      ELSE
        NEWKV = KV+(KV-OLDKV)*(PREQ-P)/(P-OLDP)
        IF (NEWKV.LE.0.) NEWKV = KV/2
      ENDIF
      OLDKV = KV
      KV = NEWKV
      OLDP = P
      GO TO 90

C IF CENTROID NOT CORRECT THEN UPDATE AND TRY AGAIN
  75  CCC = CC
      CC = C
      C = CN/CD
      IF (ABS(CC-C).LT..5) GOTO 260
      IF (((CC.GT.CCC).AND.(C.LT.CC)).OR.
     & ((CC.LT.CCC).AND.(C.GT.CC))) THEN
        FLAG = .TRUE.
        C = (CC+CCC)/2
      ELSE
        IF (FLAG) THEN
          C = 2*CC-CCC
        ELSE
          C = (2*CC+C)/3
        ENDIF
      ENDIF
      GO TO 90

C IF DETECTION INDEX NOT AS REQUIRED THEN UPDATE KD
C AND TRY AGAIN.
 260  D = 10*ALOG10(CD*977/2000)

C IF DETECTION CONSTRAINT MET WITHOUT ADDING AN MDI
C COMPONENT TO THE POWER SPECTRUM THEN DONT BOTHER.
      IF ((D.GT.DREQ).AND.(KD.EQ.0.)) GOTO 660

C IF DETECTION CONSTRAINT NOT MET AND MV COMPONENT
C OF THE POWER SPECTRUM IS NEGLIGIBLE THEN GIVE UP.
C DO NOT WORRY ABOUT TRI CONSTRAINT.
      IF ((D.LT.DREQ).AND.(PV.LT..01*PD)) THEN
        DONLY = .TRUE.
        GOTO 760
      ENDIF

      IF (ABS(DREQ-D).LT..1) GOTO 660
      IF (DFIRST) THEN
C FOR FIRST ATTEMPT GUESS A REASONABLE VALUE FOR MDI COEFFICIENT

        DFIRST = .FALSE.
      ELSE
        IF ((D-OLDD).EQ.0) THEN
```

```
C HEURISTIC TO PREVENT LOCK-UP
          NEWKD = 2.*KD
        ELSE
          NEWKD = KD+(KD-OLDKD)*(DREQ-D)/(D-OLDD)
        ENDIF
C DONT ALLOW NEGATIVE CONTRIBUTIONS TO POWER SPECTRUM
        IF (NEWKD.LE.0.) NEWKD = 0.
      ENDIF
 265  OLDKD = KD
      KD = NEWKD
      OLDD = D
      OLDKV = 0.
      OLDP = 0.
      CC = C
      FLAG = .FALSE.
      GO TO 90

C IF TRI NOT AS REQUIRED THEN UPDATE KT AND TRY AGAIN
 660  TRI = 0.0
      DO 220 I=I1,I2
      IF ((S(I).LE.0).AND.(NSPEC(I).LE.0)) THEN
       DEL = 0.
      ELSE
        DEL = (FLOAT(I)**2)*S(I)*LPSPEC(I)
        DEL = DEL/(NSPEC(I)+S(I)*LPCLUT(I))
      ENDIF
 220  TRI = TRI+DEL
      TRI = (977**3)*TRI
      TRI = 8*3.1416*.0005*TRI
      TRI = TRI/(340*340)

C IF TRI CONSTRAINT IS MET WITHOUT ANY MTRI CONTRIBUTION
C TO THE POWER SPECTRUM THEN DONT BOTHER.
       IF ((TRI.GT.TREQ).AND.(KT.EQ.0.)) GOTO 760

C IF TRI CONSTRAINT IS NOT MET AND THE MV CONTRIBUTION
C TO THE POWER SPECTRUM IS NEGLIGIBLE THEN GIVE UP.
C SINCE THE DETECTION CONSTRAINT IS DOMINANT, NO
C FURTHER FAT REMAINS TO BE TRADED OFF.
       IF ((TRI.LT.TREQ).AND.(PV.LT..01*PT)) GOTO 760

       TC = ABS(1-TRI/TREQ)*100.
       IF (TC.LE.1.) GOTO 760
       IF (TFIRST) THEN
C FOR FIRST ATTEMPT GUESS A REASONABLE VALUE FOR MTRI COEFFICIENT
         NEWKT = ((I2-I1)+2*KD/977)/(4*(I2+I1))
         TFIRST = .FALSE.
       ELSE
         IF ((TRI-OLDT).EQ.0) THEN
C HEURISTIC TO PREVENT LOCK-UP
           NEWKT = 2.*KT
         ELSE
           NEWKT = KT+(KT-OLDKT)*(TREQ-TRI)/(TRI-OLDT)
         ENDIF
         IF (NEWKT.LE.0.) NEWKT = 0.
       ENDIF
  665  DFIRST = .TRUE.
       KD = 0.
       OLDKT = KT
       KT = NEWKT
       OLDT = TRI
```

```
      OLDKV = 0.
      KV = 1.E4
      OLDP = 0.
      CC = C
      FLAG = .FALSE.
      GO TO 90

C WRITE OUT OPTIMUM SPECTRUM
 760  DO 263 I=1,I1-1
 263  S(I) = 0.
      DO 266 I=I2+1,128
 266  S(I) = 0.
      DO 110 I=1,128
 110  WRITE(3) S(I)

C IF NECESSARY COMPUTE TRI
      IF (DONLY) THEN
        TRI = 0.0
        DO 1220 I=I1,I2
        IF ((S(I).LE.0).AND.(NSPEC(I).LE.0)) THEN
          DEL = 0.
        ELSE
          DEL = (FLOAT(I)**2)*S(I)*LPSPEC(I)
          DEL = DEL/(NSPEC(I)+S(I)*LPCLUT(I))
        ENDIF
 1220   TRI = TRI+DEL
        TRI = (977**3)*TRI
        TRI = 8*3.1416*.0005*TRI
        TRI = TRI/(340*340)
      ENDIF

C COMPUTE THE VARIANCE OF THE DELAY ESTIMATE USING THE OPTIMUM
C SIGNAL SPECTRUM CORRESPONDING TO K
      SIGMA = 0.0
      DO 20 I=I1,I2
      IF ((S(I).LE.0).AND.(NSPEC(I).LE.0)) THEN
        DEL = 0.
      ELSE
        DEL = ((FLOAT(I)-C)**2)*S(I)*LPSPEC(I)
        DEL = DEL/(NSPEC(I)+S(I)*LPCLUT(I))
      ENDIF
  20  SIGMA = SIGMA+DEL
      SIGMA = 2000/(8*3.1416*3.1416*(977**3)*SIGMA)

C WRITE OUT RESULTS
      WRITE(5,31)
  31  FORMAT(1H ,//)
      WRITE(5,30) SIGMA
  30  FORMAT(1H ,'DELAY ESTIMATE VARIANCE IS ',E9.3,' SECS**2')
      SIGMA = SQRT(SIGMA)*1.0E6
      WRITE(8) SIGMA
      WRITE(5,50) SIGMA
  50  FORMAT(1H ,'CORRESPONDING TO AN RMS ERROR OF ',F9.3,' US')
      WRITE(4) TRI
      WRITE(5,230) TRI
 230  FORMAT(1H ,'TRANSVERSE RES. INDEX IS ',E9.3)
      WRITE(7) D
      WRITE(5,120) D
 120  FORMAT(1H ,'THE DETECTION INDEX IS ',F6.2,' dB')

      CLOSE(3)
```

```
      STOP

100   WRITE(5,40)
 40   FORMAT(1H ,'ERROR DURING FILE OPENING')
      STOP
      END
```

§AP3B.4 Non-linear Chirp Design Program

```
      PROGRAM GENSIG

C PROGRAM TO GENERATE A NONLINEAR CHIRP WITH APPROXIMATELY THE
C POWER SPECTRUM SPECIFIED IN OPTSPEC.
C INPUT FILE IS ASSIGNED TO LUN 1 AND OUTPUT FILE TO LUN 2.

      DIMENSION TRAJ(148)

      DO 30 I=1,20
 30   TRAJ(I) = 0.
      ETOT = 0.0
C GENERATE TRAJECTORY
      DO 10 I=21,148
      READ(1) SPEC
      ETOT = ETOT + SPEC
      TRAJ(I) = ETOT
 10   CONTINUE
      SCALE = FLOAT(1024)/ETOT

      FT = 0.0
      LSAMP = 0
      DO 20 I=21,148
C COMPUTE REQUIRED NUMBER OF SAMPLES AT FREQUENCY I
      NSAMP = INT(TRAJ(I)*SCALE+0.5)
      ISAMP = NSAMP-LSAMP
      LSAMP = NSAMP

C GENERATE AND OUTPUT SAMPLES AT FREQUENCY I
      F = FLOAT(I)
      DO 20 J=1,ISAMP
      FT = FT + F/1024
      S = SIN(6.283185*FT)
      WRITE(2) S
 20   CONTINUE
      STOP
      END
```

APPENDIX 3C: PROOF OF THEOREM 4

The proof of theorem 4 can be most simply undertaken by reducing the constrained extremization to the maximization of a single integral. In this way we can obtain an equation to replace 3A.4 in the proof of theorem 1 in appendix 3A. From there on the proof parallels that of theorem 1.

Reduction to a Single Integral

Now for this optimization problem there are three constraint equations to satisfy, given in R_1 by (from 3.15, 3.37 and 3.38):

$$\int_{R_1} G_{ss}(f)df \;=\; P_s/2, \tag{3C.1}$$

$$\int_{R_1} \frac{G_{ss}(f)\,|H_T(f)|^2}{G_{nn}(f)+G_{ss}(f)\,|H_c(f)|^2}df \;=\; \frac{\Re_{min}}{2T}, \tag{3C.2}$$

and

$$\int_{R_1} \frac{f^2 G_{ss}(f)\,|H_T(f)|^2}{G_{nn}(f)+G_{ss}(f)\,|H_c(f)|^2}df \;=\; \frac{c^2 T R I_{min}}{8\pi T}. \tag{3C.3}$$

Subject to these constraints, we wish to maximize (from 3.23):

$$\frac{1}{8\pi^2 T\sigma_\tau^2} \;=\; \int_{R_1} \frac{(f-f_0)^2\, G_{ss}(f)\,|H_T(f)|^2}{G_{nn}(f)+G_{ss}(f)\,|H_c(f)|^2}df. \tag{3C.4}$$

Now, 3C.2 may be written as:

$$\int_{R_1} \frac{|H_T(f)|^2\, G_{nn}(f)}{|H_c(f)|^2\, G_{nn}(f)+|H_c(f)|^4\, G_{ss}(f)}df \;=\; \int_{R_1} \frac{|H_T(f)|^2}{|H_c(f)|^2}df - \frac{\Re_{min}}{2T}. \tag{3C.5}$$

Similarly, 3C.3 may be rewritten as:

$$\int_{R_1} \frac{f^2 |H_T(f)|^2 G_{nn}(f)}{|H_c(f)|^2 G_{nn}(f) + |H_c(f)|^4 G_{ss}(f)} df = \int_{R_1} \frac{f^2 |H_T(f)|^2}{|H_c(f)|^2} df - \frac{c^2 T R I_{min}}{8\pi T}. \quad (3C.6)$$

From 3C.4, subject to 3C.1, 3C.5 and 3C.6, we wish to minimize:

$$\int_{R_1} \frac{(f - f_0)^2 |H_T(f)|^2}{|H_c(f)|^2} df - \frac{1}{8\pi^2 T \sigma_\tau^2}$$

which, after substitution for σ_τ^2 from 2.33, becomes:

$$\int_{R_1} \frac{(f - f_0)^2 |H_T(f)|^2 G_{nn}(f)}{|H_c(f)|^2 G_{nn}(f) + |H_c(f)|^4 G_{ss}(f)} df. \quad (3C.7)$$

This constrained extremization reduces to minimizing:

$$\Upsilon = \int_{R_1} \left[\frac{\left((f - f_0)^2 + \lambda_1 f^2 + \lambda_2\right) |H_T(f)|^2 G_{nn}(f)}{|H_c(f)|^2 G_{nn}(f) + |H_c(f)|^4 G_{ss}(f)} + \lambda_3 G_{ss}(f) \right] df. \quad (3C.8)$$

where λ_1, λ_2 and λ_3 are Lagrange multipliers.

Substitution Step

From the similarity of equations 3C.8 and 3A.4, we can deduce immediately from equation 3A.7 that the solution in R_1 is given by:

$$G_{ss}(f) = \frac{1/\lambda_3 \left((f - f_0)^2 + \lambda_1 f^2 + \lambda_2\right)^{1/2} |H_T(f)| \left(G_{nn}(f)\right)^{1/2} - G_{nn}(f)}{|H_c(f)|^2} \quad (3C.9)$$

where λ_3, λ_1 and λ_2 must be chosen to meet the three constraints, 3C.1, 3C.2 and 3C.3.

3C.9 can be rewritten as:

$$G_{ss}(f) = \frac{\left(k_v^2 (f - f_0)^2 + k_T^2 f^2 + k_d^2\right)^{1/2} |H_T(f)| \left(G_{nn}(f)\right)^{1/2} - G_{nn}(f)}{|H_c(f)|^2} \quad (3C.10)$$

The rest of the proof is almost identical to the second stage of the proof of theorem 1 in appendix 3A. However, $|H_T(f)|$ is replaced by

$$\left((f-f_0)^2+\left(\frac{k_T}{k_v}\right)^2 f^2+\left(\frac{k_d}{k_v}\right)^2\right)^{1/2}|H_T(f)|$$

wherever it appears and $\frac{\mathfrak{R}}{2T}$ is replaced by Ω where :

$$\Omega = \int_0^\infty \frac{\left((f-f_0)^2+\left(\frac{k_T}{k_v}\right)^2 f^2+\left(\frac{k_d}{k_v}\right)^2\right) G_{ss}(f)\,|H_T(f)|^2}{G_{nn}(f)+|H_c(f)|^2 G_{ss}(f)}df. \qquad (3C.11)$$

Ω is the function to be maximized overall subject to the power constraint, 3C.1.

APPENDIX 4: PROOF OF THEOREM 5.

In order to prove Theorem 5 it is necessary to show that a saddlepoint solution of the form given in 4.21 - 4.27 exists and satisfies the double inequality 4.20 with the definition 4.19.

Now the right hand inequality of 4.20 is satisfied because H_R and G_R are optimized for H_{TR} and $|H_{cR}|^2$. It remains to be shown that the left hand inequality of 4.20 is valid. Repeating that inequality here, we have to show that

$$p\left(H_{TR}, |H_{cR}|^2 ; H_R, G_R\right) \leq p\left(H_T, |H_c|^2 ; H_R, G_R\right).$$

The proof will be undertaken by showing firstly that the denominator of the left hand side of this inequality is maximum while the numerator is minimum. In doing so we will see that equations 4.25 and 4.26 will arise as conditions under which the extremization is achieved. Equation 4.27 arises as a constraint in the problem definition. The remainder of the proof involves proving that equations 4.25 to 4.26 can be simultaneously satisfied. In order to do this it is necessary to first manipulate the solution of equations 4.21 to 4.27 from an implicit form into an explicit form.

Maximization of Denominator

Consider first the denominator in 4.19 and denote it by $d\left(|H_c|^2 ; H, G_{ss}\right)$. Then:

$$\begin{aligned}
\triangle d &= d\left(|H_c|^2 ; H_R, G_R\right) - d\left(|H_{cR}|^2 ; H_R, G_R\right) \\
&= \int_{R_T} G_R(f) H_R(f) \left(|H_c(f)|^2 - |H_{cR}(f)|^2\right) df \\
&= \int_{R_U} G_R(f) \, |H_R(f)|^2 \left(|H_c(f)|^2 - U_c(f)\right) df \\
&\quad + \int_{R_L} G_R(f) \, |H_R(f)|^2 \left(|H_c(f)|^2 - L_c(f)\right) df \\
&\quad + \int_{R_M} G_R(f) \, |H_R(f)|^2 \left(|H_c(f)|^2 - |H_{cR}(f)|^2\right) df
\end{aligned} \qquad (A4.1)$$

Now, for $f \in R_M$, we have, by substitution for $H_R(f)$ from (2.24):

$$G_R(f) \, |H_R(f)|^2 = \frac{|H_{TR}(f)|^2 \, G_R(f)^2}{\left(G_{nn}(f) + G_R(f) \, |H_{cR}(f)|^2\right)^2} = k_1^2. \qquad (A4.2)$$

Also, the integral over R_U in (A4.1) is non-positive because $|H_c(f)|^2 \leq U_c(f)$. Similarly, because $|H_c(f)|^2 \geq L_c(f)$, the integral over R_L is non-negative . Meanwhile, in R_U, $G_R(f) \, |H_R(f)|^2 > k_1^2$ and in R_L, $G_R(f) \, |H_R(f)|^2 \leq k_1^2$.

It follows that:

$$\begin{aligned}
\triangle d &\leq k_1^2 \int_{R_T} \left(H_{TT}(f) - H_0(f)\right) df \\
&\leq \int_{R_T} |H_c(f)|^2 \, df - k_1^2 \sigma_c^2 \\
&\leq 0.
\end{aligned} \qquad (A4.3)$$

That is, $d\left(|H_c|^2 ; H_R, G_R\right)$ has its maximum at $|H_c(f)|^2 = |H_{cR}(f)|^2$, and we see that this part of the proof requires the constraint, 4.25.

Minimization of Numerator

Now consider the numerator in 4.19 and denote it by $N(H_T; G_{ss}, H_s)$. Then,

$$N(H_T; G_R, H_{sR}) = \left| T \int_{R_T} \frac{G_R(f) H_0^*(f) H_T(f)}{\left(G_{nn}(f) + G_R(f)\left(|H_{cR}(f)|^2 + c\right)\right)} df \right|^2 . \qquad (A4.4)$$

To minimize $N(H_T; G_R, H_{sR})$ by choice of $H_T(f)$ it is necessary to choose $A = A_{min}$ and to minimize:

$$\triangle N(H_{TT}; G_R, H_{sR}) = \left[\int_{R_T} \frac{G_R(f) H_0^*(f) (H_{TT}(f) - H_0(f))}{\left(G_{nn}(f) + G_R(f)\left(|H_{cR}(f)|^2 + c\right)\right)} df \right], \qquad (A4.5)$$

but

$$\triangle N(H_{TT}; G_R, H_{sR}) = \int_{R_T} \frac{G_R(f) |H_0(f)| |H_{TT}(f) - H_0(f)|}{\left(G_{nn}(f) + G_R(f)\left(|H_{cR}(f)|^2 + c\right)\right)} \cos\left(\arg\left(H_0^*(f)(H_{TT}(f) - H_0(f))\right)\right) df. \qquad (A4.6)$$

To minimize A4.6, we need the cosine factor to equal -1 from which we conclude:

$$\arg(H_{TR}(f)) = \arg(H_0(f)), \qquad (A4.7)$$

$$and |H_0(f)| > \frac{|H_{TR}(f)|}{A_{min}}. \qquad (A4.8)$$

In addition we must maximize the integral:

$$\triangle\triangle N(H_{TT}; G_R, H_{sR}) = \int_{R_T} \frac{G_R(f) |H_0(f)| |H_{TT}(f) - H_0(f)|}{\left(G_{nn}(f) + G_R(f)\left(|H_{cR}(f)|^2 + c\right)\right)} df. \qquad (A4.9)$$

Now,by the Schwartz inequality, we have:

$$\triangle\triangle N(H_{TT}; G_R, H_{sR}) \leq \sqrt{\int_{R_T} \frac{G_R(f)^2 |H_0(f)|^2}{\left[\left(G_{nn}(f) + G_R(f)\left(|H_{cR}(f)|^2 + c\right)\right)\right]^2} df \int_{R_T} |H_{TT}(f) - H_0(f)|^2 df}. \qquad (A4.10)$$

If we add the constraint,

$$e_T = \delta_T, \tag{A4.11}$$

where e_T is defined in 4.16, then the right hand side of A4.10 is independent of $H_T(f)$. Note that this added constraint confines our attention to the least favourable bound of the class definition, 4.16, and gives rise to equation 4.26.

We now see that $\triangle\triangle N(H_T T; G_R, H_{eR})$ is maximized by equality in A4.10. Hence, taking account of A4.7 and A4.8, we have:

$$\frac{H_{TR}(f)}{A_{min}} - H_0(f) = \frac{BG_R(f)\,|H_0(f)|}{\left(G_{nn}(f) + G_R(f)\left(|H_{cR}(f)|^2 + c\right)\right)}, \tag{A4.12}$$

where B is a constant to be selected to satisfy the constraint, A4.11. Choosing $B = -c$, which can be made to satisfy A4.11, we obtain:

$$H_{TR}(f) = \frac{A_{min}H_0(f)\left(G_{nn}(f) + G_R(f)\,|H_{cR}(f)|^2\right)}{\left(G_{nn}(f) + G_R(f)\left(|H_{cR}(f)|^2 + c\right)\right)}$$

which must be made to meet the constraint, A4.11. This requirement gives rise to 4.26.

The proof, so far, has shown that the numerator in 4.19 is at a minimum for $H_T(f) = H_{TR}(f)$ provided 4.26 is met and the denominator is maximized for $|H_c(f)|^2 = |H_{cR}(f)|^2$ provided 4.25 is satisfied. We also know that 4.27 must be satisfied as it arises in the problem definition but has not yet been taken into account. It remains to be proven, therefore, that 4.25,4.26 and 4.27 can be simultaneously satisfied by choice of k_1, k_2 and c.

Manipulation into Explicit Forms

The first step in proving this is to manipulate 4.21 to 4.27 into explicit forms such that the right hand sides of 4.21 to 4.23 are independent of the solution functions, $H_{TR}(f)$, $|H_{cR}(f)|^2$ and $G_R(f)$ and these have been substituted into 4.24 to 4.27.

Derivation of an Expression for $|H_{cR}(f)|^2$ in R_M

Firstly, consider $|H_{cR}(f)|^2$ in R_M. Substituting from 4.21 into 4.22 we have:

$$|H_{cR}(f)|^2 = \frac{A_{min}\,|H_0(f)|\left(G_{nn}(f)+G_R(f)\,|H_{cR}(f)|^2\right)}{k_1\left(G_{nn}(f)+G_R(f)\left(|H_{cR}(f)|^2+c\right)\right)} - \frac{G_{nn}(f)}{G_R(f)}$$

or

$$\begin{aligned} k_1 G_R(f)\,|H_{cR}(f)|^2\left(G_{nn}(f)+G_R(f)\left(|H_{cR}(f)|^2+c\right)\right) \\ = A_{min}H_0(f)G_R(f)\left(G_{nn}(f)+G_R(f)\,|H_{cR}(f)|^2\right) \\ - k_1 G_{nn}(f)\left(G_{nn}(f)+G_R(f)\left(|H_{cR}(f)|^2+c\right)\right). \end{aligned}$$

i.e.

$$\begin{aligned} |H_{cR}(f)|^4 + \left(\frac{2G_{nn}(f)}{G_R(f)} + c - \frac{A_{min}\,|H_0(f)|}{k_1}\right)|H_{cR}(f)|^2 + \frac{G_{nn}(f)^2}{G_R(f)^2} \\ + \frac{cG_{nn}(f)}{G_R(f)} - \frac{A_{min}\,|H_0(f)|\,G_{nn}(f)}{k_1 G_R(f)} = 0. \end{aligned}$$

Thus:

$$\begin{aligned} |H_{cR}(f)|^2 = \frac{1}{2}\left(\frac{A_{min}\,|H_0(f)|}{k_1} - c - \frac{2G_{nn}(f)}{G_R(f)}\right) \\ \pm\left(\frac{c^2}{4} + \frac{A_{min}^2\,|H_0(f)|^2}{4k_1^2} - \frac{A_{min}c\,|H_0(f)|}{2K_1}\right). \end{aligned}$$

i.e.

$$\begin{aligned} |H_{cR}(f)|^2 &= \frac{A_{min}\,|H_0(f)|}{k_1} - c - \frac{G_{nn}(f)}{G_R(f)} \\ &= \frac{A_{min}\,|H_0(f)|\,G_R(f) - k_1 cG_R(f) - k_1 G_{nn}(f)}{k_1 G_R(f)}. \end{aligned} \qquad (A4.13)$$

Derivation of an Expression for $|H_{TR}(f)|$ in R_M

Now consider $|H_{TR}(f)|$ in R_M. Substituting from A4.13 into 4.21, we obtain:

$$|H_{TR}(f)| = \frac{A_{min}\,|H_0(f)|\,(A_{min}\,|H_0(f)|\,G_R(f) - k_1 cG_R(f))}{A_{min}\,|H_0(f)|\,G_R(f)}.$$

i.e.

$$|H_{TR}(f)| = A_{min}\,|H_0(f)| - k_1 c. \qquad (A4.14)$$

Derivation of an Expression for $G_R(f)$ in R_M

Now, consider $G_R(f)$ in R_M. Substituting from A4.13 and A4.14 into 4.23, we obtain:

$$G_R(f) = \frac{\left(k_2\left(A_{min}\,|H_0(f)| - k_1 c\right)\left(G_{nn}(f)\right)^{1/2} - G_{nn}(f)\right) k_1 G_R(f)}{A_{min}\,|H_0(f)|\,G_R(f) - k_1 c G_R(f) - k_1 G_{nn}(f)}$$
$$= \frac{k_1 k_2 A_{min}\,|H_0(f)|\,G_R(f)\left(G_{nn}(f)\right)^{1/2} - k_1^2 k_2 c G_R(f)\left(G_{nn}(f)\right)^{1/2} - k_1 G_R(f) G_{nn}(f)}{A_{min}\,|H_0(f)|\,G_R(f) - k_1 c G_R(f) - k_1 G_{nn}(f)}.$$

It is readily apparent that this equation is satisfied by:

$$G_R(f) = k_1 k_2 \left(G_{nn}(f)\right)^{1/2}. \qquad (A4.15)$$

Hence, substituting A4.15 into A4.13, we obtain:

$$|H_{cR}(f)|^2 = \frac{A_{min} k_2\,|H_0(f)| - \left(G_{nn}(f)\right)^{1/2}}{k_1 k_2} - c. \qquad (A4.16)$$

Derivation of an Expression for $G_R(f)$ in R_U

In R_U,

$$G_R(f) = \frac{k_2\,|H_{TR}(f)|\left(G_{nn}(f)\right)^{1/2} - G_{nn}(f)}{U_c(f)}$$
$$= \frac{k_2 A_{min}\,|H_0(f)|\left(G_{nn}(f) + G_R(f) U_c(f)\right)\left(G_{nn}(f)\right)^{1/2}}{U_c(f)\left(G_{nn}(f) + G_R(f)\left(U_c(f) + c\right)\right)} - \frac{G_{nn}(f)}{U_c(f)}.$$

i.e.

$$U_c(f)\left(U_c(f) + c\right) G_R(f)^2 + U_c(f) G_{nn}(f) G_R(f) - k_2 A_{min}\,|H_0(f)|\,G_{nn}(f)^{3/2} + G_{nn}(f)^2$$
$$- k_2 A_{min}\,|H_0(f)|\,U_c(f)\left(G_{nn}(f)\right)^{1/2} G_R(f) + G_{nn}(f)\left(U_c(f) + c\right) G_R(f) = 0$$

or

$$G_R(f)^2 + \frac{\left(2G_{nn}(f) + \frac{c G_{nn}(f)}{U_c(f)} - k_2 A_{min}\,|H_0(f)|\left(G_{nn}(f)\right)^{1/2}\right)}{U_c(f) + c} G_R(f)$$
$$+ \frac{G_{nn}(f)^2 - k_2 A_{min}\,|H_0(f)|\,G_{nn}(f)^{3/2}}{U_c(f)\left(U_c(f) + c\right)} = 0.$$

Hence:

$$G_R(f) = \frac{1}{2}\left(\frac{k_2 A_{min}\,|H_0(f)|\,(G_{nn}(f))^{1/2} - \left(2+\frac{c}{U_c(f)}\right)G_{nn}(f)}{U_c(f)+c}\right) \pm \frac{\sqrt{k_2^2 A_{min}^2\,|H_0(f)|^2\,G_{nn}(f)^2 + 2\frac{c}{U_c(f)}k_2 A_{min}\,|H_0(f)|\,G_{nn}(f)^{3/2} + \frac{c^2}{U_c(f)^2}G_{nn}(f)}^2}{2\,(U_c(f)+c)}.$$

i.e.

$$G_R(f) = \frac{k_2 A_{min}\,|H_0(f)|\,(G_{nn}(f))^{1/2} - G_{nn}(f)}{U_c(f)+c}. \qquad (A4.17)$$

Derivation of an Expression for $G_R(f)$ in R_L

Similarly, in R_L,

$$G_R(f) = \frac{k_2 A_{min}\,|H_0(f)|\,(G_{nn}(f))^{1/2} - G_{nn}(f)}{L_c(f)+c}. \qquad (A4.18)$$

Derivation of an Expression for $H_{TR}(f)$ in R_U

Now 4.22 and A4.17 may be substituted into 4.21 to obtain $H_{TR}(f)$ in R_U as follows:

$$H_{TR}(f) = \frac{A_{min}H_0(f)\,(G_{nn}(f)+G_R(f)U_c(f))}{A_{min}k_2\,|H_0(f)|\,(G_{nn}(f))^{1/2}},$$

by substitution for $G_R(f)$ in the denominator. Hence:

$$\arg(H_{TR}(f)) = \arg(H_0(f))$$

and

$$|H_{TR}(f)| = \frac{G_{nn}(f)+G_R(f)U_c(f)}{k_2\,(G_{nn}(f))^{1/2}}.$$

i.e.

$$|H_{TR}(f)| = (G_{nn}(f))^{1/2}/k_2 + \left(A_{min}H_0(f) - (G_{nn}(f))^{1/2}/k_2\right)\frac{U_c(f)}{U_c(f)+c}$$

or

$$|H_{TR}(f)| = \frac{A_{min}\,|H_0(f)|\,U_c(f) + c/k_2\,(G_{nn}(f))^{1/2}}{U_c(f) + c}. \qquad (A4.19)$$

Derivation of an Expression for $|H_{TR}(f)|$ in R_L

Similarly, in R_L, we obtain:

$$|H_{TR}(f)| = \frac{A_{min}\,|H_0(f)|\,L_c(f) + c/k_2\,(G_{nn}(f))^{1/2}}{L_c(f) + c}. \qquad (A4.20)$$

Redefinition of R_U

Finally, we come to the inequalities defining R_U, R_L, R_M and R_0. In R_U, we have:

$$G_R(f)\,|H_{TR}(f)| = \frac{A_{min}k_2\,|H_0(f)|\,(G_{nn}(f))^{1/2} - G_{nn}(f)}{U_c(f) + c}\,|H_{TR}(f)|$$

and:

$$\begin{aligned} k_1\,[G_R(f)U_c(f) + G_{nn}(f)] &= \frac{k_1\,(G_{nn}(f) + G_R(f)\,(U_c(f) + c))}{A_{min}\,|H_0(f)|}\,|H_{TR}(f)| \\ &= k_1k_2\,(G_{nn}(f))^{1/2}\,|H_{TR}(f)|. \end{aligned}$$

Hence, if we assume $G_{nn}(f) > 0$ and thus $|H_{TR}(f)| > 0$, we obtain:

$$\begin{aligned} &G_R(f)\,|H_{TR}(f)| > k_1\,[G_R(f)U_c(f) + G_{nn}(f)] \Rightarrow \\ &\qquad A_{min}k_2\,|H_0(f)| - (G_{nn}(f))^{1/2} > k_1k_2\,(U_c(f) + c). \end{aligned} \qquad (A4.21)$$

Redefinition of R_L

Similarly, in R_L we have:

$$A_{min}k_2\,|H_0(f)| - (G_{nn}(f))^{1/2} \leq k_1k_2\,(L_c(f) + c). \qquad (A4.22)$$

Redefinition of R_0

From A4.17 and A4.18 we see that, provided $G_{nn}(f) > 0$, R_0 is defined by:

$$k_2 A_{min} |H_0(f)| - (G_{nn}(f))^{1/2} \leq 0. \qquad (A4.23)$$

Substitution into Constraint Equations

We are now in a position to derive explicit forms of equations 4.25 to 4.27. Equation 4.25 becomes:

$$\int_{R_U} U_c(f)df + \int_{R_L} L_c(f)df + \int_{R_M} \left(\frac{A_{min} k_2 |H_0(f)| - (G_{nn}(f))^{1/2}}{k_1 k_2} - c \right) df = \sigma_c^2. \qquad (A4.24)$$

Equation 4.26 becomes:

$$c^2 \int_{R_U} \frac{|H_0(f)|^2}{[U_c(f)+c]^2} df + c^2 \int_{R_L} \frac{|H_0(f)|^2}{[L_c(f)+c]^2} df + c^2 k_1 k_2 \int_{R_M} \frac{|H_0(f)|^2}{\left[A_{min} k_2 |H_0(f)| - (G_{nn}(f))^{1/2}\right]^2} df = \delta_T. \qquad (A4.25)$$

Equation 4.27 becomes:

$$k_1 k_2 \int_{R_M} (G_{nn}(f))^{1/2} df + \int_{R_U} (G_{nn}(f))^{1/2} \frac{A_{min} k_2 |H_0(f)| - (G_{nn}(f))^{1/2}}{U_c(f)+c} df + \int_{R_0} (G_{nn}(f))^{1/2} \frac{A_{min} k_2 |H_0(f)| - (G_{nn}(f))^{1/2}}{L_c(f)+c} df = P_e. \qquad (A4.26)$$

Existence of the Constants in the Solution

We need to show that k_1, k_2 and c, satisfying A4.24 to A4.26, do exist. We will assume that $G_{nn}(f)$, $|H_0(f)|$, $L_c(f)$ and $U_c(f)$ are all finite and non-negative on R_T and δ_T, σ_c^2 and P_e are finite and non-negative.

Constraint Equation 4.25

Consider first A4.24. Now, if $k_1 = 0$ then $R_U = R_T$ and the left hand side becomes:

$$\int_{R_T} U_c(f)df$$

But

$$\int_{R_T} U_c(f)df \geq \int_{R_T} |H_c(f)|^2 df \geq \sigma_c^2$$

Also, as $k_1 \rightarrow \infty$ then $R_L \rightarrow R_T$ and the left hand side becomes:

$$\int_{R_T} L_c(f)df$$

But

$$\int_{R_T} L_c(f)df \leq \int_{R_T} |H_c(f)|^2 df \leq \sigma_c^2$$

Now, we can establish by inspection of A4.21, A4.22 and A4.24 that the left hand side of A4.24 is continuous in k_1 between these extremes. It therefore follows that, regardless of the values of k_2 and c, there always exists a finite non-negative number, k_1, satisfying A4.24.

Constraint Equation 4.26

Now consider A4.25. For $c = 0$, we have on the left hand side:

$$c^2 \int_{R_U} \frac{|H_0(f)|^2}{[U_c(f)+c]^2} df = 0 \leq \delta_T.$$

Similarly, for $c \rightarrow \infty$, we have on the left hand side:

$$c^2 \int_{R_L} \frac{|H_0(f)|^2}{[U_c(f)+c]^2} df \rightarrow \int_{R_L} |H_0(f)|^2 df = E_0.$$

Hence, provided $\delta_T \leq E_0$ (a condition normally satisfied in practice as it simply means that the unknown component of the target path transfer power is less than the known component), then the left hand side of equation A4.25 will exceed the right as $c \rightarrow \infty$.

Again, inspection reveals that the left hand side of A4.25 is continuous in A4. It follows that A4.25 can always be satisfied by choice of c for any values of k_1 and k_2 provided $\delta_T \leq E_0$.

Constraint Equation 4.27

Finally we consider A4.26. For $k_2 = 0$ we find $R_0 = R_T$ and the left hand side is $0 \leq P_s$. For $k_2 \rightarrow \infty$, R_0 is empty and the positions of the other region boundaries become independent of k_2. The left hand side of A4.26 tends to ∞ ($> P_s$). By inspection, the left hand side of A4.26 is continuous in k_2 and it follows, therefore, that A4.26 can be solved for k_2 given any finite real non-negative numbers for k_1 and c.

Statement of Conditions for Solution Existence

Hence, since A4.24 can be solved for k_1, A4.25 for c and A4.26 for k_2, it follows that finite non-negative real values exist, satisfying 4.21 to 4.27. Thus a saddlepoint solution exists and is given by 4.21 to 4.27 provided:

1) δ_T, σ_c^2 and P_s are finite and non-negative.

2) $|H_0(f)|$, $L_c(f)$ and $U_c(f)$ are all finite and non-negative on R_T.

3) $G_{nn}(f)$ is finite and positive on R_T.

4) $\delta_T \leq E_0$.

Q. E. D.

APPENDIX 6: PROGRAM LISTINGS FOR CHAPTER 6

§AP6.1 Class Description Program

```
      PROGRAM CLASS
C PROGRAM TO CONSTRUCT A CLASS DESCRIPTION FROM A REPRESENTATIVE SET
C OF TRANSMISSION PATH MODELS. INPUT FILES ARE ASSUMED TO REPRESENT
C COMPONENTS OF THE MODEL AS FOLLOWS:
C       "SIGSPC*.BIN" CONTAINS THE SQUARED MAGNITUDE OF THE TARGET
C                     PATH TRANSFER FUNCTION.
C       "CLSPC*.BIN"  CONTAINS THE SQUARED MAGNITUDE OF THE CLUTTER
C                     PATH TRANSFER FUNCTION.
C OUTPUT FILES ARE AS FOLLOWS:
C       "NOMSIG.BIN"  CONTAINS THE NOMINAL TARGET IMPULSE RESPONSE.
C       "USPEC.BIN"   CONTAINS THE UPPER BOUND ON THE CLUTTER T/F SQUARED.
C       "LSPEC.BIN"   CONTAINS THE LOWER BOUND ON THE CLUTTER T/F SQUARED.
C IN ADDITION, VARIOUS PARAMETERS OF THE CLASS DESCRIPTION ARE OUTPUT TO
C THE USER AND TO FILE "CLASPRM.BIN". ALL SIGNALS ARE ASSUMED SAMPLED AT
C 500KHZ AND ALL SPECTRA ARE ASSUMED TO BE BASED ON 512-POINT FFT.

      CHARACTER*11 FNAME
      LOGICAL*1 FNAM(11)
      EQUIVALENCE (FNAME,FNAM)
      COMPLEX HI(5,1:100),HO(1:100),X(512)
      DIMENSION A(5),E(5),EI(5),U(1:100)
      REAL L(1:100)
      INTEGER F1,F2

      TYPE *,'SPECIFY FIRST AND LAST TRANSFER FUNCTIONS:'
      ACCEPT *,ITF,NTF
      TYPE *,'SPECIFY FIRST AND LAST FREQ. BIN NOS.'
      ACCEPT *,F1,F2

      DO 100 J=ITF,NTF
      ENCODE(8,101,FNAME) J
      DO 105 I=9,11
 105  FNAM(I) = 0
 101  FORMAT('SIG',O1,'.BIN')
      OPEN(1,ERR=100,FILE=FNAM,
     & STATUS='OLD',ACCESS='SEQUENTIAL',FORM='UNFORMATTED')

C READ IN THE TARGET PATH T/F
      ISAMP = 0
  10  READ(1,END=20) SAMP
      ISAMP = ISAMP+1
      X(ISAMP) = CMPLX(SAMP,0.)
      GO TO 10

C TRANSFORM TARGET PATH T/F
  20  DO 30 I=ISAMP+1,512
  30  X(I) = (0.,0.)
      CALL FFT(X,9)
      DO 40 I=F1,F2
  40  HI(J,I) = X(I)

      CLOSE(1)
 100  CONTINUE
```

```
C INITIALIZE COEFFICIENTS OF NOMINAL T/F
      DO 50 J=ITF,NTF
  50  A(J) = 1./(NTF-ITF+1)

C COMPUTE T/F ENERGIES
      DO 60 J=ITF,NTF
      E(J) = 0.
      DO 60 I=F1,F2
  60  E(J) = E(J)+REAL(HI(J,I)*CONJG(HI(J,I)))

C ITERATE TO GET NOMINAL T/F
  70  E0 = 0.
C COMPUTE NEW TRIAL T/F
      DO 90 I=F1,F2
  90  H0(I) = (0.,0.)
      DO 85 J=ITF,NTF
      DO 85 I=F1,F2
  85  H0(I) = H0(I)+A(J)*HI(J,I)
      DO 80 I=F1,F2
  80  E0 = E0+REAL(H0(I)*CONJG(H0(I)))
      A0 = SQRT(E0)
      DO 95 I=F1,F2
  95  H0(I) = H0(I)/A0
C COMPUTE ALL ERROR ENERGIES
      DO 110 J=ITF,NTF
      EI(J) = 0.
      DO 120 I=F1,F2
 120  EI(J) = EI(J)+REAL(H0(I)*CONJG(HI(J,I)))
      EI(J) = 1.-EI(J)*EI(J)/E(J)
 110  CONTINUE

C IF ALL ERROR ENERGIES APPROXIMATELY THE SAME THEN TERMINATE
      JMAX = ITF
      EMAX = 0.
      EMIN = 10.*E0
      DO 130 J=(ITF+1),NTF
      IF (ABS(EI(J)-EI(ITF)).GT.EMAX) THEN
        EMAX = ABS(EI(J)-EI(ITF))
        JMAX = J
      ENDIF
 130  CONTINUE
      DIFF = EMAX/EI(ITF)
      IF (DIFF.LT.0.01) GOTO 140

C ADJUST NOMINAL T/F COEFFICIENTS
      A(JMAX) = A(JMAX)*SQRT(EI(JMAX)/EI(ITF))

      GO TO 70

C COMPUTE AND OUTPUT SMALLEST SCALE FACTOR
 140  AMIN = 1.E10
      DO 180 J=ITF,NTF
      AA = 0.
      DO 190 I=F1,F2
 190  AA = AA+REAL(H0(I)*CONJG(HI(J,I)))
      AA = E(J)/AA
      IF (AA.LT.AMIN) AMIN = AA
 180  CONTINUE
      OPEN(3,ERR=100,FILE='CLASPRM.BIN',
     & STATUS='NEW',ACCESS='SEQUENTIAL',FORM='UNFORMATTED')
      TYPE *,'AMIN IS UNITY'
      WRITE(3) 1.
```

```
C COMPUTE AND OUTPUT NOMINAL TARGET PATH IMPULSE RESPONSE
      OPEN(1,ERR=100,FILE='NOMSIG.BIN',
     & STATUS='NEW',ACCESS='SEQUENTIAL',FORM='UNFORMATTED')
      DO 150 I=1,512
 150  X(I) = (0.,0.)
      DO 160 I=F1,F2
      X(514-I) = H0(I)*AMIN
 160  X(I) = H0(I)*AMIN
      CALL FFT(X,9)
      DO 170 I=1,100
 170  WRITE(1) REAL(X(I))/256.
      CLOSE(1)


C OUTPUT MAXIMUM ERROR ENERGY
      EE = EI(ITF)*AMIN*AMIN
      TYPE *,'MAXIMUM TARGET PATH MODELING ERROR ENERGY IS '
     & ,EE
      WRITE(3) EE
      TYPE *,'NOMINAL TARGET PATH T/F ENERGY IS ',AMIN*AMIN

C COMPUTE BOUNDS ON CLUTTER T/F SQUARED
      PCMAX = 0.
      DO 210 I=F1,F2
      U(I) = 0.
      L(I) = 1.E20
 210  CONTINUE
      DO 220 J=ITF,NTF
      ENCODE(10,102,FNAME) J
      FNAM(11) = 0
 102  FORMAT('CLSPC',01,'.BIN')
      OPEN(1,ERR=100,FILE=FNAM,
     & STATUS='OLD',ACCESS='SEQUENTIAL',FORM='UNFORMATTED')
      DO 230 I=1,(F1-1)
 230  READ(1)
      PC = 0.
      DO 240 I=F1,F2
      READ(1) SAMP
      IF (SAMP.GT.U(I)) U(I) = SAMP
      IF (SAMP.LT.L(I)) L(I) = SAMP
      PC = PC+SAMP
 240  CONTINUE
      IF (PC.GT.PCMAX) PCMAX = PC
      CLOSE(1)
 220  CONTINUE

C OUTPUT BOUNDS ON CLUTTER PATH T/F SQUARED
      OPEN(1,ERR=100,FILE='USPEC.BIN',
     & STATUS='NEW',ACCESS='SEQUENTIAL',FORM='UNFORMATTED')
      OPEN(2,ERR=100,FILE='LSPEC.BIN',
     & STATUS='NEW',ACCESS='SEQUENTIAL',FORM='UNFORMATTED')
      DO 250 I=1,(F1-1)
      WRITE(1) 0.
 250  WRITE(2) 0.
      DO 260 I=F1,F2
      WRITE(1) U(I)
```

```
 260  WRITE(2) L(I)
      DO 270 I=11,128
      WRITE(1) 0.
 270  WRITE(2) 0.
      CLOSE(1)
      CLOSE(2)

C OUTPUT MAXIMUM CLUTTER TRANSFER POWER
      TYPE *,'Pc IS LESS THAN ',PCMAX
      WRITE(3) PCMAX
      CLOSE(3)

      STOP
      END
```

§AP6.2 Robust Optimization Program

```
      PROGRAM ROBUST
C PROGRAM TO FIND THE LEAST FAVOURABLE TRANSMISSION PATH WITHIN A
C CLASS DESCRIPTION FOR THE PURPOSE OF ROBUST JOINT OPTIMIZATION OF
C SIGNAL AND RECEIVER FILTER. INPUT FILES ARE ASSUMED TO REPRESENT
C COMPONENTS OF THE CLASS DESCRIPTION AS FOLLOWS:
C       "NOMSIG.BIN"   CONTAINS THE NOMINAL TARGET IMPULSE RESPONSE.
C       "USPEC.BIN"    CONTAINS THE UPPER BOUND ON THE CLUTTER T/F SQUARED.
C       "LSPEC.BIN"    CONTAINS THE LOWER BOUND ON THE CLUTTER T/F SQUARED.
C       "CLASPRM.BIN" CONTAINS THE THREE PARAMETERS OF THE CLASS DESCRIPTION.
C OUTPUT FILES REPRESENT THE LEAST FAVOURABLE TRANSMISSION PATH AS FOLLOWS:
C       "ROBSIG.BIN"   CONTAINS THE LEAST FAVOURABLE TARGET PATH
C                      IMPULSE RESPONSE.
C       "ROBSPEC.BIN" CONTAINS THE SQUARE OF THE LEAST FAVOURABLE
C                      CLUTTER PATH T/F.
C SIGNALS ARE ASSUMED SAMPLED AT  500KHZ AND ALL SPECTRA ARE ASSUMED TO
C BE BASED ON 512-POINT FFT.

      COMPLEX H0(100),X(512)
      DIMENSION U(100)
      REAL L(100),NSPEC(100),K1,K2,HTR(100)
      REAL HCR(100),NN,NEWK,LVAL,NEWC
      INTEGER F1,F2

      TYPE *,'SPECIFY FIRST AND LAST FREQ. BIN NOS.:'
      ACCEPT *,F1,F2

C GET SIGNAL POWER IN UNITS COMPATIBLE WITH THOSE USED IN "DETENTE"
C AND CONVERT TO INTERNAL UNITS
      TYPE *,'SPECIFY SIGNAL POWER AS FOR "DETENTE" (dB) '
      ACCEPT *,PS
      PS = 10**(PS/10.)

C READ IN NOMINAL TARGET PATH IMPULSE RESPONSE AND COMPUTE
C NOMINAL TARGET PATH T/F WHICH MUST BE DIVIDED BY THE
C TRANSMITTED IMPULSE RESPONSE MAGNITUDE (10V) EXPRESSED IN
C UNITS OF THE QUANTIZATION STEP (.1*9/256 V).
      OPEN(1,ERR=100,FILE='NOMSIG.BIN',
     & STATUS='OLD',ACCESS='SEQUENTIAL',FORM='UNFORMATTED')
      DO 150 I=1,512
  150 X(I) = (0.,0.)
      DO 160 I=1,100
      READ(1) SAMP
  160 X(I) = CMPLX(SAMP/2840.,0.)
      CALL FFT(X,9)
      DO 170 I=F1,F2
  170 H0(I) = X(I)
      CLOSE(1)

C READ IN PARAMETERS OF CLASS DESCRIPTION AND CONVERT TO
C STANDARD UNITS.
      OPEN(1,ERR=100,FILE='CLASPRM.BIN',
     & STATUS='OLD',ACCESS='SEQUENTIAL',FORM='UNFORMATTED')
      READ(1) AMIN
      READ(1) EMAX
      EMAX = EMAX/(2840.*2840.)
      READ(1) PCMAX
      PCMAX = PCMAX/(2840.*2840.)
      CLOSE(1)
```

```
C INPUT BOUNDS ON CLUTTER PATH T/F SQUARED WHICH MUST BE
C DIVIDED BY THE SQUARE OF THE TRANSMITTED IMPULSE RESPONSE
C MAGNITUDE (10V) EXPRESSED IN UNITS OF THE QUANTIZATION
C STEP (.1*9/256 V).
      OPEN(1,ERR=100,FILE='USPEC.BIN',
     & STATUS='OLD',ACCESS='SEQUENTIAL',FORM='UNFORMATTED')
      OPEN(2,ERR=100,FILE='LSPEC.BIN',
     & STATUS='OLD',ACCESS='SEQUENTIAL',FORM='UNFORMATTED')
      DO 250 I=1,(F1-1)
      READ(1)
 250  READ(2)
      DO 260 I=F1,F2
      READ(1) SAMP
      U(I) = SAMP/(2840.*2840.)
      READ(2) SAMP
 260  L(I) = SAMP/(2840.*2840.)
      CLOSE(1)
      CLOSE(2)

C INPUT NOISE SPECTRUM
      OPEN(1,ERR=100,FILE='NSPEC.BIN',
     & STATUS='OLD',ACCESS='SEQUENTIAL',FORM='UNFORMATTED')
      DO 270 I=1,(F1-1)
 270  READ(1)
      DO 280 I=F1,F2
 280  READ(1) NSPEC(I)
      CLOSE(1)

C SOLVE FOR THE CONSTANTS

C INITIALIZE K2 AND C
      NN = 0.
      HH = 0.
      UU = 0.
      DO 290 I=F1,F2
      NN = NN+NSPEC(I)
      HH = HH+CABS(H0(I))
      UU = UU+U(I)
 290  CONTINUE
      NN = NN/(F2-F1+1)
      HH = HH/(F2-F1+1)
      UU = UU/(F2-F1+1)
      K2 = 10*SQRT(NN)/(AMIN*HH)
      C = UU/10.
      FIRSTC = C
      OLDC = EMAX/62
      E = EMAX/2
      OLDK2 = 0.
      P = 0.
      OLDK1 = 0.
      PC = 2*PCMAX

C COMPUTE INITIAL VALUE FOR K1
      PM = 0.
      PCM = 0.
      DO 300 I=F1,F2
      TVAL = AMIN*K2*CABS(H0(I))-SQRT(NSPEC(I))
      PM = PM+TVAL
      PCM = PCM+C
 300  CONTINUE
      K1 = 100*PM/((PCMAX+PCM)*K2)
      FIRSTK = K1
```

```
C COMPUTE SIGNAL POWER
 310  PU = 0.
      PM = 0.
      PL = 0.
      OLDP = P
      DO 360 I=F1,F2
      TVAL = AMIN*K2*CABS(HO(I))-SQRT(NSPEC(I))
      IF (TVAL.GT.0.) THEN
        LVAL = (L(I)+C)*K1*K2
        IF (TVAL.GT.LVAL) THEN
          UVAL = (U(I)+C)*K1*K2
          IF (TVAL.GT.UVAL) THEN
            PU = PU+TVAL*SQRT(NSPEC(I))/(U(I)+C)
          ELSE
            PM = PM+SQRT(NSPEC(I))
          ENDIF
        ELSE
            PL = PL+TVAL*SQRT(NSPEC(I))/(L(I)+C)
        ENDIF
      ENDIF
 360  CONTINUE
      P = K1*K2*PM+PU+PL
      P = P*26E-12*977

C IF P SIGNIFICANTLY DIFFERENT FROM PS THEN
C UPDATE K2 AND TRY AGAIN
      VAL = 2*ABS(P-PS)/(P+PS)
      IF (VAL.LE.0.01) GOTO 350
      NEWK = K2+(K2-OLDK2)*(PS-P)/(P-OLDP)
      OLDK2 = K2
      K2 = NEWK
      GOTO 310

C COMPUTE VALUE OF PC
 350  PU = 0.
      PM = 0.
      PL = 0.
      OLDPC = PC
      DO 320 I=F1,F2
      TVAL = AMIN*K2*CABS(HO(I))-SQRT(NSPEC(I))
      LVAL = (L(I)+C)*K1*K2
      IF (TVAL.GT.LVAL) THEN
        UVAL = (U(I)+C)*K1*K2
        IF (TVAL.GT.UVAL) THEN
          PU = PU+U(I)
        ELSE
          PM = PM+TVAL/(K1*K2)-C
        ENDIF
      ELSE
        PL = PL+L(I)
      ENDIF
 320  CONTINUE
      PC = PU+PM+PL
```

```
C IF NEW PC SIGNIFICANTLY DIFFERENT FROM PCMAX THEN
C UPDATE AND TRY AGAIN.
      VAL = 2*ABS(PC-PCMAX)/(PC+PCMAX)
      IF (VAL.LE.0.01) GOTO 330
      IF (PC.EQ.OLDPC) THEN
        NEWK = 3*K1-2*OLDK1
      ELSE
        NEWK = K1+(K1-OLDK1)*(PCMAX-PC)/(PC-OLDPC)
      ENDIF
      IF (NEWK.LT.0.) NEWK = 0.
      OLDK1 = K1
      K1 = NEWK
      P=0.
      OLDK2 = 0.
      GOTO 310

C COMPUTE ERROR ENERGY
 330  PU = 0.
      PM = 0.
      PL = 0.
      OLDE = E
      DO 340 I=F1,F2
      TVAL = AMIN*K2*CABS(HO(I))-SQRT(NSPEC(I))
      LVAL = (L(I)+C)*K1*K2
      IF (TVAL.GT.LVAL) THEN
        UVAL = (U(I)+C)*K1*K2
        IF (TVAL.GT.UVAL) THEN
          PP = SQRT(NSPEC(I))/(AMIN*K2)-CABS(HO(I))
          PU = PU+PP*PP/((U(I)+C)*(U(I)+C))
        ELSE
          PM = PM+K1*K1/(AMIN*AMIN)
        ENDIF
      ELSE
        PP = SQRT(NSPEC(I))/(AMIN*K2)-CABS(HO(I))
        PL = PL+PP*PP/((L(I)+C)*(L(I)+C))
      ENDIF
 340  CONTINUE
      E = PM+PU+PL
      E = C*C*E
      TYPE *,'E=',E,'EMAX=',EMAX

C IF E SIGNIFICANTLY DIFFERENT FROM EMAX THEN
C UPDATE C AND TRY AGAIN
      VAL = 2*ABS(E-EMAX)/(E+EMAX)
      IF (VAL.LE.0.01) GOTO 370
      NEWC = C+(C-OLDC)*(EMAX-E)/(E-OLDE)
      IF (NEWC.LT.0.) NEWC = C/10.
      OLDC = C
      C = NEWC
      P = 0.
      OLDK2 = 0.
      PC = 2*PCMAX
      OLDK1 = 0.
      GOTO 310
```

```
C COMPUTE LEAST FAVOURABLE TRANSFER FUNCTIONS
 370  DO 380 I=F1,F2
      TVAL = AMIN*K2*CABS(HO(I))-SQRT(NSPEC(I))
      LVAL = (L(I)+C)*K1*K2
      IF (TVAL.GT.LVAL) THEN
        UVAL = (U(I)+C)*K1*K2
        IF (TVAL.GT.UVAL) THEN
          SAMP = AMIN*CABS(HO(I))*U(I)
          SAMP = SAMP+C*SQRT(NSPEC(I))/K2
          SAMP = SAMP/(U(I)+C)
          HTR(I) = SAMP
          HCR(I) = U(I)
        ELSE
          HTR(I) = AMIN*CABS(HO(I))-K1*C
          HCR(I) = TVAL/(K1*K2)-C
        ENDIF
      ELSE
        SAMP = AMIN*CABS(HO(I))*L(I)
        SAMP = SAMP+C*SQRT(NSPEC(I))/K2
        SAMP = SAMP/(L(I)+C)
        HTR(I) = SAMP
        HCR(I) = L(I)
      ENDIF
 380  CONTINUE

C COMPUTE AND OUTPUT THE LEAST FAVOURABLE TARGET PATH I/R.
      OPEN(1,ERR=100,FILE='ROBSIG.BIN',
     & STATUS='NEW',ACCESS='SEQUENTIAL',FORM='UNFORMATTED')
      DO 390 I=1,512
 390  X(I) = (0.,0.)
      DO 400 I=F1,F2
      X(I) = HTR(I)*HO(I)/CABS(HO(I))
 400  X(514-I) = X(I)
      CALL FFT(X,9)
      DO 410 I=1,100
      SAMP = REAL(X(I))*2840./256.
      WRITE(1) SAMP
 410  CONTINUE
      CLOSE(1)

C SCALE AND OUTPUT THE SQUARED MAGNITUDE OF THE LEAST FAVOURABLE
C CLUTTER PATH TRANSFER FUNCTION
      OPEN(1,ERR=100,FILE='ROBSPEC.BIN',
     & STATUS='NEW',ACCESS='SEQUENTIAL',FORM='UNFORMATTED')
      DO 420 I=1,(F1-1)
 420  WRITE(1) 0.
      DO 430 I=F1,F2
 430  WRITE(1) HCR(I)*2840.*2840.
      DO 440 I=(F2+1),128
 440  WRITE(1) 0.
      CLOSE(1)

 100  STOP
      END
```

LIST OF REFERENCES

1.1 Bryant, R.C. and Bogner, R.E.
"Ultrasonic Surface Imaging in Adverse Environments"
IEEE Trans. SU-31 No.4 P.373
July, 1984

1.2 Moritz, W.E. et al
"Ultrasonic Technique for Imaging The Ventricle in Three Dimensions
And Calculating Its Volume"
IEEE Trans. BME-30 No.8 P.482
Aug., 1983

1.3 Blessing, G.V. et al
"The Effect of Surface Roughness On Ultrasonic Echo Amplitude
in Steel"
Proc. IEEE Ultrasonics Symposium, P.923
Oct., 1983

1.4 Pasqualucci, F.
"Millimeter - Wave Radar Applications in Meteorology"
Atmos. Tech. Vol.13 P.46
1981

1.5 Alfano, L. et al
"Analysis Procedure And Equipment For Deep Geoelectrical Soundings
in Noisy Areas"
Geothermics Vol.11 No.4 P.269
1982

2.1 Woodward, P.M.
"Probability And Information Theory With Applications To Radar"
Pergamon Press
1953

2.2 Woodward, P.M. and Davies, I.L.
"A Theory of Radar Information"
Phil. Mag. Ser.7 Vol.41 No.321 P.1001
Oct., 1950

2.3 Van Trees, H.L.
"Detection, Estimation and Modulation Theory" Vol.1
Wiley
1969

2.4 Helstrom, C.W.
"Statistical Theory of Signal Detection"
Pergamon Press
1968

2.5 Swerling,
"Parameter Estimation Accuracy Formulas"
IEEE Trans. IT-10 No.4 P.302
Oct., 1964

2.6 Moose, P.H.
"Signal Processing in Reverberant Environments"
from "Signal Processing" P.413
in the NATO Advanced Study Institute series
Academic Press
1973

2.7 Kooij, T.
"Optimum Signals in Noise and Reverberation"
from the proceedings of the NATO Advanced Study Institute
held in Enschede, The Netherlands.
1968

2.8 Zapalowski, L. et al
"Imaging Within A Weak Scattering Approximation"
from "Acoustical Imaging '83"
Plenum Press
1984

2.9 Klauder, J.R. et al
"The Theory and Design of Chirp Radars"
Bell Laboratory Technical Journal Vol.XXXIX No.4
July, 1960

2.10 Gabor, D.
"Theory of Communication"
JIEE Vol.93 No.3 P.429
1946

2.11 Evans, S. and Kong, F.N.
"Gain And Effective Area For Impulse Antennas"
from the proceedings of ICAP '83 P.421
IEE
April, 1983

2.12 Carter, G.C.
"The Role Of Coherence in Time Delay Estimation"
from "Aspects of Signal Processing" P.25
in the NATO Advanced Study Institute series
Academic Press
1977

2.13 Macdonald, V.H. and Schultheiss, P.M.
"Optimum Passive Bearing Estimation in a Spatially Incoherent
Noise Environment"
JASA Vol.46 No.1 Pt.1 P.37
1969

2.14 Quazi, A.H.
"An Overview on The Time Delay Estimate in Active And Passive
Systems For Target Localization"
IEEE Trans. ASSP-29 No.3 P.527
June, 1981

2.15 Arques, P.Y.
"Detection, Estimation ET Performances de Signaux Certains de
Arrivee et de Direction Inconnues"
Annales Des Telecommunications Vol.26 No.9-10 P.371
Oct., 1971

2.16 Ziv, J. and Zakai, M.
"Some Lower Bounds on Signal Parameter Estimation"
IEEE Trans. IT-15 No.3
May, 1969

2.17 Weiss, A.J. and Weinstein E.
"Fundamental Limitations in Passive Time Delay Estimation
- Part I: Narrow-Band Systems"
IEEE Trans. ASSP-31 No.2 P.472
April, 1983

3.1 Helstrom, C.W.
"The Statistical Theory of Signal Detection" PP.256-257
Pergamon Press
1968

3.2 Bates, R.H.T.
"A Theorem For Wide Bandwidth Echo-Location Systems"
J. Sound Vib. Vol.16 No.2 P.223
1971

3.3 Delong, D.F., Jr. and Hofstetter, E.M.
"The Design of Clutter Resistant Radar Waveforms With
Limited Dynamic Range"
IEEE Trans. IT-15 No.3 P.376
1969

3.4 Delong, D.F., Jr. and Hofstetter, E.M.
"On The Design of Optimum Radar Waveforms for Clutter Rejection"
IEEE Trans. IT-13 No.3 P.454
1967

3.5 Westerfield, E.C. et al
"Processing Gains Against Clutter Using Matched Filters"
IRE Trans. IT-6 No.3 P.342
1960

3.6 Rihaczek, A.W. and Mitchell R.L.
"Radar Waveforms For Suppression of Extended Clutter"
IEEE Trans. AES-3 No.3 P.510
1967

3.7 Makhoul, J.
"Linear Prediction: A Tutorial Review"
Proc. IEEE Vol.63 No.4 P.561
April, 1975

3.8 Ulrych, T.J. and Bishop, T.N.
"Maximum Entropy Spectral Analysis and Autoregressive Decomposition"
Reviews of Geophysics and Space Physics Vol.13 No.1 P.183
Feb., 1975

3.9 Cook, C.E. and Bernfield, M.
"Radar Signals - An Introduction To Theory And Application"
Academic Press
1967

3.10 Lee, B.B. and Furgason, E.S.
"Golay Codes For Simultaneous Multi-Mode Ultrasonic Imaging"
from "Acoustical Imaging" Vol. 11
Plenum Press
Sept., 1983

3.11 *See [2.9]*

4.1 Kassam, S.A. et al
"Two-Dimensional Filters For Signal Processing Under
Modeling Uncertainties"
IEEE Trans. GE-18 No.4
Oct., 1980

4.2 Kassam, S.A. and Poor, H.V.
"Robust Signal Processing For Communications Systems"
IEEE Communications Mag. P.20
Jan., 1983

4.3 Turin, G.L.
"Minimax Strategies For Matched Filter Detection"
IEEE Trans. COM-23 p.1370
Nov., 1975

4.4 Verdu, S. and Poor, H.V.
"Minimax Robust Discrete-Time Matched Filters"
IEEE Trans. COM-31 No.2
Feb., 1983

4.5 Kuznetsov, V.P.
"Stable Detection When The Signal And Spectrum of Normal Noise
Are Inaccurately Known"
Telecom. Radio Eng. Vol.30-31 P.58
Mar., 1976

4.6 Vastola, K.S. and Poor, H.V.
"An Analysis of The Effects of Spectral Uncertainty
On Wiener Filtering"
Automatica Vol.19
1983

4.7 Poor, H.V.
"On Robust Wiener Filtering"
IEEE Trans. AC-25 P.513
Jun., 1980

4.8 Moustakides, G. and Kassam, S.A.
"Robust Wiener Filters For Random Signals in Correlated Noise"
IEEE Trans. IT-29
1983

4.9 Malkevitch, J. and Meyer, W.
"Graphs, Models And Finite Mathematics" P.368
Prentice-Hall
1974

4.10 Maki, D.P. and Thompson, M.
"Mathematical Models And Applications" PP.208-226
Prentice-Hall
1973

5.1 Papoulis, A.
"Probability, Random Variables And Stochastic Processes"
McGraw-Hill
1965

5.2 Jaynes, E.T.
"Where Do We Stand On Maximum Entropy"
from "The Maximum Entropy Formalism" P.15
M.I.T. Press
May, 1978

5.3 Schwartz, M. and Shaw, L.
"Signal Processing - Discrete Spectral Analysis, Detection,
And Estimation"
McGraw-Hill
1975

5.4 Pryor, C.N.
"An Adaptive Kalman Filter Tracker For Multi-Mode
Range-Doppler Sonar"
Proc. of Nato Advanced Study Institute on Signal Processing, Pt.I P.265
- held in Portovenere, Italy
30 Aug. - 11 Sep., 1976

5.5 Trevelyan, J.P. et al
"Techniques for Surface Representation and Adaptation in
Automated Sheep Shearing"
Presented at the seminar on Robots in Manufacturing Industry
in Adelaide, South Australia
1981

6.1 Trevelyan, J.P. and Key, S.
"Automated Sheep Shearing"
Presented at the seminar on Robots in Manufacturing Industry
in Adelaide, South Australia
1981

6.2 *See 5.5*

6.3 Oppenheim, A.V. and Schafer, R.W.
"Digital Signal Processing"
Prentice-Hall
1975

6.4 Eshraghian, K. et al
"The Transform and Filter Brick: A New Architecture for Signal Processing"
Proc. VLSI 85 P.129
Elsevier Science Publishers B.V.
Aug. 1985

6.5 Johnston, J.
"Parallel Pipeline Fast Fourier Transformer"
Proc. IEE Vol.130 Part F No.6
Oct. 1983

6.6 Barnwell, T. III et al
"Optimum Implementation of Single Time Index Signal Flow Graphs
On Synchronous Multiprocessor Machines"
Proc. ICASSP
1982